Mechanical, Durability and Structural Evaluation of Geopolymer Concretes

Mohammad Albitar

B.Eng. Building Engineering (Hons)
M.Eng. Civil & Structural Engineering (MS)

Thesis submitted to the Faculty of Engineering, Computer and Mathematical Sciences in total to fulfilment of the requirements for the degree of

Doctor of Philosophy

School of Civil, Environmental and Mining Engineering

The University of Adelaide

Australia

–October 2016–

ABSTRACT

Alkali–activated aluminosilicates, known as geopolymers, have the potential to be used for sustainable concrete. Geopolymers encompass any binder systems derived from the reaction of an alkalis reagent with aluminosilicate rich materials that can harden at room (ambient) or elevated temperatures. The use of industrial waste materials in the manufacture of concrete not only introduces economic and structural performance benefits, but it also provides environmental benefits associated with reducing large volumes of disposed waste materials, such as ashes from coal–fired power stations and slags from metal production operations.

Despite the commercial promise of geopolymer concrete technology, its widespread use is hindered by the lack of fundamental understanding of its potential long–term behaviour. Moreover, an understanding of the behaviour of reinforced geopolymer concrete, including the interaction between the reinforcement and surrounding concrete and its resistance to corrosion is sparse. This lack of information is significant, as it delays compliance with regulatory design standards and hence limits practical structural applications.

This thesis explores the mechanical and structural characteristics of geopolymer concretes that are derived from class–F fly ash and granulated lead smelter slag. Significant aspects of these geopolymer concretes are investigated and the results are presented by compiling a series of journal papers. Firstly, mix designs utilising fly ash and lead smelter slags are developed and appropriate mix design guidelines are prescribed. For these mix designs, the material and mechanical properties of the concretes at both fresh and hardened states are then investigated. Having developed mix designs and quantified basic material behaviour, the long–term durability characteristics of both fly ash and lead smelter slag–based geopolymer concretes are extensively investigated. Particular attention is paid to the long–term durability of geopolymer concrete through consideration of the bond strengths of corroded and non–corroded steel reinforcement. The structural mechanisms related to the bond strength are investigated to quantify the formation of cracks, tension–stiffening and crack widening. Finally, the structural behaviour of granulated lead smelter slag–based geopolymer concrete short and slender columns was investigated through axial compression subjected to different eccentricities.

From the investigation conducted in this thesis, it is shown that fly ash geopolymer concrete has comparable mechanical and structural behaviour to that of Ordinary Portland Cement (OPC) concrete. For a given compressive strength of concrete, the mechanical properties, durability, bond strength, tension–stiffening, and structural performance exhibited in geopolymer concrete are slightly higher than the corresponding measures of these properties in OPC concrete. Similarly, granulated lead smelter slag–based geopolymer concrete is shown to have potential as a cementitious material if the slag particles are crushed to a size similar to that of fly ash and OPC. Alternatively, granulated lead smelter slag is shown to be of use as a partial replacement for fly ash, which results in a blended binder.

Significantly, based on the results obtained from this research, it can be stated that the current design provisions contained in the standards for Ordinary Portland Cement concrete can easily be modified and adopted for the applications of geopolymer concrete.

TABLE OF CONTENT

STATEMENT OF ORIGINALITY

I certify that this work contains no material which has been accepted for the award of any other degree or diploma in my name, in any university or other tertiary institution and, to the best of my knowledge and belief, contains no material previously published or written by another person, except where due reference has been made in the text. In addition, I certify that no part of this work will, in the future, be used in a submission in my name, for any other degree or diploma in any university or other tertiary institution without the prior approval of the University of Adelaide and where applicable, any partner institution responsible for the joint-award of this degree.

I give consent to this copy of my thesis when deposited in the University Library, being made available for loan and photocopying, subject to the provisions of the Copyright Act 1968.

I acknowledge that copyright of published works contained within this thesis resides with the copyright holder(s) of those works.

I also give permission for the digital version of my thesis to be made available on the web, via the University's digital research repository, the Library Search and also through web search engines, unless permission has been granted by the University to restrict access for a period of time.

…….. ……..

Mohammad Albitar Date

LIST OF PUBLICATIONS

Albitar, M., Visintin, P., Mohamed Ali, M. S. and Drechsler, M. (2014). "Assessing behaviour of fresh and hardened geopolymer concrete mixed with class–F fly ash." *Korean Society of Civil Engineers*, Vol. 19, No. 5, pp 1445–1455, DOI: 10.1007/s12205-014-1254-z.

Albitar, M., Mohamed Ali, M. S., Visintin, P., and Drechsler, M. (2015). "Effect of granulated lead smelter slag on strength of fly ash–based geopolymer concrete." *Construction and Building Materials*, Vol. 83, pp. 128–135, DOI: 10.1016/j.conbuildmat.2015.03.009.

Albitar, M., Mohamed Ali, M. S. and Visintin, P. (2016). "Durability evaluation of geopolymer and conventional concretes." *Construction and Building Materials*, in press.

Albitar, M., Visintin, P., Mohamed Ali, M. S., Lavigne, O. and Gamboa, E. (2016). "Bond slip models for uncorroded and corroded steel reinforcement in class–F fly ash geopolymer concrete." *Journal of Materials in Civil Engineering*, DOI: 10.1061/(ASCE)MT.1943-5533.0001713.

Albitar, M., Mohamed Ali, M.S. and Visintin, P. (2016). "Evaluation of tension stiffening, crack spacing and crack width of geopolymer concretes." *Engineering Structures*, submitted.

Albitar, M., Mohamed Ali, M. S. and Visintin, P. (2016). "Experimental study on fly ash and lead smelter slag–based geopolymer concrete columns." *Construction and Building Materials*, submitted.

ACKNOWLEDGEMENTS

This thesis was completed under the supervision of Dr Mohamed Ali Sadakkathulla, Dr Phillip Visintin and Mr Mark Drechsler. It is with great sincerity that the author wishes to thank Dr Sadakkathulla and Dr Visintin for their advice, guidance, encouragement and support, all of which led to the completion of this research within a flexible time and in a professional manner. My thanks extend to Mr Mark Drechsler for his input and guidance in the field of his expertise.

I am grateful to the laboratory staff of Adelaide University, Mr. Ian Ogier, Mr. Dale Hodson, Mr. Jon Ayoub, Mr. Gary Bowman, Mr. Simon Golding and Mr. Ian Cates, for their assistance with the experimental work and impressive craftsmanship in the test configuration.

Special thanks go to my parents for their encouragement, love and support. I am also eternally grateful to my Australian family who has provided me with confidence and unwavering support. Finally, to my close friends who were always there to offer support and motivation, I sincerely thank them.

INTRODUCTION

Geopolymers are innovative substances made of geo materials (aluminium and silicon) and activated through synthesis with an alkaline solution to form a long chain, which is similar to that of a polymer. Thus, the term geopolymer was coined to describe the material and its chemistry. Gepolymer materials generally, but not exclusively, go through a geopolymerisation reaction when they are activated with an alkaline solution, which usually contains variable amounts of dissolved silicon. The economic, environmental and technical advantages of this new binding material, such as abundance, comparable mechanical properties and durability characteristics have contributed to its popularity. Moreover geopolymers can be produced from a wide variety of by–product waste aluminosilicate–bearing raw materials, such as fly ash, silica fume, granulated blast–furnace slag, rice–husk ash, metakaolin, and granulated lead smelter slag (GLSS). The ability to utilise industrial by–product waste materials in concrete is of a significant benefit, as it reduces the environmental risks associated with disposal and storage in landfills of industrial wastes.

Given that geopolymer concrete is relatively new, substantial investigation is needed to prove its potential prior to widespread acceptance by the engineering community. Thus, to expedite its widespread use, existing design methodologies for conventional concrete must be proven to be applicable, or alternatively new design methodologies must be developed.

This thesis covers several aspects of the behaviour of two different geopolymer concretes, namely fly ash– and GLSS–based geopolymer concretes. These aspects are presented in a series of journal papers in which geopolymers are investigated from mix design to mechanical and durability properties to structural performance. Each chapter of the thesis presents a number of journal papers in which can be read individually without the need for the cumulative knowledge of former or following chapters. The manuscripts presented in this thesis are published, submitted or to be submitted to internationally recognised journals.

Chapter 1 investigates the material and mechanical properties of fly ash– and GLSS–based geopolymer concretes. The investigated material properties include the influence of water content, superplasticiser amount and chemical dosage on the workability and compressive strength. The investigated mechanical properties include compressive strength development, stress–strain relationship, splitting tensile strength, flexural strength and elastic modulus. Formulations based on empirical correlations are proposed to predict the mechanical properties of fly ash–based geopolymer.

Chapter 2 presents the durability characteristics of geopolymer concretes, as well as the bond properties of fly ash geopolymer concrete. Firstly, the effect of several chemicals attack on the compressive strength, splitting tensile strength and flexural strength is studied and hence the resistivity of fly ash, GLSS and OPC concretes against sodium chloride, sodium sulphate, sodium sulphate with magnesium sulphate and sulphuric acid

is quantified. In the second manuscript, the bond between reinforcement and geopolymer concrete is investigated and the influence of reinforcement corrosion on the bond stress is quantified. The bond–slip properties of uncorroded and corroded steel reinforcement in geopolymer concrete are quantified, analysed and compared to that of conventional concrete. Models to predict the key points, such as bond stress, slip at peak bond stress, frictional stress and maximum slip are established.

Chapter 3 investigates the tension–stiffening mechanisms of geopolymer concrete and analyses cracks formation, crack width and crack spacing. The manuscript also investigates the tension–stiffening mechanisms of OPC concrete for comparison purposes. Design provisions developed for OPC concrete were compared with the experimental results of geopolymer concrete in order to verify the accuracy of existing models. The study also incorporates mechanics–based solutions developed for OPC concrete with bond properties between reinforcing steel and concrete set for geopolymer concrete.

Chapter 4 contains an investigation into the structural performance of the developed geopolymer concretes in Chapter 1. The performance of geopolymer concrete columns and beam was studied in a manuscript that investigates the structural behaviour of blended fly ash with granulated lead smelter slag–based geopolymer concrete short and slender columns subjected to axial compression with different eccentricities. The paper investigates the slenderness and eccentricity effects on the performance of geopolymer concrete columns. Furthermore, the experimental results are subsequently compared with predictions from the design provisions developed for OPC concrete.

Chapter 5 of this thesis consists of concluding remarks that summarise major findings of this research. Suggestions for future research that will broaden the understanding of the behaviour of geopolymer concrete and hence expedite its widespread in the real world are also given. The widespread applications of geopolymer concrete provides a novel environmentally friendly binder–manufacturing technologies in the foreseeable future.

CHAPTER 1: Material and Mechanical Properties of Geopolymer Concrete

Background

This chapter focuses on the material and mechanical properties of class–F fly ash and granulated lead smelter slag (GLSS) as cementitious or filler materials for concrete. The first manuscript "Assessing behaviour of fresh and hardened geopolymer concrete mixed with class–F fly ash" presents an experimental study into the behaviour of class–F fly ash–based geopolymer concrete in its both wet and hardened states. Furthermore, the manuscript establishes new generic models for the hardened properties of fly ash–based geopolymer concrete to describe the mechanical properties of hardened geopolymer concrete as a function of the compressive strength. It is shown that the variation in mechanical properties with compressive strength is similar to that seen in OPC concrete, which suggests the possibility that only minor changes to design guidelines are required to incorporate geopolymer concretes.

The second manuscript of this chapter broadens the investigation into geopolymers through consideration of a new material. The manuscript "Effect of granulated lead smelter slag on strength of fly ash–based geopolymer concrete" presents an experimental study on the manufacture and behaviour of geopolymer concrete produced with a combination of granulated lead smelter slag (GLSS) and fly ash. The study aims at introducing a new industrial waste material that is a by–product of heavy metal extraction during lead smelting process. The investigation involved the use of GLSS as a supplementary or binder replacement for fly ash in order to further drive commercialisation and reduce costs, as well as to fill gaps in supply left by increased regulation around coal–fired power stations. Therefore, the manuscript studies the mechanical properties of GLSS incorporated with fly ash as binder and fine aggregate. It is shown that blended fly ash and GLSS–based geopolymer has the potential to be used in concrete industry.

List of Manuscripts

Albitar, M., Visintin, P., Mohamed Ali, M. S. and Drechsler, M. (2014). "Assessing behaviour of fresh and hardened geopolymer concrete mixed with class–F fly ash." *Korean Society of Civil Engineers*, Vol. 19, No. 5, pp 1445–1455, DOI: 10.1007/s12205-014-1254-z.

Albitar, M., Mohamed Ali, M. S., Visintin, P., and Drechsler, M. (2015). "Effect of granulated lead smelter slag on strength of fly ash–based geopolymer concrete." *Construction and Building Materials*, Vol. 83, pp. 128–135, DOI: 10.1016/j.conbuildmat.2015.03.009.

Statement of Authorship

Title of Paper	Assessing Behaviour of Fresh and Hardened Geopolymer Concrete Mixed with Class–F Fly Ash
Publication Details	Albitar, M., Visintin, P., Mohamed Ali, M. S. and Drechsler, M. (2014). "Assessing behaviour of fresh and hardened geopolymer concrete mixed with class–F fly ash." *KSCE Journal of Civil Engineering*, Vol. 19, No. 5, pp. 1445-1455, DOI 10.1007/s12205-014-1254-z.
Publication Status	Published

Principal Author

Name of Principal Author (Candidate)	Albitar, M		
Contribution to the Paper	Performed the experiment, interpreted and analysed data and wrote manuscript.		
Overall percentage (%)	85%		
Certification:	This paper reports on original research I conducted during the period of my Higher Degree by Research candidature and is not subject to any obligations or contractual agreements with a third party that would constrain its inclusion in this thesis. I am the primary author of this paper.		
Signature		Date	

Co-Author Contributions

By signing the Statement of Authorship, each author certifies that:

i. the candidate's stated contribution to the publication is accurate (as detailed above);
ii. permission is granted for the candidate in include the publication in the thesis; and
iii. the sum of all co-author contributions is equal to 100% less the candidate's stated contribution.

Name of Co-Author	Visintin, P.		
Contribution to the Paper	Supervised development of work, helped in data interpretation and manuscript evaluation and acted as corresponding author.		
Signature		Date	20/10/2016

Name of Co-Author	Mohamed Ali, M.S.		
Contribution to the Paper	Supervised development of work, helped to evaluate and edit the manuscript.		
Signature		Date	20/10/16

Name of Co-Author	Drechsler, M.		
Contribution to the Paper	Assisted in manuscript evaluation.		
Signature		Date	21/10/16

Assessing Behaviour of Fresh and Hardened Geopolymer Concrete Mixed with Class–F Fly Ash

M. Albitar, P. Visintin, M.S. Mohamed Ali, and M. Drechsler

ABSTRACT

Geopolymer binders have been shown to be a potential green replacement for Ordinary Portland Cement (OPC) in concrete manufacture. This paper presents an experimental study into the behaviour of geopolymer concrete in both its wet and hardened states using Class–F fly ash. The experimental program included 15 mix designs to investigate the influence of water–to–binder and superplasticiser–to–binder ratios on the workability and strength of fly ash–based geopolymer concrete. The results show that the addition of naphthalene sulphonate polymer–based superplasticiser has little to no influence on workability and a detrimental effect on strength. Furthermore, the indirect tensile strength, flexural tensile strength and elastic modulus of fly ash–based geopolymer concrete were recorded in this experimental program and have been added to a database of available tests in the open literature. The experimentally determined results are subsequently compared with prediction models developed for OPC–based concrete. The comparison suggests that existing OPC models provide reasonably accurate predictions of the elastic moduli and stress–strain relationships, whereas they slightly underestimate flexural and splitting tensile strengths.

KEYWORDS: Fly ash; Geopolymer concrete; Engineering properties; Workability; Tensile strength; Elastic moduli.

1. INTRODUCTION

The global production of Ordinary Portland Cement (OPC) is nearly four billion tonnes per year. The production of cement, in fact, contributes to the emission of carbon dioxide (CO_2) through the combustion of fossil fuels and calcining of limestone. Globally, the production of one tonne of OPC generates around 0.95 tonnes of CO_2 (Eliasson *et al.*, 1999; Bosoaga *et al.*, 2009), with the total CO_2 released by manufacturing OPC estimated to be between 5% and 8% of the global anthropogenic CO_2 emissions into the atmosphere (Davidovits, 1991; Sofi *et al.*, 2007a and 2007b; Duxson *et al.*, 2007; Nowak, 2008; Vijai *et al.*, 2010; Shi *et al.*, 2011; van Deventer *et al.*, 2012). The environmental impact of global OPC manufacture has therefore provided increased impetus for research into alternative concrete binders, such as geopolymers. Geopolymer binders utilise waste materials that contain a high volume of aluminium and silicon species, typically fly ash from coal–burning power plants which are activated in a highly alkali solution, such as sodium hydroxide (NaOH).

The chemistry of geopolymer binders has been widely studied (Davidovits, 1991 and 1994; Bijen, 1995; Palomo *et al.*, 1999; Xu and van Deventer, 2000; van Jaarsveld *et al.*,

2002; Yip and van Deventer, 2003; Duxson *et al.*, 2007) and it has been shown that it is possible to use geopolymers as an alternative binder to OPC in concrete manufacture. However, due to several limitations regarding production process, such as workability, necessity of heat curing and delay in setting time (Vijai *et al.*, 2012; Naik and Kumar, 2013), more widespread applications of geopolymer concrete are needed at both concrete manufacture and structural design levels.

The properties of geopolymer concretes (GPC) are highly dependent on the source materials, which are generally industrial waste materials that are not subject to the strict quality control procedures used in OPC manufacture. To address the uncertainty in using specific sources of waste materials, generic models describing the wet and hardened properties of geopolymer concrete are required.

To establish new generic models for the hardened properties of geopolymer concretes, the results of this experimental program are added to a database of available test results in the literature (Sofi *et al.*, 2007a; Hardjito and Rangan, 2005; Raijiwala and Patil, 2010; Nguyen *et al.*, 2010; Yildirim *et al.*, 2011; Olivia and Nikraz, 2011; Ivan Diaz-Loya *et al.*, 2011). Through a regression analysis of the database, models to describe the mechanical properties of hardened geopolymer concrete as a function of the compressive strength are then developed. The results of this analysis show the variation in mechanical properties with compressive strength is similar to that seen in OPC concrete, which suggests the possibility that only minor changes to design guidelines are required to incorporate geopolymer concretes.

2. EXPERIMENTAL PROGRAM

A total of 15 mixes described in *Table 1* were carried out to quantify the influence of naphthalene sulphonate polymer–based superplasticiser and water on workability and strength. In these tests, the superplasticiser–to–binder (sp:b) ratio and water–to–binder (w:b) ratios were varied within the started range up to where sufficient slump was obtained, so the sp:b ratio was varied between 0 and 0.115 and the w:b ratio was varied between 0 and 0.14.

Table 1. Mix Designs

Mix no	w:b	sp:b	Quantity (kg/m^3)					
			Coarse aggregate	Sand	Fly ash	Activator solution	SP	Water
1	0	0.0203	1200	600	424.8	158.4	8.64	0
2	0	0.0331	1197.12	598.56	424.8	158.4	13.92	0
3	0	0.1146	1179.84	589.92	424.8	158.4	48	0
4	0.0525	0.1129	1168.8	584.4	424.8	158.4	48	22.32
5	0.0079	0.0576	1192.8	594.48	424.8	158.4	24	3.36
6	0.0169	0.0576	1192.8	587.52	424.8	158.4	24	7.2

7	0.0225	0.0576	1192.8	584.16	424.8	158.4	24	9.6
8	0.0960	0	1180.8	580.8	424.8	158.4	0	40.8
9	0.0887	0.0197	1185.6	585.6	424.8	158.4	0.84	35.28
10	0.0225	0.0745	1183.2	585.6	424.8	158.4	31.68	9.6
11	0.0225	0.0858	1183.2	585.6	424.8	158.4	36.48	9.6
12	0.0225	0.0971	1183.2	585.6	424.8	158.4	41.28	9.6
13	0.0225	0.1129	1183.2	585.6	424.8	158.4	48	9.6
14	0.1073	0	1183.2	585.6	424.8	158.4	0	45.6
15	0.1412	0	1183.2	585.6	424.8	158.4	0	60

w:b = water-to-binder ratio, sp:b = superplasticiser-to-binder ratio, sp = superplasticiser

2.1. Material Specifications

In this study, low–calcium Class–F (ASTM C618-08 2008) fly ash produced at Port Augusta Power Station in South Australia was used. The selection of class–F fly ash was based on several reasons (i) its abundance worldwide, and (ii) the absence of tricalcium aluminate (C_3A) reaction, which is the main reason of concrete deterioration in the presence of sulphate attack (Tosun-Felekoğlu 2012). The chemical compositions of the fly ash were determined by x–ray fluorescence (XRF) and are presented in *Table 2* together with chemical composition of OPC for comparison reason.

Table 2. Chemical Composition of Fly Ash and OPC

Oxides	SiO_2	Al_2O_3	Fe_2O_3	CaO	Na_2O	K_2O	TiO_2	MgO	P_2O_5	SO_3	SrO	Mn_2O_3	*LOI
Fly ash	49	31	2.8	5.4	3.76	1.17	2.1	2.5	0.9	0.3	>0.1	>0.1	0.3
OPC	20.2	5.8	3.2	64.1	0.3	0.7	-	2.5	-	2.66	-	-	2.5

*Loss on Ignition

For all of the mixes, the alkaline solution phase consisted of a sodium silicate (Na_2SiO_3) and sodium hydroxide (NaOH) 14 M pre–mixed with a Na_2SiO_3–to–NaOH ratio of 1.5, and the ratio of activator–to–binder (a:b) was kept at 0.37.

2.2. Specimen Preparation

Mixing was carried out in either a 20 kg planetary mixer or a 150 kg pan mixer, depending on the mix volume. The mixing procedure consisted of initially mixing the dry constituents for three minutes. Following this, the water and activator solution were added. Once sufficient wetting of the concrete was observed, usually after one minute, the superplasticiser was added and mixed in for seven more minutes. Immediately following mixing, the workability was measured using slump test in accordance with Australian Standards AS 1012.3.1 (1998); standard 100mm x 200mm cylinders were then cast in accordance with Australian Standards AS 1012.3.2 (1998). The specimens were then either covered at a constant 23°C ambient room temperature or heat–cured in an oven at 70ºC for 24 hours and then placed in a fog room until the testing day.

3. RESULTS AND DISCUSSION

The results of the workability and strength tests for the mixes identified in *Table 1* are presented in *Table 3*. The general trends of superplasticiser influence are shown in *Fig. 1*, where it can be seen that increasing the *sp:b* ratio results in a reduction in the compressive strength of the geopolymer concrete.

Table 3. Influence of *w:b* and *sp:b* Ratios on Workability and Strength

Mix	w:b	sp:b	Slump (mm)	3 day compressive strength MPa (heat cured 24 hr)
1	0	0.020	4	53.8
2	0	0.033	6	34.8
3	0	0.115	70	29.4
4	0.052	0.113	210	36.3
5	0.008	0.058	5	74.5
6	0.017	0.058	15	67.6
7	0.026	0.058	25	64.4
8	0.096	0	125	55.6
9	0.089	0.020	200	44.4
10	0.023	0.075	65	66.9
11	0.023	0.086	85	62.4
12	0.026	0.097	125	57.1
13	0.026	0.113	165	40.9
14	0.107	0	165	46.2
15	0.141	0	230	27.2

w:b = water-to-binder ratio, sp:b = superplasticiser-to-binder ratio

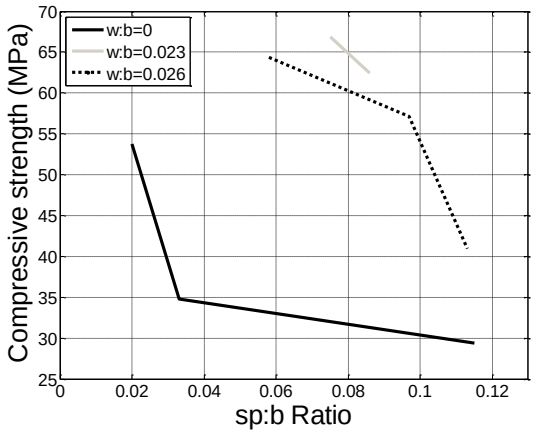

Figure 1. Influence of *sp:b* ratio on compressive strength

3.1. Workability

To investigate the influence of the *w:b* and *sp:b* ratios on workability, slump tests were performed on each mix design. The results are presented in *Table 3* and represented graphically in *Fig. 2.* It is shown that the addition of superplasticiser leads to increase concrete slump. This increase can be expressed mathematically through a linear regression of the data, as shown in *Fig. 2(a)*, which yields

$$slump = 2112(w{:}\,b) + 1275(sp{:}\,b) - 61 \tag{1}$$

A clear indication of the influence of the superplasticiser on the workability can be seen in *Fig. 2(b)* in which the solid superplasticiser–to–binder (solid *sp:b*) ratio and total water–to–binder (total *w:b*) ratio are plotted. Repeating the regression analysis for the data in *Fig. 2(b)* gives

$$slump = 2112(total\ w{:}\,b) - 279.8(solid\ sp{:}\,b) - 60.1 \tag{2}$$

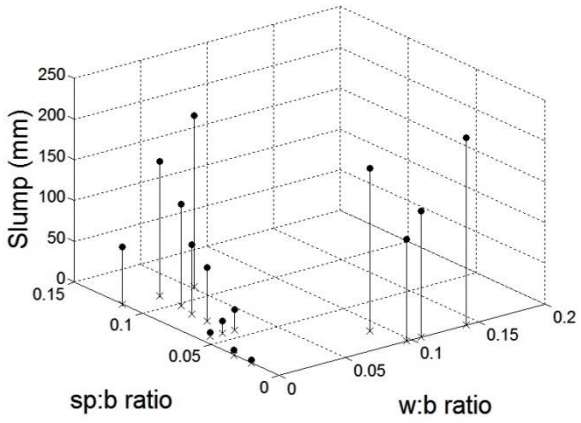

Figure 2a. Superplasticiser–to–binder ratio vs. water–to–binder ratio

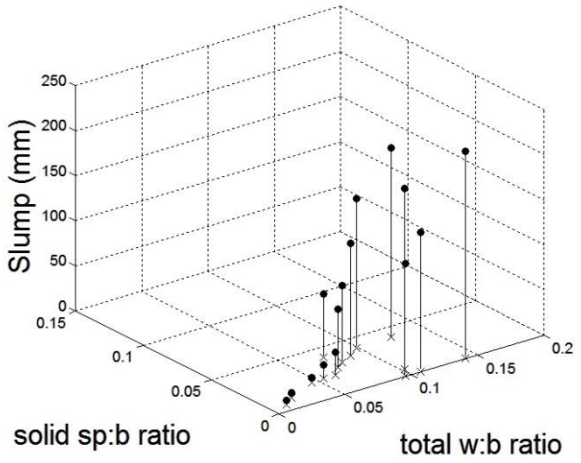

Figure 2b. Solid superplasticiser–to–binder ratio vs. total water–to–binder ratio

When the reactive component of superplasticiser is considered only to be its solid contents, which makes up 35% of the total quantity of the superplasticiser, it becomes clear that the reactive component of naphthalene sulphonate polymer–based superplasticiser has little to no effect on the workability of geopolymer concrete and the influence on the workability is raised due to the free water in the superplasticiser.

It is worth mentioning that Laskar and Bhattacharjee (2013) studied the influence of lignin–based plasticiser and polycarboxylic–ether–based superplasticiser on the rheology of fly ash–based geopolymer concrete, and found similar results. It was found that the superplasticiser additives only improved the slump of the geopolymer concrete when the alkalinity of the activator solution was lower than 4 M, and all mixtures containing NaOH solutions with molar strength above 4 M showed a reduction in the slump with increasing the amount of superplasticiser.

Other studies into the workability of geopolymer concrete have found similar findings and it has been suggested that the workability of geopolymer concrete is more strongly influenced by other factors, such as molarity of NaOH, Na_2SiO_3:NaOH ratio and ambient temperature. For example, a major study by Hardjito and Rangan (2005) on the influence of the molarity of NaOH was conducted and it was observed that increasing molarity leads to a reduction in the workability. Similar results were also found by Rattanasak and Chindaprasirt (2009) in a study where different molar strengths of NaOH were used as an activator solution. Furthermore, Heah *et al.* (2012) found that the workability of the geopolymer concrete decreases with increasing the ratio of Na_2SiO_3:NaOH. The ambient temperature was noticed to affect the workability of geopolymer concrete, as higher temperature improves the workability. This can be attributed to the polymerisation reaction mentioned by Shi *et al.* (2011).

3.2. Mechanical Properties of Hardened Concrete

Knowledge of modulus of elasticity and tensile strength of concrete are fundamental to structural concrete design. For OPC, these properties are typically defined empirically as a function of compressive strength in national design standards, such as ACI 318-08 (2008). For GPC's comparatively little experimental testing has been performed (Hardjito *et al.*, 2004; Hardjito and Rangan, 2005; Sofi *et al.*, 2007a; Ivan Diaz-Loya *et al.*, 2011); hence, tests to determine the full compression stress–strain relationships, the elastic modulus, the flexural strength and indirect tensile strength of the GPC have been undertaken on both ambient– and heat–cured specimens manufactured from mix 13. In order to enable a meaningful comparison, the obtained data have been added to a database of available test results for fly ash–based geopolymer concrete manufactured from both class–C and class–F for each engineering property, and then a regression analysis was performed to provide updated generic material models.

3.2.1. Stress–Strain Relationship

The full stress–strain relationships for both heat and ambient cured specimens are shown in *Fig. 3(a)*, together with Hognestad (1951) and Collins *et al.* (1993)'s expressions. The axial strains have been determined based on the average of four linear variable displacement transformers (LVDTs) readings measuring the total deformation over the full height of the specimen. It is evident from *Fig. 3(a)* that the expressions of Hognestad (1951) and Collins *et al.* (1993) provide reasonable accuracy for fly ash–based geopolymer concrete stress–strain relationships. *Fig. 3(b)* shows the stress–lateral strain relationships measured by three lateral strain gauges located at the mid–height of the specimens. The readings are provided up until the point at which damage to the concrete prevented any further accurate measurements.

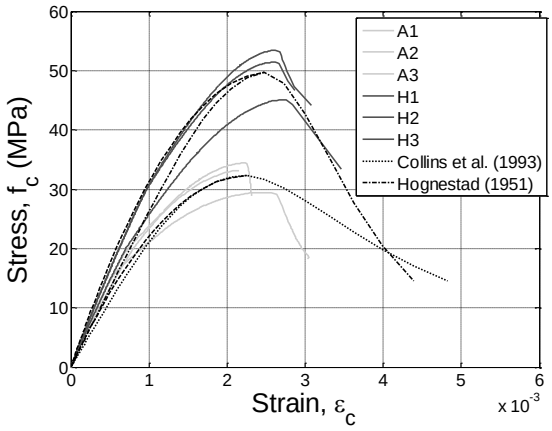

(a)

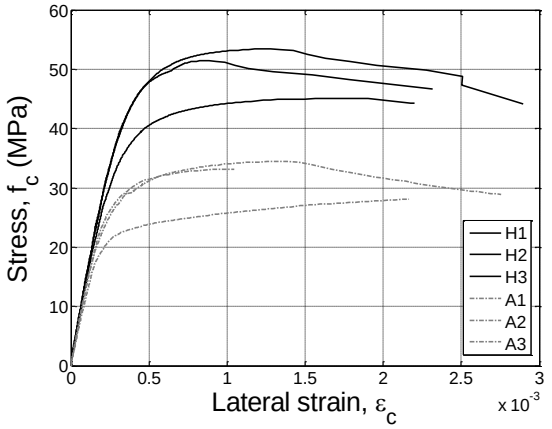

(b)

Figure 3. Stress-Strain Relationships: (a) Axial Stress-Axial Strain, (b) Axial Stress-Lateral Strain

It can be noticed that there is significant difference in the compressive strengths of the heat– and ambient–cured specimens, but in general, the strain at peak stress varied between 0.0022 and 0.0026. The relationship between compressive strength and the strain at peak stress is plotted in *Fig. 4* using the results of the current study, as well as the results of Hardjito and Rangan (2005), Yost *et al.* (2013), and Fernández-Jiménez *et al.* (2006). The results were then compared with several models set for OPC–based concrete, including Chen *et al.* (2013), as given in *Eq. 3*, and Ahmad and Shah (1985), as given in *Eq. 4*.

$$\varepsilon_{co} = 4.76 \times 10^{-6} f'_c + 2.13 \times 10^{-3} \quad (3)$$

$$\varepsilon_o = 0.001648 + 1.65 \times 10^{-5} f'_c \quad (4)$$

It can be seen from *Fig. 4* that the model of Chen *et al.* (2013) is in line with the trend-line of the geopolymer data of the investigated studies, which yields

$$\varepsilon_{co} = 4 \times 10^{-6} f'_c + 2.2 \times 10^{-3} \quad (5)$$

These findings indicate that the strain behaviour of GPC is quite similar to that of OPC, and hence the same equations can be used in order to predict the stress–strain relationships, as well as the strain at peak stress.

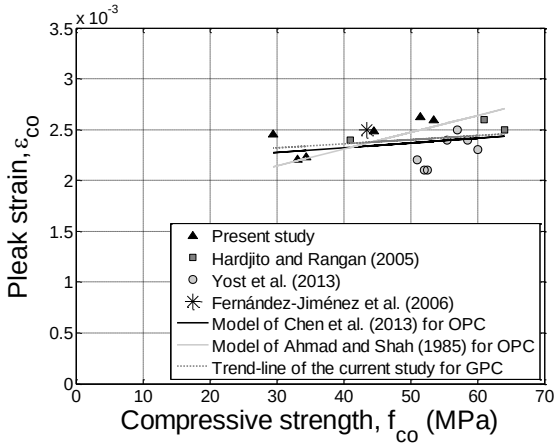

Figure 4. Compressive Strength-Peak Strain Relationship

3.2.2. Compressive Strength

The compressive strength results for all of the mixes are presented in *Table 3*. It can be observed that the compressive strength decreases with an increase in *sp:b* ratio, as can be seen in *Fig. 1*. The compressive strength developments of heat– and ambient–cured specimens of mix 13 are shown in *Fig. 5*. It can be seen that the strength development of ambient–cured cylinders is slower than that of the heat–cured cylinders, reflecting the process of the polymerisation reaction, which can be accelerated with heat curing. In fact, Bijen (1995) stated that the curing sensitivity of fly ash–based geopolymer is slower than that of OPC–based concrete. Nevertheless, the compressive strength development is sensitive to the liquid in the mix design. For instance, mix 13, which contains superplasticiser, gained the strength at a slower rate than mix 14, which does not contain superplasticiser, as can be seen in *Fig. 6*. It was deduced that while the naphthalene sulphonate–based superplasticiser may improve the strength of the conventional concrete, it reduces the compressive strength of fly ash–based geopolymer concrete. This observation was also reported by Al Bakri *et al.* (2012).

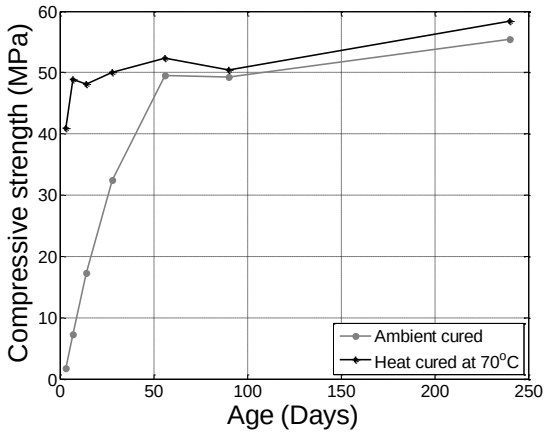

Figure 5. Compressive Strength Developments of Ambient and Heat Cured

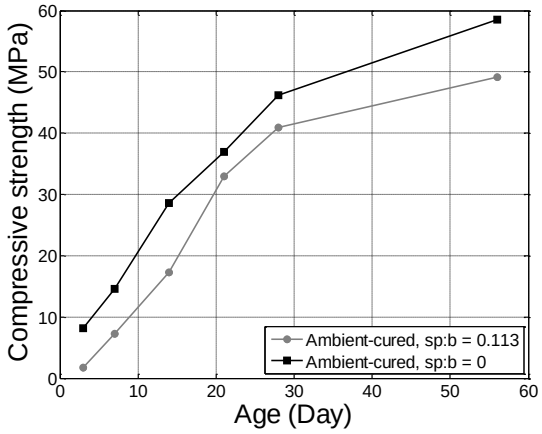

Figure 6. Compressive Strength Developments of Mixes with and without Superplasticiser

3.2.3. Splitting Tensile and Flexural Strength

The splitting tensile and flexural strength tests for mix 13 were experimentally determined in accordance with Australian Standards AS 1012.10 (2000) and AS 1012.11 (2000), respectively. The results of the splitting tensile and flexural tests are tabulated in *Table 4* and *Table 5*, respectively, together with other available results.

Table 4. Summary of Splitting Tensile Strength and Models (MPa)

Experimentally determined		Models			
f'_c	f'_{ct}	ACI 318-08 (2008)	Eurocode (2002)	Sofi et al. (2007a)	Proposed
Present study - Class–F					
18.66	2.04	2.29	2.11	2.07	2.59
33.17	3.08	3.05	3.10	2.76	3.46
34.41	3.14	3.11	3.17	2.82	3.52
29.45	2.96	2.88	2.86	2.60	3.26
51.42	4.23	3.80	3.85	3.44	4.30
53.42	5.55	3.87	3.92	3.51	4.39
44.58	5.51	3.54	3.77	3.20	4.01
Hardjito & Rangan (2005) - Class–F					
89.00	7.43	5.00	4.86	4.53	5.66
68.00	5.52	4.37	4.35	3.96	4.95
55.00	5.45	3.93	3.97	3.56	4.45
44.00	4.43	3.52	3.74	3.18	3.98
Sofi et al. (2007a) - Class–F					
55.40	3.40	3.94	3.98	3.57	4.47
54.00	2.80	3.89	3.94	3.53	4.41
48.60	2.80	3.69	4.00	3.35	4.18
56.50	4.10	3.98	4.02	3.61	4.51
47.00	3.90	3.63	3.91	3.29	4.11
52.80	3.30	3.85	3.90	3.49	4.36
35.20	3.20	3.14	3.22	2.85	3.56
44.40	2.90	3.53	3.76	3.20	4.00
37.60	2.40	3.25	3.37	2.94	3.68
41.80	3.60	3.43	3.61	3.10	3.88
42.00	3.50	3.43	3.62	3.11	3.89
38.30	2.70	3.28	3.41	2.97	3.71
Nguyen et al. (2010) - Class–F					
35.00	3.90	3.14	3.21	2.84	3.55
42.80	4.90	3.47	3.67	3.14	3.93
Raijiwala and Patil (2010) - Class–F					
20.18	2.24	2.38	2.22	2.16	2.70
23.10	2.38	2.55	2.43	2.31	2.88
24.12	2.54	2.60	2.50	2.36	2.95
25.02	3.02	2.65	2.57	2.40	3.00
28.33	2.60	2.82	2.79	2.55	3.19
30.14	3.06	2.91	2.91	2.64	3.29

33.16	3.50	3.05	3.10	2.76	3.46
34.28	3.80	3.10	3.17	2.81	3.51
35.10	4.16	3.14	3.22	2.84	3.55
34.22	3.22	3.10	3.16	2.81	3.51
35.24	3.48	3.15	3.22	2.85	3.56
39.12	4.48	3.31	3.46	3.00	3.75
40.18	4.64	3.36	3.52	3.04	3.80
41.18	5.18	3.40	3.58	3.08	3.85
37.36	4.00	3.24	3.35	2.93	3.67
40.29	4.20	3.36	3.53	3.05	3.81
42.44	4.80	3.45	3.65	3.13	3.91
43.00	5.00	3.48	3.68	3.15	3.93
44.14	5.24	3.52	3.75	3.19	3.99
Olivia and Nikraz (2011) - Class–F					
56.49	4.13	3.98	4.02	3.61	4.51
56.51	4.18	3.98	4.02	3.61	4.51
56.24	3.96	3.97	4.01	3.60	4.50
58.85	4.10	4.07	4.09	3.68	4.60
60.20	4.29	4.11	4.13	3.72	4.66
63.29	4.79	4.22	4.22	3.82	4.77

Table 5: Summary of Flexural Strength and Models (MPa)

Experimentally determined		Predictive Models			
f'_c	f'_{cf}	ACI 318-08 (2008)	Sofi *et al.* (2007a)	Ivan Diaz-Loya *et al.* (2011)	Proposed Model
Present study - Class–F					
18.66	3.56	2.68	3.02	2.98	3.24
18.66	3.56	2.68	3.02	2.98	3.24
33.17	4.12	3.57	4.03	3.97	4.32
34.41	4.35	3.64	4.11	4.05	4.40
51.42	5.30	4.45	5.02	4.95	5.38
53.42	5.25	4.53	5.12	5.04	5.48
Sofi *et al.* (2007a) - Class–F					
35.20	4.90	3.68	4.15	4.09	4.45
44.40	4.80	4.13	4.66	4.60	5.00
37.60	4.50	3.80	4.29	4.23	4.60
41.80	5.30	4.01	4.53	4.46	4.85
42.00	5.30	4.02	4.54	4.47	4.86
38.30	4.20	3.84	4.33	4.27	4.64
55.40	6.10	4.61	5.21	5.14	5.58

54.00	4.90	4.56	5.14	5.07	5.51
48.60	5.40	4.32	4.88	4.81	5.23
56.50	6.20	4.66	5.26	5.19	5.64
47.00	5.90	4.25	4.80	4.73	5.14
52.80	5.30	4.51	5.09	5.01	5.45
Raijiwala and Patil (2010) - Class–F					
16.42	2.28	2.51	2.84	2.80	3.04
20.18	3.44	2.79	3.14	3.10	3.37
23.10	3.50	2.98	3.36	3.32	3.60
24.12	3.55	3.04	3.44	3.39	3.68
25.02	3.72	3.10	3.50	3.45	3.75
28.33	3.52	3.30	3.73	3.67	3.99
30.14	3.98	3.40	3.84	3.79	4.12
33.16	4.30	3.57	4.03	3.97	4.32
34.28	4.34	3.63	4.10	4.04	4.39
35.10	4.68	3.67	4.15	4.09	4.44
34.22	4.21	3.63	4.09	4.04	4.39
35.24	5.50	3.68	4.16	4.10	4.45
39.12	5.76	3.88	4.38	4.32	4.69
40.18	5.82	3.93	4.44	4.37	4.75
41.18	6.04	3.98	4.49	4.43	4.81
37.36	5.20	3.79	4.28	4.22	4.58
40.29	6.00	3.94	4.44	4.38	4.76
42.44	6.60	4.04	4.56	4.50	4.89
43.00	6.66	4.07	4.59	4.52	4.92
44.14	7.18	4.12	4.65	4.58	4.98
Olivia and Nikraz (2011) - Class–F					
56.49	7.39	4.66	5.26	5.19	5.64
56.51	9.21	4.66	5.26	5.19	5.64
56.24	8.99	4.65	5.25	5.17	5.62
58.85	9.36	4.76	5.37	5.29	5.75
60.20	8.38	4.81	5.43	5.35	5.82
63.29	9.85	4.93	5.57	5.49	5.97
Ivan Diaz-Loya *et al.* (2011) - Class–F					
40.30	4.10	3.94	4.44	4.38	4.76
47.50	5.50	4.27	4.82	4.76	5.17
46.69	5.30	4.24	4.78	4.71	5.12
46.79	4.60	4.24	4.79	4.72	5.13
46.11	4.70	4.21	4.75	4.69	5.09
47.44	5.10	4.27	4.82	4.75	5.17
12.20	2.20	2.17	2.44	2.41	2.62

12.80	2.30	2.22	2.50	2.47	2.68
20.60	3.50	2.81	3.18	3.13	3.40
10.30	2.70	1.99	2.25	2.21	2.41
46.50	6.30	4.23	4.77	4.71	5.11
49.20	4.66	4.35	4.91	4.84	5.26
43.38	4.24	4.08	4.61	4.54	4.94
Ivan Diaz-Loya *et al.* (2011) - Class–C					
59.50	4.48	4.78	5.40	5.32	5.79
52.20	4.70	4.48	5.06	4.99	5.42
55.80	4.30	4.63	5.23	5.15	5.60
80.37	5.27	5.56	6.28	6.19	6.72
61.30	6.23	4.85	5.48	5.40	5.87
39.10	4.19	3.88	4.38	4.31	4.69
53.70	4.43	4.54	5.13	5.06	5.50
36.54	3.58	3.75	4.23	4.17	4.53
57.18	5.27	4.69	5.29	5.22	5.67
42.81	5.18	4.06	4.58	4.51	4.91
62.10	4.83	4.89	5.52	5.44	5.91
2.70	0.62	1.02	1.15	1.13	1.23

Fig. 7 shows the results of splitting tensile tests of the present study, as well as available results on geopolymer concrete, including Sofi *et al.* (2007a); Hardjito and Rangan (2005); Raijiwala and Patil (2010); Nguyen *et al.* (2010); Olivia and Nikraz (2011); and Ivan Diaz-Loya *et al.* (2011), and compared with predictions models developed for OPC–based concrete and GPC, including ACI 318-08 (2008), Eurocode (2002) and Sofi *et al.* (2007a). A regression analysis was then performed, and the following expression is proposed in terms of the compressive strength:

$$f'_{ct} = 0.6\sqrt{f'_c} \qquad \text{(MPa)} \qquad (6)$$

which is in the same form as that of the ACI 318-08 (2008).

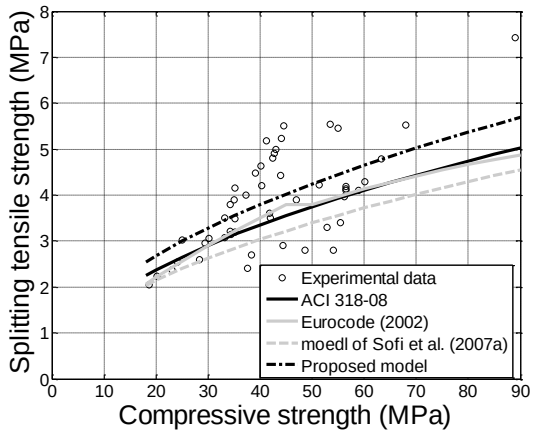

Figure 7. Splitting Tensile Strength versus Compressive Strength

Fig. 8 shows the results of the flexural tensile tests conducted in the present study, as well as available results on class–F fly ash–based geopolymer concrete (Sofi *et al.*, 2007a; Raijiwala and Patil, 2010; Olivia and Nikraz, 2011; Ivan Diaz-Loya *et al.*, 2011) and compared with predictions models developed for OPC–based concrete and GPC, including ACI 318-08 (2008); Sofi *et al.* (2007a); Ivan Diaz-Loya *et al.* (2011). In addition, results on class–C fly ash (Ivan Diaz-Loya et al., 2011) were also included for comparison purpose. A regression analysis was then performed to propose the following expression in terms of the compressive strength:

$$f'_{cf} = 0.75\sqrt{f'_c} \qquad \text{(MPa)} \qquad (7)$$

which is again in the same form of the ACI 318-08 (2008).

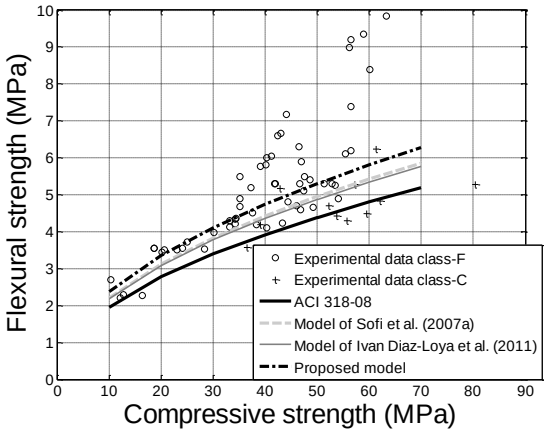

Figure 8. Flexural strength versus Compressive Strength

It should be noted that the expressions set for conventional OPC concrete, such as ACI (2008), underestimate the values of class–F fly ash–based geopolymer concrete, yet they accurately enough estimate the values of class–C fly ash–based geopolymer concrete, as can be seen in *Fig. 8*. This indicates that the mechanical properties of class–C fly ash–based geopolymer concrete are similar to those of conventional OPC–based concrete.

3.2.4. Modulus of Elasticity

The modulus of elasticity (E_c) was determined from the linear elastic portion of the stress−strain curves. The results of the present study are tabulated in *Table 6*, together with other available results.

Table 6. Summary of Modulus of Elasticity

Experimentally determined		Predictive Models (MPa)			
f'_c (MPa)	E_c (GPa)	ACI 318-08 (2008)	AS 3600 (2001)	Carrasquillio *et al.* (1981)	Ahmad and Shah (1985)
Present study - Class–F					
56.97	30.2	31.959	36.97	32.581	33.664
45.52	41.6	29.300	33.05	29.870	31.297
47.3	28.4	29.733	33.69	30.312	31.690
46.58	29.2	29.559	33.43	30.134	31.532
33.17	28.07	26.021	28.21	26.527	28.238
34.41	25.05	26.375	28.74	26.888	28.576
29.45	27.81	24.917	26.58	25.402	27.167
51.42	30.88	30.707	35.13	31.305	32.561
53.42	31.02	31.166	35.80	31.772	32.968
44.58	28.55	29.067	32.71	29.633	31.085
Nguyen *et al.* (2010) - Class–F					
30	35.04	25.084	26.83	25.573	27.331
35	31.31	26.541	28.98	27.058	28.735
35.4	32.9	26.653	29.15	27.172	28.841
40.9	30.93	28.132	31.33	28.680	30.227
44	27.8	28.922	32.49	29.485	30.953
40.3	37.5	27.976	31.10	28.521	30.082
Hardjito & Rangan (2005) - Class–F					
89	30.8	38.221	46.21	38.965	38.917
68	27.3	34.277	40.39	34.944	35.658
55	26.1	31.522	36.33	32.135	33.282
44	23	28.922	32.49	29.485	30.953
Yildirim *et al.* (2011) - Class–F					
40.2	35.97	27.950	31.06	28.494	30.058

38.75	34.89	27.567	30.49	28.103	29.701
40.25	35.65	27.963	31.08	28.507	30.070
39.25	34.95	27.700	30.69	28.239	29.825
36.49	32.79	26.955	29.59	27.480	29.127
38.14	33.06	27.404	30.25	27.937	29.548
40.06	34.96	27.913	31.00	28.456	30.024
47.81	37.82	29.856	33.87	30.437	31.800
46.81	36.85	29.615	33.52	30.191	31.582
47.93	38.12	29.885	33.91	30.466	31.826
46.96	37.95	29.651	33.57	30.228	31.615
45.9	37.31	29.393	33.19	29.965	31.382
46.23	37.84	29.474	33.31	30.047	31.455
47.52	38.11	29.786	33.77	30.366	31.737
60.49	42.64	32.721	38.10	33.358	34.327
57.76	41.89	32.132	37.23	32.757	33.815
61.1	43.64	32.851	38.29	33.491	34.439
63.31	42.65	33.316	38.98	33.965	34.839
55.27	36.22	31.582	36.42	32.197	33.335
58.44	40.45	32.280	37.45	32.908	33.944
61.12	43.63	32.856	38.30	33.495	34.443
Yildirim *et al*. (2011) - Class–C					
40.2	35.97	27.950	31.06	28.494	30.058
40.5	36.31	28.028	31.17	28.574	30.131
41.3	36.91	28.236	31.48	28.785	30.323
42.5	37.66	28.544	31.93	29.099	30.606
38.7	33.03	27.553	30.47	28.090	29.689
39.8	34.01	27.845	30.90	28.387	29.960
41.2	36.01	28.210	31.44	28.759	30.299
47.8	37.82	29.854	33.87	30.435	31.798
48.6	37.25	30.045	34.15	30.630	31.970
50.8	37.92	30.563	34.91	31.158	32.433
50.5	36.89	30.493	34.81	31.086	32.371
48.2	38.11	29.950	34.01	30.532	31.884
50.5	39.7	30.493	34.81	31.086	32.371
51.2	40.62	30.656	35.05	31.253	32.516
60.5	42.64	32.724	38.10	33.360	34.329
57.9	42.59	32.163	37.27	32.788	33.842
60.8	42.01	32.787	38.20	33.426	34.384
63.2	42.89	33.293	38.94	33.941	34.819
58.8	40.49	32.358	37.56	32.988	34.012
60.1	42.5	32.638	37.98	33.273	34.255

62.9	43.62	33.231	38.85	33.877	34.765
Olivia and Nikraz (2011) - Class–F					
56.49	25.33	31.853	36.82	32.473	33.572
56.51	27.18	31.857	36.82	32.477	33.576
56.24	26.95	31.798	36.74	32.417	33.524
58.85	28.03	32.369	37.58	32.999	34.022
60.2	29.05	32.659	38.01	33.295	34.273
63.29	26.8	33.312	38.97	33.960	34.835
Ivan Diaz-Loya *et al.* (2011) - Class–F					
40.300	28.599	27.976	31.10	28.521	30.082
47.500	29.475	29.782	33.76	30.361	31.733
46.690	29.358	29.586	33.47	30.161	31.556
46.790	28.517	29.610	33.51	30.186	31.578
46.110	26.455	29.444	33.26	30.017	31.428
47.440	25.635	29.767	33.74	30.346	31.720
46.500	28.744	29.539	33.40	30.114	31.514
43.380	25.607	28.767	32.26	29.326	30.811
Ivan Diaz-Loya *et al.* (2011) - Class–C					
59.500	33.633	32.509	37.79	33.142	34.143
52.200	34.377	30.887	35.39	31.488	32.721
55.800	37.108	31.700	36.59	32.317	33.438
80.370	42.878	36.664	43.92	37.377	37.648
61.300	31.447	32.894	38.35	33.534	34.476
53.700	28.91	31.229	35.90	31.837	33.024
36.540	26.972	26.969	29.61	27.494	29.140
57.180	29.448	32.005	37.04	32.628	33.705
42.810	22.567	28.623	32.05	29.180	30.679
62.100	29.896	33.063	38.60	33.706	34.621

Fig. 9 shows the results of the present study, together with results from database of available test data for comparison purpose, including class–C (Yildirim *et al.*, 2011; Ivan Diaz-Loya *et al.*, 2011) and class–F (Hardjito and Rangan, 2005; Nguyen *et al.*, 2010; Yildirim *et al.*, 2011; Olivia and Nikraz, 2011; Ivan Diaz-Loya *et al.*, 2011) fly ash–based geopolymer concrete. As seen in *Fig. 9*, while there is a large scatter of experimental results, the expression of the ACI 318-08 (2008) shown in *Eq. 8* for OPC provides a reasonable estimate of the mean test results.

$$E_c = 3320\sqrt{f'_c} + 6900 \qquad \text{(MPa)} \qquad (8)$$

Moreover, the upper and lower bounds of Australian Standards AS 3600 (2001) shown in *Eq. 9* capture the scatter of the results.

$$E_c = 0.043\,\rho^{1.5}\sqrt{f_{cm}} \pm 20\% \qquad \text{(MPa)} \qquad (9)$$

where f_{cm} is the mean value of concrete cylinder compressive strength.

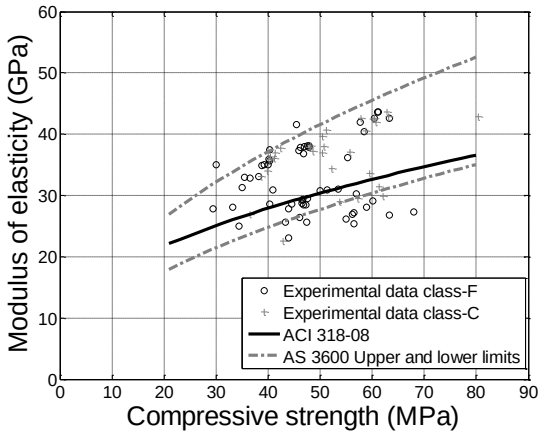

Figure 9. Modulus of Elasticity of Fly Ash (Class–F and Class–C)

The results reported by Hardjeto and Rangan (2005) are found to be beneath the lower limit of AS 3600 (2001). This can be attributed to the size of the coarse aggregates used in the experimental program. The effective elastic modulus of concrete can be increased by increasing the maximum aggregate size, as well as by reducing the water/cement ratio, which will lead to increasing the elastic modulus of the cement paste (Neville, 2000; Shah and Ribakov, 2011).

3.2.5. Poisson's Ratio

Poisson's ratios were calculated in accordance with Australian Standard AS 1012.17 (1997). The values of the longitudinal and lateral strains were recorded simultaneously on the same samples using strain gauges and LVDTs. For each specimen, Poisson's ratio was calculated from the average strain from the second and successive loadings according to the following equation:

$$\upsilon = (\varepsilon\_4 - \varepsilon\_3\,)/(\varepsilon\_1 - 0.00005) \qquad (10)$$

where υ is the Poisson's ratio, ε_4 is the average transverse strain at test load, ε_3 is the average of transverse strain coincident with average longitudinal strain of 50×10^{-6} m/m, and ε_1 is the average of longitudinal strain at test load.

Table 7 presents the experimental values obtained in the present study, as well as other studies including, Hardjito and Rangan (2005); Ivan Diaz-Loya *et al.* (2011).

Table 7: Summary of Poisson's Ratios

Compressive strength	Poisson's ratio
Present study	
32.3	0.12
49.8	0.14
Hardjito and Rangan (2005)	
89	0.16
68	0.12
55	0.14
44	0.13
Ivan Diaz-Loya *et al.* (2011)	
40.3	0.14
47.5	0.16
46.7	0.14
46.8	0.13
46.1	0.12
47.4	0.14
12.2	0.17
12.8	0.10
20.6	0.08
10.3	0.10
46.5	0.15
49.2	0.15
43.3	0.13

The majority of experimentally determined Poisson's ratio of geopolymer concrete ranged between 0.12 and 0.16 (*Table 7*) with an average value of 0.13. For Portland cement concrete, the Poisson's ratio is usually ranged between 0.11 and 0.21, with an average value of 0.15 (Warner *et al.*, 1998). Thus, it can be concluded that the Poisson's ratio of fly ash–based geopolymer concrete is similar to that of conventional OPC–based concrete.

4. CONCLUSION

This paper presented the results of an experimental study that was conducted to obtain a greater understanding of the behaviour of typical Class–F fly ash–based geopolymer concrete. The results from the current study augmented the existing database of geopolymer concrete, as it involved compressive strength development, flexural strength, tensile strength, elastic modulus and the stress–strain relationship. The following conclusions can be drawn based on the results and discussions reported in this paper.

1. The polymerisation reaction can be accelerated with heat curing, as the compressive strength can be developed at an early age.
2. Naphthalene sulphonate polymer–based superplasticiser has little to no effect on the slump and an adverse effect on the strength of fly ash–based geopolymer concrete where high molarity NaOH is used.
3. The experimentally determined values of splitting tensile and flexural strength were higher than those in the expressions prescribed by national standards for

OPC–based concrete, indicating that class–F fly ash–based geopolymer concrete exhibits higher tensile strength than the OPC-based concrete.

4. Elastic modulus and Poisson's ratio of class–F fly ash–based geopolymer concrete were found to be similar of those of conventional OPC–based concrete.
5. Stress–strain expressions developed for conventional OPC–based concrete can be applied with reasonable accuracy for determination of fly ash–based geopolymer concrete stress–strain relationships.
6. The results have shown that geopolymer–based concrete using Class–F fly ash has a great potential for utilisation in construction industries as a replacement for OPC–based concrete, as it has comparable structural properties.

ACKNOWLEDGEMENT

The authors would like to acknowledge the support of The South Australian Department of Further Education, Employment, Science and Technology through Catalyst Research Grant "Development of Geopolymer Concrete."

REFERENCES

ACI Committee 318 (2008). "Building code requirements for structural concrete (ACI 318-08) and commentary." *American Concrete Institute*, Farmington Hills, MI, ISBN: 978-0-87031-264-9, ISBN: 9780870317446 .

Ahmad, S. H., and Shah, S. P. (1985). "Structural properties of high strength concrete and its implication for precast prestressed concrete." *Portland Cement Instituted Journal*, Vol. 30, No. 6, pp. 92–119.

Al Bakri, A. M., Kamarudin, H., Bnhussain, M., Nizar, I., Rafiza, A. R., and Zarina, Y. (2012). "The processing, characterization, and properties of fly ash based geopolymer concrete." *Reviews on Advanced Materials Science*, Vol. 30, pp. 90–97.

AS 1012.3.1. (1998). "Methods of testing concrete: determination of properties related to the consistency of concrete - Slump test." Australian Standards, ISBN: 0-7337-2156-7.

AS 1012.3.2. (1998). "Methods of testing concrete: determination of properties related to the consistency of concrete - Compacting factor test." Australian Standards, ISBN: 0-7337-2157-5.

AS 1012.10. (2000). "Method of testing concrete: determination of indirect tensile strength of concrete cylinders (Brazil or Splitting Test)." Australian Standards, ISBN: 0-7337-3391-3.

AS 1012.11. (2000). “Method of testing concrete: determination of the modulus of rupture.” Australian Standards, ISBN: 0-7337-3392-1.

AS 1012.17. (1997). “Methods of testing concrete: determination of the static chord modulus of elasticity and Poisson's ratio of concrete specimens.” Australian Standards, ISBN: 0-7337-1310-6.

AS 3600 (2001). “Concrete structure.” Australian Standards, ISBN: 0-7337-3931-8.

ASTM C618-08 (2008). “Standard Specification for Coal Fly Ash and Raw or Calcined Natural Pozzolan for Use in Concrete,” Philadelphia: Amirican Society for Testing and Materials, DOI: 10.1520/C0618-08.

Bijen, J. (1995). “Benefits of slag and fly ash.” *Construction and Building Materials*, Vol. 10, No. 5, pp. 309–314, DOI: 10.1016/0950-0618(95)00014-3.

Bosoaga, A., Masek, O., Oakey, J. E. (2009). “CO_2 capture technologies for cement industry.” *Energy Procedia*, pp. 133–40, DOI: 10.1016/j.egypro.2009.01.020.

Cement Industry Federation (2011). “Australian Cement Industry.” *Sustainability Report*.

Chen, Y., Visintin, P., Oehlers, D. J., and Alengaram, U. J. (2013). “Size-dependent stress-strain model for unconfined concrete.” *Journal of Structural Engineering*, 04013088–1–04013088–11, DOI: 10.1061/(ASCE)ST.1943-541X.0000869.

Collins, M. P., Mitchell, D., and MacGregor, G. J. (1993). “Structural design considerations for high strength concrete.” *ACI Concrete International*, Vol. 15, No. 5, pp. 27–34, ISSN: 0162-4075.

Davidovits, J. (1991). “Geopolymers: inorganic polymeric new materials.” *Journal of Thermal Analysis*, Vol. 37, pp. 1633–1656, DOI: 10.1007/BF01912193.

Davidovits, J. (1994). “Global warming impact on the cement and aggregates industries.” *World Resource Review*, Vol. 6, No. 2, pp. 263–278.

Duxson, P., Provis, J. L., Lukey, G. C., and van Deventer, J. S. J. (2007). “The role of inorganic polymer technology in the development of ‘green concrete’.” *Cement and Concrete Research*, Vol. 37, pp. 1590–1597, DOI: 10.1016/j.cemconres.2007.08.018.

Eliasson, B., Riemer, P. W. F., and Wokaun, A. (1999). “Greenhouse gas control technologies.” *Elsevier Science Ltd*, UK.

European Standard. (2002). “Eurocode 2: Design of Concrete Structure – Part 1: General Rules and Rules for Buildings.” ref. no. prEN 1992–1–1, ISBN: 978 0 580 73752 7.

Fernández-Jiménez, A., Palomo, A., and López-Hombrados, C. (2006). “Engineering properties of alkali-activated fly ash concrete.” *ACI Materials Journal*, pp. 106–112, DOI: 10.14359/15261.

Hardjito, D., and Rangan, B. V. (2005). “Development and properties of low-calcium fly ash-based geopolymer concrete.” Research report GC1, Faculty of Engineering Curtin University of Technology, Perth, Australia.

Hardjito, D., Wallah, S. E., Sumajouw, D. M. J., and Rangan, B. V. (2004). “Factors influencing the compressive strength of fly ash-based geopolymer concrete.” *Journal of Civil Engineering Dimension*, Vol. 6, No. 2, pp. 88–93, ISSN: 1410-9530.

Heah, C. Y., Kamarudin, H., Al Bakri, A. M. M., Bnhussain, M., Luqman, M., Nizar, I. K., Ruzaidi, C. M., and Liew, Y. M. (2012). “Study on solids-to liquid and alkaline activator ratios on kaolin-based geopolymers.” *Construction and Building Materials*, Vol. 35, pp. 912–922, DOI: 10.1016/j.conbuildmat.2012.04.102.

Hognestad, E. N. (1951). “A study of combined bending and axial load in reinforced concrete members.” *University of Illinois at Urbana-Champaign*, Vol. 49, No. 22, USA, DOI: 5308743.

Ivan Diaz-Loya, E., Allouche, E. N., Vaiday, S. (2011). “Mechanical properties of fly-ash-based geopolymer concrete.” *ACI Materials Journal*, pp. 300–306, ISSN: 0889-325X.

Laskar, A. I., Bhattacharjee, R. (2013). “Effect of plasticizer and superplasticizer on rheology of fly-ash-based geopolymer concrete.” *ACI Materials Journal*, pp. 513–518, ISSN: 0889-325X.

Naik, T. R., Kumar, R. (2013). “Geopolymer concrete for sustainable developments: opportunities, limitations, and future needs.” *Third International Conference on Sustainable Construction Materials and Technologies*, pp. 1–8.

Neville, A. M. (2000). “Properties of concrete.” Prentice Hall, London, ISBN: 978-0-273-78633-7.

Nguyen, N. H., Smith, S. M., Staniford, M. D., and van Senden, M. F. (2010). “Geopolymer concrete - concrete goes green.” Research report, School of Civil, Environmental and Mining Engineering, The University of Adelaide, Adelaide, Australia.

Nowak, R. (2008). “Build ‘em high, and make them green’.” *New Scientist*, Vol. 197, No. 2640, pp. 28–29, DOI: 10.1016/S0262-4079(08)60229-8.

Olivia, M., and Nikraz, H. (2011) “Properties of fly ash geopolymer concrete designed by Taguchi method.” *Materials and Design*, pp. 1–27, DOI: 10.1016/j.matdes.2011.10.036.

Palomo, A., Grutzek, M., and Blanco, M. (1999). “Alkali-activated fly ashes. A cement for the future.” *Cement and Concrete Research*, Vol. 29, pp. 1323–1329, DOI: 10.1016/S0008-8846(98)00243-9.

Raijiwala, D. B., and Patil, H. S. (2010). “Geopolymer concrete: a green concrete.” *2nd International Conference on Chemical, Biological and Environmental Engineering*, pp. 202–206, DOI: 10.1109/ICBEE.2010.5649609.

Rattanasak, U., and Chindaprasirt, P. (2009). “Influence of NaOH solution on the synthesis of fly ash geopolymer.” *Minerals Engineering*, Vol. 22, pp. 1073–1078, DOI: 10.1016/j.mineng.2009.03.022.

Shah, A. A., and Ribakov, Y. (2011). “Recent trends in steel fibered high-strength concrete.” *Materials and Design*, Vol. 32, pp. 4122–4151, DOI: 10.1016/j.matdes.2011.03.030.

Shi, C., Jiménez, A. F., and Palomo, A. (2011). “New cements for the 21st century: The pursuit of an alternative to Portland cement.” *Cement and Concrete Research*, Vol. 41, pp. 750–763, DOI: 10.1016/j.cemconres.2011.03.016, DOI: 10.1016/j.cemconres.2011.03.016.

Sofi, M., van Deventer, J. S. J., Mendis, P.A., and Lukey, G. C. (2007a). “Engineering properties of inorganic polymer concretes (IPCs).” *Cement and Concrete Research*, Vol. 37, pp. 251–257, DOI: 10.1016/j.cemconres.2006.10.008.

Sofi, M., van Deventer, J. S. J., Mendis, P. A., and Lukey, G. C. (2007b). “Bond performance of reinforcing bars in inorganic polymer concrete (IPC).” *Advances in Geopolymer Science & Technology*, Vol. 42, pp. 3107–3116, DOI: 10.1007/s10853-006-0534-5.

Tosun-Felekoğlu, K. (2012). “The effect of C3A content on sulfate durability of Portland limestone cement mortars.” *Construction and Building Materials*, Vol. 36, pp. 437–447, DOI: 10.1016/j.conbuildmat.2012.04.091.

van Deventer, J. S. J., Provis, J. L., and Duxson, P. (2012). “Technical and commercial progress in the adoption of geopolymer cement.” *Minerals Engineering*, Vol. 29, pp. 89–104, DOI: 10.1016/j.mineng.2011.09.009.

van Jaarsveld, J. G. S., van Deventer, J. S. J., and Lukey, G. C. (2002). "The effect of composition and temperature on the properties of fly ash-and kaolinite-based geopolymers." *Chemical Engineering Journal*, Vol. 89, pp. 63–73, DOI: 10.1016/S1385-8947(02)00025-6.

Vijai, K., Kumutha, R., and Vishnuram, B. G. (2010). "Influence of curing types on strength of: Geopolymer concrete." *Athena Information Solutions Pvt. Ltd. NBM & CW 2010*, Available from: http://www.nbmcw.com/articles/concrete/19630-influence-of-curing-types-on-strength-of-geopolymer-concrete.html.

Vijai, K., Kumutha, R., and Vishnuram, B. G. (2012). "Experimental investigations on mechanical properties of geopolymer concrete composites." *Asian Journal of Civil Engineering (Building and Housing)*, Vol. 13, No. 1, pp. 89–96.

Warner, R. F., Rangan, B. V., Hall, A. S., and Faulkes, K. A. (1998). "Concrete Structures." Melbourne, Addison Wesley Longman Australia Ltd.

Xu, H., and van Deventer, J. S. J. (2000). "The geopolymerisation of alumino-silicate minerals." *International Journal of Mineral Processing*, Vol. 59, No. 3, pp. 247–266, DOI: 10.1016/S0301-7516(99)00074-5.

Yildirim, H., Sümer, M., Akyüncü, V., and Gürbüz, E. (2011). "Comparison on efficiency factors of F and C types of fly ashes." *Construction & Building Materials*, Vol. 25, No. 6, pp. 2939–2947, DOI: 10.1016/j.conbuildmat.2010.12.009.

Yip, C. K., and van Deventer, J. S. J. (2003). "Microanalysis of calcium silicate hydrate gel formed within a geopolymeric binder." *Journal of Materials Science*, Vol. 38, No. 18, pp. 3851–3860, DOI: 10.1023/A:1025904905176.

Yost, J. R., Radlińska, A., Ernst, S., and Salera, M. (2013). "Structural behaviour of alkali activated fly ash concrete. Part 1: mixture design, material properties and sample fabrication." *Materials and Structures*, Vol. 45, pp. 435–447, DOI: 10.1617/s11527-012-9919-x.

Statement of Authorship

Title of Paper	Effect of Granulated Lead Smelter Slag on Strength of Fly Ash–based Geopolymer Concrete
Publication Details	Albitar, M., Mohamed Ali, M. S., Visintin, P., Drechsler, M. (2015). "Effect of granulated lead smelter slag on strength of fly ash–based geopolymer concrete." *Construction and Building Materials*, vol. 83, pp. 128–135, DOI: 10.1016/j.conbuildmat.2015.03.009.
Publication Status	Published

Principal Author

Name of Principal Author (Candidate)	Albitar, M		
Contribution to the Paper	Performed the experiment, interpreted and analysed data and wrote manuscript.		
Overall percentage (%)	85%		
Certification:	This paper reports on original research I conducted during the period of my Higher Degree by Research candidature and is not subject to any obligations or contractual agreements with a third party that would constrain its inclusion in this thesis. I am the primary author of this paper.		
Signature		Date	

Co-Author Contributions

By signing the Statement of Authorship, each author certifies that:

i. the candidate's stated contribution to the publication is accurate (as detailed above);
ii. permission is granted for the candidate in include the publication in the thesis; and
iii. the sum of all co-author contributions is equal to 100% less the candidate's stated contribution.

Name of Co-Author	Mohamed Ali, M.S.		
Contribution to the Paper	Supervised development of work, helped to evaluate and edit the manuscript.		
Signature		Date	20/10/2016

Name of Co-Author	Visintin, P.		
Contribution to the Paper	Supervised development of work, helped in data interpretation and manuscript evaluation and acted as corresponding author.		
Signature		Date	20/10/2016

Name of Co-Author	Drechsler, M.		
Contribution to the Paper	Assisted in manuscript evaluation.		
Signature		Date	21/10/16

Effect of Granulated Lead Smelter Slag on Strength of Fly Ash–Based Geopolymer Concrete

M. Albitar, M.S. Mohamed Ali, P. Visintin and M. Drechsler

ABSTRACT

Geopolymer concretes are manufactured from high–volume industrial waste materials in order to produce concrete that is low energy consuming, has a low carbon footprint, is sustainable and Portland cement–free. This paper presents an experimental study on the manufacture and behaviour of geopolymer concrete produced with a combination of granulated lead smelter slag (GLSS) and fly ash. The experimental program included 32 mix designs to investigate the influence of: fly ash replacement with slag as a binder, washed river sand replacement with slag as a filler, slag particle size to reactivity, alkaline activator–to–binder ratio, and curing period. It was found that incorporating 75% of slag as fly ash replacement and 100% of slag as fine aggregate produces concrete exhibiting compressive strength of 31 MPa. It was also found that significant improvements in the compressive strength of the hardened concrete (i.e., from 6 MPa to 65 MPa) could be obtained by super fine crushing the slag to a fineness similar to Portland cement and fly ash (<20μm). The results showed that the mechanical properties of the fly ash/slag–based geopolymer concrete were similar to that of fly ash–based geopolymer concrete, whilst the drying shrinkage of geopolymer concrete containing high volume of GLSS was lower than that of fly ash–based geopolymer concrete.

KEYWORDS: slag concrete, lead smelter slag, fly ash, geopolymer, particle size.

1. INTRODUCTION

Geopolymer concrete, also known as alkali–activated cement [1], inorganic polymer concrete [2], and geocement [3], has emerged as an innovative engineering material with the potential to form Ordinary Portland Cement (OPC) –free concrete for both structural and non–structural applications [4]. Geopolymer concretes are commonly formed by synthesising industrial aluminosilicate waste materials, such as metakaolin, fly ash and slags, with a highly alkaline activator solution. The use of industrial waste materials in the manufacture of concrete not only introduces economic and environmental benefits [5], but it also resolves issues associated with the disposal of large volumes of waste materials, such as ash from coal–fired power stations and slags from metal production operations, which may otherwise jeopardise the environment [6]. There is therefore a compelling case to explore the use of geopolymer concretes manufactured from a range of waste materials as a sustainable alternative to traditional OPC concrete technologies.

The use of fly ash as the cementitious source in the manufacture of geopolymer concrete has been intensively investigated with regard to both the mechanism of geopolomorisation, as well as the mechanical properties of the resulting concrete. It has

been shown that in general Class–F fly ash is the most suitable binder for manufacturing geopolymer concrete as the resulting product exhibits superior mechanical properties [7-14] and durability under thermal loading and in the presence of aggressive chemicals [15-18].

In industrially advanced countries increasing stringency in greenhouse gas emission regulations have created a degree of uncertainty in the longevity and sustainability of fly ash resources as coal–fired thermal power plants are increasingly being replaced with greener energy production technologies. There is therefore a need to develop suitable alternatives to fly ash in order to further drive the commercialisation of geopolymer concrete technology. A potential alternative can be found in slags obtained from various mineral processing operations. As shown in Figure 1 and Table 2 these slags can have markedly different chemical compositions to typical Class–F fly ash [19] and as a result have been shown to improve the strength of geopolymer concretes manufactured using fly ash. For example, ground granulated blast furnace slag (GGBFS) was found to increase the compressive strength of Class–F fly ash–based geopolymer concrete due to the presence of calcium oxide (CaO). Yip and van Deventer [20] and Yip et al. [21] proved that it is possible to have geopolymeric aluminosilicate hydrate (A–S–H) gel and calcium silicate hydrate (C–S–H) gel forming simultaneously within a single binder. Copper slag was successfully integrated with OPC as cement clinkers, fine aggregate and coarse aggregate [22-25].

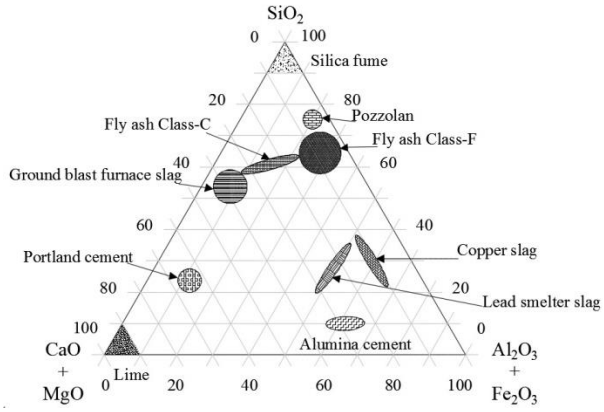

Figure 1. Illustration of chemical compositions in cementitious materials

While it has been shown that GGBFS is a viable cementitious material for the manufacture of geopolymer concrete, other forms of slags that are abundant have received less research attention. For instance, granulated lead smelter slag (GLSS), which is the focus of this paper, is an industrial waste material that is a by–product of heavy metal extraction during lead smelting process. The production of lead world–wide was estimated to be 3.9 million tonnes in 2009 from both primary and secondary resources [26], and the production of each ton of metallic lead generates around 100-350 kg of slag that is known as granulated lead smelter slag [27]. Despite its abundance, the studies on the behaviour of GLSS have so far focused on their characterisation and stability [27-31], and only one study to date has investigated the mechanical behaviour of geopolymer concretes and was limited in

that only up to 10% maximum substitution of fly ash with GLSS was investigated [26]. Given the availability and potential suitability of GLSS for the use in structural and non–structural geopolymer concrete manufacture, it is of particular importance to understand the mechanical behaviour of GLSS–based geopolymer concrete.

1.1. Research Significance

Geopolymer concrete has been the focus of a significant recent research interest due to its ability to solve environmental issues surrounding the greenhouse gas emissions of OPC manufacture, as well as those associated with the dumping of industrial waste materials. With this research effort, geopolymer concrete has moved beyond a laboratory–based technology into the real world; for example, the building of Global Change Institute (GCI) in the University of Queensland was completely built out of geopolymer concrete using fly ash as a binder [32].

Alternatives to Class–F fly for use as a cementitious material in the manufacture of geopolymer concrete are required in order to further drive commercialisation and reduce costs, as well as to fill gaps in supply left by increased regulation around coal–fired power stations. Thus, the aim of this research is to find a supplementary or replacement binder for fly ash in the form of a previously untapped source of slags, namely granulated lead smelter slag (GLSS). This work is undertaken with the primary aim of identifying if GLSS can be used as a partial or full replacement for fly ash in the manufacture of structural grade geopolymer concretes.

The secondary aim of the research is to investigate the reactivity of the GLSS of various grain size distributions. This is done with the intent of identifying the minimum level of grinding required to achieve specific grades of concrete thereby minimising the greenhouse gas emissions associated with the energy intensive process of grinding. Finally, the potential of using GLSS as a filler is investigated to determine if it can be utilised in high volumes in the geopolymer concrete industry, thus reducing current stockpiles. Each of these aims represents the first investigations in the use of GLSS at high proportions, with previous studies reporting only on the use of GLSS as a replacement of up to 10% of the primary binder.

2. EXPERIMENTAL PROGRAM

A total of 32 mix designs were trialled to quantify the influence of granulated lead smelter slag (GLSS) on the compressive strength of fly ash geopolymer concrete. The mixes are based on the results of previous studies conducted at the University of Adelaide by Nguyen et al. [33] who investigated the particle size of ashes, including bottom ash, middle ash and fly ash, and Albitar et al. [7] who investigated the water–to–binder (w/b), superplasticiser–to–binder (sp/b) and activator–to–binder (a/b) ratios of fly ash–based geopolymer concrete. It should be noted that both of these studies used identical materials to the current study. The mix proportions of the current study are presented in Table 1.

Table 1. Mixture proportions

Materials	Mixture proportions (kg/m^3)
Binder	424.8
Coarse aggregate	1180.8
Fine aggregate	595.2
*NaOH with Na_2SiO_3	156.7
Superplasticiser	31.2
Water	9.84
*Except for mixes 17 and 19, which had 212.4 kg/m^3 of NaOH with Na_2SiO_3, and mixes 18 and 20, which had 318.4 kg/m^3 of NaOH with Na_2SiO_3.	

To investigate the influence of fly ash replacement with GLSS as a binder, five different fly ash–to–GLSS ratios were investigated (0, 0.25, 0.5, 0.75, and 1). To investigate the influence of washed river sand (WRS) replacement with GLSS as fine aggregate, four different WRS–to–GLSS ratios were considered, namely 0, 0.5, 0.75, and 1. To investigate the influence of GLSS particle size, four different fractions of unground GLSS were examined, including 550 μm, sub 400 μm, sub 250 μm, and sub 150 μm, additionally seven different grading of ground GLSS, these gradings were identified based on their D_{50}, that is the grain size of which 50% material passes namely 70 μm, 63 μm, 43 μm, 20 μm, 11 μm, 8.2 μm, and 5.8 μm. Finally, in order to examine the degree of reactivity of the GLSS, three different alkaline–to–binder (a/b) ratios were investigated (0.37, 0.5, and 0.75). The mechanical properties of the optimised GLSS mix design were experimentally obtained and subsequently compared to those of fly ash–based geopolymer concrete.

2.1. Material Specifications

The basis of the mixes used in this study was low–calcium Class–F according to ASTM C618-08 [19] fly ash produced at Port Augusta Power Station in South Australia and granulated lead smelter slag (GLSS), locally called ‘black sand’, from the Nystar lead zinc smelter in Port Pirie. The chemical compositions of the fly ash and GLSS were determined by X–ray fluorescence (XRF) and are documented in Table 2. Also shown in Table 2 are typical compositions of different cementitious materials of which have previously been used in the manufacture of geopolymer concrete. It can be seen that the chemical composition of GLSS used in the current study is similar to that used by de Andrade Lima et al. [27] who investigated the durability and stability of lead smelter slags. Moreover, it can also be seen that the GLSS contains larger amount of Fe_2O_3 and CaO, and substantial lower amount of SiO_2 and Al_2O_3 than fly ash, which can be expected to reduce the geopolymeric aluminosilicate hydrate (A–S–H) gel and instead provide calcium silicate hydrate (C–S–H) gel. It is also seen in Table 2 that the amount of CaO in GLSS is considerably lower than that in OPC and GGBFS and hence the production of C–S–H gel will not be as significant.

Table 2. Chemical compositions by mass (%)

Oxides	Fe_2O_3	SiO_2	Al_2O_3	CaO	MgO	SO_3
Granulated lead smelter slag (Current study)	33.8	27.5	7.4	19.4	2.1	-
Lead smelter slag (de Andrade Lima et al. [27])	28.1	21.4	3.6	23.1	5.44	-
Fly ash (Current study)	2.8	49.0	31.0	5.4	2.5	0.3
OPC (Chi and Huang [8])	2.9	21.0	5.4	63.5	2.5	2.0
GGBFS (Chi and Huang [8])	0.44	34.5	13.7	40.6	7.1	0.56

For all mixes, the alkaline solution phase consisted of a combination of sodium silicate (Na_2SiO_3) and 14 molar sodium hydroxide (NaOH), pre–mixed with a ratio of Na_2SiO_3-to-NaOH of 1.5. In order to study the relationship of GLSS reactivity with grain size, three different super–fine crushed trial products of GLSS were investigated. Each trial product is separated into two different size fractions in the classification process, designated fine (F) and oversize (OS). The final grading fraction designated (combined) is produced by combining the overall product of the super fine crushing process and consists of a material which is comprised of 60% fine and 40% oversize fractions. For direct comparison, Figure 2 shows the particle size grading of all cementitious products used in this study. The grain size of which 50% material passes (D_{50}) is written next to each classification for easy identification of the ground materials.

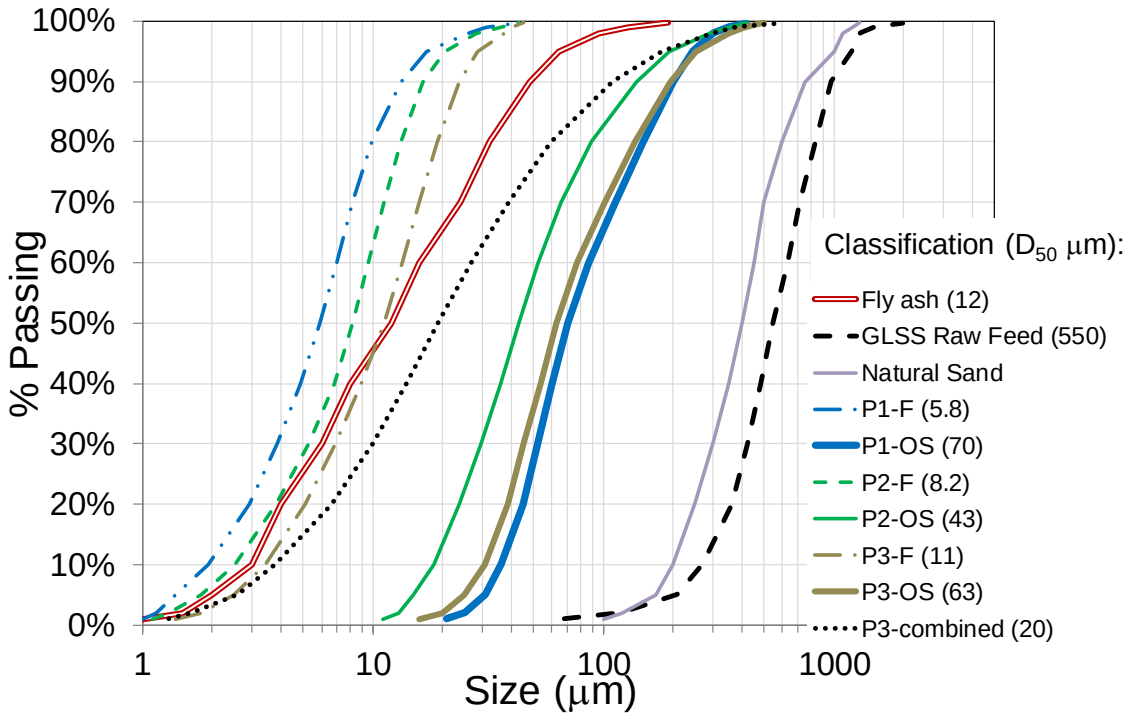

Figure 2. Grading of particle sizes

2.2. Testing Procedures

The experimental program consisted of the following two stages: (i) examining the behaviour of geopolymer concrete mixes utilising high–volumes of GLSS as either a binder or a filler and (ii) examining the engineering properties of the mixes considered to be optimal, that is those with compressive strengths and sufficient workability such that they are suitable for structural applications.

The mixing procedures of all stages was to first mix the dry components for three minutes, following this, the water, alkaline solution and superplasticiser, where applicable, were added.

In the first stage of the study, that is where the aim was to investigate the behaviour of mixes utilising high volumes of GLSS, all specimens were heat–cured at a temperature of 70^{o}C for 24 hours with the exception of mixes 12 and 21, which were cured for 48 hours to provide some indication of the influence of heat curing period. Heat curing was undertaken as it is well established that it accelerates the curing period such that the final strength can be obtained in a shorter period [34]. In this study, the heat curing period is based on previous work which identified that the final strength was obtained after a period of 7 days [11]. After the heat curing period, all specimens were placed in a fog room until the day of testing in order to ensure they were subjected to the same environmental conditions. In all tests, three replications were made for each mix.

In the second stage, the optimised mix design was manufactured at a larger scale to examine the engineering material properties, including: compressive strength, stress–strain relationships, splitting tensile strength, flexural strength and modulus of elasticity. In this stage both 24-hours heat curing and ambient curing were considered in order to investigate the influence of the curing regime on the mechanical properties. All specimens in this series of tests were tested at 28-day of age.

3. RESULTS AND DISCUSSION

Table 3 summarises the mix designs in terms of the parameter investigated. The mixes were designed to investigate (1) the influence of granulated lead smelter slag (GLSS), which includes (i) effect of GLSS as fine aggregate, (ii) effect of GLSS as a binder, and (iii) effect of GLSS particle size, (2) the influence of activator dosage, and (3) influence of curing period.

Table 3. Description of mixtures

Mix No	Binder			Fine aggregates		GYP	a:b	Heat-curing period (Hour)	Slump (mm)	Density (kg/m^3)	Strength at 7 days (MPa)
	FA Ratio	GLSS		WRS	GLSS						
		Ratio	D_{50} (μm)								
1	0.5	0.5	550	1	0	-	0.37	24	75	2355	37.2
2	0.5	0.5	400	1	0	-	0.37	24	27	2355	35.86
3	0.5	0.5	250	1	0	-	0.37	24	50	2355	36.06
4	0.5	0.5	150	1	0	-	0.37	24	50	2355	37.4
5	0.5	0.5	550	0	1	-	0.37	24	180	2360	51.94
6	0.5	0.5	400	0	1	-	0.37	24	130	2360	46.04
7	0.5	0.5	250	0	1	-	0.37	24	75	2360	50.06
8	0.5	0.5	150	0	1	-	0.37	24	100	2360	49.5
9	0.5	0.5	250	1	0	5%	0.37	24	0	2355	13.6
10	0.5	0.5	250	1	0	10%	0.37	24	0	2355	1.06
11	0.5	0.5	250	1	0	15%	0.37	24	0	2355	3.1
12	0.5	0.5	250	1	0	-	0.37	48	80	2355	36.4
13	1	0	-	1	0	-	0.37	24	155	2350	66.78
14	1	0	-	0.5	0.5	-	0.37	24	140	2355	63.8
15	1	0	-	0.25	0.75	-	0.37	24	200	2360	62.5
16	1	0	-	0	1	-	0.37	24	200*	2350	63.22
17	0.5	0.5	250	1	0	-	0.50	24	235	2355	28.91
18	0.5	0.5	250	1	0	-	0.75	24	270	2355	16.85
19	0.5	0.5	250	0	1	-	0.50	24	240	2370	40.8
20	0.5	0.5	250	0	1	-	0.75	24	275	2370	23.19
21	1	0	-	0	1	-	0.37	48	155*	2350	63.7
22	0.75	0.25	550	0	1	-	0.37	24	200	2360	62.41
23	0.5	0.5	550	0	1	-	0.37	24	200	2370	51.13
24	0.25	0.75	550	0	1	-	0.37	24	130	2400	31.52
25	0	1	550	0	1	-	0.37	24	0	2469	6.75
26	0	1	43	0	1	-	0.37	24	0	2548	11.9
27	0	1	63	0	1	-	0.37	24	0	2552	13.4
28	0	1	70	0	1	-	0.37	24	0	2548	16.4
29	0	1	20	0	1	-	0.37	24	0	2646	48.1
30	0	1	8.2	0	1	-	0.37	24	0	2702	52.4
31	0	1	11	0	1	-	0.37	24	0	2701	60.1
32	0	1	5.8	0	1	-	0.37	24	0	2643	64.9

FA = fly ash, GLSS = granulated lead smelter slag, WRS = washed river sand, a/b = alkaline-to-binder ratio, GYP = gypsum, D_{50}= grainsize of which 50% material passes.

* Although the mixes were identically manufactured, the slump values were different due to the difference in the ambient conditions on the day of casting [35].

3.1. Influence of granulated lead smelter slag

In order to study the influence of granulated lead smelter slag (GLSS) on the behaviour of fly ash–based geopolymer concrete, the GLSS was substituted as fine aggregate, binder or both fine aggregate and binder.

3.1.1. Effect of granulated lead smelter slag as fine aggregate

The particle size of the GLSS is similar to that of WRS, and both are relatively coarse compared to the particle size of fly ash as shown in Figure 2. Thus, GLSS is not expected to show high reactivity as a primary binder material; however, there is a potential for the GLSS to be used as fine aggregate replacement. The usage of GLSS in this way has the environmental benefit of utilising large volumes of GLSS without the need for further processing. Additionally, if used in sufficient quantities it could contribute to the polymerisation reaction by acting as a secondary binder and thus allow for a reduction in the quantity of fly ash required.

In order to investigate the influence of GLSS as fine aggregate replacement, it was used as a total replacement for WRS in a mix utilising only fly ash as the cementitious material. The results of this investigation, which are shown in Figure 3(a) and in which mixes 13 and 16 are compared, indicate that the replacement of WRS with GLSS has little to no effect on the compressive strength. This result occurs as the condensation polymerisation reaction occurs preferentially within fly ash due to its particle size.

In the second part of the investigation, the fly ash content was halved, whilst maintaining the same volume of activator solution to identify the potential for using unground GLSS as both a filler and a partial binder replacement. This was identified as a goal of the research as while it is known that grinding will increases the reactivity of the GLSS, it reduces the green credentials of the concrete due to the energy consumption required to grind the slag. A comparison of mixes 3 and 7 in Figure 3(b) shows that the utilisation of GLSS as fine aggregate results in a significant improvement in the compressive strength when the fly ash acting as a binder is reduced by 50%. This indicates that the GLSS also contributes to the polymerisation reaction and can act partially as a binder. That is, given a sufficient quantity the polymerisation reaction will occur with the GLSS and thus the strength is enhanced (as seen in mixes 5 to 8), this supplementary reaction will however only take place when an absence of sufficient fly ash to consume all the activator solution as seen in mixes 13 to 16. Therefore, GLSS may act as a supplementary binder when there is insufficient fly ash to complete polymerisation reaction, or alternatively, as a filler when the polymerisation reaction occurs entirely within the fly ash, which is the preferential reaction site due to the finer grain size

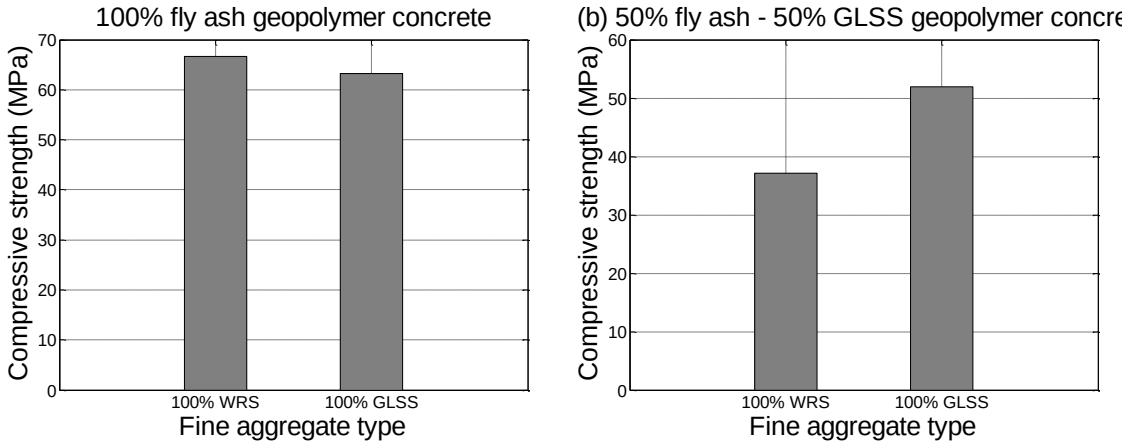

(a) (b)

Figure 3. Effect of GLSS as fine aggregate on compressive strength of: (a) 100% fly ash geopolymer concrete (b) 50% fly ash geopolymer concrete

3.1.2. Effect of granulated lead smelter slag as a binder

It was demonstrated above that the utilisation of GLSS as fine aggregate can partially compensate for a reduction of fly ash binder content. Thus, in order to investigate how much fly ash binder can be replaced, the fly ash was progressively replaced with GLSS to have fly ash–to–GLSS ratios of 1, 0.75, 0.50, 0.25 and 0, with GLSS as fine aggregate in all mixes. Figure 4 shows the influence of fly ash replacement with GLSS as a binder (mixes 21-25). It is evident that the compressive strength decreases with a reduction in the fly ash content. This reduction occurs as the fly ash content affects the heterogeneous reaction that is involved in the geopolymerisation between solid aluminosilicate oxides and alkali silicate solutions. Nevertheless, GLSS improves the reactivity, especially when the volume of fly ash is reduced. This is due to the primary constituents of the GLSS, namely the Ca and Si, of which as shown in Table 2 the oxides account for 46.9% of the weight. The presence of calcium oxide (CaO) may result in forming calcium silicate hydrate (C-S-H) gel simultaneously with the geopolymeric aluminosilicate hydeate (A–S–H) [21]. However, the reaction contribution of GLSS is not optimum due to the particle size, which as seen in Figure 2 is relatively coarse compared to the particle size of fly ash. Moreover, it can be seen that a 25% reduction in fly ash content can occur with little change in compressive strength and in all cases GLSS improves the reactivity over that, which would occur if the fly ash content were replaced with an inert material. This observation is in agreement with the findings previously reported by Ogundiran et al. [26] who investigated the replacements of fly ash with GLSS up to 10%.

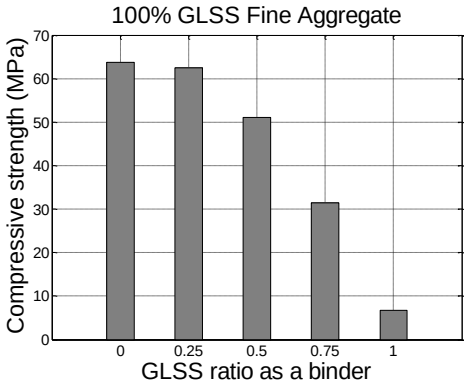

Figure 4. Influence of fly ash-to-GLSS ratio on compressive strength

As the significance of the research is to utilise high volume of GLSS while maintaining the compressive strength in the range of the normal concrete strength (>25 MPa), mixture 24 (25% FA and 75% GLSS) was chosen to be optimised.

3.1.3. Effect of granulated lead smelter slag particle size

Granulated lead smelter slag (GLSS) demonstrates different properties for different size fractions, as its reactivity generally increases with fineness [36-37]. In fact, the fineness of the binder has the most significant influence on the properties of the hardened concrete, even more so than the chemical and mineralogical composition of the binder [38-39]. Figure 4 shows the reduction in the compressive strength with increasing GLSS content, which is partly due to the coarseness of the GLSS and poor reactivity. Nguyen et al. [33] investigated the particle size of power station ashes from South Australia, including bottom ash, middle ash and fly ash and found that the compressive strength decreases with increasing the size of the particles as seen in Figure 5.

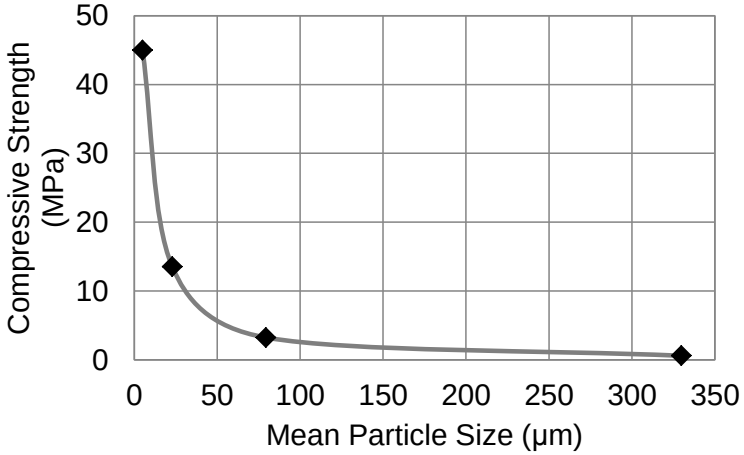

Figure 5. Compressive strength-particle size relationship of ash in geopolymer concrete [33]

The natural particles of GLSS are relatively large, angular and irregular, and for handling, health and environmental reasons, GLSS is produced as sand with particle sizes of less than 2 mm. To allow comparisons in reactivity of the GLSS particle size, different fractions of GLSS were examined, that is the fractions retained on the 550 μm, 400 μm, 250 μm and 150 μm sieves and these were used as 50% substitution for fly ash (mixes 1-4 and mixes 5-8). The results showed that those size fractions did not have any significant influence on the final compressive strength. This can be attributed to the significantly different particle size of fly ash compared to GLSS, as slag particle of 150 μm grading is still coarse compared to that of fly ash (D_{50} of 12 μm) and hence the polymerisation reaction occurs preferentially with the fly ash.

To determine the influence of particle size of GLSS, different super fine crushed fractions of the slag were tested (mixes 25-32). It was found that the fineness of the binder has a significant effect on the reactivity of GLSS in geopolymer concrete, as can be seen in Figure 6. These results clearly demonstrate the effectiveness of super fine crushing the GLSS to grain sizes equal to or even finer than that of fly ash (D_{50} of 12 μm). These results can be attributed to the significant increase in the surface area with reducing grain size, which consequently improves the reactivity of GLSS. Nevertheless, super fine crushing GLSS does require additional processing and energy, thus the potential use of the oversize fraction was studied using a combination of fine GLSS and over size GLSS (mix 29). The combined fraction (D_{50} of 20 μm) achieved a compressive strength of 48 MPa, suggesting that the fine fraction is providing most of the binder reactivity. The relationship between strength and various grain sizes (D_5, D_{20}, D_{50} and D_{80}) is plotted in Figure 7 and can be used as a tool for optimising the grinding requirement to achieve a specific strength target.

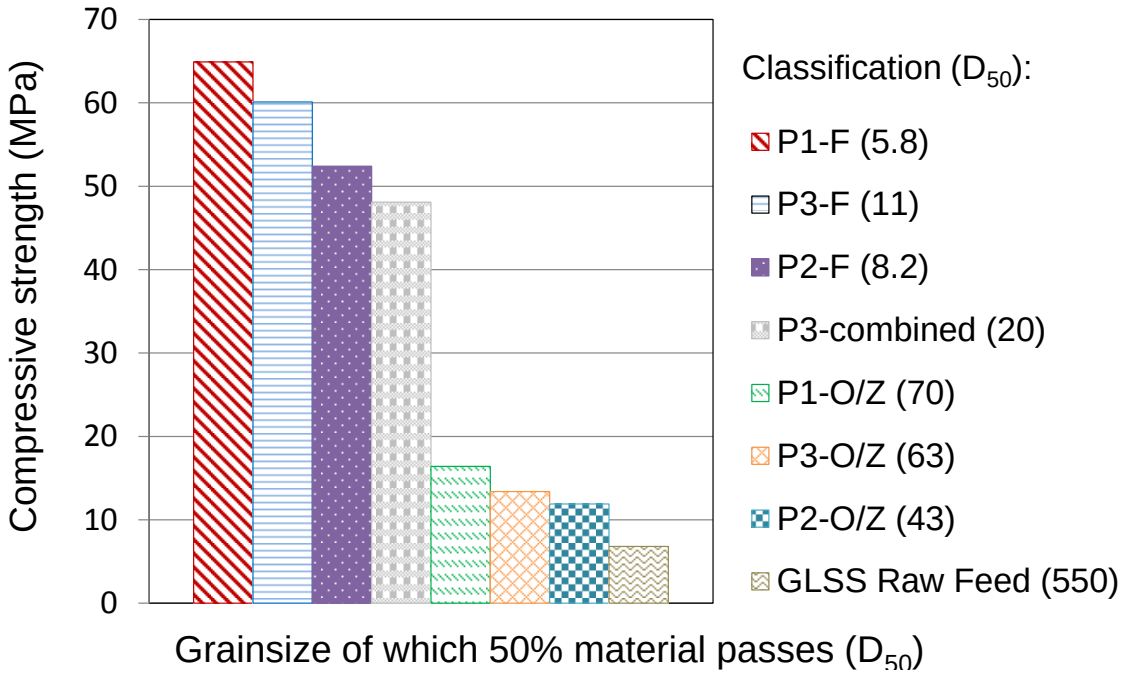

Figure 6. Influence of grainsize on strength of 100% GLSS geopolymer concrete

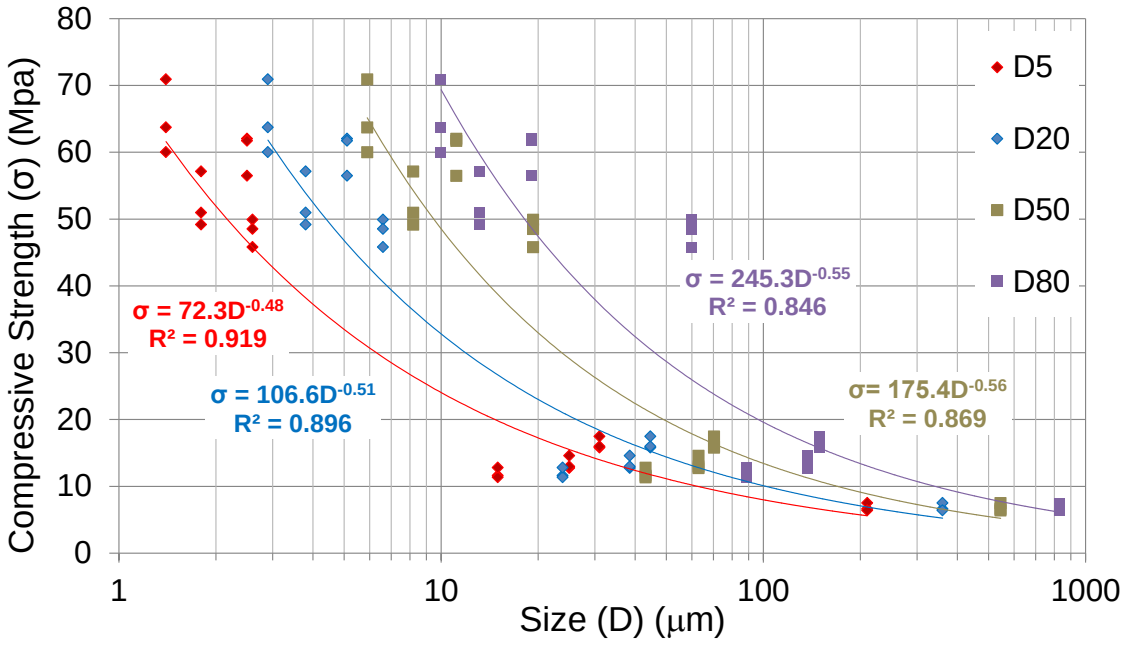

Figure 7. Strength versus grain size relationship of 100% GLSS geopolymer concrete

3.2. Influence of activator dosage

The activator dosage has a strong relationship with the formation of the aluminosilicate binder because the aluminium and silicon particles soluble in highly alkaline solutions and thus allow the polycondensation reaction to occur. For low activator–to–binder (a/b) ratios (i.e., less than 0.2), the polymerisation reaction is low; hence, there is less leaching of silica and alumina from the binder material. In contrast, at high a/b ratio (i.e., higher than 0.45), the mixture becomes very viscous, which hinders the leaching of the silica and alumina, resulting in a lesser degree of polymerisation reaction as compared to that of an optimal a/b ratio of 0.3-0.4 [40].

In the present study, three different activator–to–binder ratios were used for the activation of slag geopolymer concrete, including 0.37, 0.5 and 0.75. These ratios were chosen to examine whether the reactivity of GLSS improves with an increase of the activator dosage using 50% fly ash and 50% GLSS geopolymer concrete mixes with two different fine aggregates, washed river sand (mixes 3, 17, 18) and GLSS (mixes 7, 19, 20). It can be seen in Figure 8 that the compressive strength declined with the increase of the activator to binder ratio. It can also be seen that the behaviour of the mixes that contain GLSS as fine aggregate attained higher compressive strength, which reflects the increase reactivity of the GLSS compared to the washed river sand.

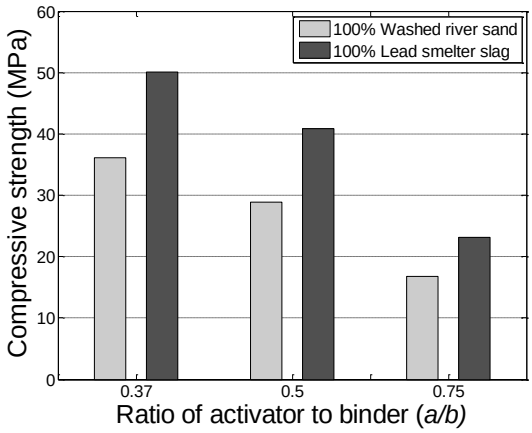

Figure 8. Influence of activator to binder (a/b) ratio in GLSS geopolymer concrete.

3.3. Influence of curing period

In order to examine the influence of curing period, mix 3 and mix 12 were identically designed, prepared and tested, but they were cured at 70^{o}C for different periods, 24 and 48 hours, respectively. As evident from the obtained results shown in Table 3, an increase in heat curing period more than 24 hours showed no further strength development.

3.4. Mechanical properties of optimised mix design

Knowledge of the in–service behaviour and strength of geopolymer concrete is fundamental to structural design, and the structural designer needs to know the modulus of elasticity in compression and tensile capacity of the geopolymer concrete and the expected shrinkage of the concrete. For OPC, these properties are typically defined empirically as a function of compressive strength in a national design standard ACI [41]. Therefore, tests to determine the full–compression stress-strain relationships, the elastic modulus, the flexural strength, the indirect tensile strength and the drying shrinkage of slag geopolymer concrete have been undertaken on both ambient– and heat–cured specimens tested after 28-day of casting. All the specimens were manufactured from mix 24, which utilises 75% of GLSS as the fly ash binder replacement. The results were then compared to that of 100% fly ash geopolymer concrete.

The full stress–strain relationships for both heat and ambient cured specimens are shown in Figure 9, together with Hognestad's [42] and Collins et al.'s [43] models. It is evident that the expressions of Hognestad [42] and Collins et al. [43] provide reasonable accuracy for slag geopolymer concrete stress–strain relationships.

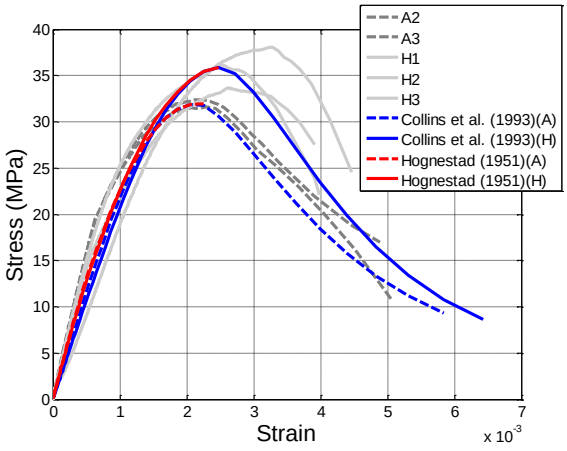

Figure 9. Stress–strain relationships

The weight of three cylinders per mix was measured in order to calculate the density (ρ) of a particular mix. The density, along with the respective compressive (f_c) of each particular mix is presented in Table 3. It can be noted that the density of fly ash geopolymer concrete is marginally lower than the equivalent OPC concretes, ranging between 2350-2355 kg/m^3. It can also be noticed that the density slightly increased with the addition of raw feed GLSS and significantly increased to 2700 kg/m^3 when utilising super fine crushed GLSS. This is probably as a result of the high iron content of the GLSS, as well as a lower porosity of the geopolymer concrete when using super fine crushed GLSS.

Table 4 presents the splitting tensile, flexural strength and elastic modulus of flyash–slag–based geopolymer concrete (mix 24), as well as fly ash–based geopolymer concrete (mix 21) results of ambient– and heat–cured specimens. The table also presents the results of predictive models of ACI [41] and Albitar et al. [7] which was derived from a database of all available tests on geopolymer concretes manufactured from Class–F fly ash. The splitting tensile and flexural proposed models of Albitar et al. [7] are presented in Equations 1 and 2, respectively. It can be observed that the mechanical properties of fly ash–slag–based geopolymer concrete are similar to those of fly ash–based geopolymer concrete.

Proposed model of Albitar et al. [7] for splitting tensile strength.

$$f'_{ct} = 0.6\sqrt{f'_c} \quad \text{(MPa)} \qquad (1)$$

Proposed model of Albitar et al. [7] for flexural strength.

$$f'_{cf} = 0.75\sqrt{f'_c} \quad \text{(MPa)} \qquad (2)$$

Table 4. Mechanical properties of slag and fly ash geopolymer concretes

Mix No.	f'_c (MPa)	f'_{ct} (MPa)	f'_{cf} (MPa)	E_c (GPa)	American Concrete Institute (ACI [41])			Albitar et al. [7]'s Proposed Model	
					f'_{ct} (MPa)	f'_{cf} (MPa)	E_c (GPa)	f'_{ct} (MPa)	f'_{cf} (MPa)
24 - Ambient	31.7	4.1	4.0	30.7	3.0	3.5	25.6	3.4	4.2
24 - Heat	35.9	4.4	4.8	29.9	3.2	3.7	26.8	3.6	4.5
21 - Ambient	32.3	3.1	4.2	27.0	3.0	3.5	25.8	3.4	4.2
21 - Heat	63.4	4.8	6.3	30.1	4.2	4.9	33.3	4.7	5.9

f'_c= compressive strength, f'_{ct}= Splitting tensile strength, f'_{cf}= Flexural strength, E_c= elastic modulus

3.4.1. Drying shrinkage

The drying shrinkage of heat– and ambient–cured 100% fly ash–based geopolymer concrete (mix 21), and heat– and ambient–cured 25% fly ash–75% GLSS–based geopolymer concrete (mix 24) were measured in order to identify the influence of GLSS replacement as both a binder and a filler. Test specimens preparation and test procedures were carried out in accordance with Australian Standards AS1012.13 [44], where 3, 75x75x285 mm prisms are monitored for length change, in this case over a period of 91 days.

The results shown in Figure 10 indicate that geopolymer concrete containing high volume of GLSS has substantially lower shrinkage than that of fly ash–based geopolymer concrete. Furthermore, when GLSS is present, heat–cured specimens do not experience significantly different levels of drying shrinkage, whereas in the case where no GLSS is present there is a marked difference in the shrinkage. This behaviour in the slag–based mixes can be attributed to the particle shape and honeycomb surface texture of the slags in comparison to the smooth surface textured of the washed river sand, which allows the concrete to absorb a large amount of water which is released to the mortar during drying. That keeps the mortar in a moist condition, which will limit the drying shrinkage [45].

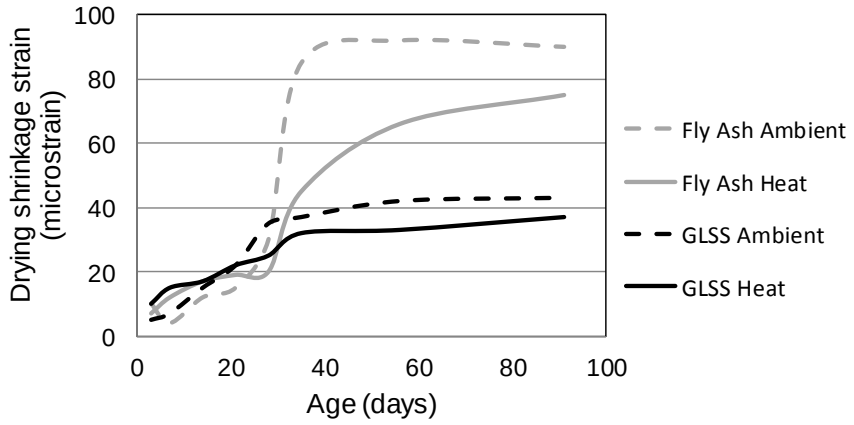

Figure 10. Drying shrinkage

4. CONCLUSIONS

This paper has presented the results of an experimental study that was undertaken to investigate the influence of granulated lead smelter slag (GLSS) on the compressive strength of fly ash–based geopolymer concrete. The investigation involved the influence of (i) GLSS as fine aggregate, (ii) GLSS as a binder, (iii) particle size of GLSS, and (iv) activator–to–binder (a/b) ratio. The study also investigated the mechanical properties of the optimised mix design. The results showed that utilising GLSS as fine aggregate improved the strength when the volume of fly ash was reduced, and had little to no effect on 100% fly ash geopolymer concrete. The compressive strength of fly ash geopolymer concretes decreased in proportion to increasing fly ash binder replacement with GLSS. Nevertheless, strengths in excess of 30 MPa were still obtained by replacing 75% of fly ash with GLSS. It was also shown that different fractions of GLSS between 550 μm and 150 μm did not have any significant influence on the compressive strength of geopolymer concrete. However, when the GLSS was super fine crushed to produce fractions with D_{50}'s less than 20 μm, the size fractions had a significant positive impact on the compressive strength and density of geopolymer concretes. Increasing the activator–to–binder ratio above 0.4 had a negative impact on the compressive strength of geopolymer concretes. Moreover, the mechanical properties of the optimised geopolymer concrete mix design, which contained 25% fly ash and 75% GLSS as a binder and 100% GLSS as fine aggregate, were found to be similar to that of 100% fly ash geopolymer concrete. Finally, the drying shrinkage of geopolymer concrete containing high volume of GLSS has substantially lower shrinkage than that of fly ash–based geopolymer concrete.

ACKNOWLEDGEMENTS

The authors wish to extend their gratitude to the South Australian Department of Further Education, Employment, Science and Technology through Catalyst Research Grant "Development of Geopolymer Concrete". The University of Adelaide research team would also like to acknowledge the following contributors: WorleyParsons Services Pty

Ltd, MSP Group, Nyrstar Port Pirie; IMP Technologies, Zero Waste SA and South Australian Department of Planning, Transport and Infrastructure (DPTI).

REFERENCES

[1] Duxson, P., Fernández-Jiménez, A., Provis, J. L., Lukey, G. C., Palomo, A., and van Deventer, J. (2007). "Geopolymer Technology: The Current State of The Art." *Journal of Materials Science*, vol. 42, pp. 2917–2933, DOI: 10.1007/s10853-006-0637-z.

[2] Sofi, M., van Deventer, J. S. J., Mendis, P. A., and Lukey, G. C. (2007). "Engineering properties of inorganic polymer concretes (IPCs)." *Cement and Concrete Research*, vol. 37, pp. 251–257, DOI: 10.1016/j.cemconres.2006.10.008.

[3] Aldred, J., and Day, J. (2012). "Is geopolymer concrete a suitable alternative to traditional concrete." *37th Conference on Our World in Concrete & Structures*, Australia, pp. 1-14.

[4] Komnitsas, K., and Zaharaki, D. (2007). "Geopolymerisation: A review and prospects for the minerals industry." *Minerals Engineering*, vol. 20, no. 14, pp. 1261–1277, DOI: 10.1016/j.mineng.2007.07.011.

[5] Barcelo, L., Kline, J., Walenta, G., and Gartner, E. (2014). "Cement and carbon emissions." *Journal of Materials and Structures*, vol. 47, pp. 1055–1065, DOI: 10.1617/s11527-013-0114-5.

[6] Gencel, O., Koksal, F., Ozel, C., and Brosow, W. (2012). "Combind effects of fly ash and waste ferrochromium on properties of concrete." *Construction and Building Materials*, vol. 29, pp. 633–640, DOI: 10.1016/j.conbuildmat.2011.11.026.

[7] Albitar, M., Visintin, P., Mohamed Ali, M. S., and Drechsler, M. (2014). "Assessing behaviour of fresh and hardened geopolymer concrete mixed with class-F fly ash." *Journal of Korean Society of Civil Engineering*, pp. 1–11, DOI: 10.1007/s12205-014-1254-z .

[8] Chi, M., and Huang, R. (2013). "Binding mechanism and properties of alkali-activated fly ash/slag mortars." *Construction and Building Materials*, vol. 40, pp.291–298, DOI: 10.1016/j.conbuildmat.2012.11.003.

[9] Yildirim, H., Sümer, M., Akyüncü, V., and Gürbüz, E. (2011). "Comparison on efficiency factors of F and C types of fly ashes." *Construction and Building Materials*, vol. 25, no. 6, pp. 2939–2947, DOI: 10.1016/j.conbuildmat.2010.12.009.

[10] Olivia, M., and Nikraz, H. (2011) "Properties of fly ash geopolymer concrete designed by Taguchi method." *Materials and Design*, pp. 1–27, DOI: 10.1016/j.matdes.2011.10.036.

[11] Raijiwala, D. B., and Patil, H. S. (2010). "Geopolymer concrete: a green concrete." *2nd International Conference on Chemical, Biological and Environmental Engineering*, pp. 202–206, DOI: 10.1109/ICBEE.2010.5649609.

[12] Bouzoubaâ, N., Zhang, M. H., and Malhotra, V. M. (2001). "Mechanical properties and durability of concrete made with high-volume fly ash blended

cements using a coarse fly ash." *Cement and Concrete Research*, vol. 31, no. 3, pp. 1393–1402.
[13] Palomo, A., Fernández-Jiménez, A., Kovalchuk, G., Ordoñez, L. M., and Naranjo, M. C. (2007). "OPC-fly ash cementitious systems: study of gel binders produced during alkaline hydration." *Material Science*, vol. 42, pp. 2958–2966, DOI: 10.1007/s10853-006-0585-7.
[14] Hardjito, D., and Rangan, B. V. (2005). "Development and properties of low-calcium fly ash-based geopolymer concrete." Research Report GC 1, Curtin University of Technology, Perth, Australia.
[15] van Deventer, J. S. J., Provis, J. L., and Duxson, P. (2012). "Technical and commercial progress in the adoption of geopolymer cement." *Minerals Engineering*, vol. 29, pp. 89–104, DOI: 10.1016/j.mineng.2011.09.009.
[16] Shi, C., Jiménez, A. F., and Palomo, A. (2011). "New cements for the 21st century: The pursuit of an alternative to Portland cement." *Cement and Concrete Research*, vol. 41, pp. 750–763, DOI: 10.1016/j.cemconres.2011.03.016.
[17] Bijen, J. (1995). "Benefits of slag and fly ash." *Construction and Building Materials*, vol. 10, no. 5, pp. 309–314, DOI: 10.1016/0950-0618(95)00014-3.
[18] Davidovits, J. (1991). "Geopolymers: inorganic polymeric new materials." *Journal of Thermal Analysis*, vol. 37, pp. 1633–1656, DOI: 10.1007/BF01912193.
[19] ASTM C618-08 (2008). "Standard Specification for Coal Fly Ash and Raw or Calcined Natural Pozzolan for Use in Concrete," Philadelphia: American Society for Testing and Materials, DOI: 10.1520/C0618-08.
[20] Yip, C. K., and van Deventer, J. S. J. (2003). "Microanalysis of calcium silicate hydrate gel formed within a geopolymeric binder." *Journal of Materials Science*, vol. 38, no. 18, pp. 3851–3860, DOI: 10.1023/A:1025904905176.
[21] Yip, C. K., Lukey, G. C., and van Deventer, J. S. J. (2005). "The coexistence of geopolymeric gel and calcium silicate hydrate at the early stage of alkaline activation." *Cement and Concrete Research*, vol. 35, pp. 1688–1697, DOI: 10.1016/j.cemconres.2004.10.042.
[22] Najimi, M., Sobhani, J., and Pourkhorshidi, A. R. (2011). "Durability of copper slag contained concrete exposed to sulfate attack." *Construction and Building Materials*, vol. 25, pp. 1895–1905, DOI: 10.1016/j.conbuildmat.2010.11.067.
[23] Al-Jabri, K. S., Taha, R. A., Al-Hashmi, A., and Al-Harthy, A. S. (2006). "Effect of copper slag and cement by-pass dust addition on mechanical properties of concrete." *Construction and Building Materials*, vol. 20, pp. 322–331, DOI: 10.1016/j.conbuildmat.2005.01.020.
[24] Alp, İ., Deveci, H., and Süngün, H. (2008). "Utilization of flotation wastes of copper slag as raw materialin cement production." *Journal of Hazardous Materials*, vol. 159, pp. 390–395, DOI: 10.1016/j.jhazmat.2008.02.056.
[25] Ariño, A. M., and Mobasher, B. (1999). "Effect of ground copper slag on strength and toughness of cementitious mixes." *American Concrete Institute Material Journal*, vol. 96, no. 1, pp. 68–75, DOI: 10.14359/430.
[26] Ogundirana, M. B., Nugterena, H. W., and Witkampb, G. J. (2013). "Immobilisation of lead smelting slag within spent aluminate-fly ash based

geopolymers." *Journal of Hazardous Materials*, vol. 248–249, pp. 29-36, DOI: 10.1016/j.jhazmat.2012.12.040.
[27] de Andrade Limaa, L. R. P., and Bernardezb, L. A. (2011). "Characterization of the lead smelter slag in Santo Amaro, Bahia, Brazil." *Journal of Hazardous Materials*, vol. 189, pp. 692–699, DOI: 10.1016/j.jhazmat.2011.02.091.
[28] Ettler, V., Legendre, O., Bodénan, F., and Touray, J. C. (2001). "Primary phases and natural weathering of old lead–zinc pyrometallurgical slag from Pribram." *The Canadian Mineralogist*, vol. 39, no. 3, pp. 873–888, DOI: 10.2113/gscanmin.39.3.873.
[29] Ettler, V., Mihaljevič, M., Touray, J. C., and Piantone, P. (2002). "Leaching of polished sections: an integrated approach for studying the liberation of heavy metals from lead–zinc metallurgical slags." *Bulletin de la Société Géologique de France*, vol. 173, no. 2, pp. 161–169, DOI: 10.2113/173.2.161.
[30] Ettler, V., Komárková, M., Jehlička, J., Coufal, P., Hradil, D., Machovič, V., and Delorme, F. (2004). "Leaching of lead metallurgical slag in citric solutions—implications for disposal and weathering in soil environments." *Chemosphere*, vol. 57, pp. 567–577, DOI: 10.1016/j.chemosphere.2004.07.022.
[31] Lewis, A. E., and Hugo, A. (2000). "Characterization and batch testing of a secondary lead slag." *Journal of the South African Institute of Mining and Metallurgy*, vol. 100, pp. 365–370.
[32] Mc Gar, J. (2013). "World first structural use of cement-free panels." <http://sourceable.net/world-first-structural-use-of-cement-free-panels/#>
[33] Nguyen, P., Pho, H., Ratanatray, M., and Yeh, H. (2012). "Full bottom ash replacement for geopolymer concrete in civil & structural applications." The University of Adelaide, Adelaide, Australia.
[34] Kupaei, R. H., Alenaram, U. J., Bin Jumaat, M. Z., and Nikraz, H. (2013). "Mix design for fly ash based oil palm shell geopolymer lightweight concrete." *Construction and Building Materials*, vol. 43, pp. 490–496, DOI: 10.1016/j.conbuildmat.2013.02.071.
[35] Neville, A. M. (2000). Properties of concrete, Prentice Hall, London.
[36] Monzó, J., Payá, J., and Peris-Mora, E. (1994). "A preliminary study of fly ash granulometric influence on mortar strength." *Cement and Concrete Research*, vol. 24, no. 4, pp. 791–796.
[37] Erdoğdu, K., and Türker, P. (1998). "Effect of fly ash particle size on strength of Portland cement fly ash mortars." *Cement and Concrete Research*, vol. 28, no. 9, pp. 1217–1222.
[38] Shi, C., Krivenko, P. V., and Roy, D. (2006). "Alkali-activated cements and concretes." USA.
[39] Slanička, Š. (1991). "The influence of fly ash fineness on the strength of concrete." *Cement and Concrete Research*, vol. 21, pp. 285–296.
[40] Sathonsaowaphak, A., Chindaprasirt, P., and Pimraksa, K. (2009). "Workability and strength of lignite bottom ash geopolymer mortar." *Journal of Hazardous Materials*, vol. 168, pp. 44–50, DOI: 10.1016/j.jhazmat.2009.01.120.
[41] ACI Committee 318 (2008). "Building code requirements for structural concrete (ACI 318-08) and commentary." American Concrete Institute, Farmington Hills, MI, ISBN: 978-0-87031-264-9, ISBN: 9780870317446 .

[42] Hognestad, E. N. (1951). “A study of combined bending and axial load in reinforced concrete members.” University of Illinois at Urbana-Champaign, vol. 49, no. 22, USA, DOI: 5308743.
[43] Collins, M. P., Mitchell, D., and MacGregor, G. J. (1993). “Structural design considerations for high strength concrete.” *ACI Concrete International*, vol. 15, no. 5, pp. 27–34, ISSN: 0162-4075.
[44] AS 1012.13 (1992). “Method 13: Determination of the drying shrinkage of concrete for samples prepared in the field or in the laboratory,” Australian Standard: Methods of Testing Concrete.
[45] Bai, Y., Darcy, F., and Basheer, P. A. M. (2005). “Strength and drying shrinkage properties of concrete containing furnace bottom ash as fine aggregate.” *Construction and Building Materials*, vol. 19, no. 9, pp. 691–697, DOI: 10.1016/j.conbuildmat.2005.02.021.

CHAPTER 2: Durability Characteristics of Geopolymer Concrete

Background

Durability of concrete is one of the most important and desired characteristics that determines the life expectancy of the concrete. Having identified the mechanical properties of fly ash– and granulated lead smelter slag (GLSS)–based geopolymer concrete, it is important to investigate the ability of concretes to resist weathering action, chemical attack, and absorption rate before the investigation of structural performance. The optimised concrete mix designs developed in Chapter 1 are used to further study the durability performance of geopolymer concrete. Thereafter, the successful mix designs will be subjected to structural investigations.

The first manuscript of this chapter "Durability evaluation of geopolymer and conventional concretes" extensively examines the durability characteristics of fly ash, GLSS and OPC concretes. It studies the resistivity of the concretes against several chemical solutions, including sodium chloride, sodium sulphate, sodium sulphate with magnesium sulphate and sulphuric acid. In addition, it investigates other durability characteristics, such as water absorption rate, sorptivity and porosity before and after chemical attack in order to draw a meaningful comparison between the conditions of concretes after the chemical attack.

The second manuscript of this chapter "Bond slip models for uncorroded and corroded steel reinforcement in class–F fly ash geopolymer concrete" further investigates the durability of geopolymer concrete. It also investigates the influence of corrosion rate on the bond strength of fly ash–based geopolymer concrete. It is shown that the fly ash–based geopolymer concrete exhibits slightly higher bond strength than the conventional OPC concrete. This study will be the bridge that links the mechanical and durability work to the structural work. That is because the bond between reinforcement and concrete strongly influences the flexural behaviour and shear capacity.

List of Manuscripts

Albitar, M., Mohamed Ali, M. S. and Visintin, P. (2016). "Durability evaluation of geopolymer and conventional concretes." *Cement and Concrete Research,* submitted.

Albitar, M., Visintin, P., Mohamed Ali, M. S., Lavigne, O. and Gamboa, E. (2016). "Bond slip models for uncorroded and corroded steel reinforcement in class–F fly ash geopolymer concrete." *Journal of Materials in Civil Engineering*, DOI: 10.1061/(ASCE)MT.1943-5533.0001713.

Statement of Authorship

Title of Paper	Durability evaluation of geopolymer and conventional concretes
Publication Details	Albitar, M., Mohamed Ali, M. S. and Visintin, P. (2016). "Durability evaluation of geopolymer and conventional concretes." *Construction and Building Materials*, in press.
Publication Status	Accepted

Principal Author

Name of Principal Author (Candidate)	Albitar, M		
Contribution to the Paper	Performed the experiment, interpreted and analysed data and wrote manuscript and acted as corresponding author.		
Overall percentage (%)	85%		
Certification:	This paper reports on original research I conducted during the period of my Higher Degree by Research candidature and is not subject to any obligations or contractual agreements with a third party that would constrain its inclusion in this thesis. I am the primary author of this paper.		
Signature		Date	

Co-Author Contributions

By signing the Statement of Authorship, each author certifies that:

i. the candidate's stated contribution to the publication is accurate (as detailed above);
ii. permission is granted for the candidate in include the publication in the thesis; and
iii. the sum of all co-author contributions is equal to 100% less the candidate's stated contribution.

Name of Co-Author	Mohamed Ali, M.S.		
Contribution to the Paper	Supervised development of work, helped to evaluate and edit the manuscript		
Signature		Date	20/10/2016

Name of Co-Author	Visintin, P.		
Contribution to the Paper	Supervised development of work and assisted in manuscript evaluation.		
Signature		Date	20/10/2016

Name of Co-Author	Drechsler, M.		
Contribution to the Paper	Assisted in manuscript evaluation.		
Signature		Date	21/10/16

Durability evaluation of geopolymer and conventional concretes

M. Albitar, M.S. Mohamed Ali, P. Visintin and M. Drechsler

ABSTRACT

Durability of concrete strongly influences the service life of structural members. Durable concrete protects embedded reinforcing steel from corrosion and reduces the potential for concrete spalling under chemical attack. This paper evaluates the performance of geopolymer concretes manufactured using either class–F fly ash or blended fly ash and granulated lead smelter slag (GLSS). The performance of Ordinary Portland Cement (OPC) is also investigated as a reference for evaluating the durability characteristics of geopolymer concretes. All concrete specimens were continuously immersed up to nine months in four different chemical solutions: 5% sodium chloride, 5% sodium sulphate, 5% sodium sulphate + 5% magnesium sulphate, and 3% sulphuric acid. Throughout the exposure period, the change in mass, compressive strength, splitting tensile strength, flexural strength, water absorption, sorptivity and porosity were evaluated. The influence of wetting–drying and heating–cooling cycles on the mass loss and compressive strength was also investigated. The results revealed that the OPC concrete has lower water absorption and sorptivity than the geopolymer concrete. Furthermore, it is shown that sodium sulphate has the greatest impact on geopolymer concretes, while OPC concrete is more susceptible to sulphuric acid attack. The results showed that, in general, the durability performance of geopolymer concrete is superior to that of OPC concrete within the range of the considered exposure.

Keywords: Durability; fly ash; lead smelter slag; OPC concrete; geopolymer concrete.

1. INTRODUCTION

Ordinary Portland Cement (OPC) concrete has long been used in construction of civil infrastructure and its deterioration over time due to sulphate attack has been widely observed and documented [1–4]. Investigations have revealed that the degradation of OPC concrete takes place due to reactions between cement hydration products and sulphate–bearing solutions. That is when concrete is exposed to poorly mineralised or acidic water, the acid leaches into the concrete and reacts with the concrete chemical components in a phenomenon known as diffusion–reaction [5]. Degradation of concrete strength due to sulphate attack takes place when the calcium and hydroxide ions dissolve out of the matrix, causing an increase in porosity and permeability of the concrete surface [5]. The most susceptible products of cement hydration to sulphate attack are alumina–bearing phases and calcium hydroxide, as these two products produce calcium sulphoaluminate (ettringite) and gypsum when they react with sulphate [6]. The calcium hydroxide $Ca(OH)_2$ decomposes at a pH level below 12, whereas calcium sulphoaluminate decomposes at a pH level below 11 [7].

Geopolymer concrete is a novel material prepared using alkali–activated binders. Geopolymers have the potential to resolve major concerns surrounding the storage and disposal of wastes from mineral extraction and process industries by utilising these wastes as cementitious materials. Before geopolymer concretes can be widely adopted in commercial applications, a clear understanding of durability characteristics of these new type of binders is required. Several studies have investigated the mechanism of fly ash geopolymer concrete degradation due to corrosion [8], sulphate attack [9], and acid attack [10], but only one study to date has investigated the selective sulfidation of lead smelter slag [11].

Despite the vast number of investigations conducted on the traditional concrete when exposed to sulphate ions, the degradation mechanism is yet to be fully understood, particularly for blended cements. Ramyar and İnan [6] stated that when calcium hydroxide reacts with sulphate ions, both monosulphate and hydrogarnet convert to ettringite and the formation of ettringite then causes expansion. This mechanism was further explained based on diffusion–reaction–based phenomenon. In a sulphate-bearing environment, the sulphate ions will react with portlandite (calcium hydroxide and calcium aluminates hydrate) and form gypsum ($CaSO.\ 2H_2O$), which in turn will react with products resulting from the hydration of C_3A to form calcium sulphoaluminate (ettringite). Both gypsum and ettringite can be expansive and this expansion results in the development of internal stresses that can damage the concrete and lead to a reduction in strength [5, 12–14]. The chemical components of geopolymer concrete are different to that of OPC concrete in which geopolymers are formed from geopolymeric aluminosilicate hydrate (A–S–H) gel instead of calcium silicate hydrate (C–S–H) gel. Therefore, it is of particular importance to investigate the diffusion–reaction of geopolymer concrete. This paper investigates the durability characteristics of two different cementitious–based geopolymer, namely low calcium class–F fly ash and granulated lead smelter slag (GLSS), and compares their behaviour to the corresponding behaviour of similar OPC concrete.

Continuous immersion of test specimens does not necessarily represent service conditions. In service, concretes are usually subjected to environmental effects such as wetting–drying and heating–cooling, especially those near the coasts or those used in piping systems [15]. Marine environments are found to be very aggressive, since sea water consists mainly of sodium chlorides and sodium sulphates. In fact, heating–cooling cycles in combination with the presence of water and salts represent several degradation scenarios, such as freezing and thawing and chemical attack. In addition, heating–cooling and wetting–drying cycles are the prerequisite for several deterioration mechanisms, such as crystallisation pressure and thermal stresses. Therefore, it is essential to evaluate the mechanisms of deterioration in this case to be able to predict the behaviour of a concrete subjected to wet–dry and heat–cool conditions during its service life.

2. EXPERIMENTAL PROGRAM

The present experimental program aims to investigate the durability characteristics of fly ash and lead smelter slag–based geopolymer concretes exposed to chemical solutions and compare their behaviours to that of OPC concrete. The investigation involves two

different programmes of accelerating the degradation: (i) continuous immersion in highly concentrated solutions up to nine months and (ii) wetting–drying and heating–cooling cycles up to ten cycles in which each cycle consists of full immersion for six days in 5% sodium chloride (NaCl) with 5% sodium sulphate (Na_2SO_4) solution and one day in an oven at a temperature of 110^oC. The chemical solutions used in the continuous immersion method were: (i) 5% sodium chloride (NaCl), (ii) 5% sodium sulphate (Na_2SO_4), (iii) 5% sodium sulphate with 5% magnesium sulphate (Na_2SO_4 with $MgSO_4$) and (vi) 3% concentric (10N) sulphuric acid (H_2SO_4). The selection of sodium chloride and sodium sulphate was based on the dominance of chloride and sulphate–based environments, which have previously been shown to have significant detrimental impact on concrete [3]. Additionally, magnesium sulphate was considered because it is generally accompanied with sodium sulphate in most coastal regions. Finally, sulphuric acid with pH level of 0.8 was considered in order to simulate the end conditions of biogenic corrosion in waste water sewers. That is because in sewer systems, the corrosion of concrete is initiated by chemical reaction in which the acidophilic sulphur oxidising microorganisms (ASOM) oxidises the hydrogen sulphide (H_2S) to sulphuric acid by bacteria of the genus *Acidithiobacillus* [16,17].

Two different exposure regimes were considered to expedite the degradation process and to simulate field conditions: (i) continuous immersion, or (ii) wetting–drying and heating–cooling conditions. Prior to undergoing exposure to chemical attack, all specimens were ambient cured for a period of 90 days. This extended curing period was considered important in order to ensure the hydration and geopolymerisation reactions were complete to avoid further strength development during the course of investigation. The selection of a 90 day curing period was based on previous research findings [18,19].

Following the commencement of exposure to chemical attack, the resistance of the concretes to the chemicals attack was observed by measuring (i) weight loss, (ii) compressive strength loss, (iii) flexural strength loss and (iv) splitting tensile strength loss. In addition, other significant parameters were also measured, such as stress–strain relationship, water absorption, sorptivity and porosity of the concretes.

2.1. Materials specifications

Three different concrete types were investigated including: a class–F fly ash–based geopolymer, a blended class–F fly ash and granulated lead smelter slag (GLSS) geopolymer and an OPC concrete. The chemical compositions of the fly ash, GLSS and OPC were determined by X–ray fluorescence (XRF) technique and the results are documented in *Table 1*. Fly ash and GLSS geopolymer concretes were activated by an alkaline solution phase consisted of a combination of sodium silicate (Na_2SiO_3) and 14 molar sodium hydroxide (NaOH), pre–mixed with a ratio of Na_2SiO_3-to-NaOH of 1:1.5. All mixes consisted of crushed coarse aggregate with a nominal maximum size of 10mm. Washed river sand was used as a fine aggregate in both fly ash and OPC concretes, whereas raw GLSS was used as the fine aggregate in GLSS geopolymer concrete. Concrete mix proportions for all mixes are tabulated in *Table 2*.

Table 1. Chemical compositions by mass (%)

Oxides	Fe_2O_3	SiO_2	Al_2O_3	CaO	MgO	SO_3
Fly ash	2.8	49.0	31.0	5.4	2.5	0.3
Granulated lead smelter slag	33.8	27.5	7.4	19.4	2.1	-
Ordinary Portland cement	3.0	21.5	5.5	65.2	2.5	2.1

Table 2. Mixtures proportions, (kg/m^3)

Ingredients	Fly ash	GLSS	OPC
OPC	0	0	391.3
Fly ash	424.8	212.4	0
Aggregate (10 mm)	1176	1176	1076
Sand	576	0	717.3
Granulated lead smelter slag	0	788.4	0
Sodium hydroxide (14M)	63.36	63.36	0
Sodium silicate	95.04	95.04	0
Superplasticiser	48*	48**	0
Water	16.8	16.8	180

* ViscoCrete 10
** Sika ViscoCrete -5-500

2.2. Test Procedure

All the solutions were made by adding laboratory grade chemicals to distilled water. Solid chemicals, such as sodium chloride, sodium sulphate and magnesium sulphate were dissolved initially in hot distilled water and then were diluted with distilled water maintained at a room temperature (23 ± 2°C). All the solutions were replaced every two months to maintain their concentrations. A summary of the test measurement regimes for each chemical exposure is given in *Table 3.*

The cyclic immersion of specimens consisted of 10 cycles in which every cycle comprised of exposure to 5% NaCl with 5% Na_2SO_4 at room temperature for 6 days and 24 hours in the oven at 110°C. The solution was replaced with a fresh solution every two cycles (i.e., 14 days). The change in weight was measured at the end of each cycle, whereas the compressive strength measurements were performed every two cycles (i.e., 2, 4, 6, 8 and 10 weeks upon drying and cooling).

The other tests including determination of stress–strain relationship, water absorption, sorptivity and porosity were performed on all the immersed specimens at the end of the chemical exposure (i.e., after 9 months) along with control specimens that were ambient cured.

Table 3. Details of measurement intervals.

	Compressive strength			Splitting and flexural tensile strengths strength		
Solutions	No. of tests	Test interval (week)	Total period (month)	No. of tests	Test interval (week)	Total period (month)
Sodium chloride	2	18, 36	9	2	18, 36	9
Sodium sulphate	5	8, 16, 24, 32, 36	9	2	18, 36	9
Sodium sulphate with magnesium sulphate	5	8, 16, 24, 32, 36	9	2	18, 36	9
Sulphuric acid	9	1, 2, 4, 8, 12, 20, 24, 28, 36	9	2	18, 36	9

2.2.1. Weight loss

The change in weight for both dry and wet conditions was measured using 100mm diameter and 200mm height cylinders. In the dry condition, the specimens were left at room temperature to dry until a constant mass was attained and then weighed using an electronic scale (accuracy of ± 0.01 g) to obtain the initial dry weight ($w_{i,dry}$). In the wet condition, the specimens were immersed in fresh distilled water for seven days and then their weights were measured after cloth–dried to obtain the initial wet weight ($w_{i,wet}$). The specimens were then immersed into their designated solutions. At the time of testing, three specimens were removed from the solution, cloth–dried, weighed for their second wet weight ($w_{s,wet}$) and left at room temperature to dry until a constant mass was reached and then weighed again to obtain the second dry weight ($w_{s,dry}$).

2.2.2. Permeable porosity test

The effective permeable porosity of concrete was obtained based on the quantum of water absorption and apparent volume of permeable voids (AVPV) tests according to ASTM C 642–06 [20]. The test was conducted on cylindrical specimens (100mm diameter and 50mm height). The specimens were dried in an oven at a temperature of 110°C for 24 hours to ensure that a constant mass was achieved. The specimens were left at a room temperature (23 ± 2°C) to obtain their initial weight (w_i); they were then immersed in water for four days to measure their saturated weight (w_s). Water absorption was then quantified using *Eq. 1* to quantify the change in weight as a percentage of the initial weight.

$$Water\ absorption, \% = \left(\frac{w_s - w_i}{w_i}\right) \times 100 \quad \text{(Eq. 1)}$$

According to ASTM C 642–06 [20], the volume of permeable voids and the effective porosity can be determined through the measurement of the bulk density of a concrete

specimen before and after immersion in boiling water. Therefore, the saturated mass after boiling was determined by immersing the specimens in boiling water for 5 hours and left to cool by natural loss of heat for 15 hours so that the final temperature was 23°C. The change in mass of boiled specimens (w_b) as a percentage of initial oven–dried mass (w_i) was then calculated using *Eq. 2*.

$$Water\ absorption\ of\ boild\ specimen, \% = \left(\frac{w_b - w_i}{w_i}\right) \times 100 \quad \text{(Eq. 2)}$$

After immersion and boiling, the specimens were suspended by a wire to obtain the apparent mass in water (w_w). Using the value of w_w, the bulk density of dry specimens, bulk density of saturated specimens, bulk density of boiled specimens, apparent density and volume of permeable voids can then be calculated using *Eqs. 3-7*, respectively.

$$Bulk\ density, dry = [w_i/(w_b - w_w)].\rho = g_1 \quad \text{(Eq. 3)}$$

$$Bulk\ density, after\ immersion = [w_s/(w_b - w_w)].\rho \quad \text{(Eq. 4)}$$

$$Bulk\ density, after\ immersion\ and\ boiling = [w_b/(w_b - w_w)].\rho \quad \text{(Eq. 5)}$$

$$Apparent\ density = [w_i/(w_i - w_w)].\rho = g_2 \quad \text{(Eq. 6)}$$

$$Volume\ of\ permeable\ voids, \% = \left(\frac{g_2 - g_1}{g_2}\right) \times 100 \quad \text{(Eq. 7)}$$

where w_i is initial weight of oven–dried sample (g), w_s is weight of saturated specimens (g), w_b is weight of boiled sample (g), w_w is weight of specimens in water after boiling (g), g_1 is bulk density of the dry sample (Mg/m^3), g_2 is apparent density of the boiled sample (Mg/m^3) and ρ is density of water (= 1 Mg/m^3 = 1 g/cm^3).

2.2.3. Sorptivity

The sorptivity of concrete is one of the most important features that characterises the durability of concrete as it relates to the tendency of concrete to absorb and transmit water

and other liquids by capillarity action. Water sorptivity tests yield significant information about the condition of concrete such as the composition and physical characteristics of the cementitious component and the entrained air content.

This study not only compares the sorptivities of different cementitious materials, such as OPC, fly ash and GLSS, but it also compares the sorptivities of each concrete before and after the exposure to different chemical solutions to examine the conditions of the concretes after the exposure to the chemicals.

The sorptivity test was carried out in accordance with ASTM C 1585–04 [21]. Cylindrical specimens with dimensions of 100mm diameter and 50mm height were dried in the oven at a temperature of 50 °C for three days in which a constant mass was achieved. The specimens were then left at room temperature (i.e., 23 ± 2°C) for 24 hours to cool down. These specimens were then placed in polyethylene storage containers and left again at room temperature (i.e., 23 ± 2°C) for 15 days. A non–absorbent coating (i.e., electrical tape) was then applied on all peripheral surfaces to prevent any flow of the water to the specimens except from one side, which was the base. Thereafter, the specimens were drowned with water level 2-3 mm above the base of specimen. The quantity of water absorbed by the concrete in time period up to 8 days was measured by weighing the specimen. Surface water on the specimen was wiped off with a dampened tissue and each weighing operation was completed within 30 seconds. The cumulative water absorption, *I*, (per unit area of the inflow surface) increases as the square root of elapsed time, $t^{1/2}$, and hence can be related to the sorptivity (*S*), which can be calculated using *Eq. 8*.

$$S = \frac{I}{t^{1/2}} \quad \text{(Eq. 8)}$$

where *t* is the elapsed time in minutes, and *I* can be calculated as *Eq. 9*:

$$I = \frac{\Delta m_t}{a \times d} \quad \text{(Eq. 9)}$$

in which Δm_t is the change in specimen mass in grams at the time *t*, *a* is the exposed area of the specimens in mm^2, and *d* is the density of water in g/mm^3.

2.2.5. Compressive strength degradation

The compressive strength was determined in accordance with Australian Standards AS 1012.9 [22]. The cylinders were instrumented with two 30mm uniaxial electrical resistance strain gauges and two Linear Variable Displacement Transformers (LVDTs) to

record the stress–strain relationship. In conjunction with measuring the strength of the immersed cylinders, three ambient–cured cylinders (control specimens) were tested at each interval to measure the strength of concrete at the designated date for a meaningful comparison.

2.2.6. Splitting and flexural tensile strengths degradation

In order to measure the splitting and flexural tensile strengths, six (100mm diameter x 200mm height) cylinders and four (100 x 100 x 500 mm) prisms were tested at 18 and 36 weeks of the immersion. Ambient–cured cylinders and prisms (control specimens) were also tested simultaneously for comparisons. These tests were carried out in accordance with Australian Standards AS 1012.10 [23] for the splitting tensile strength and AS 1012.11 [24] for the flexural tensile strength.

3. RESULTS AND DISCUSSION

3.1. Appearance of exposed specimens

All specimens immersed in sodium chloride and sodium sulphate + magnesium sulphate solutions had no visual signs of deterioration, as can be seen in *Fig. 1*. *Fig. 2(a)* shows that OPC concrete specimens exposed to sodium sulphate had no visual signs of deterioration, while geopolymer concrete specimens developed a white layer of sodium carbonate on their surfaces after they were dried. The thickness of this layer increased gradually with time to a maximum thickness of 1mm for cylinders and 5mm for prisms as can be seen in *Fig. 2(b)*. It is worth noting that all the specimens were cloth–dried once they were taken out of their designated solutions, and the white layer developed after exposure to air. A similar result was observed in previous studies such as those reported by Singh et al. [25]. Moreover, Bakharev [9] noted that sodium hydroxide seeps out in a migration process from geopolymer specimens when exposed to solutions containing Na_2SO_4. Therefore, it can be said that the formation of this white layer is due to the reaction of leached sodium hydroxide with the atmospheric carbon dioxide (CO_2) and subsequently yielding a white layer of sodium carbonate (Na_2CO_3).

(a) Fly ash (b) GLSS (c) OPC

Figure 1. Specimens immersed in sodium sulphate with magnesium sulphate for nine months

(a) OPC, GLSS and fly ash cylinders (b) GLSS prism

Figure 2. Specimens immersed in sodium sulphate for nine months

Specimens immersed in sulphuric acid solutions deteriorated gradually with time to a degree where the coarse aggregates of the OPC concrete was apparently visible, as can be seen in *Fig. 3(a)*. *Figs. 3(b-e)* show the specimens after several periods of immersion in sulphuric acid solutions. It can be seen that GLSS specimens were covered with a yellow layer of sulphur, which started as a small patch (*Fig. 3(b-ii)*) and kept on increasing to cover the whole sample. This yellow layer can be attributed to the formation of sulphur dioxide (SO_2), which was yielded through the reaction of ferric oxide (Fe_2O_3) with H_2SO_4 and resulted in dissolving the ferric oxide to produce $Fe_2(SO_4)_3+H_2O$. The influence of H_2SO_4 on the appearance of fly ash concrete was minimal in comparison with that of specimens manufactured from OPC concrete, which experienced the most significant deterioration in sulphuric acid solutions due to the formation of calcium sulphate ($CaSO_4$).

(a) GLSS, fly ash and OPC prisms exposed to solphuric acid for 9 months

(i) Fly ash (ii) GLSS (iii) OPC

(b) Four weeks of immersion in sulphric acid

(i) Fly ash (ii) GLSS (iii) OPC

(c) Eight weeks of immersion in sulphric acid

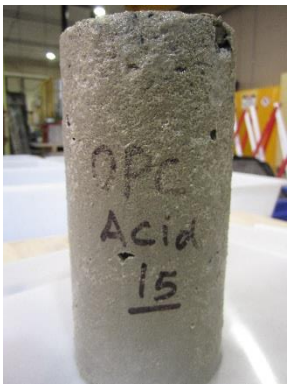

(i) Fly ash (ii) GLSS (iii) OPC

(d) Twenty-four weeks (six months) of immersion in sulphric acid

(i) Fly ash (ii) GLSS (iii) OPC

(e) Thirty-six weeks (nine months) of immersion in sulphric acid

Figure 3. Specimens immersed in sulphuric acid up to nine months

3.2. Porosity, sorptivity and water absorption

The results of density, water absorption and porosity determined through the apparent volume of permeable voids (AVPV) are summarised in *Table 4*, together with the critical mechanical properties that have an influence on absorption mechanisms such as compressive strength, elastic modulus and strain at peak stress.

Table 4. Test results of porosity, sorptivity and water absorption after nine months exposure to chemical attack

Concrete type	f_c (MPa)	E_c (MPa)	ε at peak σ	Density, ρ (kg/m^3)	Water absorption (%)	AVPV (%)
Fly ash control	49.51	30093.02	0.00217	2463.87	3.51	8.64
Fly ash sodium chloride	47.37	29542.34	0.00241	2268.38	2.28	5.98
Fly ash sodium sulphate	42.88	27119.94	0.00203	2250.04	3.72	9.14
Fly ash sodium sulphate + magnesium sulphate	46.95	30278.87	0.00184	2183.67	3.37	8.63
Fly ash sulphuric acid	44.12	34572.66	0.00170	2169.28	3.42	8.77
GLSS control	34.20	28880.28	0.00171	2412.11	3.17	9.95
GLSS sodium chloride	32.78	29707.30	0.00173	2435.80	2.69	9.35
GLSS sodium sulphate	30.01	28028.48	0.00197	2413.90	3.38	9.71
GLSS sodium sulphate + magnesium sulphate	32.91	28146.79	0.00158	2452.80	3.00	9.14
GLSS sulphuric acid	31.72	29977.94	0.00170	2311.48	3.22	10.08
OPC control	71.06	42900.28	0.00192	2344.40	2.44	5.85
OPC sodium chloride	67.25	39962.53	0.00246	2340.11	0.94	2.61
OPC sodium sulphate	60.12	41319.13	0.00204	2342.23	2.16	6.92
OPC sodium sulphate + magnesium sulphate	63.45	41675.87	0.00182	2333.48	2.14	6.79
OPC sulphuric acid	52.17	39698.47	0.00193	2326.58	2.93	9.31

The water absorption rates and sorptivities at early stages, which reveal the transport mechanism for water movement within concrete are shown in *Figs. 4* and *5* respectively. It is evident from *Fig. 4* that OPC concrete has a much lower water absorption rate than the corresponding fly ash and GLSS geopolymer concrete specimens. This is partially attributed to the difference in the compressive strength and mainly due to the capillary mechanism, which reveals that OPC concrete has a lower absorption rate than geopolymer concrete. The difference between the absorption rates of fly ash and GLSS geopolymer concretes is mainly due to the difference in the compressive strength because the absorption rate difference is only in the secondary absorption. The secondary absorption is usually controlled by the air voids, which in turn is controlled by the water–to–cement ratio that strongly influences the strength of concrete. In contrast, the initial absorption is controlled by the capillary forces.

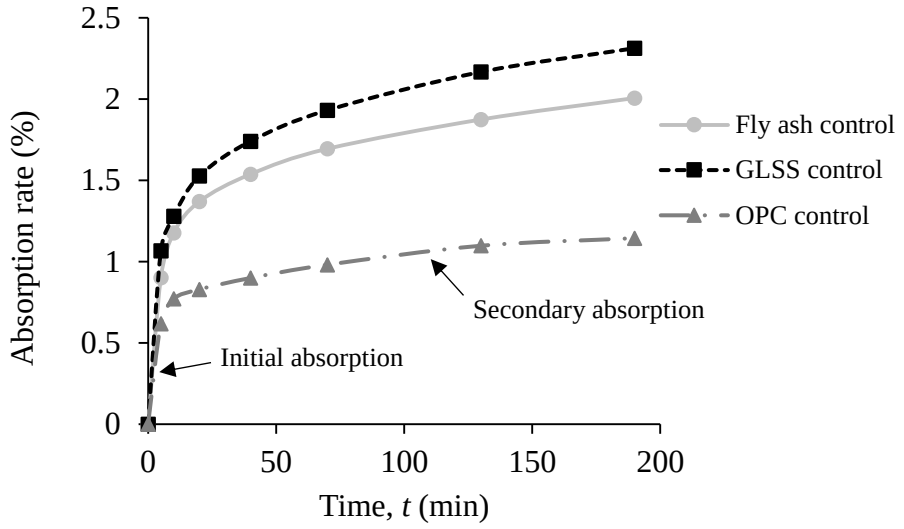

Figure 4. Water absorption of different concretes

Figs. S1(a-c), which are available in the supplementary data, show the effect of chemicals attack on the absorption rates of fly ash, GLSS and OPC concretes respectively. It can be observed that the exposure of all the concretes to sodium chloride resulted in a reduction of the water absorption. From *Fig. S1(a),* it can be seen that sodium sulphate had the greatest impact on the water absorption of fly ash geopolymer concrete, whereas the water absorption of OPC concrete was most susceptible to sulphuric acid, as can be seen in *Fig. S1(c).* The water absorption of GLSS geopolymer concrete was equally influenced by sodium sulphate and sulphuric acid (*Fig. S1(b)*).

It is evident from *Figs. 5(a and b)* that OPC concrete has the lowest cumulative water absorption and water sorptivity, followed by fly ash concrete and then GLSS concrete. These results indicate that the capillary forces of OPC concrete transport less water content than its fly ash and GLSS geopolymer concrete peers. This phenomenon reveals that OPC concrete is more durable and sustainable in regards to limiting the water access.

Figs. S2(a-f), which are available in the supplementary data, show the effect of chemicals attack on the cumulative water absorption and water sorptivity of different concretes. It can be observed that sodium sulphate has the greatest impact on fly ash and GLSS geopolymer concretes, whereas OPC concrete is more affected by sulphuric acid.

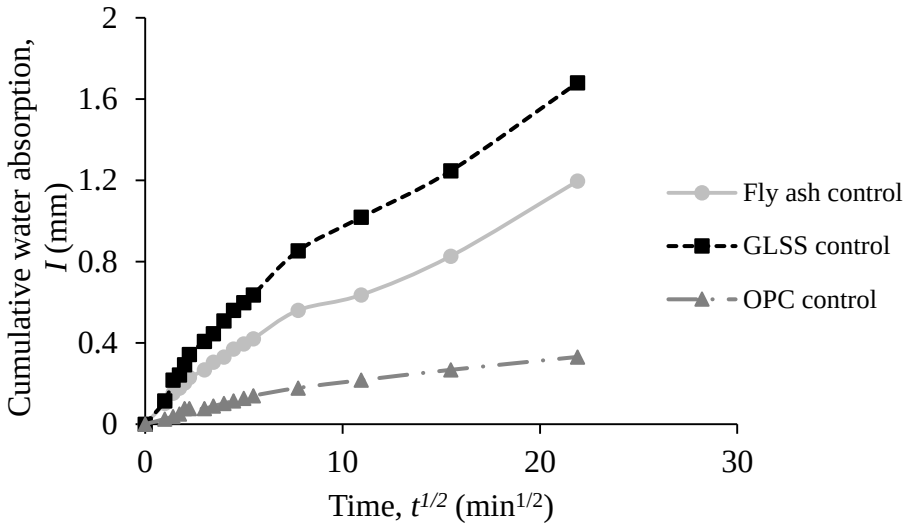

(a) Cumulative water absorption comparison among ambient cured fly ash, GLSS and OPC concretes

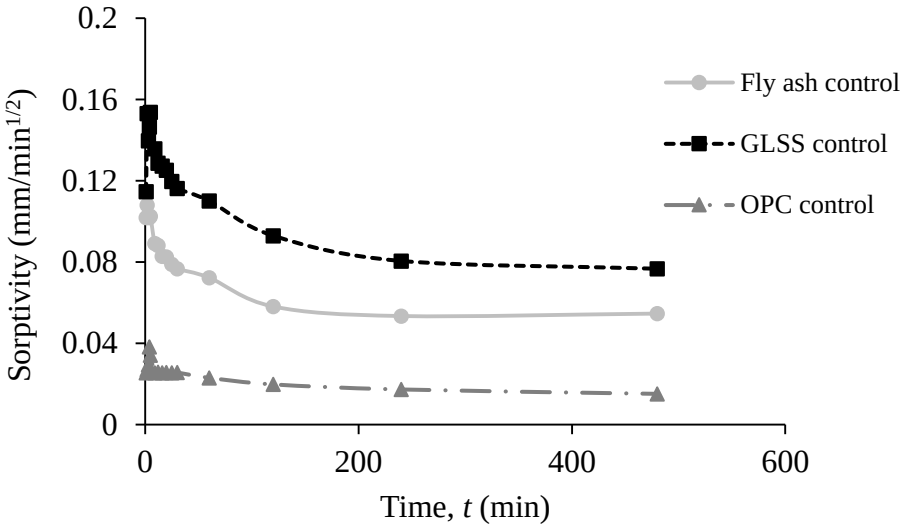

(b) Sorptivity comparison among ambient cured fly ash, GLSS and OPC concretes

Figure 5. Cumulative water absorption and water sorptivity of different concretes

3.3. Mass loss

The weight–change results of the concretes exposed to sodium chloride, sodium sulphate, sodium sulphate + magnesium sulphate and sulphuric acid solutions are illustrated in *Fig. 6*. It is evident from *Fig. 6* that the weight of the immersed specimens in the chemical solutions tends to increase and then decrease. The initial increase of the weight can be attributed to (i) the inclusion of the weight of the chemical particles that penetrated the concrete within the solution and resulted in an increase in the concrete weight, and (ii) the expansion of some elements in the concrete, which has a beneficial effect in terms of increasing the volume of the concrete. However, once the internal expansion causes the formation of internal micro–cracks, the expansion mechanism will have a detrimental impact. This phenomenon is known as reaction–diffusion, which occurs between the chemical solutions and the binder constituent of concrete. As a result of the reaction, the calcium hydroxide will be converted to calcium sulphate (gypsum), which results in increasing the volume of about 124% [16,17]. Subsequently, a more distractive reaction occurs between gypsum and tricalcium aluminates within the cement matrix, which results in forming calcium sulphoaluminate (ettringite). The ettringite possesses a larger volume and is susceptible to expansion by a factor of about two [26].

Figs. 6(a-c) show the influence of the chemicals on the mass loss of fly ash, GLSS and OPC concrete specimens respectively. It can be seen in *Fig. 6* that the influence of sodium chloride on the mass of fly ash, GLSS and OPC concrete was beneficial even after nine months of exposure, as the mass increased by 1.8%, 1.0% and 1.7% respectively. On the other hand, sodium sulphate, magnesium sulphate and sulphuric acid had a beneficial influence initially followed by a detrimental impact. *Fig. 6(a)* shows that fly ash specimens gained 1.6% after four months of sodium sulphate exposure, and it gained 2.1% after eight months of sodium sulphate + magnesium sulphate exposure. Thereafter, the increase in the weight dropped to 1.1% after nine months in the sodium sulphate solution and 1.9% in the sodium sulphate + magnesium sulphate solution. *Fig. 6(b)* shows that the weight change of GLSS concrete was the least influenced by chemical attack, as the increase and decrease in the weight were limited in which the weight increased by 1.1% after six months in the sodium sulphate solution and 1.8% after eight months in the sodium sulphate + magnesium sulphate solution. Thereafter, the increase dropped to 0.9% and 1.6% after nine months in the sodium sulphate and sodium sulphate + magnesium sulphate solutions respectively. OPC concrete specimens had the most significant changes in weight as can be seen in *Fig. 6(c)*, which shows that the weight increased by 1.8% after four months in the sodium sulphate solution and 1.8% after six months in the sodium sulphate + magnesium sulphate solution. Thereafter, the increase dropped to 0.7% and 1.0% after nine months in the sodium sulphate and sodium sulphate + magnesium sulphate solutions respectively. Therefore, it can be stated that both fly ash and GLSS concretes are more chemically stable than OPC concrete. This observation is in agreement with the results reported by de Andrade Lima et al. [27], which indicate that the chemical analysis of lead slag was relatively stable in a weak acidic environment.

The changes in the weight due to sulphuric acid exposure were the most pronounced in which the weight of all of the specimens started to decline after seven days of exposure. Specimens made of OPC concrete were the most susceptible, as after nine months of

exposure they lost 11.0% of their weight, while GLSS concrete had lost 9.6% and fly ash concrete lost 5.4%. Therefore, it is evident that geopolymer concretes have performed better than OPC concrete in an acidic environment.

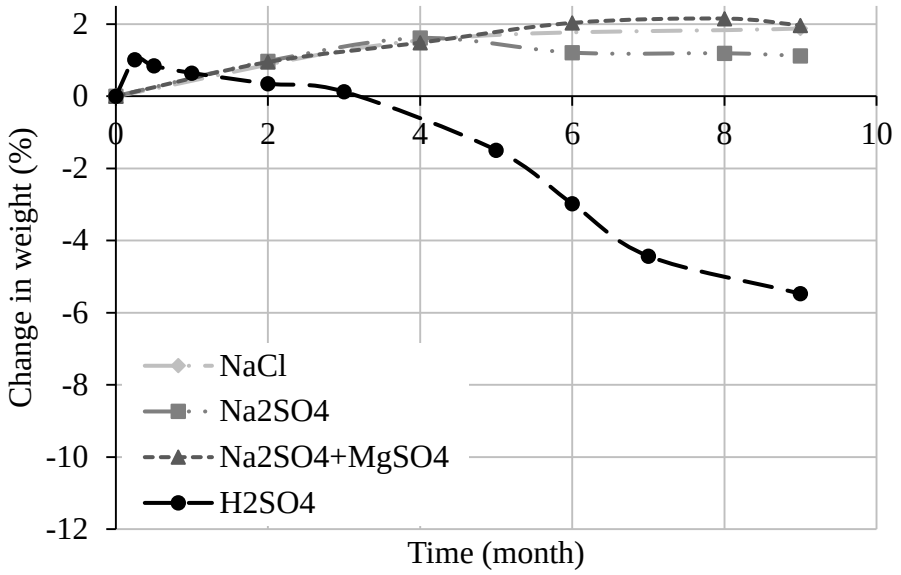

(a) Change in weight of fly ash

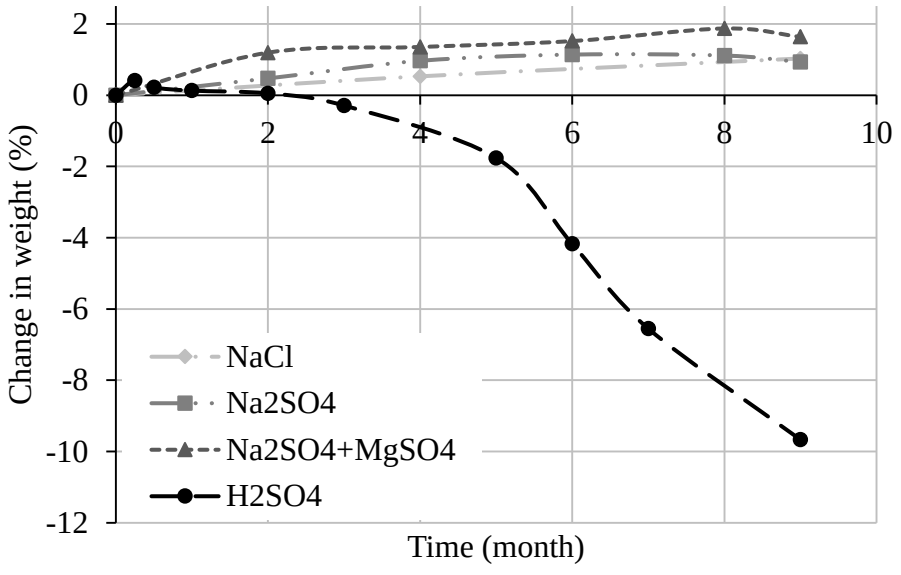

(b) Change in weight of GLSS

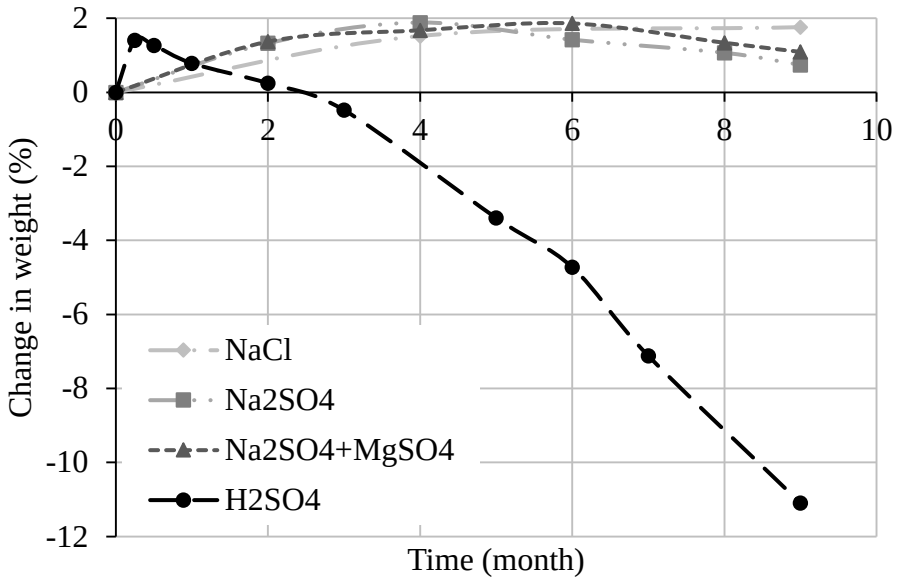

(c) Change in weight of OPC

Figure 6. Mass loss of different concretes exposed to different chemicals

3.4. Strength degradation

The strength degradation of the specimens exposed to different chemical solutions was evaluated through measuring compressive strength, splitting tensile strength and flexural tensile strength at regular intervals. It is worth noting that the strength degradation is shown in terms of the percentage of the equivalent ambient–cured specimens that were tested on the same day as the immersed specimens in the chemical solutions.

3.4.1. Compressive strength

The compressive strengths of fly ash, GLSS and OPC concretes at all the intervals are summarised in *Table 5*. *Figs. 7(a-c)* depict the change in the compressive strength of fly ash, GLSS and OPC concretes, respectively, as a percentage of their ambient–cured specimens peers. It is evident that all of the concretes exhibited an initial increase in the compressive strength, followed by either a drastic decrease or a trivial decrease. The initial increase is attributed to the hydration of calcium silicates and pozzolanic reactions, which result in an internal confinement due to the pressure that the expanded elements exert. The integrity of the concrete specimens is similar to that of a structural member in which the load travels through the particles to be transmitted to the base, where the load can be transferred finally [28]. In the case of normal ambient–cured specimens where voids are present, the specimens will fail once the weakest part can no longer transfer the load. In contrast, when specimens are immersed in a chemical solution that causes the internal components of the concrete such as calcium to expand, the integrity of the specimens will be enhanced. However, once the pressure produced by the expansion of the ettringite

formation exceeds the available voids and starts to cause internal cracks, the strength will decline.

It is evident from *Figs. 7(a)* and *(b)* that sodium sulphate had the greatest effect on the performance of fly ash and GLSS concretes after nine months of exposure. This is attributed to the leaching of the sodium hydroxide, which was caused by sodium sulphate (*Fig. 2*). Therefore, it can be inferred that the performance of fly ash geopolymer concrete in sodium sulphate environment can be significantly enhanced if it is activated by a different alkaline solution. *Fig.7(c)* shows that OPC concrete was most susceptible to sulphuric acid, with its strength being reduced by 26.6%. It can be observed from *Table 5* that the exposure to sodium sulphate + magnesium sulphate had lower impact on all of the concretes than sodium sulphate alone. This was mainly due to the high ionic strength of the solution, which led to less diffusion. This observation is in agreement with the results reported by Bakharev [9].

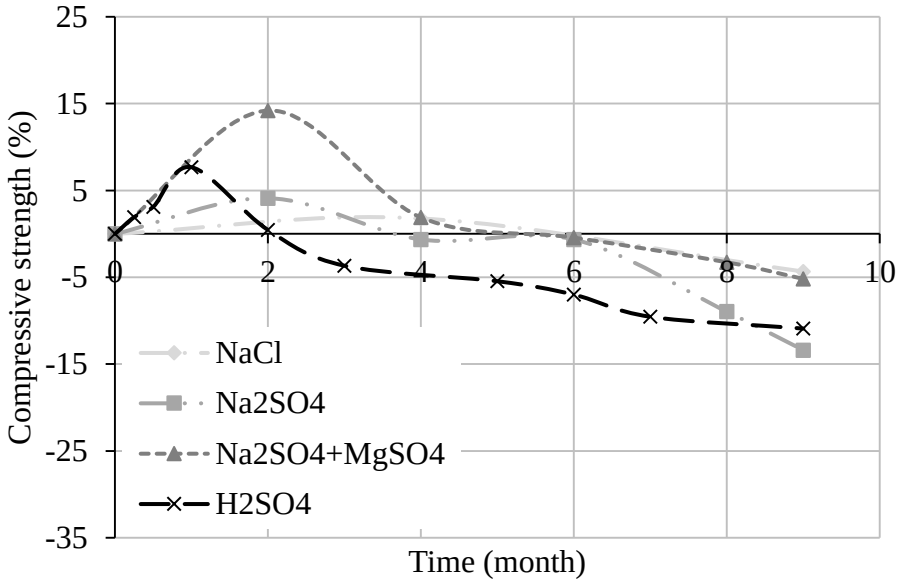

(a) Compressive strength degradation of fly ash

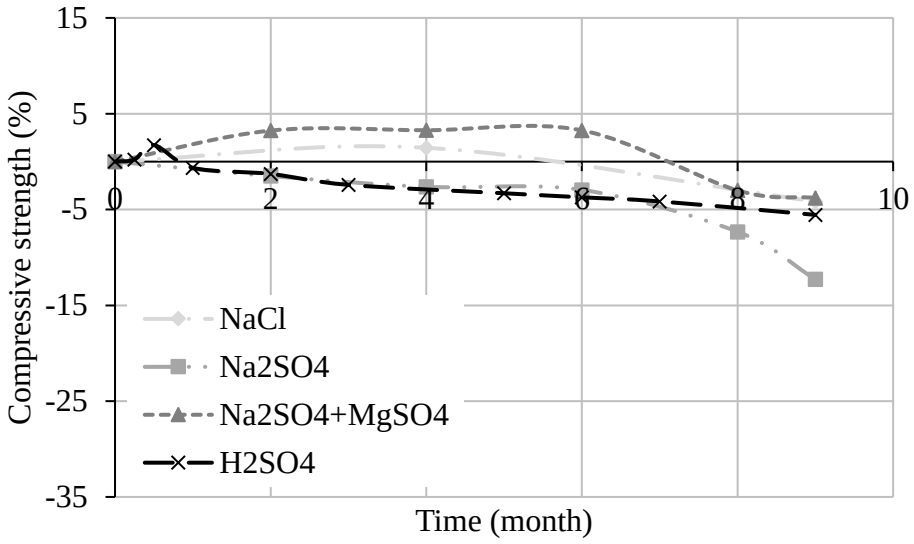

(b) Compressive strength degradation of GLSS

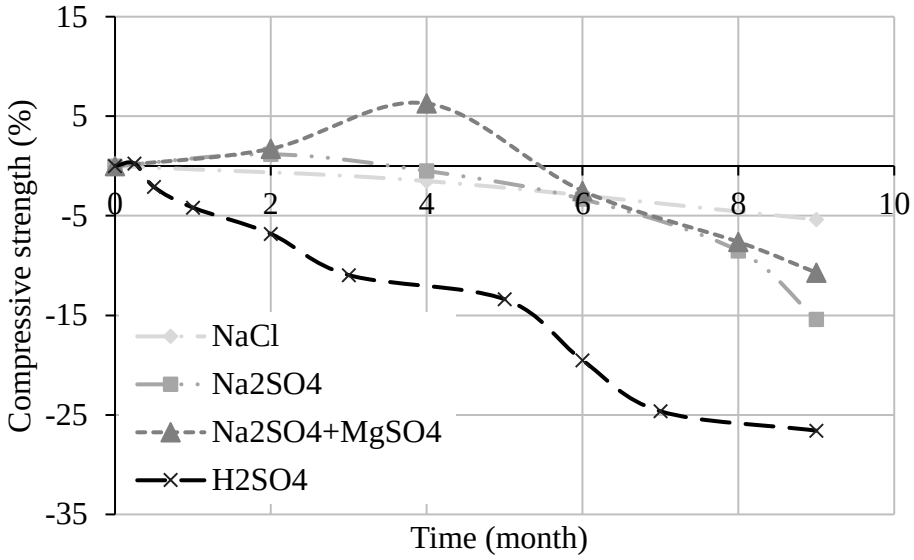

(c) Compressive strength degradation of OPC

Figure 7. Compressive strength degradation

It is worth mentioning the vast contrast between the compressive degradation of fly ash and OPC concretes due to sulphuric acid exposure. This significant deterioration in OPC concrete strength is attributed to the magnitude of $Ca(OH)_2$ and C_3A in hydrated concrete in which they are highly available in OPC concrete. The hydrated cement that contains high amount of calcium hydroxide produces gypsum ($CaSO_4.2H_2O$) when it is attacked by sulphuric acid (H_2SO_4), as shown in *Eq. 10*. Furthermore, calcium silicate hydrate (C–

S–H) gel that is exhibited in OPC concrete produces SiO_2 in an aqueous state in a sulphuric acid environment, as shown in *Eq. 11* [4].

$$Ca(OH)_2 + H_2SO_4 \rightarrow CaSO_4 . 2H_2O \quad \text{(Eq. 10)}$$

$$xCaO . SiO_2 + xH_2SO_4 + xH_2O \rightarrow xCaSO_4 . 2H_2O + SiO_2 . aq \quad \text{(Eq. 11)}$$

The full stress–strain relationship under axial compression of fly ash, GLSS and OPC concretes exposed to different chemical attack are shown in *Figs. 8 (a-c)* respectively. It is evident that in general the strain at peak stress increases after the exposure to chemical attack due to concrete softening. Nevertheless, all the specimens exhibited stress–strain relationship similar to the expression given by Popovics [29].

Table 5. Compressive strength degradation

Control – Ambient cured specimens						
Age (Month)	OPC	(%)	Fly ash	(%)	GLSS	(%)
0	62.85	-	40.97	-	29.53	-
2	62.85	-	40.97	-	29.53	-
4	65.70	-	46.32	-	31.2	-
6	68.12	-	47.02	-	32.79	-
8	70.63	-	48.70	-	33.20	-
9	71.06	-	49.51	-	34.20	-
Specimens immersed in 5% sodium chloride (NaCl) solution						
Age (Month)	OPC	(%)	Fly ash	(%)	GLSS	(%)
0	62.85	0	40.97	0	29.53	0
4	64.71	-1.51	47.14	1.77	31.70	1.44
9	67.25	-5.36	47.37	-4.33	32.78	-4.16
Specimens immersed in 5% sodium sulphate (Na_2SO_4) solution						
Age (Month)	OPC	(%)	Fly ash	(%)	GLSS	(%)
0	62.85	0	40.97	0	29.53	0
2	63.59	1.180	42.65	4.10	29.09	-1.50
4	65.38	-0.49	46.02	-0.64	30.43	-2.62
6	65.85	-3.32	46.72	-0.63	31.83	-2.94
8	64.6	-8.52	44.34	-8.95	30.78	-7.31
9	60.12	-15.40	42.88	-13.38	30.01	-12.27
Specimens immersed in 5% sodium sulphate + 5% magnesium sulphate ($Na_2SO_4 + MgSO_4$) solution						
Age (Month)	OPC	(%)	Fly ash	(%)	GLSS	(%)

0	62.85	0	40.97	0	29.53	0
2	63.94	1.73	46.79	14.20	30.49	3.23
4	69.83	6.28	47.20	1.89	32.27	3.27
6	66.42	-2.49	46.82	-0.43	33.86	3.26
8	65.24	-7.62	47.10	-3.27	32.21	-3.00
9	63.45	-10.70	46.95	-5.18	32.91	-3.78
Specimens immersed in 3% sulphuric acid (H_2SO_4) solution						
Age (Month)	OPC	(%)	Fly ash	(%)	GLSS	(%)
0	62.86	0.00	40.97	0.00	29.54	0.00
0.25	63.02	0.26	41.76	1.93	29.60	0.22
0.5	61.53	-2.10	42.25	3.13	30.05	1.73
1	60.23	-4.17	44.12	7.68	29.35	-0.64
2	58.57	-6.82	41.16	0.45	29.16	-1.29
3	58.51	-10.96	44.63	-3.67	30.49	-2.43
5	56.91	-13.39	43.80	-5.45	30.22	-3.30
6	54.83	-19.52	43.74	-7.00	31.58	-3.72
7	53.23	-24.64	44.05	-9.54	31.83	-4.15
9	52.17	-26.59	44.12	-10.90	31.72	-7.28

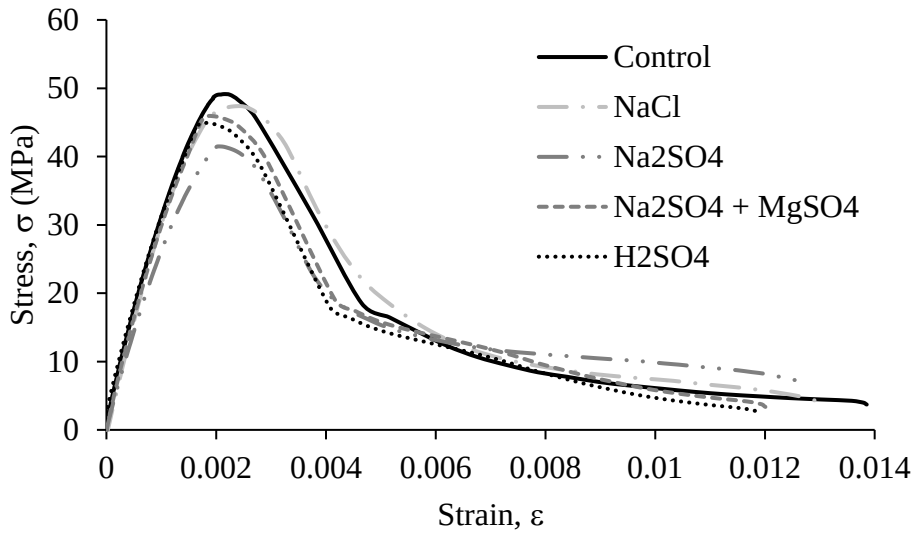

(a) Fly ash concrete

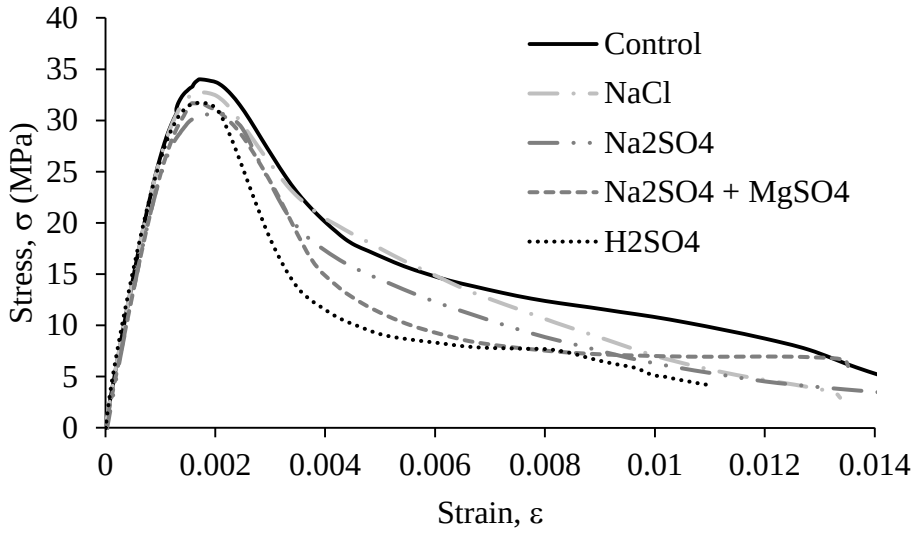

(b) GLSS concrete

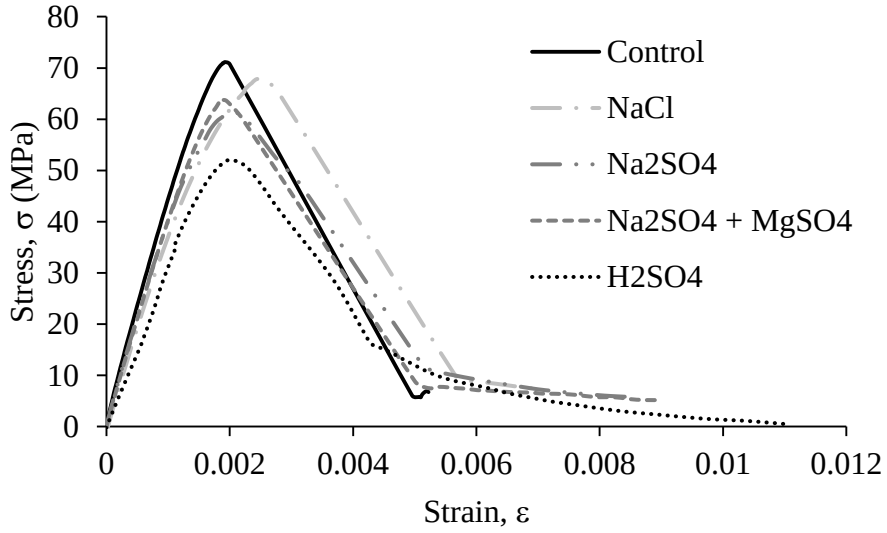

(c) OPC concrete

Figure 8. Stress–strain relationship

3.4.2. Splitting and flexural tensile strengths

The degradation of the splitting tensile strength of fly ash, GLSS and OPC is shown in *Figs. 9(a-c)* respectively, whereas *Figs. 10(a-c)* show the degradation of the flexural tensile strength of fly ash, GLSS and OPC respectively. It can be seen in *Figs. 9 and 10* that both the splitting and flexural tensile strengths of fly ash, GLSS and OPC concretes

were more sensitive towards sulphuric acid; they respectively lost 13.1%, 16.5% and 18.8% of their tensile strength and 25.3%, 30.8% and 43.5% of their flexural tensile strength after nine months of exposure. It is worth mentioning that fly ash concrete exhibited the least degradation, followed by GLSS concrete and then OPC concrete. Fly ash concrete also had the least amount of splitting and flexural tensile strength degradation in sodium sulphate, which was the second most influential solution as can be seen in *Table 6*.

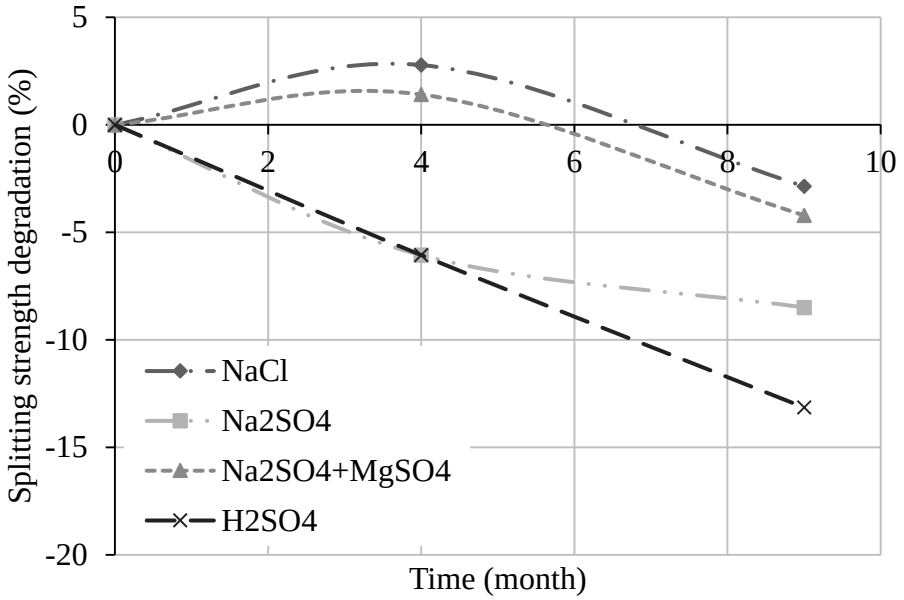

(a) Splitting tensile degradation of fly ash

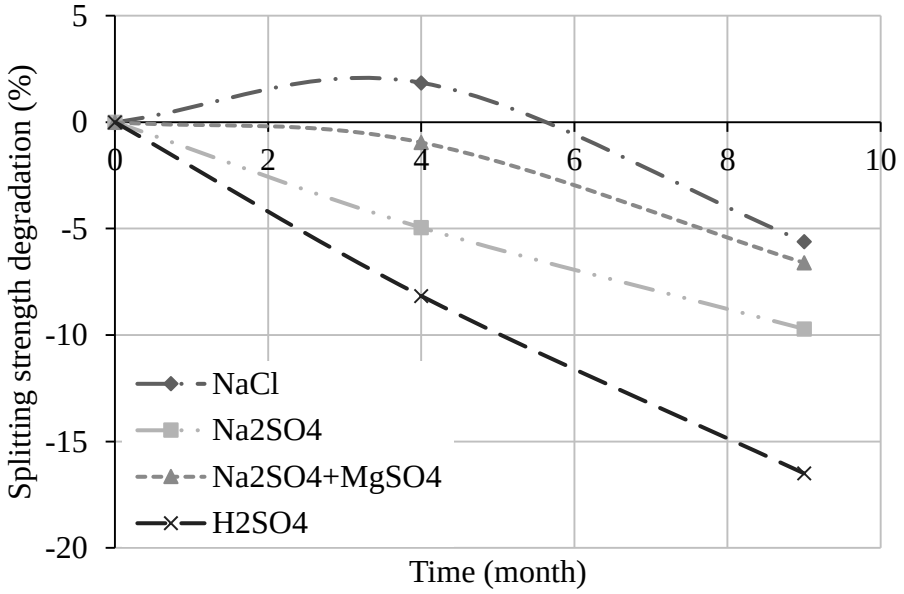

(b) Splitting tensile degradation of GLSS

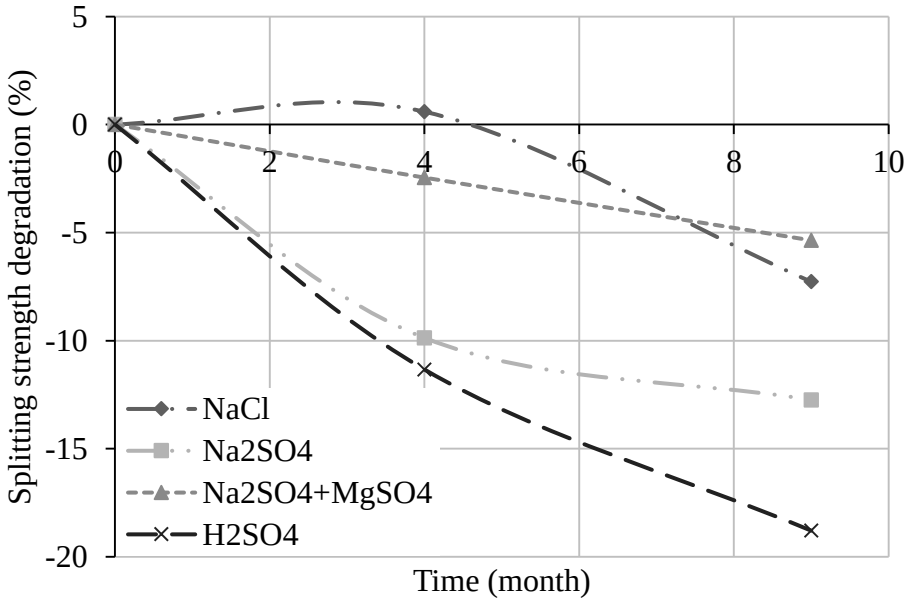

(c) Splitting tensile degradation of OPC

Figure 9. Splitting tensile strength degradation

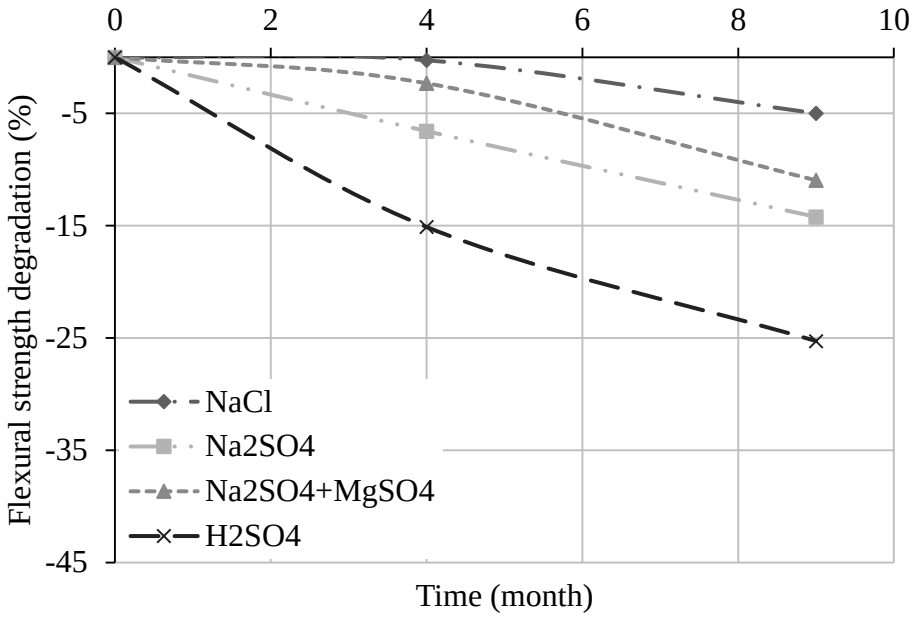

(a) Flexural tensile strength degradation of fly ash

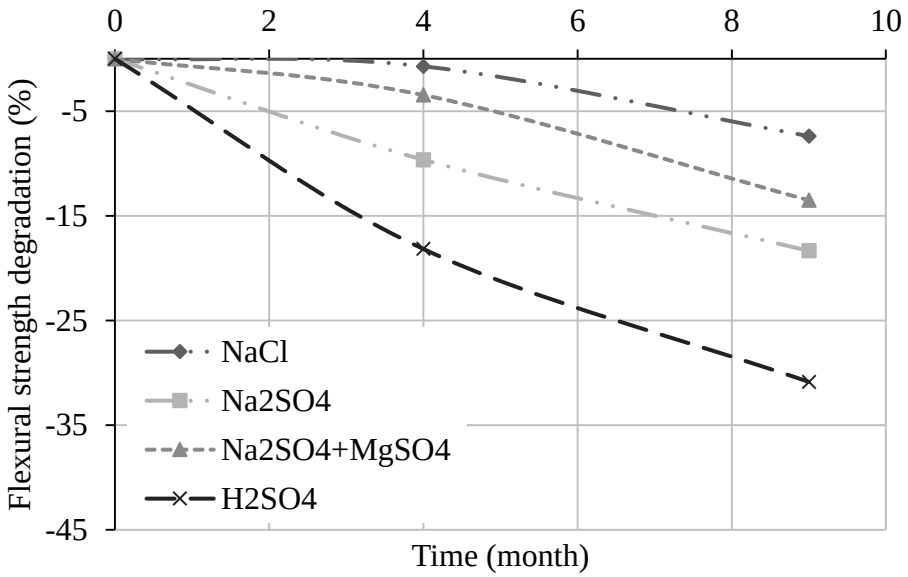

(b) Flexural tensile strength degradation of GLSS

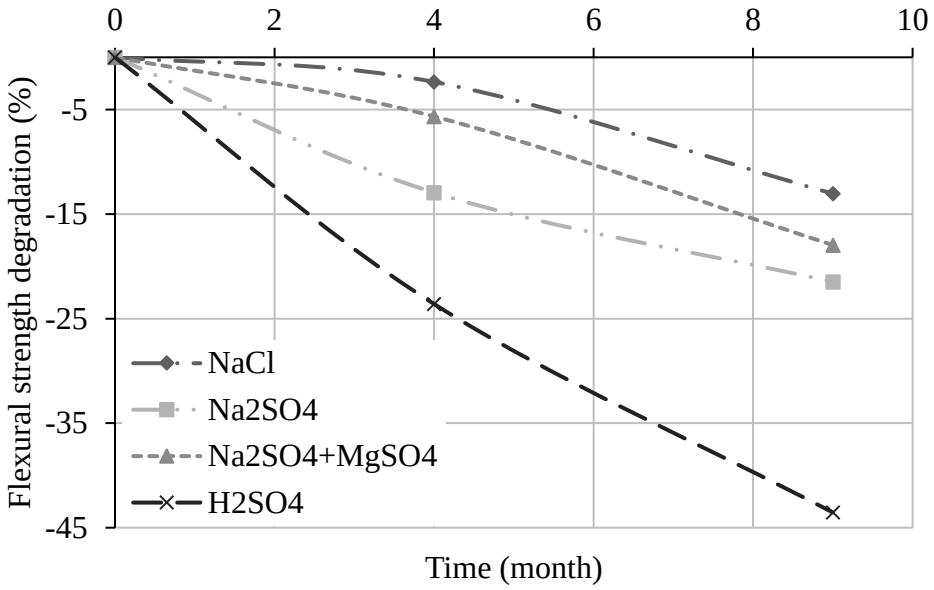

(c) Flexural tensile strength degradation of OPC

Figure 10. Flexural tensile strength degradation

Table 6. Splitting and flexural tensile strength degradation after nine months of chemical exposure

Concrete type	5% sodium chloride	5% sodium sulphate	5% sodium sulphate with 5% magnesium sulphate	3% sulphuric acid
Splitting tensile strength				
Fly ash	-2.8	-8.5	-4.2	-13.1
GLSS	-5.6	-9.7	-6.6	-16.5
OPC	-7.2	-12.7	-5.3	-18.8
Flexural strength				
Fly ash	-4.9	-14.2	-10.9	-25.3
GLSS	-7.3	-18.3	-13.5	-30.8
OPC	-13.0	-21.5	-17.9	-43.5

3.5. Wetting–drying cycles

The influence of wetting–drying and heating–cooling cycles on the weight change and compressive strength degradation is depicted in *Figs. 11(a)* and *(b)* respectively. *Fig. 11(a)* shows that the weight changes of fly ash, GLSS and OPC concretes displayed similar behaviours in which the weights of all the concretes increased, decreased and then increased again. It is evident from *Fig. 11(b)* that the compressive strength of geopolymer concretes experienced a rapid increase in the first two cycles followed by a slight decrease and then an increase again. On the other hand, OPC concrete experienced a reduction in the compressive strength followed by an increase and then a decrease. This fluctuation in

the weight and compressive strength was anticipated and it is attributed to the severity of the exposure regime in which staggers the integrity of concrete, which is the case under service conditions. The wetting–drying and heating–cooling cycles; in fact, cause several changes in the concrete due to the repetitive crystallisation of chlorides and sulphates by repeated hydration and evaporation, which causes expansion and then contraction and leads to forming internal stresses in the pores that may enhance or reduce the strength of the concrete.

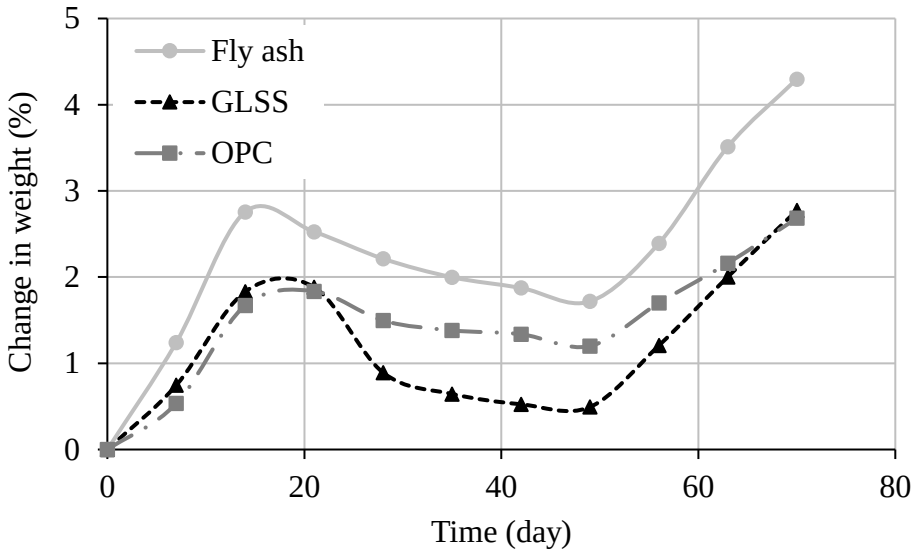

(a) Change in weight

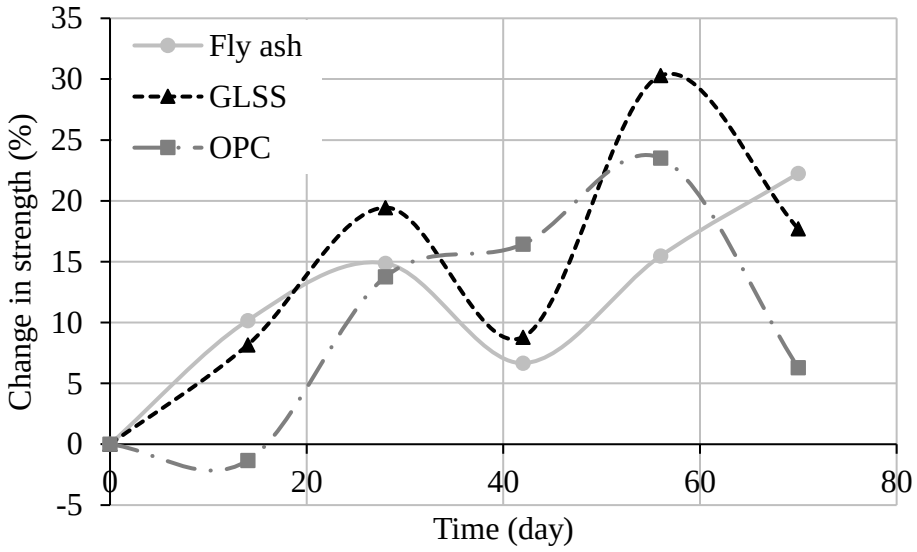

(a) Compressive strength

Figure 11. Influence of wetting–drying and heating–cooling cycles

4. CONCLUSION

This paper has presented the results of an experimental study that was undertaken to investigate the behaviour geopolymer concretes exposed to 5% sodium chloride, 5% sodium sulphate, 5% sodium sulphate + 5% magnesium sulphate and 3% sulphuric acid. The following conclusions can be drawn based on the results and discussions reported in this paper:

1. Ordinary Portland Cement (OPC) concrete has lower water absorption and sorptivity rate than fly ash and GLSS geopolymer concretes.
2. OPC concrete suffers more deterioration than geopolymer concretes due to sodium sulphate exposure with a reduction magnitude of 15.4% compared to 13.4% and 12.3% corresponding reduction magnitude of fly ash and GLSS geopolymer concretes respectively.
3. Sulphuric acid has a more detrimental impact on OPC concrete with a reduction in compressive strength of 26.6% compared to 10.9% and 7.3% reduction of fly ash and GLSS geopolymer concrete compressive strengths respectively.
4. The wetting–drying and heating–cooling cycles reflected service conditions in which the compressive strength fluctuated due to the imbalance in the internal stresses caused by the elevated temperature and penetrated chlorides and sulphates.
5. Sodium sulphate has significant detrimental impact on the compressive strength of geopolymer concretes due to leaching of sodium hydroxide when interacting with sodium sulphate. Therefore, the study highlighted the need to investigate the effect of sodium sulphate on the performance of geopolymer concrete activated with a different activator solution to that used in the present study.

Notwithstanding the superiority of OPC concrete in terms of capillarity mechanism that limits water access into concrete, geopolymer concrete showed superior durability performance when exposed to chemical attack. This performance reflects the stability of the geopolymer concrete chemical matrix and should lead to the emergence of durable geopolymer binder technologies in the foreseeable future.

ACKNOWLEDGEMENTS

The authors would like to acknowledge the support of the Department of Planning, Transport and Infrastructure of South Australia and The South Australian Department of Further Education, Employment, Science and Technology through Catalyst Research Grant “Development of Geopolymer Concrete.”

REFERENCES

[1] P.K. Mehta, Sulfate attack on concrete: a critical review, in: R.R. Villarreal (Ed.), Concrete Durability, Univ. Autonoma de Nuevo Leon, 1993.

[2] L.D. Wakely, T.S. Poole, J.J. Ernzen, B.D. Neeley, Salt saturated mass concrete under chemical attack, in: P. Zia (Ed.), High Performance Concrete in Severe Environments, Am. Concr. Inst., vol. SP-140, 1993, pp. 239–267.
[3] E.F. Irassar, A. Di Maio, O.R. Batic, Sulfate attack on concrete with mineral admixtures, Cem. Concr. Res. 26 (1) (1996) 113– 123.
[4] K. Tosun-Felekoğlu, The effect of C_3A content on sulfate durability of Portland limestone cement mortars, Constr. Build. Mater. 36 (2012) 437–447, DOI: 10.1016/j.conbuildmat.2012.04.091.
[5] E. Rozière, A. Loukili, R. El Hachem, F. Grondin, Durability of concrete exposed to leaching and external sulphate attacks. Cem. Concr. Res. 39 (2009) 1188-1198.
[6] K. Ramyar, G. İnan, Sodium sulfate attack on plain and blended cements, Build. Environ. 42 (2007) 1368–1372.
[7] C. Shi, P.V. Krivenko, D. Roy, Alkali-activated cements and concretes. Taylor & Francis, (2006) ISBN-I 0: 0-415-70004-3,376.
[8] M. Albitar, P. Visintin, M.S. Mohamed Ali, O. Lavigne, E. Gamboa, Bond slip models for uncorroded and corroded steel reinforcement in class-F fly ash geopolymer concrete, (ASCE) J. Mater. Civ. Eng. (2016) DOI: 10.1061/(ASCE)MT.1943-5533.0001713.
[9] T. Bakharev, Durability of geopolymer materials in sodium and magnesium sulfate solutions, Cem. Concr. Res. 35 (2005) 1233–1246.
[10] T. Bakharev, Resistance of geopolymer materials to acid attack, Cem. Concr. Res. 35 (2005) 658–670.
[11] J. Han, W. Liu, D. Wang, F. Jiao, T. Zhang, W. Qin, Selective sulfidation of lead smelter slag with pyrite and flotation behavior of synthetic ZnS, Metall. Mater. Trans. B. 47B (2016) 2400–2410.
[12] O.A. Hodhod, G. Salama, Simulation of expansion in cement based materials subjected to external sulfate attack, Ain. Shams. Eng. J. 5 (1) (2014) 7–15.
[13] A.M. Ramezanianpour, D.R. Hooton, Sulfate resistance of Portland-limestone cements in combination with supplementary cementitious materials, Mater. Struct. 46 (2013) 1061–1073.
[14] E.K. Attiogbe, S.H. Rizkalla, Response of concrete to sulfuric acid attack, ACI Mater. J. (1987) 481–488.
[15] K. Abora, I. Beleña, S.A. Bernal, A. Dunster, P.A. Nixon, J.L. Provis, A. Tagnit-Hamou, F. Winnefeld, Durability and testing – Chemical matrix degradation processes, in: J.L. Provis, J.S.J. van Deventer (Eds.), Alkali activated materials, State-of-the-Art Report, RILEM TC 224-AAM, London, 2014, pp. 177–222.
[16] A.P. Joseph, J. Keller, H. Bustamante, P.L. Bond, Surface neutralization and H_2S oxidation at early stages of sewer corrosion: influence of temperature, relative humidity and H_2S concentration, Water. Res. 46 (13) (2012) 4235–4245.
[17] H. Yuan, P. Dangla, P. Chatellier, T. Chaussadent, Degradation modelling of concrete submitted to sulfuric acid attack, Cem. Concr. Res. 53 (2013) 267–277.

[18] M. Albitar, M.S. Mohamed Ali, P. Visintin, M. Drechsler, Effect of granulated lead smelter slag on strength of fly ash-based geopolymer concrete, Constr. Build. Mater. 83 (2015) 128–135.
[19] M. Albitar, P. Visintin, M.S. Mohamed Ali, M. Drechsler, Assessing behaviour of fresh and hardened geopolymer concrete mixed with class-F fly ash, KSCE J. Civ. Eng. 19 (5) (2014) 1445–1455.
[20] ASTM C 642–06, Standard test method for density, absorption, and voids in hardened concrete, ASTM International, 100 Barr Harbor Drive, PO Box C700, West Conshohocken, PA 19428-2959, United States, 2008.
[21] ASTM C 1585–04, Standard test method for measurement of rate of absorbtion of water by hydraulic-cement concretes, ASTM International, 100 Barr Harbor Drive, PO Box C700, West Conshohocken, PA 19428-2959, United States, 2007.
[22] AS 1012.9, Method of testing concrete - Determination of properties related to the consistency of concrete, Australian Standard: Methods of Testing Concrete, 1999.
[23] AS 1012.10, Method of testing concrete - Determination of indirect tensile strength of concrete cylinders (Brazil or Splitting Test), Australian Standards, 2000.
[24] AS 1012.11, Method of testing concrete - Determination of the modulus of rupture, Australian Standards, 2000.
[25] N. Singh, S. Vyas, R.P. Pathak, P. Sharma, N.V. Mahure, S.L. Gupta, Effect of aggressive chemical environment on durability of green geopolymer concrete, Inter. J. Eng. Innova. Technology. (IJEIT). 3 (4) (2013) 277–284.
[26] I. Soroka, Portland cement, paste and concrete, Macmillan Education UK, London, 1979.
[27] L.R.P. de Andrade Lima, L.A. Bernardez, Characterization of the lead smelter slag in Santo Amaro, Bahia, Brazil, J. Haz. Mat. 189 (2011) 692–699.
[28] R.F. Warner, B.V. Rangan, A.S. Hall, K.A. Faulkes, Concrete structures, Addison Wesley Longman Australia Ltd., Melbourne, 1998.
[29] S. Popovics, A numerical approach to the complete stress-strain curves of concrete, Cem. Concr. Res., 3 (5) (1973) 583–599.

Statement of Authorship

Title of Paper	Bond slip models for uncorroded and corroded steel reinforcement in class–F fly ash geopolymer concrete
Publication Details	Albitar, M., Visintin, P., Mohamed Ali, M.S., Lavigne, O. and Gamboa, E. (2016). "Bond slip models for uncorroded and corroded steel reinforcement in class–F fly ash geopolymer concrete." *Journal of Materials in Civil Engineering (ASCE)*, pp. 04016186-1–04016186-10.
Publication Status	Published

Principal Author

Name of Principal Author (Candidate)	Albitar, M		
Contribution to the Paper	Performed the experiment, interpreted and analysed data and wrote manuscript.		
Overall percentage (%)	85%		
Certification:	This paper reports on original research I conducted during the period of my Higher Degree by Research candidature and is not subject to any obligations or contractual agreements with a third party that would constrain its inclusion in this thesis. I am the primary author of this paper.		
Signature		Date	

Co-Author Contributions

By signing the Statement of Authorship, each author certifies that:

i. the candidate's stated contribution to the publication is accurate (as detailed above);
ii. permission is granted for the candidate in include the publication in the thesis; and
iii. the sum of all co-author contributions is equal to 100% less the candidate's stated contribution.

Name of Co-Author	Visintin, P.		
Contribution to the Paper	Supervised development of work, helped in data interpretation and manuscript evaluation and acted as corresponding author.		
Signature		Date	20/10/2016

Name of Co-Author	Mohamed Ali, M.S.		
Contribution to the Paper	Supervised development of work, helped to evaluate and edit the manuscript.		
Signature		Date	20/10/16

Name of Co-Author	Lavigne, O.		
Contribution to the Paper	Supervised corrosion work.		
Signature		Date	23 / 09 / 2016

Name of Co-Author	Gamboa, E.		
Contribution to the Paper	Supervised corrosion work.		
Signature		Date	15 Sep 2016

Bond Slip Models for Uncorroded and Corroded Steel Reinforcement in Class–F Fly ash Geopolymer Concrete

M. Albitar, P. Visintin, M.S. Mohamed Ali, O. Lavigne, and E. Gamboa

ABSTRACT

Geopolymer concrete is an innovative construction material that utilises industrial by–product waste materials to form a cement replacement for concrete manufacture. In order to simulate the behaviour of reinforced concrete at all load levels, an understanding of the bond between the reinforcement and the concrete is required. That is at the serviceability limit state, the bond between the reinforcement and the concrete controls the formation of cracks, crack widening and tension–stiffening. Similarly, adequate bond between the reinforcement and the concrete is required at the ultimate limit state to ensure the full capacity of the reinforcement is obtained. Over time the bond between the reinforcement and concrete can deteriorate due to corrosion thus impacting on the overall performance of a structure. This paper presents a wide ranging study of the bond between reinforcement and geopolymer concrete including an investigation of the influence of corrosion. This study involved 102 pull–out test specimens covering a range of parameters including: bar diameter, concrete cover–to–diameter ratio, compressive strength and level of corrosion. Significantly, this study shows that the bond between reinforcement and geopolymer concrete is stronger than that between reinforcement and Ordinary Portland Cement.

KEYWORDS: Geopolymer concrete; Bond; Corrosion.

INTRODUCTION

Knowledge of the bond between reinforcement and the surrounding concrete is essential in the analysis and design of reinforced concrete (RC) members. The bond between reinforcement and concrete strongly influences the flexural behaviour at both the serviceability (Visintin et al. 2013) and ultimate limit states (Visintin et al. 2012), as well as the shear capacity (Zhang et al. 2014). That is bond between the reinforcement and the concrete controls the formation of cracks, crack widening, tension–stiffening (Gupta and Maestrini 1990; Choi and Cheung 1996; Marti et al. 1998; Knight et al. 2013) and anchorage of reinforcement (Castel et al. 2015). Corrosion of reinforcement not only reduces the strength of reinforcement, but also leads to deterioration of the bond, which can cause increased deflections, reduced strengths, debonding of reinforcement and ultimately lead to premature failure of a member. Therefore, there is a strong need to quantify the degradation of the bond between reinforcement and concrete in such it can be used to predict the long term performance of a structure.

While there is a significant number of publications empirically quantifying both the bond strength (Al-Sulaimani et al. 1990; Almusallam et al. 1996; Lee et al. 2002) and the change in local bond properties due to corrosion for concrete manufactured from Ordinary

Portland Cement (OPC) (Cabrera 1996; Lee et al. 2002; Chung et al. 2008; Feng et al. 2015), there is little information regarding the bond and durability of reinforced geopolymer concrete (Sofi et al. 2007; Chang 2009; Sarker 2010; Selby 2011; Reddy et al. 2013; Castel and Foster 2015; Kim and Park 2015) which is manufactured by activating an alternate silica source such as fly ash with a strong alkali solution (Davidovits 1991 and 1994).

This paper presents the results of a comprehensive experimental study on the bond characteristics of geopolymer concrete. The test programme involves 102 pull–out tests to quantify the bond between conventional ribbed steel reinforcement and class–F fly ash geopolymer concrete, including 78 pull–out tests to quantify the change in bond properties due to corrosion levels ranging from 0 to 85% mass loss.

Importantly, based on the test results obtained in this study, it is shown that the bond between reinforcement and geopolymer concrete is equal to or better than that between reinforcement and OPC concrete. This suggests that in the absence of more refined models for geopolymer concrete, those developed for OPC concrete may be suitable as a lower bound approximation for geopolymer concrete.

EXPERIMENTAL PROGRAMME

In order to quantify the durability of the local bond stress–slip (τ/δ) properties between conventional ribbed steel reinforcement and geopolymer concrete, a series of 102 pull tests were conducted on class–F fly ash–based geopolymer concrete. The key parameters chosen for investigation were the concrete cover–to–bar diameter (C_c/d_b) ratio, which was varied between 2 and 7.8; the mass loss corrosion level, *CL*, which ranged between 0% and 85% and the compressive strength, f_c, which were 33, 38 or 43 MPa.

When considering changes in concrete cover (C_c) a variation in bar diameter from 12 mm to 16 mm was also considered; this is important as Rasheeduzzafar et al. (1992) showed that changes to the concrete cover without the consideration of the diameter leads to misleading results, especially when considering reinforcement corrosion. It should also be noted that the range of C_c considered in this programme satisfies the requirements for all exposure classes for ACI 318 (1995) as well as the Australian Standard for concrete structures AS3600 (2003).

To complement the pull–out test data and allow the results of this study to be used in advanced analysis procedures, such as those which quantify the progression of corrosion (Otieno et al. 2011), additional material tests were conducted to quantify the full–compression stress–strain relationships, elastic modulus, indirect tensile strength, sorptivity and water absorption of the geopolymer concrete.

Pull–out Test Specimens

The experimental pull–out test programme consisted of two phases. In the first phase, concrete blocks with a cross section of 150x150mm, and a height of 200mm, as shown in *Fig. 1* were used and the concrete cover varied as in *Table 1*. This series of tests was conducted in order to quantify the change in failure mode from concrete cover splitting to reinforcement pull out as C_c increases.

In the second phase, the specimens were designed such that splitting failure would not occur; thus, the specimens were designed to have large concrete cover and as such had a cross section of 200x200mm, and a height of 350mm with a centrally located bar. This series of tests was conducted in order to obtain the backbone curve, which typically define τ/δ relationships, such as the well–known CEB-FIP (1993) model.

For both phases, the reinforcement embedment length was taken to be 5 times the steel bar diameter ($5d_b$) to ensure that the steel bars do not yield prior to debonding.

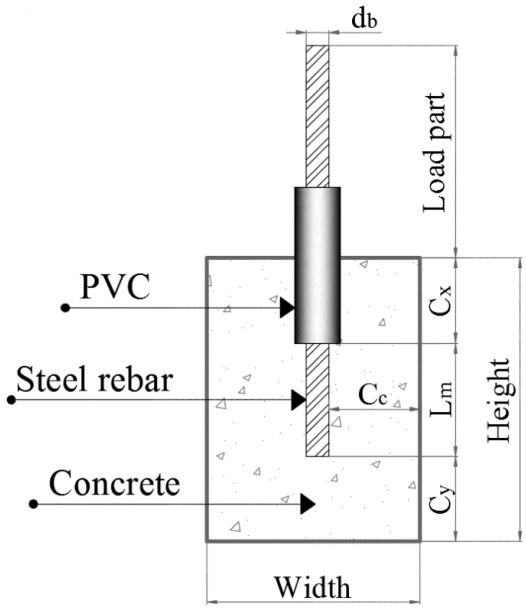

Figure 1. Details of pull–out test specimens

Table 1. Geometric Properties of Pull–out Test Specimens

Specimens	f_c (MPa)	Height (mm)	Width (mm)	C_c (mm)	d_b (mm)	L_m (mm)	C_x (mm)	C_y (mm)
Specimens: 1, 2, 15, 16, 23, 24, 31, 32, 39, 40, 47, 48	33	200	150	24	12	60	60	80
Specimens: 3, 4, 17, 18, 25, 26, 33, 34, 41, 42, 49, 50	33	200	150	36	12	60	60	80
Specimens: 5, 6,	33	200	150	48	12	60	60	80
Specimens 7, 8, 19, 20, 27, 28, 35, 36, 43, 44, 51, 52	33	200	150	32	16	80	60	60
Specimens: 9, 10, 21, 22, 29, 30, 37, 38, 45, 46, 53, 54	33	200	150	48	16	80	60	60
Specimens: 11, 12	33	200	150	64	16	80	60	60
Specimens: 13, 14	33	200	250	177	16	80	60	60
Specimens: 55, 56, 59, 60, 63, 64, 67, 68, 71, 72, 75, 76	43	200	150	24	12	60	60	80
Specimens: 57, 58, 61, 62, 65, 66, 69, 70, 73, 74, 77, 78	43	200	150	36	16	80	60	60
Specimens: 79, 80, 81, 82, 83, 84, 85, 86, 87, 88, 89, 90	38	350	200	94	12	60	120	170
Specimens: 91, 92, 93, 94, 95, 96, 97, 98, 99, 100, 101, 102	38	350	200	92	16	80	120	150

Material Properties

Low calcium class–F fly ash was used as the cementitious material to manufacture geopolymer concrete according to the mix designs in *Table 2*, which were developed by the authors in previous works (Albitar et al. 2014; 2015). The activator solution was a combination of sodium silicate (Na_2SiO_3) and 14-molar sodium hydroxide (NaOH) pre–mixed with a ratio of Na_2SiO_3-to-NaOH of 1.5. Washed river sand and crushed bluestone with a maximum size of 10mm was used as fine and coarse aggregates respectively. Deformed steel bars with two different diameters, namely 12mm and 16mm were embedded in the concrete. Steel tensile tests were performed on three bars of each

diameter from which the yield strengths were determined to be 560 MPa and 520 MPa for the 12 and 16 mm bars respectively.

Table 2. Mixture Proportions of Concrete (kg/m^3)

Ingredients	Mixture 1	Mixture 2	Mixture 3
Fly ash	430.11	430.11	430.11
Aggregate (10 mm)	1172.23	1195.56	1182.95
Sand	583.20	588.06	583.20
Sodium hydroxide (14 M)	63.83	63.18	63.83
Sodium silicate	95.75	94.77	95.75
Water	85.05	79.22	74.11
Slump (mm)	250	210	180
Compressive strength (MPa)	33	38	43

Mixing, Casting and Curing

All pull–out test specimens and associated material durability test specimens were manufactured at The University of Adelaide in three batches in a 750 L planetary mixer. The concrete was manufactured by mixing the dry components (i.e., fly ash, sand and course aggregate) for three minutes. Once well combined, the water and activator solution were added and mixing continued for seven minutes. The concrete was then cast into plywood moulds, which were greased with a conventional mould–releasing compound to prevent water absorption by the plywood. The specimens were de–moulded after two weeks and left at ambient room temperature for 84 days prior to the commencement of testing.

It has been widely shown that the development of strength can be slow in low calcium fly ash geopolymer concretes and that the rate of strength gain can be significantly increased by heat curing (Chindaprasirt et al. 2007; Winnefeld et al. 2010). In this study, it was chosen not to heat cure in order to avoid any potential damage to the bond due to thermal stresses. The geopolymer concretes considered in this study have previously been shown to be able to be demoulded after two days of casting and to achieve approximately 70% of their final heat cured compressive strength by day 28 and approximately 100% by day 56 (Albitar et al. 2014). Hence it can be expected that all specimens had reached their full strength by the commencement of testing at day 84.

In addition to pull–out tests, sixty cylinders with a diameter of 100mm diameter and height of 200mm were manufactured from mix 1 in *Table 2* for compressive strength, splitting tensile strength, and durability tests. The durability tests included sodium chloride exposure, water absorption, and sorptivity tests. It should be noted that test cylinders of each concrete were subjected to the same curing condition as the pull–out test specimens in terms of curing period and immersion in the sodium chloride solution such that the compressive strength of the concrete in the pull–out tests could be quantified.

Accelerated Corrosion Method

Corrosion of the reinforcement in the pull–out test specimens was induced electrochemically. Specimens were initially fully immersed in an aqueous solution of 3.5% sodium chloride (NaCl) by weight for 4 days at a constant temperature of 22°C (±2°C) in order to saturate the concrete and introduce NaCl to the concrete. To accelerate corrosion of the reinforcement, specimens were removed from the NaCl solution, cloth–dried, and then fully immersed in an aqueous solution of 5% NaCl by weight. The corrosion was induced electrochemically using a direct current supply by connecting the exposed reinforcement to the positive terminal of a constant current source to serve as the anode, while the negative terminal of the power source was connected to a stainless steel mesh, which was placed in the solution next to the specimens to act as a cathode.

The magnitude of corrosion was measured using gravimetric weight–loss according to Faraday's law:

$$mass\ loss = \frac{t\ (s) \times M_{Fr}\left(\frac{g}{mol}\right) \times i\ (\frac{A}{cm^2})}{\rho\left(\frac{g}{cm^3}\right) \times Z \times r\ (cm) \times F\ (\frac{A.S}{mol})} \quad (1)$$

where, t is the duration of exposure in seconds, ρ is the density of iron (ρ=7.87g/cm^3), Z is the ionic charge (2 for Fe), r is the radius of corroded bar (cm), F is Faraday's constant (96487 A.S/mol), M_{Fr} is the atomic weight of the metal (55.847g/mol for steel), and i is the average current density in (A/cm^2).

After the completion of bond tests, the corroded reinforcement was removed from the concrete block and cleaned with hydrochloric acid to remove the corrosion products from the surface of the bars in accordance with ASTM G1-03 (2003). The bars were then weighed to determine the final corroded weight (G_1) and this was compared with the initial weight (G_0) to determine the corrosion level, CL, as follows

$$CL = \frac{G_0 - G_1}{g_0 \times l} \times 100\% \quad (2)$$

in which l is the bond length.

The rate at which corrosion of the reinforcement is accelerated can be a significant factor in the deterioration of the bond between steel bar and concrete. Applying a high current will result in a relatively sudden expansion in the steel bar due to a rapid growth of the corroded (oxide) layer, forcing the concrete to expand and split. Additionally, artificially high potentials would cause water to break down into hydrogen and oxygen, altering the chemistry at the steel–concrete interface in a manner not representative of field conditions. Thus accelerated corrosion tests performed with a high current density may not represent real world conditions (Song and Shayan 1998). In order to avoid the scenario in which the induced corrosion does not represent actual field conditions, the current density (i) was maintained at a low rate (≈100 μA/cm^2).

Loading and Measurements

Pull–out tests were performed for corroded and uncorroded specimens in accordance with ASTM C234-91a (1991). The pull–out tests were carried out on a universal testing machine with a capacity of 2,000 kN. The specimens were placed vertically on a platen and reacted against a 25mm thick steel bearing plate by applying a tensile load to the reinforcing bar. The slip of the reinforcement was measured relative to concrete using 2 linear variable displacement transducers (LVDTs).

Sorptivity and Water Absorption Tests

Sorptivity and water absorption tests were conducted on cylindrical specimens with dimensions of 100mm diameter and 50mm height which were cut from standard compressive strength cylinders. The tests which were carried out in accordance with ASTM C1585 and ASTM C642 were conducted to examine the porosity and tendency of the specimen to absorb and transmit water by capillarity action.

EXPERIMENTAL RESULTS

Mechanical Properties of Concrete

For a given type of reinforcing bar, the local τ–δ bond properties are primarily influenced by mechanical properties of the concrete and the geometric properties of the reinforcement. When considering a scenario in which reinforcement may corrode over time, the bond stress is strongly dependent on the level of corrosion, which itself depends on factors, such as the sorptivity and porosity of the concrete mix. Therefore, tests to determine the full–compression stress–strain relationships, elastic modulus, indirect tensile strength, sorptivity and water absorption have been undertaken on specimens manufactured from mix 1 in *Table 2*, which has an average compressive strength of 33 MPa.

The results of the mechanical testing of the concrete are summarised in *Table 3. Fig. 2* shows the compressive stress–strain relationship of cylinders subjected to either ambient conditions or immersed in sodium chloride solution. From *Table 3* and *Fig. 2* it can be concluded that the influence of immersion in sodium chloride has a negligible influence on the mechanical properties of the geopolymer concrete.

Table 3. Durability and Mechanical Properties of Mix 1

Age, *t* (Week)	f_c (ambient condition) (MPa)	f_c (after immersion in NaCl solution), (MPa)	f_{ct}, (ambient condition) (MPa)	f_{ct} (after immersion in NaCl solution), (MPa)	Elastic modulus, (ambient condition) (MPa)	Elastic modulus (after immersion in NaCl solution), (MPa)
8	30.2	30.2	3.0	3.0	28198.3	28199.3
12	30.9	30.9	3.1	3.1	281200.2	28205.2
18	32.8	32.8	3.1	3.2	28204.5	28201.5
24	33.5	33.5	3.1	3.2	28201.7	28202.7
30	34.2	33.3	3.2	3.2	28205.5	28200.5
36	35.6	33.1	3.7	3.2	28203.4	28201.4

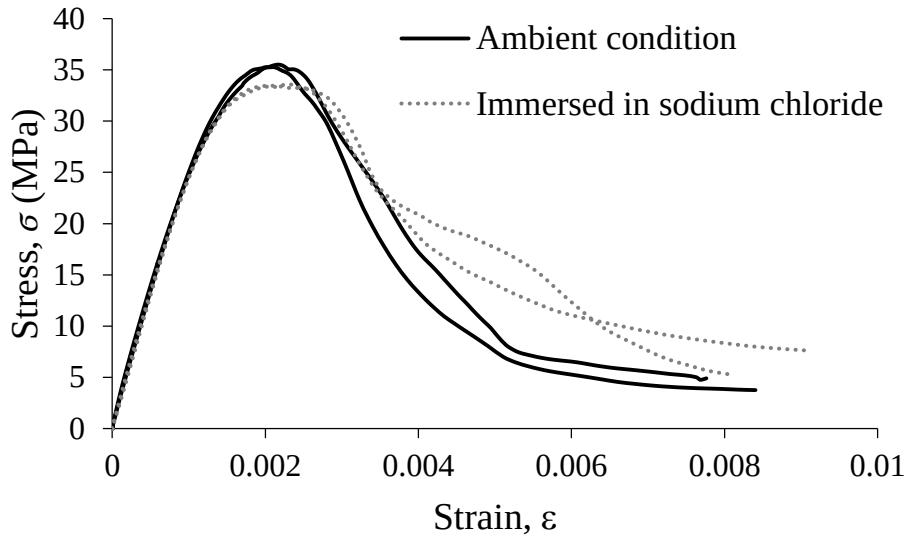

Figure 2. Stress–strain relationship of specimens cured under ambient condition and specimens immersed for 36 weeks in sodium chloride

The results of sorptivity and water absorption tests are shown in *Figs. 3a, b* and *c*. It can be seen that the curves in *Figs. 3a* and *b* consist of two portions, non–linear and linear. Each portion reflects a different transport mechanism for water movement within concrete. The rapid saturation of capillary pores of concrete can be observed in the initial portion, which corresponds to the period immediately after the concrete is exposed to the water source following this behaviour stabilises indicating the slow movement of the water within concrete overtime.

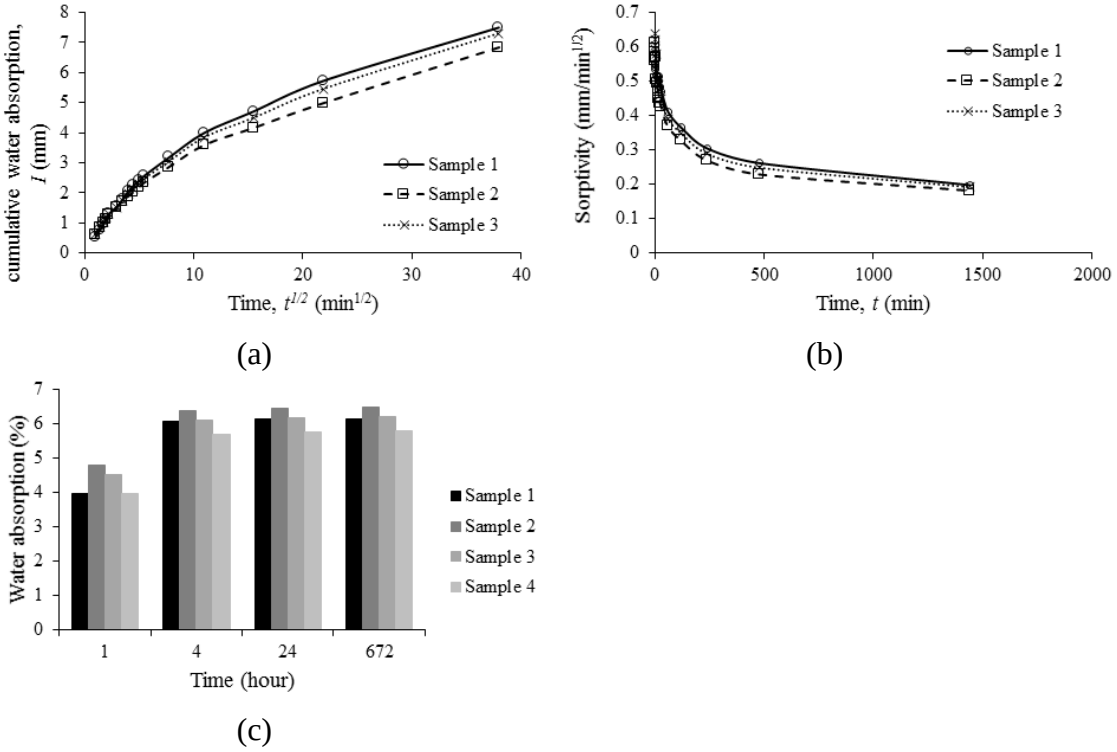

Figure 3. Sorptivity and water absorption tests: (a) cumulative water absorption; (b) sorptivity; and (c) water absorption.

Pull out Test Results

The full bond stress–slip (τ/δ) relationship of all 102 uncorroded and corroded test specimens is given in *Figs. S1* and *S2* in the supplementary material, where in the experimental designation in each subplot refers to the specimen number–concrete compressive strength–bar diameter–clear cover to the reinforcement and corrosion level. It should be noted that the bond stress has been calculated from the recorded force in the reinforcement using *Eq. 3*

$$\tau = \frac{P}{\pi \times d_b \times L} \tag{3}$$

in which P is the is the force applied to the reinforcement, d_b is the steel bar diameter, and L is the bond length of the steel bar.

Local Bond Stress–Slip Model for Uncorroded and Corroded Reinforcement

In this section the local τ–δ properties extracted from experimental tests in *Figs. S1* and *S2*, which are available in the supplementary material, will be used to develop a local τ–δ constitutive relationship shown generically in *Fig. 4*. The form of the model is the same as that defined by CEB-FIB (1993) in which the ascending branch is defined as

$$\tau = \tau_{max}(\frac{\delta}{\delta_1})^{0.4} \quad (4)$$

and the descending and frictional branches are approximated as linear.

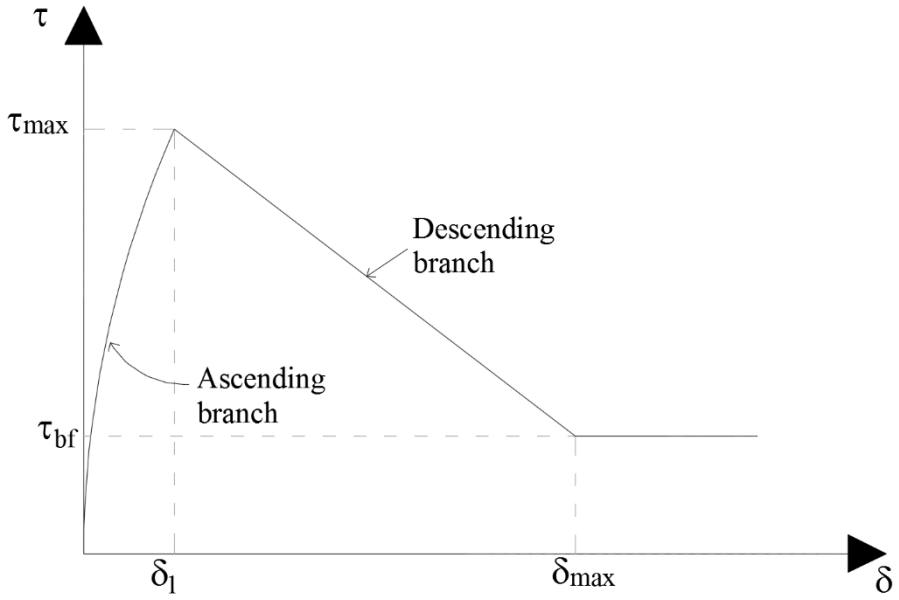

Figure 4. Idealised bond–slip

In *Table S1*, which is available in the supplementary material, the critical results associated with each local bond stress–slip relationships in *Figs. S1* and *S2* are summarised including: corrosion level, *CL*; crack width before testing, cw_b; crack width after testing, cw_a; maximum bond strength, τ_{max}; slip at maximum bond strength, δ_1; maximum slip, δ_{max}; and frictional strength, τ_{bf}. From *Table S1*, specimens can be classified into five different categories, namely (i) uncorroded and uncracked (ii) uncorroded and cracked after testing (iii) corroded and uncracked before and after testing (iv) corroded and uncraked before testing, but cracked after testing, and (v) corroded and cracked before and after testing. The changes in (δ_1/τ_{max}) and (δ_{max}/τ_{bf}) with varying material and geometric properties are now considered.

It should be noted that when developing a bond stress–slip relationship for geopolymer concrete it is assumed that the differing reaction mechanism between geopolymer and OPC concretes does not directly influence the bond properties. That is as suggested by Ciampi et al. (1982) the local bond stress–slip relationship is controlled by localised cracking and crushing of the concrete as the reinforcement slips relative to the concrete. Hence it is suggested that the major difference between the bond behaviour of geopolymer and OPC concretes will arise due to the variation in mechanical properties of the concrete.

DISCUSSION

Uncorroded Reinforcement

Influence of Concrete Strength on Bond Strength

In previous research on bond of geopolymer concrete, both Selby (2011) and Castel and Foster (2015) found that the ultimate bond strength of geopolymer concrete is slightly higher than that of OPC concrete of an equivalent compressive strength. This behaviour was attributed to the higher tensile strength of geopolymer concrete compared to an equivalent OPC.

In *Fig.* 5 the variation in bond strength with concrete compressive strength is shown and in which the concrete compressive strength varies from 33 MPa to 43 MPa. It should be noted that as is commonly done (Darwin 2005) the bond strength is considered to be function of the square root of the concrete strength which is analogous to the tensile capacity of the concrete.

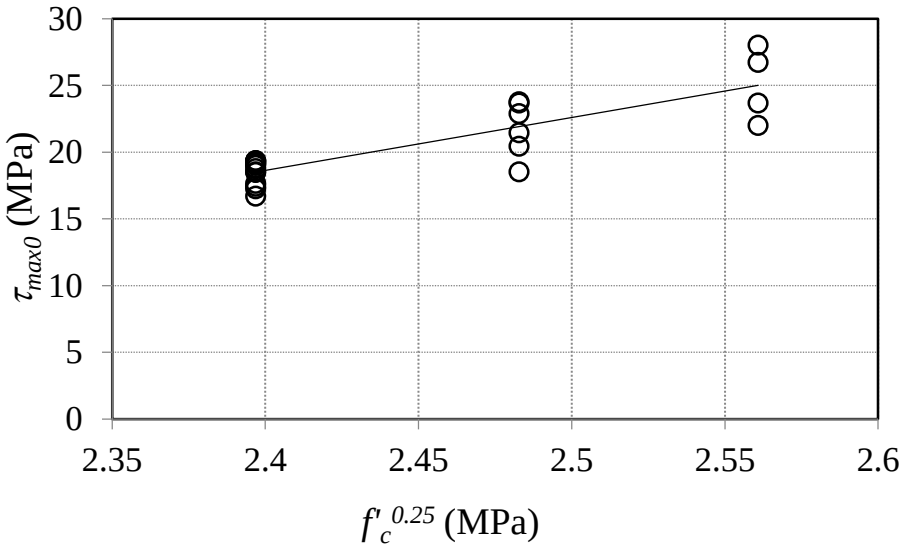

Figure 5. Influence of concrete compressive strength on bond strength

From a linear regression of the results in *Fig. 5*, the change in bond strength with concrete compressive strength is given by

$$\tau_{max0} = 39.6 f'^{0.25}_c - 76.5 \quad (5)$$

where the increase in τ_{max0} with concrete compressive strength can be considered to arise due to an increase in splitting, bearing, cohesion and friction strengths of the concrete.

Although a relationship between the maximum bond strength and concrete compressive strength is proposed here, the scatter of results in *Fig. 5* suggests that further experiments are required to determine the influence of compressive strength.

Influence of Concrete Cover to Bar Diameter Ratio on Bond Strength

The influence of C_c/d_b ratio on the bond strength of uncorroded specimens is given in *Fig. 6*, in which the bond stress is normalised by the concrete strength in order to remove its influence. In *Fig. 6* it can be seen that there is a minor increase in bond strength as the C_c/d_b ratio increases from 2 to 3 beyond which there is negligible influence.

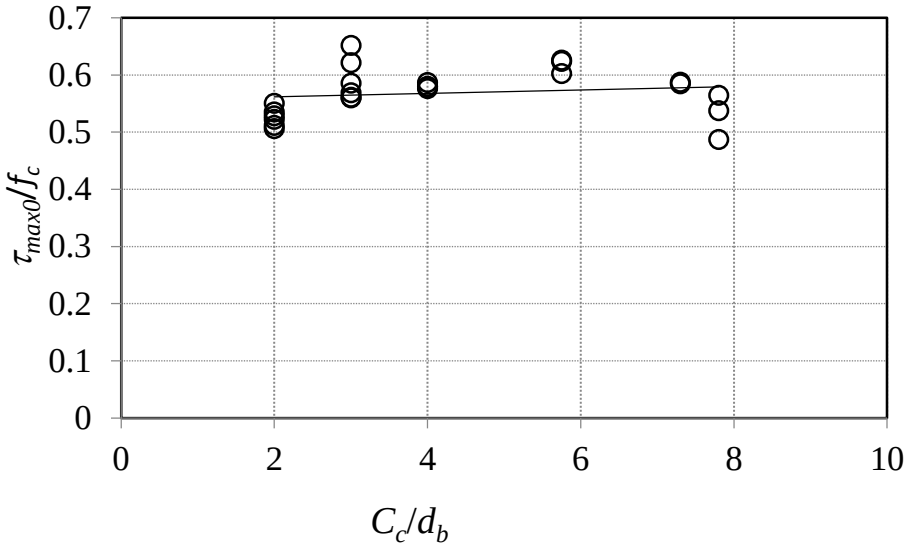

Figure 6. Influence *of* C_c/d_b ratio on bond strength

As the scatter of test results for any given C_c/d_b ratio is in the same order of magnitude as the increase in bond strength due to increases in C_c/d_b the influence of this parameter is not considered further in the development of the model. It should, however, be noted that an increase in bond strength with increases in cover is a well–established phenomenon and hence further research may need to be conducted with a wider range of bar diameters to clarify the influence of C_c/d_b ratio.

Slip at Peak Stress

Having defined the bond strength τ_{max} as a function of key parameters, a regression of the slip at peak stress (δ_1) against τ_{max} allows for the transition between pull–out and splitting failure. The results of this regression are summarised in *Fig. 7* in which the slip at peak stress can be defined as

$$\delta_1 = 0.088\tau_{max0} - 0.320 \quad (6)$$

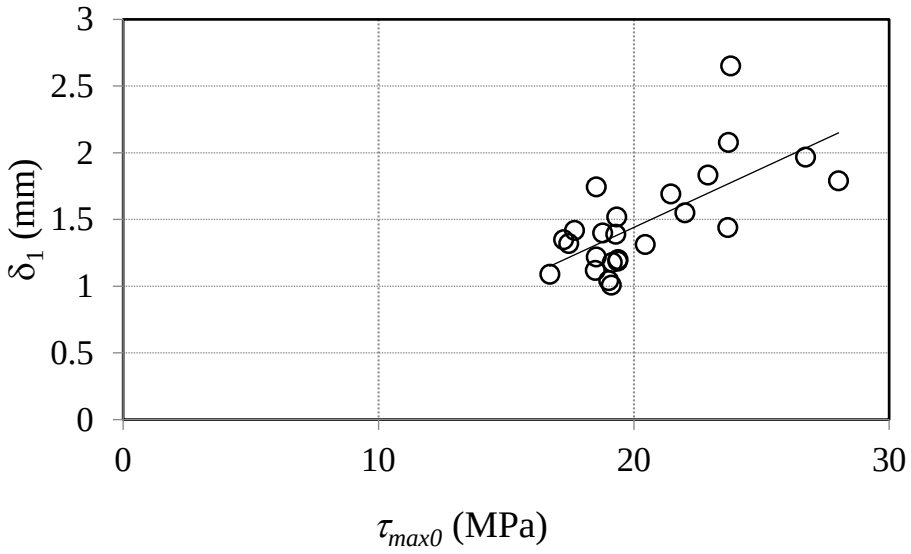

Figure 7. Influence of τ_{max0} on δ_1

Frictional Strength and Maximum Slip

The frictional strength (τ_{bf}) and maximum slip (δ_{max}) occur when pulling out of the reinforcement is resisted only by friction between the reinforcement and concrete. Both τ_{bf} and δ_{max} are highly dependent on the failure mode, as splitting of the concrete significantly reduces confinement of the reinforcement by the surrounding concrete. The width of splitting cracks post pull–out failure, cw_a, is summarised in *Table S1*.

The relationships between τ_{bf} and τ_{max0} and δ_{max} and τ_{max0} for uncorroded reinforcement are shown in *Fig. 8* and *Fig. 9* respectively. As expected, there is a clear relationship between the frictional behaviour and the peak bond strength as both these behaviours are strongly influenced by the formation of splitting cracks.

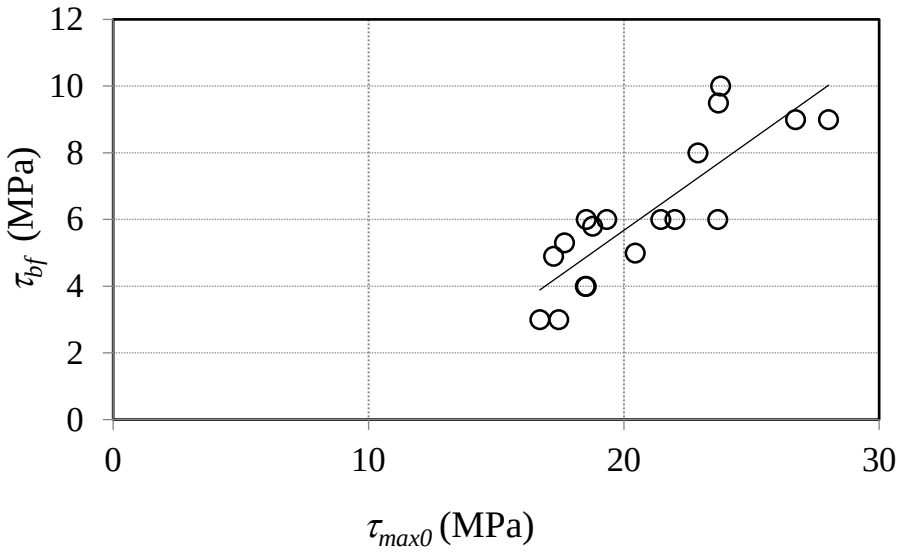

Figure 8. Influence of τ_{max0} on τ_{bf}

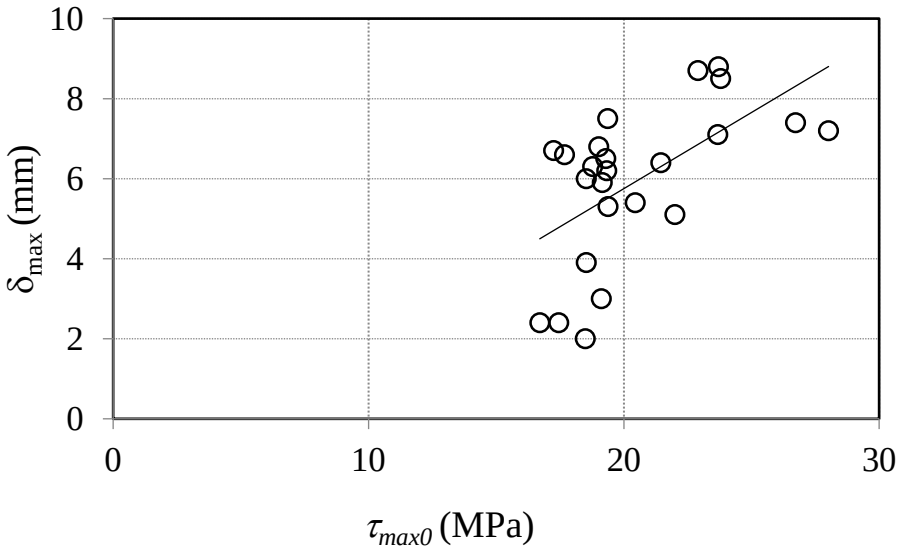

Figure 9. Influence of τ_{max0} on δ_{max}

Performing a linear regression on the results in *Figs. 8* and *9* can be described by:

$$\tau_{bf} = 0.543\tau_{max0} - 5.18 \quad (7)$$

$$\delta_{max} = 0.380\tau_{max0} - 1.86 \leq s_r \quad (8)$$

in which it should be noted that the maximum slip prior to frictional resistance is taken as the clear spacing between ribs, s_r, as this defines the point at which shearing of the concrete keys between ribs occurs (Ciampi et al. 1982).

Corroded Reinforcement

Local Bond Stress–Slip Relationship of Corroded Specimens

Examining the test results for τ/δ relationships for corroded reinforcement in *Fig. S2*, it can be seen that corrosion levels of less than 1% are in general beneficial, leading to an increase in bond strength; however, at levels greater than 1% a rapid reduction in strength occurs. In *Table S1* it can also be noted that the most significant reduction in bond strength occurs when splitting cracks of width cw_a form prior to testing as a result of the formation of the corrosion products.

Influence of Corrosion on the Ultimate Bond Strength

When considering the change in bond behaviour, there are several approaches available for quantifying the corrosion level. For example, Vidal et al. (2004), François et al. (2013) and Castel et al. (2015) consider the quantum of corrosion product as it is the corrosion product which exerts a pressure to the surrounding concrete resulting in cracking and a reduction in bond strength. In the works of Cabrera (1996), Lee et al. (2002), Bhargava et al. (2007) and Chung et al. (2008) the bond behaviour of corroded reinforcement has been considered to be adequately modelled as a function of the percentage cross sectional area reduction due to corrosion. In these approaches, for a given corrosion level, the change in total quantity of corrosion product with bar diameter cannot be allowed for and hence their application over a wide variety of bar diameters may be questionable. Alternatively, models such as those reported by Feng et al. (2015) consider cross sectional reduction which is weighted by the concrete cover to diameter ratio which has been shown by Rasheeduzzafar et al. (1992) to be a significant parameter when predicting corrosion cracking. Hence these approaches indirectly allow for the change in quantum of corrosion product with bar diameter.

The relationship between maximum bond strength and the quantity of corrosion in terms of mass loss is shown in *Fig. 10*. It should be noted that the change in the bond strength τ_{max} with corrosion is given in terms of the change in bond strength away from that expected when there is no corrosion τ_{max0}. This approach is the same as that taken by Feng et al. (2015) and is done in order to remove the scatter which arises due to the definition of the bond properties without corrosion.

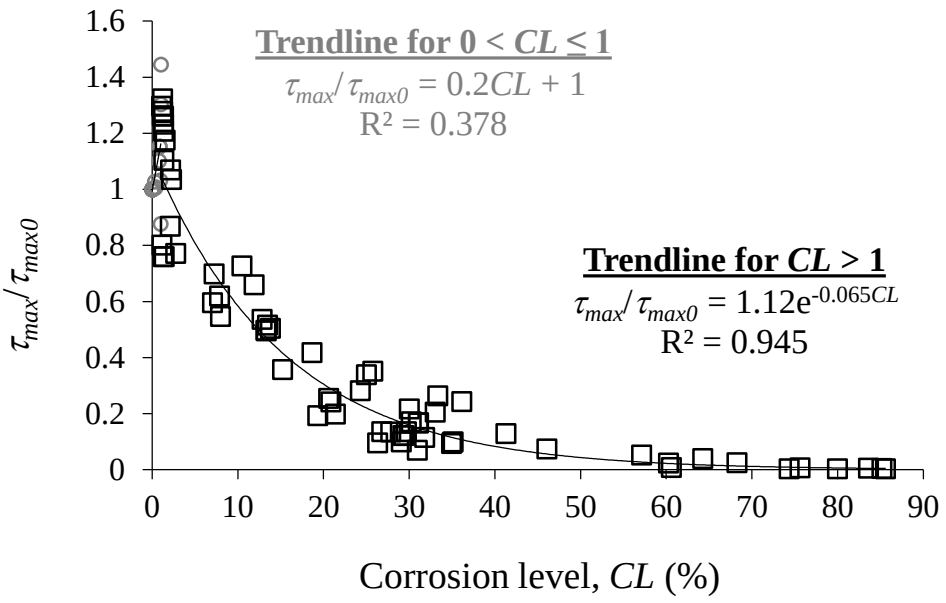

Figure 10. Relationship between ultimate bond stress and different degrees of corrosion

From *Fig 10* it can be observed that, in general, the maximum bond strength increases as the degree of corrosion increases from 0 to 1%, and thereafter the bond strength decreases with increasing the corrosion level. Hence for the purpose of defining the change in τ_{max} with corrosion, two stages have been defined: (i) where corrosion leads to an increase in bond strength; and (ii) where corrosion causes a reduction in bond strength. Based on a regression analysis, the change in bond strength for each range of corrosion is defined in *Eqns. 9* and *10* as a function of the percentage of mass loss due to corrosion (*CL*)

$$\frac{\tau_{max}}{\tau_{max0}} = 0.20CL + 1;\ 0\% \leq CL \leq 1\% \quad (9)$$

$$\frac{\tau_{max}}{\tau_{max0}} = 1.12e^{-0.065CL};\ CL > 1\% \quad (10)$$

Unexpectedly, regression analysis to obtain *Eqs. 9* and *10* did not show a statistically significant dependence on either the C_c/d_b ratio or the bar diameter alone. This result may be because although the C_c/d_b ratio varied from 2 to 3, the variation in bar diameter was small, that is from 12 to 16mm. It is therefore suggested that further experimental work is needed in order to consider a wider range of reinforcement diameter.

It is worth mentioning here that there can be significant scatter in the bond strength for a given level of corrosion. For example, consider the duplicate specimens 31 and 32, which had the same corrosion level but in which τ_{max} varied from 3.6 to 4.6 MPa, this scatter can be attributed to heterogeneity of the concrete, different degrees of cleanliness at the interface (Fu and Chung 1997) as well as non–uniformity in the localised intensity of the corrosion.

Slip at Peak Stress

The relationship between the slip at peak stress (δ_1) and the change in the peak bond stress due to corrosion (τ_{max}/τ_{max0}) is shown in *Fig 11*. The slip at peak stress for corroded reinforcement equation as a result of linear regression analysis can be described by

$$\delta_1 = -0.223\frac{\tau_{max}}{\tau_{max0}} + 2.00 \quad (11)$$

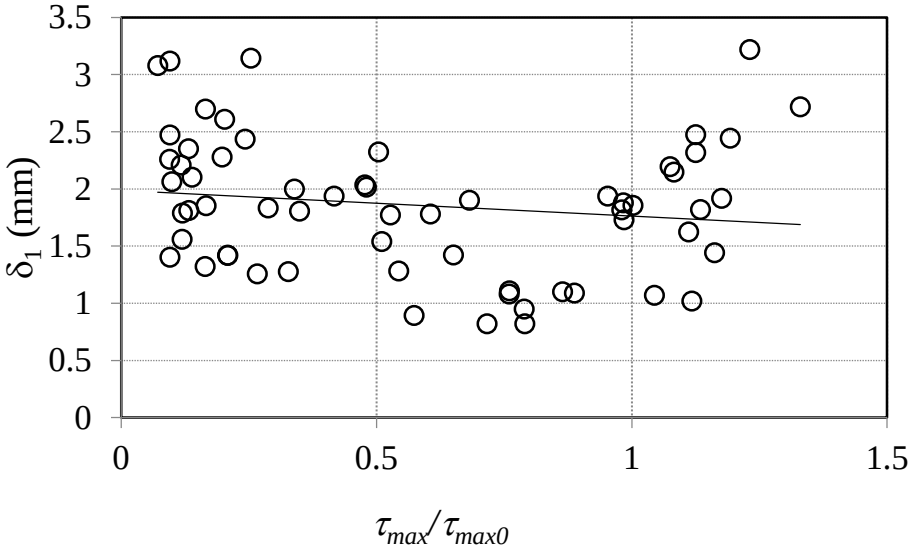

Figure 11. Influence of τ_{max}/τ_{max0} on δ_1

Frictional Strength and Maximum Slip

The relationships between τ_{bf} and τ_{max}/τ_{max0} and between δ_{max} and τ_{max}/τ_{max0} for corroded specimens are shown in *Fig. 12* and *Fig. 13* respectively. The influence of τ_{max}/τ_{max0} on the frictional properties is taken from regression analysis of the data in *Fig. 12* and *Fig. 13*, given by

$$\tau_{bf} = 7.77(\frac{\tau_{max}}{\tau_{max0}})^2 - 2.15\frac{\tau_{max}}{\tau_{max0}} + 0.69 \quad (12)$$

$$\delta_{max} = 0.367\frac{\tau_{max}}{\tau_{max0}} + 5.13 \quad (13)$$

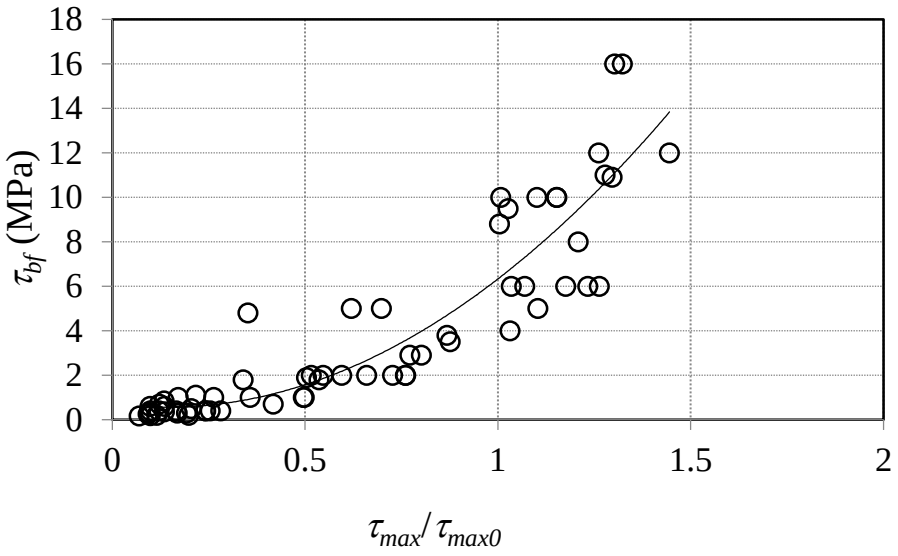

Figure 12. Influence of τ_{max}/τ_{max0} on τ_{bf}

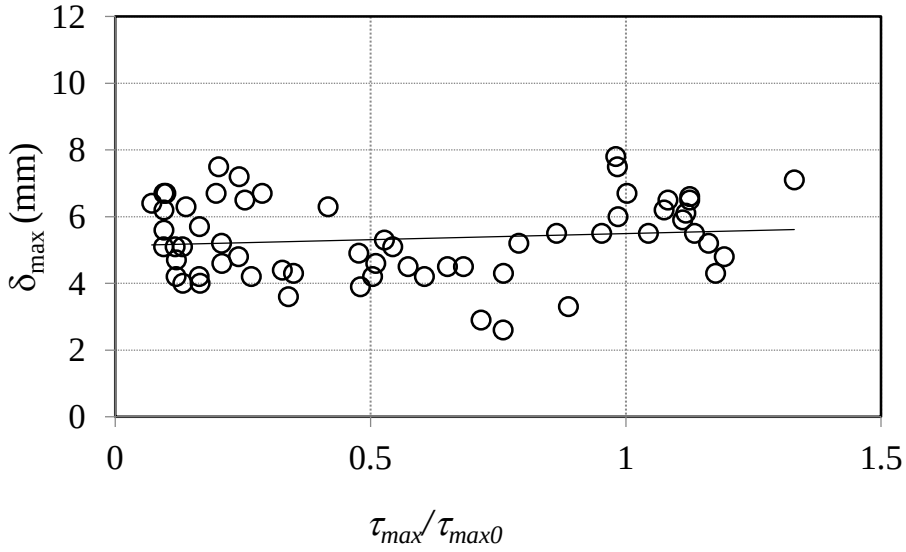

Figure 13. Influence of τ_{max}/τ_{max0} on δ_{max}

Corrosion induced cracking

The level of corrosion required to cause longitudinal splitting cracks has been widely investigated, with several empirical (Zhao et al. 2012; Vu et al. 2005; Vidal et al. 2004) and analytical (Pantazopoulou and Papoulia 2001; Koteš 2013) formulations proposed. The importance of this parameter can be clearly seen in *Fig. 14(a)* in which it is shown that upon formation of a splitting crack due to corrosion, the bond strength is reduced by more than 50%.

In *Fig. 14(b)* the splitting crack widths prior to loading is plotted for various corrosion levels. It can be observed that there is significant scatter in test results, with splitting cracks occurring at vastly different corrosion levels regardless of concrete cover to bar diameter ratio. This can be attributed to the heterogeneous nature of corrosion along the bonded length. A similar observation was also made by Vidal et al. (2007) on beams subjected to corrosion and sustained loading. In *Fig. 14(b)* it can also be seen that there is only a weak correlation between the corrosion crack width and the C_c/d_b relationship which is contrary to the results available for OPC concrete (Vidal et al. 2007, Koteš 2013, Zhao et al. 2012, Vu et al. 2005).

As a comparison of the behaviour of OPC concrete to geopolymer concrete, the models of Vidal et al. (2004) and Koteš (2013) for OPC concrete are plotted in *Fig. 14(b)*, where it can be noted that the geopolymer test results generally lie above those predicted by OPC models. However, given the scatter of test results, the suggestion of a corrosion crack width model based on currently available test data is premature.

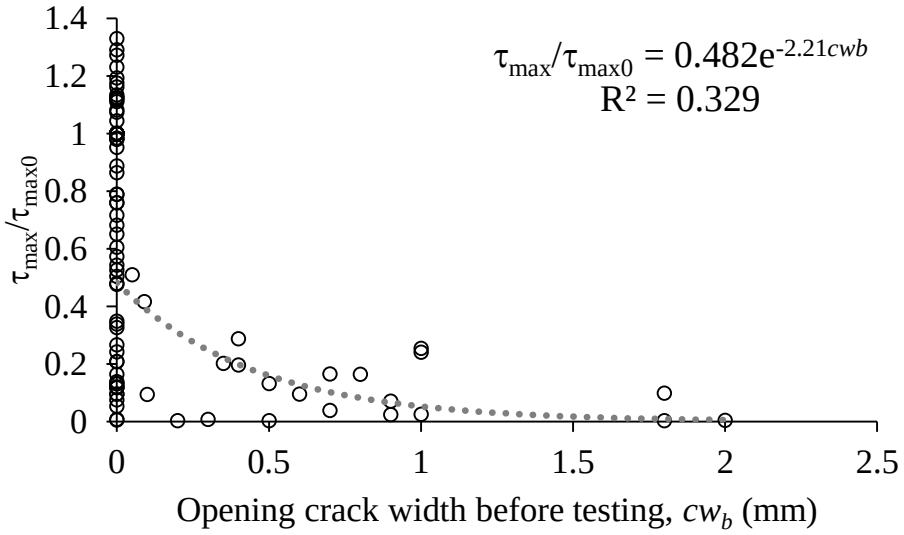

(a) τ_{max}/τ_{max0} versus cw_b

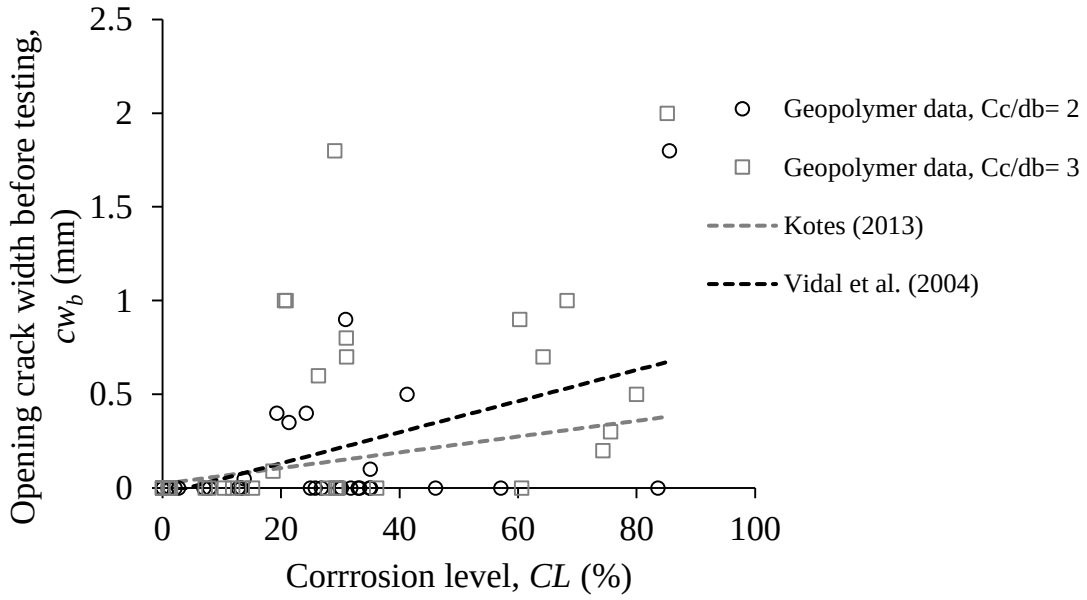

(b) cw_b versus *CL*

Figure 14. Crack width due to corrosion

Comparison of Experimental Results with Predictive models

Table 4 summarises the accuracy and precision of *Eqs. 4-13* in predicting the key points of the idealised bond stress slip relationship presented in *Fig. 4*. It can be seen that, in general, the model performs well at predicting the strength parameters, that is τ_{max} and τ_{bf}, as well as at predicting the slip parameters δ_1 and δ_{max}. The scatter in these parameters arises due to the difficulty in identifying a single slip corresponding to the peak stress or the frictional resistance in *Figs. S1* and *S2*.

Table 4. Comparison of Test Results with Predictive Proposed Models

Statistics	$(\tau_{max})_{exp}/(\tau_{max})_{pre}$	$(\delta_1)_{exp}/(\delta_1)_{pre}$	$(\tau_{bf})_{exp}/(\tau_{bf})_{pre}$	$(\delta_{max})_{exp}/(\delta_{max})_{pre}$
Mean	1.06	1.00	1.01	1.01
Standard Deviation	0.34	0.46	0.28	0.70
COV	0.32	0.46	0.28	0.69

To show the difference in the bond strength between OPC concrete and geopolymer concrete, an experimental database of 196 test results compiled by Feng et al. (2015) for OPC concrete is compared to the test results obtained in this study in *Fig. 15*.

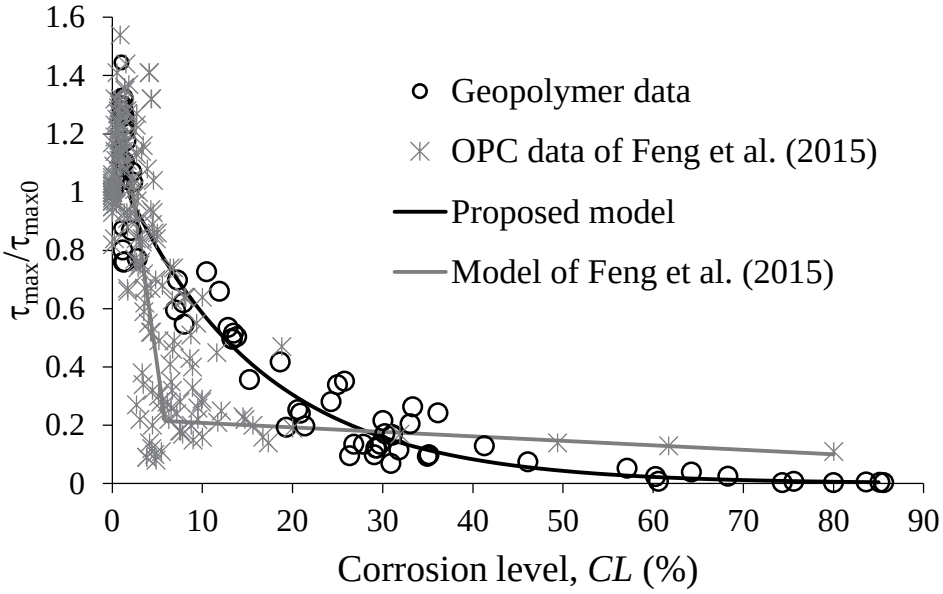

Figure 15. Comparison of OPC and geopolymer concrete test data and predictive models

As further comparison, the predictive model of Feng et al. (2015) for quantifying the bond strength of OPC concrete with corroded reinforcement is plotted along with the geopolymer bond strength model given by *Eqs. 9* and *10*. It should be noted that while several bond strength models for corroded reinforcement are available, in *Fig. 15*, for clarity only the model of Feng et al. (2015) is plotted as it has been shown to predict the bond strength of OPC concrete with the most accuracy and the least scatter. Further comparison to other well–known models (Cabrera 1996; Lee et al. 2002; Bhargava et al. 2007; Chung et al. 2008) is summarised in *Table 5*.

Table 5. Comparison of Bond Strength Predictive Models to OPC Concrete Experimental Data

Statistics	Feng et al. (2015)	Chung et al. (2008)	Bhargava et al. (2007)	Lee et al. (2002)	Cabrera (1996)
Mean	0.97	1.17	1.12	1.12	1.14
COV	0.16	0.22	0.22	0.25	0.24
Confidence intervals	0.72 - 1.22	0.74 - 1.59	0.71 - 1.54	0.66 - 1.58	0.68 - 1.60

Considering the test data plotted in *Fig. 15*, it can be seen that for corrosion levels less than 2% and greater than 30% there is not a significant difference between the variation in bond strength for geopolymer and OPC concretes. However when the corrosion level is between 5% and 30% a slower reduction in bond strength occurs. It is suggested that this may be because of the increased tensile strength of geopolymer concrete compared to OPC concrete which allows for the development of a larger volume of corrosion product prior to the formation of cracking.

Given there is minimal variation in the test results obtained for OPC and geopolymer concretes, it is suggested that the model of Feng et al. (2015) may be applied accurately to OPC and as a lower bound to geopolymer concrete. A comparison of the statistics of accuracy and scatter to the geopolymer model given by *Eqs. 9* and *10* and of Feng's OPC model when applied to geopolymer concrete is also given in *Table 5* where it is shown to be a reliable lower bound solution with similar scatter to that obtained for conventional concrete.

CONCLUSION

Knowledge of the bond between reinforcement and the surrounding concrete is essential in the analysis and design of RC members at both the serviceability and ultimate limit states. Corrosion of reinforcement not only reduces the strength of reinforcement, but also leads to deterioration of the bond which can cause increased deflections, reduced strengths ultimately failure. Therefore, there is a need to quantify the bond between reinforcement and geopoymer concrete, as well as the durability of the bond to corrosion. In this paper, the results of 102 pull tests conducted on class–F fly ash–based geopolymer concrete were presented. In these tests concrete cover–to–bar diameter (C_c/d_b) varied between 2 and 7.8; the level of corrosion ranged between 0% and 85% mass loss and the compressive strength between 33, 38 or 43 MPa. From statistical analyses of the test results a new bond model for geopolymer concrete with corroded reinforcement was proposed, alternatively it was shown that existing models for OPC concrete can be used as a safe lower bound for geopolymer concrete with corrosion levels up to 30%.

SUPPLEMENTARY MATERIAL:

Table S1. Summary of critical τ/δ test results

Specimens ID	d_b (mm)	C_c (mm)	C_c/d_b	CL (%)	cw_b (mm)	cw_a (mm)	τ_{max} (MPa)	δ_1 (mm)	δ_{max} (mm)	τ_{bf} (MPa)
Compressive strength, f'_c= 33 MPa										
Specimen 1	12	24	2	0	0	0	17.68	1.42	6.60	5.30
Specimen 2	12	24	2	0	0	0	17.25	1.35	6.70	4.90
Specimen 3	12	36	3	0	0	0	18.78	1.40	6.30	5.80
Specimen 4	12	36	3	0	0	0	19.33	1.52	6.20	6.00
Specimen 5	12	48	4	0	0	0	19.01	1.04	6.80	10.00
Specimen 6	12	48	4	0	0	0	19.12	1.01	3.00	10.00
Specimen 7	16	32	2	0	0	0.55	17.44	1.32	2.40	3.00
Specimen 8	16	32	2	0	0	0.4	16.71	1.09	2.40	3.00
Specimen 9	16	48	3	0	0	1.1	18.49	1.12	2.00	4.00
Specimen 10	16	48	3	0	0	0.2	18.52	1.22	3.90	6.00
Specimen 11	16	64	4	0	0	0	19.15	1.18	5.90	10.50
Specimen 12	16	64	4	0	0	0	19.37	1.19	7.50	10.50
Specimen 13	16	117	7.3	0	0	0	19.38	1.20	5.30	14.00
Specimen 14	16	117	7.3	0	0	0	19.29	1.39	6.50	11.00
Specimen 15	12	24	2	1.33	0	0	19.52	1.02	6.10	5.00
Specimen 16	12	24	2	0.95	0	0.1	18.24	1.07	5.50	4.00
Specimen 17	12	36	3	1.14	0	0.5	15.06	0.82	5.20	2.90
Specimen 18	12	36	3	0.96	0	0.2	16.46	1.10	5.50	3.50
Specimen 19	16	32	2	2.11	0	0.3	15.15	1.09	3.30	3.80
Specimen 20	16	32	2	2.74	0	0.6	13.47	0.95	1.80	2.90
Specimen 21	16	48	3	1.22	0	0.5	14.06	1.08	2.60	2.00
Specimen 22	16	48	3	1.38	0	0.45	14.07	1.11	4.30	2.00
Specimen 23	12	24	2	12.82	0	0	9.49	1.28	5.10	1.80
Specimen 24	12	24	2	13.77	0.05	0.2	8.91	1.54	4.60	1.90
Specimen 25	12	36	3	11.86	0	0	12.40	1.42	4.50	2.00
Specimen 26	12	36	3	10.45	0	0.8	13.66	0.82	2.90	2.00
Specimen 27	16	32	2	24.26	0.4	0.8	4.92	1.84	6.70	0.40
Specimen 28	16	32	2	21.35	0.35	0.5	3.46	2.61	7.50	0.20
Specimen 29	16	48	3	20.57	1	1.5	4.71	3.14	6.50	0.40
Specimen 30	16	48	3	20.85	1	1.6	4.47	0.44	4.80	0.40
Specimen 31	12	24	2	33.30	0	0	4.66	1.26	4.20	1.00
Specimen 32	12	24	2	33.01	0	0	3.63	1.42	5.20	0.50
Specimen 33	12	36	3	31.02	0.8	1.1	3.13	1.32	4.20	0.40
Specimen 34	12	36	3	31.07	0.7	0.9	3.17	1.85	4.00	0.30
Specimen 35	16	32	2	19.30	0.4	0.7	3.37	2.28	6.70	0.30

Specimen 36	16	32	2	26.78	0	0	2.37	2.10	6.30	0.60
Specimen 37	16	48	3	18.63	0.09	0.12	7.72	1.94	6.30	0.70
Specimen 38	16	48	3	36.12	0	0	4.49	2.44	7.20	0.40
Specimen 39	12	24	2	46.07	0	0	1.32	3.19	6.00	0.30
Specimen 40	12	24	2	31.77	0	0	2.05	2.21	5.10	0.20
Specimen 41	12	36	3	64.23	0.7	0.9	0.75	1.22	6.40	0.16
Specimen 42	12	36	3	68.25	1	1.2	0.48	1.70	4.10	0.25
Specimen 43	16	32	2	34.93	0	0	1.63	3.12	6.20	0.25
Specimen 44	16	32	2	30.91	0.9	1.3	1.22	3.08	6.40	0.17
Specimen 45	16	48	3	26.30	0.6	0.8	1.77	2.47	6.70	0.30
Specimen 46	16	48	3	29.05	1.8	1.9	1.84	2.06	6.70	0.18
Specimen 47	12	24	2	57.09	0	0	0.94	0.78	3.20	0.20
Specimen 48	12	24	2	83.59	0	0	0.10	0.07	3.00	0.05
Specimen 49	12	36	3	60.58	0	0	0.15	0.10	3.20	0.09
Specimen 50	12	36	3	79.97	0.5	0.7	0.08	1.81	5.50	0.03
Specimen 51	16	32	2	85.55	1.8	1.9	0.06	1.00	4.50	0.01
Specimen 52	16	32	2	41.26	0.5	0.6	2.26	2.56	6.30	0.18
Specimen 53	16	48	3	60.25	0.9	1	0.46	2.06	6.80	0.07
Specimen 54	16	48	3	85.14	2	2.1	0.09	2.41	7.80	0.05
Compressive strength, f'_c= 43 MPa										
Specimen 55	12	24	2	0.00	0	0	22.00	1.55	5.10	6.00
Specimen 56	12	24	2	0.00	0	0	23.68	1.44	7.10	6.00
Specimen 57	12	36	3	0.00	0	0	26.73	1.97	7.40	9.00
Specimen 58	12	36	3	0.00	0	0	28.02	1.78	7.20	9.00
Specimen 59	12	24	2	7.95	0	0	12.04	1.77	5.30	2.00
Specimen 60	12	24	2	7.01	0	0.2	13.10	0.89	4.50	2.00
Specimen 61	12	36	3	7.85	0	0	16.58	1.78	4.20	5.00
Specimen 62	12	36	3	7.22	0	0	18.67	1.90	4.50	5.00
Specimen 63	12	24	2	13.29	0	0	10.90	2.03	4.90	1.00
Specimen 64	12	24	2	13.25	0	0	10.96	2.02	3.90	1.00
Specimen 65	12	36	3	15.22	0	0	9.56	1.81	4.30	1.00
Specimen 66	12	36	3	13.45	0	0	13.80	2.32	4.20	2.00
Specimen 67	12	24	2	24.98	0	0	7.47	1.28	4.40	1.80
Specimen 68	12	24	2	25.75	0	0	7.75	2.00	3.60	4.80
Specimen 69	12	36	3	29.34	0	0	3.26	1.56	4.20	0.40
Specimen 70	12	36	3	29.23	0	0	3.28	1.79	4.70	0.70
Specimen 71	12	24	2	30.22	0	0	3.77	2.70	5.70	1.00
Specimen 72	12	24	2	30.01	0	0	4.77	1.42	4.60	1.10
Specimen 73	12	36	3	27.84	0	0	3.61	2.35	5.10	0.85
Specimen 74	12	36	3	29.67	0	0	3.63	1.81	4.00	0.35
Specimen 75	12	24	2	35.04	0.1	0.15	2.16	2.26	5.10	0.60
Specimen 76	12	24	2	35.12	0	0	2.18	1.40	5.60	0.40
Specimen 77	12	36	3	74.31	0.2	0.5	0.11	2.11	4.60	1.10
Specimen 78	12	36	3	75.58	0.3	0.5	0.20	0.42	3.40	0.08

Compressive strength, f'_c= 38 MPa										
Specimen 79	12	94	7.8	0.00	0	0	18.53	1.75	6.00	4.00
Specimen 80	12	94	7.8	0.00	0	0	20.44	1.31	5.40	5.00
Specimen 81	12	94	7.8	0.00	0	0	21.45	1.69	6.40	6.00
Specimen 82	12	94	7.8	1.00	0	0	26.78	2.72	7.10	12.00
Specimen 83	12	94	7.8	1.20	0	0	23.68	1.92	4.30	11.00
Specimen 84	12	94	7.8	1.10	0	0	24.02	2.44	4.80	10.90
Specimen 85	12	94	7.8	1.32	0	0	22.38	1.63	5.90	8.00
Specimen 86	12	94	7.8	1.50	0	0	21.80	2.15	6.50	6.00
Specimen 87	12	94	7.8	1.15	0	0	23.40	1.44	5.20	6.00
Specimen 88	12	94	7.8	2.25	0	0	19.18	1.94	5.50	6.00
Specimen 89	12	94	7.8	2.14	0	0	19.83	1.73	6.00	6.00
Specimen 90	12	94	7.8	1.32	0	0	22.84	1.82	5.50	6.00
Specimen 91	16	92	5.8	0.00	0	0	23.70	2.08	8.80	9.50
Specimen 92	16	92	5.8	0.00	0	0	22.90	1.83	8.70	8.00
Specimen 93	16	92	5.8	0.00	0	0	23.79	2.65	8.50	10.00
Specimen 94	16	92	5.8	0.35	0	0	23.00	1.82	7.80	8.80
Specimen 95	16	92	5.8	0.31	0	0	23.52	1.86	6.70	9.50
Specimen 96	16	92	5.8	0.37	0	0	23.07	1.88	7.50	10.00
Specimen 97	16	92	5.8	0.80	0	0	25.22	2.20	6.20	10.00
Specimen 98	16	92	5.8	0.86	0	0	26.39	2.32	6.50	10.00
Specimen 99	16	92	5.8	0.85	0	0	26.40	2.47	6.60	10.00
Specimen 100	16	92	5.8	1.00	0	0	29.84	5.23	9.30	16.00
Specimen 101	16	92	5.8	1.20	0	0	30.30	6.12	10.20	16.00
Specimen 102	16	92	5.8	1.30	0	0	28.88	3.22	8.80	12.00

d_b= steel bar diameter, C_c= concrete cover, C_c/d_b= concrete cover-to-bar diameter ratio, CL= corrosion level, cw_b= opening crack width before testing, cw_a= opening crack width after testing, τ_{max}= ultimate bond stress, δ_1= displacement at maximum bond stress, δ_{max}= maximum displacement, τ_{bf}= frictional bond stress.

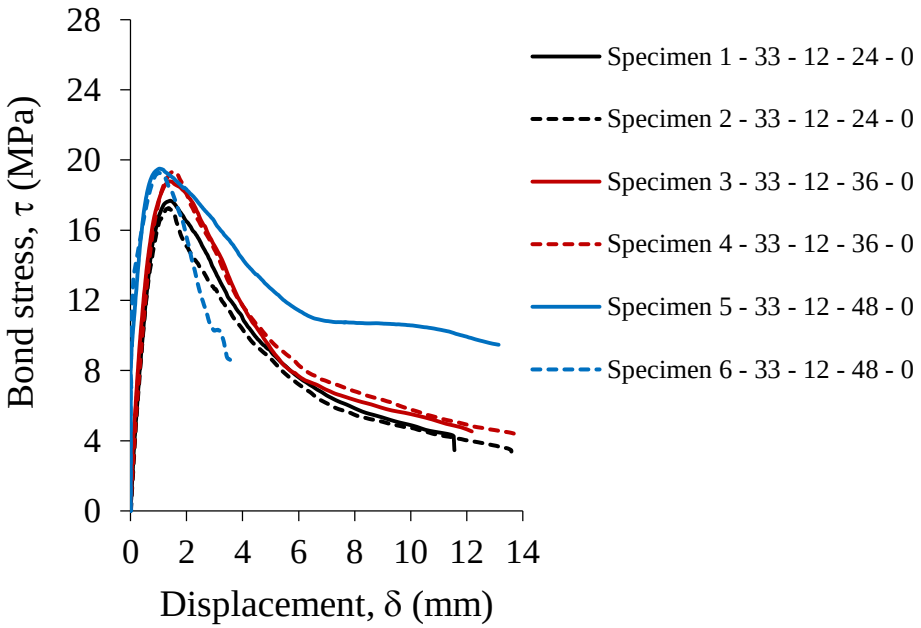

(a) f'_c = 33MPa, d_b= 12mm, C_c= 24, 36 or 48mm, CL= 0%

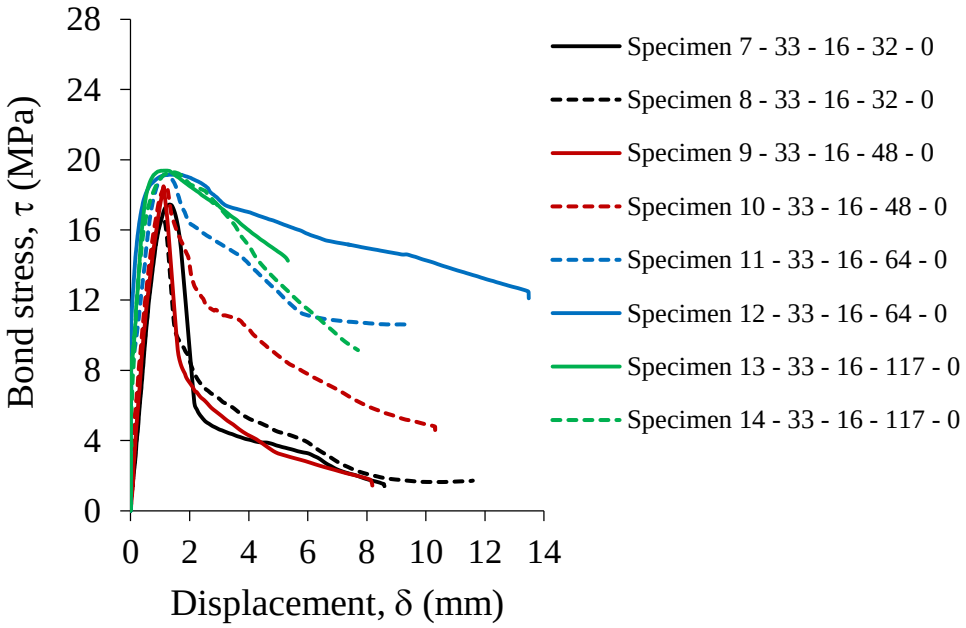

(b) f'_c = 33MPa, d_b= 16mm, C_c= 32, 48, 64 or 117mm, CL= 0%

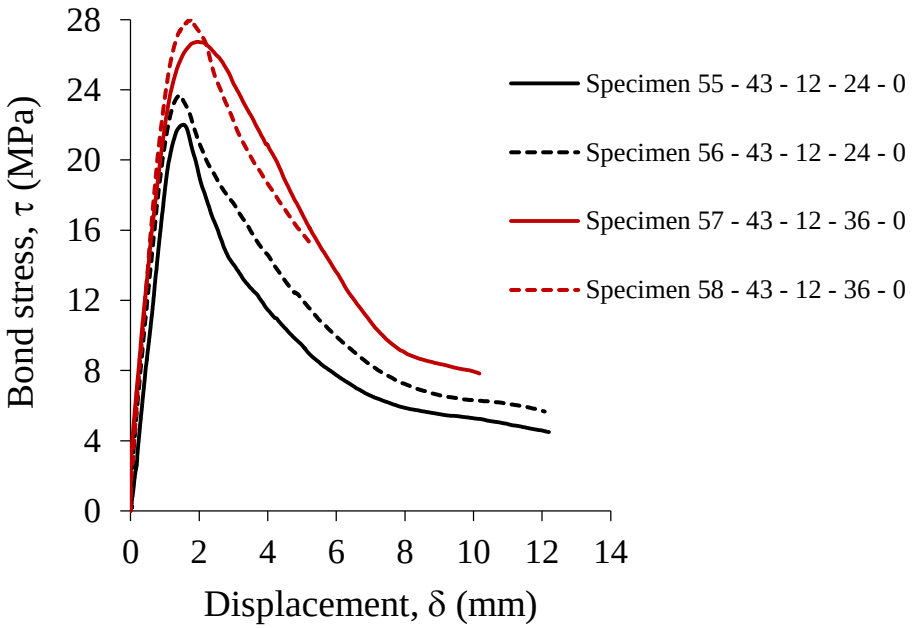

(c) f'_c = 43MPa, d_b= 12mm, C_c= 24 or 36mm, CL= 0%

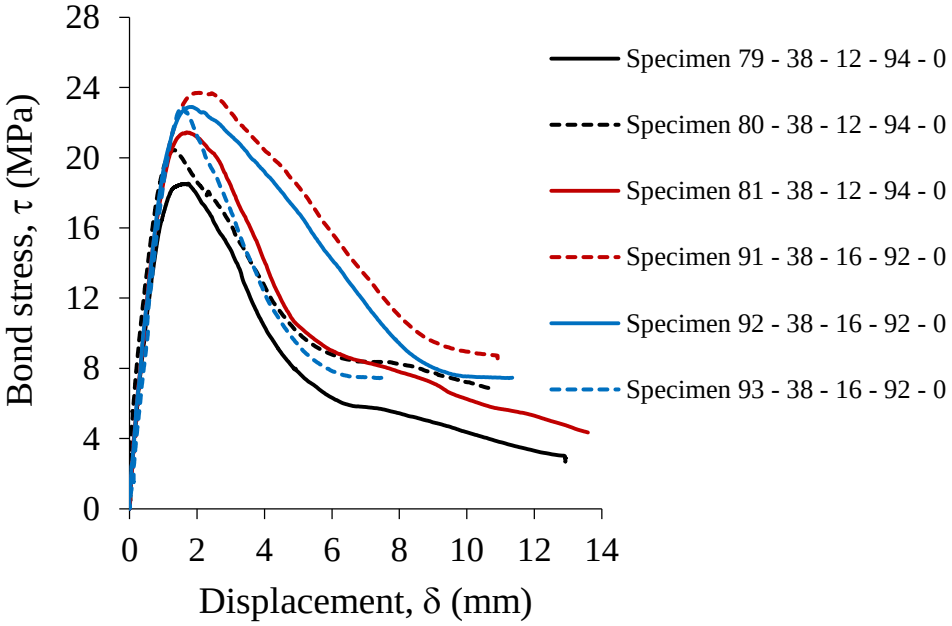

(d) f'_c = 38MPa, d_b= 12 or 16mm, C_c= 94 or 92mm, CL= 0%

Figure S1. Local bond stress–slip relationship of uncorroded specimens

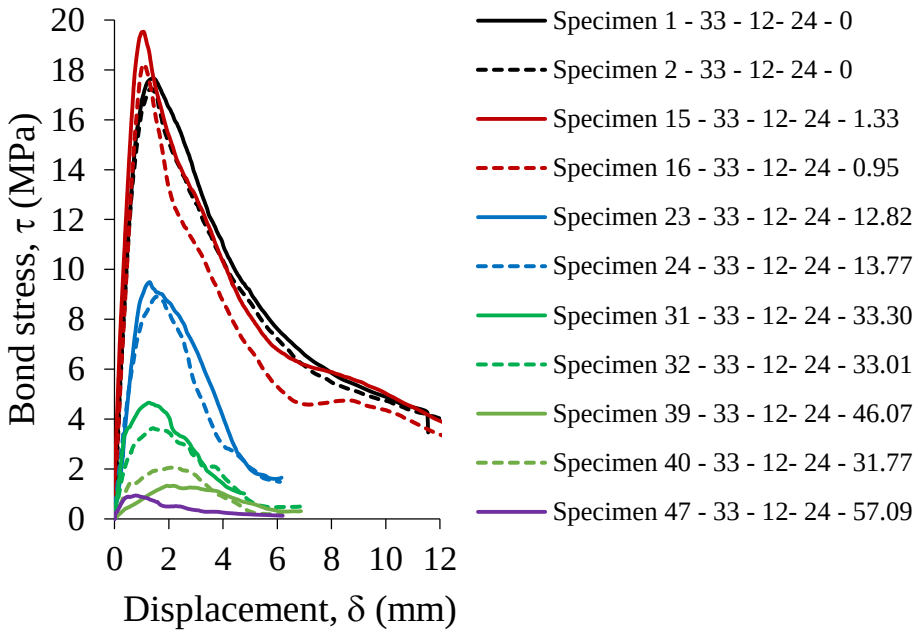

(a) f'_c = 33MPa, d_b= 12mm, C_c= 24mm, C_c/d_b = 2

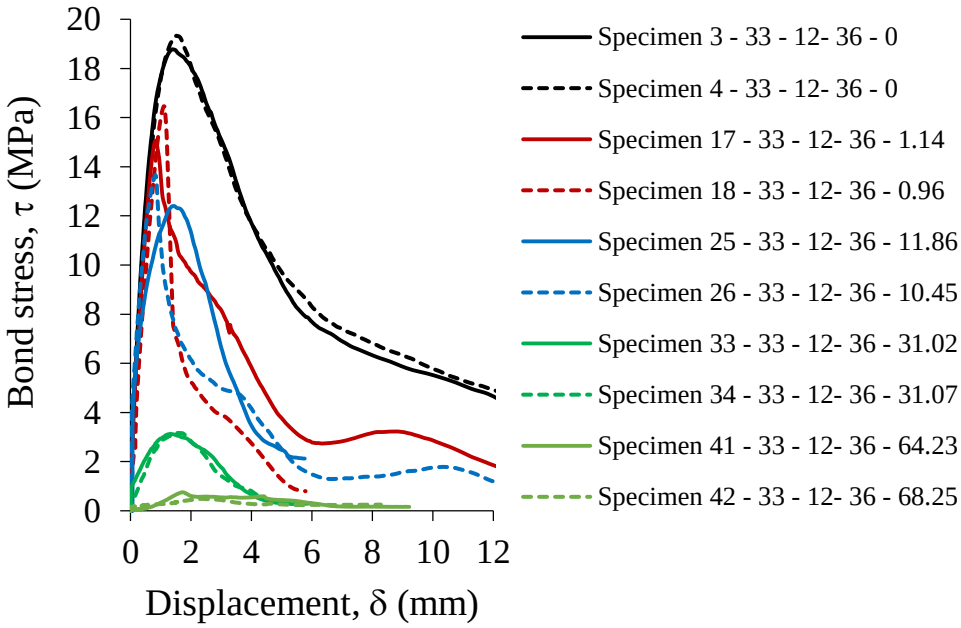

(b) f'_c = 33MPa, d_b= 12mm, C_c= 36mm, C_c/d_b = 3

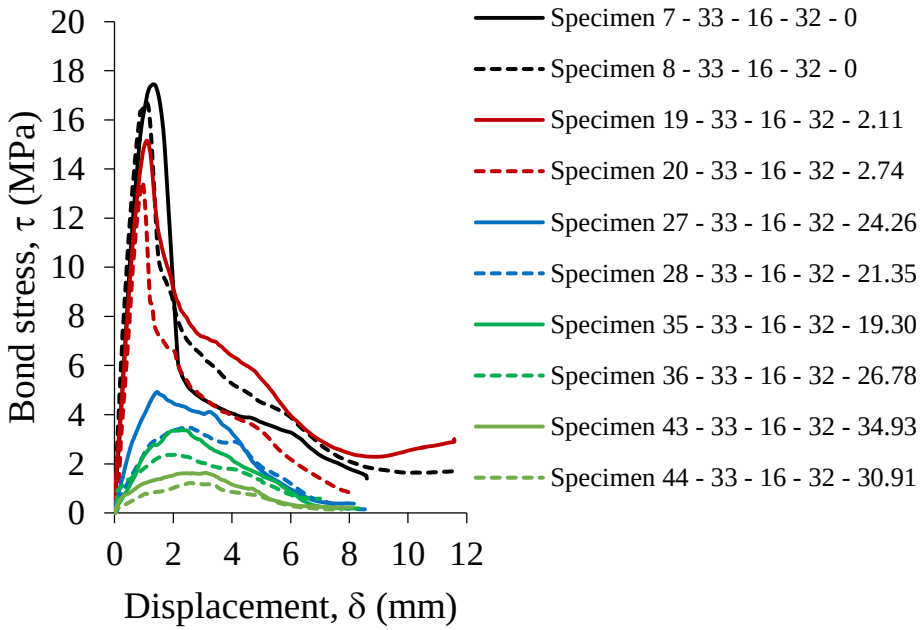

(c) f'_c = 33MPa, d_b= 16mm, C_c= 32mm, C_c/d_b = 2

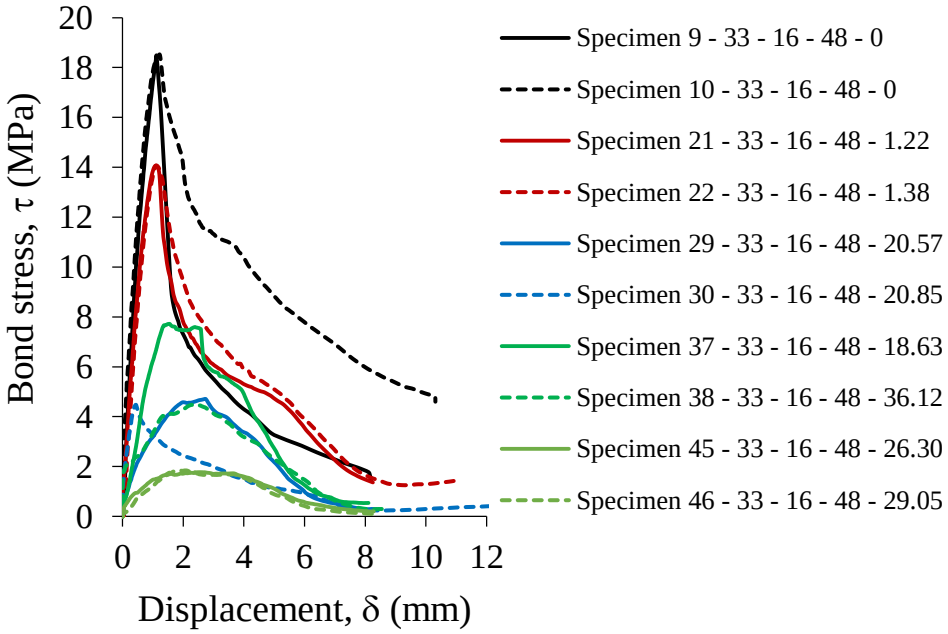

(d) f'_c = 33MPa, d_b= 16mm, C_c= 48mm, C_c/d_b = 3

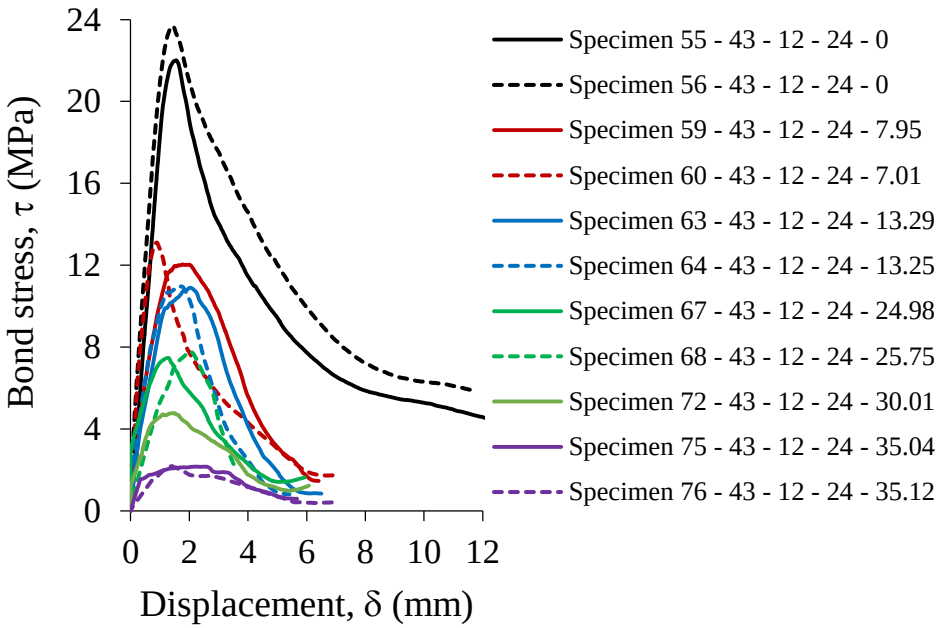

(e) f'_c = 43MPa, d_b= 12mm, C_c= 24mm, C_c/d_b = 2

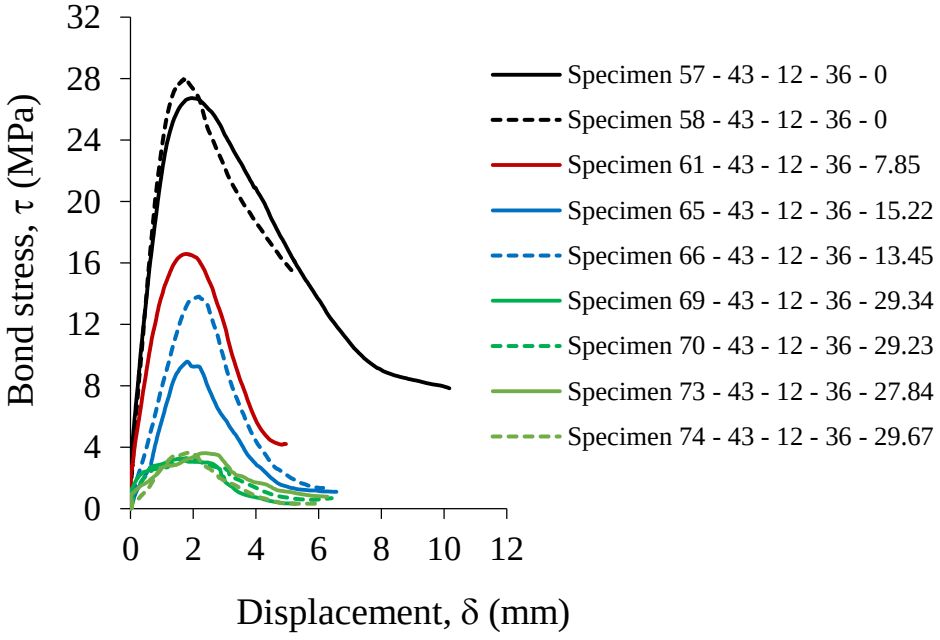

(f) f'_c = 43MPa, d_b= 12mm, C_c= 36mm, C_c/d_b = 3

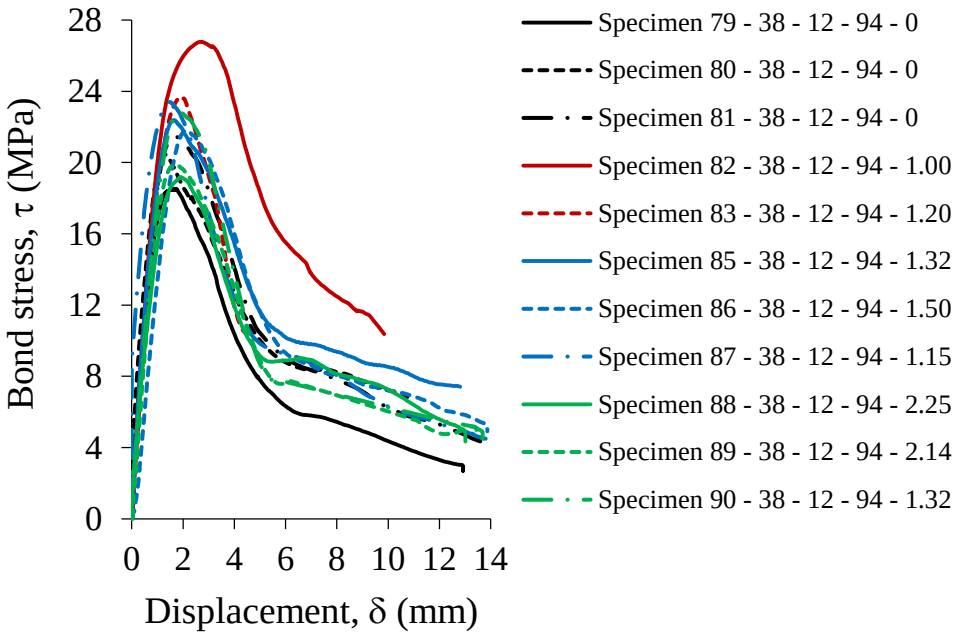

(g) f'_c = 38MPa, d_b= 12mm, C_c= 94mm, C_c/d_b = 7.8

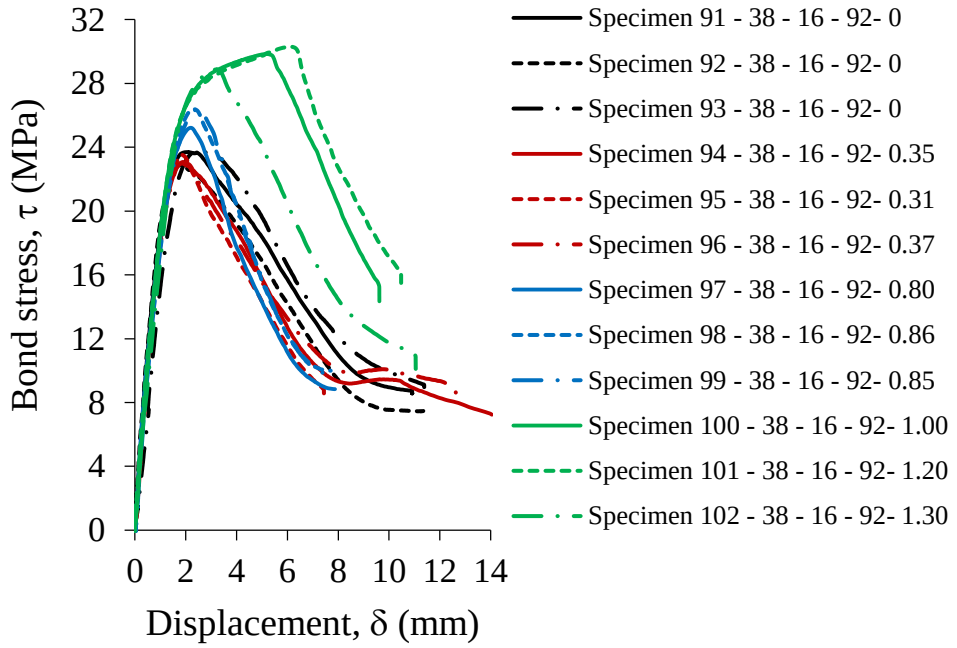

(h) f'_c = 38MPa, d_b= 16mm, C_c= 92mm, C_c/d_b = 5.75

Figure S2. Local bond stress–slip relationships of corroded specimens

REFERENCES

ACI 318 – 02 (2002). *Building Code Requirements for Structural Concrete*, Reported by ACI Committee 318.

ACI 318 (1995). *Building Code Requirements for Reinforced Concrete*, American Concrete Institute, Farmington Hills MI 48333.

ACI 408R-03 (2003). *Bond and Development of Straight Reinforcing Bars in Tension*, American Concrete Institute, Farmington Hills.

Albitar, M., Mohamed Ali, M. S., Visintin, P., Drechsler, M. (2015). "Effect of granulated lead smelter slag on strength of fly ash-based geopolymer concrete." *Construction and Building Materials*, vol. 83, pp. 128–135, DOI: 10.1016/j.conbuildmat.2015.03.009.

Albitar, M., Visintin, P., Mohamed Ali, M. S. and Drechsler, M. (2014). "Assessing behaviour of fresh and hardened geopolymer concrete mixed with class-F fly ash." *KSCE Journal of Civil Engineering*, Vol. 19, No. 5, pp. 1445-1455, DOI 10.1007/s12205-014-1254-z.

Almusallam, A. A., Al-Gahtani, A. S., Aziz, A. and Rasheeduzzafart (1995). "Effect of reinforcement corrosion on bond strength." *Construction and Building Materials*, Vol. 10, No. 2, pp. 123–129, DOI:10.1016/0950-0618(95)00077-1.

Almusallam, A. A., Al-Gahtani, A. S., Aziz, A. R., Rasheeduzzafar (1996). "Effect of reinforcement corrosion on bond strength." *Construction and Building Materials*, Vol. 10, No. 2, pp. 123–129, DOI:10.1016/0950-0618(95)00077-1 .

Al-Sulaimani, G., Kaleemullah, M., Basunbul, I., Rasheeduzzafar (1990). "Influence of corrosion and cracking on bond behavior and strength of reinforced concrete members." *ACI Structural Journal*, Vol. 87, No. 2, pp. 220–231.

AS 3600 (2003). *Concrete Structures Code*, Standard Association of Australia, Sydney.

ASTM C234-91a (1991) *Standard Test Method for Comparing Concretes on the Basis of the Bond Developed with Reinforcing Steel*, American Society for Testing and Materials annual book of standards.

ASTM C1585 – 13 (2007). *Standard Test Method for Measurement of Rate of Absorption of Water by Hydraulic-Cement Concretes*, American Society for Testing and Materials annual book of standards, DOI: 10.1520/C1585-13.

ASTM C 642 – 06 (2008). *Standard test method for density, absorption, and voids in hardened concrete,* American Society for Testing and Materials annual book of standards, DOI: 10.1520/C0642-13.

ASTM G1-03 (2003). *Standard Practice for Preparing, Cleaning, and Evaluating Corrosion Test Specimens,* American Society for Testing and Materials.

Bhargava, K., Ghosh, A. K., Mori, Y. and Ramanujam, S. (2007). "Corrosion induced bond strength degradation in reinforced concrete – analytical and empirical models." Nuclear Engineering and Design, Vol. 237, pp. 1140–1157, DOI: 10.1016/j.nucengdes.2007.01.010.

Cabrera, J. G. (1996). "Deterioration of concrete due to reinforcement steel corrosion." *Cement & Concrete Composites,* vol. 18, pp. 47–59, DOI: 10.1016/0958-9465(95)00043-7.

Castel, A. and Foster, S. J. (2015). "Bond strength between blended slag and class F fly ash geopolymer concrete with steel reinforcement." *Cement and Concrete Research,* Vol. 72, pp. 48–53, DOI: 10.1016/j.cemconres.2015.02.0160008-8846.

Castel, A., Khan, I., Gilbert, R. I. (2015). "Development length in reinforced concrete structures exposed to steel corrosion: A correction factor for AS3600 provisions Australian." *Journal of Structural Engineering*, Vol. 16, No. 2, pp. 89–98, DOI: 10.7158/S14-006.2015.16.2.

CEB-FIP (1993). *Design of concrete structures,* CEB-FIP-Model-Code 1990, British Standard Institution, London, UK.

Chang, E. H. (2009). "Shear and bond behaviour of reinforced fly ash-based geopolymer concrete beams." Thesis presented for the degree of Doctor of Philosophy, Curtin University of Technology, Perth.

Chindaprasirt, P., Chareerat, T. and Siricicatnanon, V, (2007). "Workability and strength of coarse high calcium fly ash geopolymer." *Cement Concrete Compos,* Vol. 29, pp. 224–229, DOI: 10.1016/j.cemconcomp.2006.11.002.

Choi, C. K., Cheung, S. H. (1996). "Tension stiffening model for planar reinforced concrete members." *Computers & Structures,* Vol. 59, No. 1, pp. 179–190, DOI: 10.1016/0045-7949(95)00146-8.

Chung, L., Jay, J. H., Yi, S. T. (2008). "Bond strength prediction for reinforced concrete members with highly corroded reinforcing bars." *Cement and concrete composites,* Vol. 30, No. 7, pp. 603–611, DOI: 10.1016/j.cemconcomp.2008.03.006.

Ciampi, V., Eligehausen, R., Bertero, V. V., and Popov, E. P. (1982). "Analytical model for concrete anchorage of reinforcing bar under generalized excitation." *Report No, 82/23,* University of California, Berkeley, California, pp. 111.

Darwin, D. (2005). "Tension development length and lap splice design for reinforced concrete members." *Progress in Structural Engineering and Materials,* Vol. 7, pp. 210–225, DOI: 10.1002/pse.206.

Davidovits, J. (1991). "Geopolymers: Inorganic polymeric new materials." *Journal of Thermal Analysis,* Vol. 37, No. 8, pp. 1633–1656, DOI: 10.1007/BF01912193.

Davidovits, J. (1994). "Global warming impact on the cement and aggregates industries." *World Resource Review,* Vol. 6, No. 2, pp. 263–278.

Feng, Q, Visintin, P. and Oehlers, D. J. (2015). "Deterioration of bond-slip due to corrosion of steel reinforcement in RC." *Magazine of Concrete Research,* in press.

Fu, X. and Chung, D. D. L. (1997). "Effect of corrosion on the bond between concrete and steel rebar." *Cement and Concrete Research,* Vol. 27, No. 12, pp. 181 l–18 15, DOI:10.1016/S0008-8846(97)00172-5.

François, R., Khan, I. and Dang, V. H. (2013). "Impact of corrosion on mechanical properties of steel embedded in 27-year-old corroded reinforced concrete beams." *Materials and Structures,* Vol. 46, No. 6, pp. 889–910, DOI: 10.1617/s11527-012-9941-z.

Gupta, A. K., Maestrini, S. R. (1990). "Tension stiffening model for reinforced concrete bars." *Journal of Structural Engineering,* Vol. 116, No. 3, pp.769–790, DOI:org/10.1061/(ASCE)0733-9445(1990)116:3(769).

Kim, J. and Park, J. H. (2015). "An experimental investigation of bond properties of reinforcements embedded in geopolymer concrete." *International Journal of Civil, Structural, Construction and Architectural Engineering,* Vol. 9, No. 2, pp. 92–95.

Knight, D., P. Visintin, D. Oehlers, and M. Jumaat. (2013). "Incorporating Residual Strains in the Flexural Rigidity of RC members with Varying Degrees of Prestress and Cracking." *Advances in Structural Engineering,* Vol. 16, No. 10, pp. 1701–1718, DOI: 10.1260/1369-4332.16.10.1701.

Koteš, P. (2013). "Influence of corrosion on crack width and pattern in an RC beam." *Concrete and Concrete Structure 2013 Conference,* Vol. 65, pp. 311–320, DOI: 10.1016/j.proeng.2013.09.048.

Lee, H., Noguchi, T. and Tomosawa, F. (2002). “Evaluation of the bond properties between concrete and reinforcement as a function of the degree of reinforcement corrosion.” *Cement and Concrete Research*, Vol. 32, pp. 1313–1318, DOI: 10.1016/S0008-8846(02)00783-4.

Marti, P., Alvarez, M., Kaufmann, W., and Sigrist, V. (1998). “Tension chord model for structural concrete.” *Structural Engineering International*, Vol. 8, No. 4, pp. 287–298, DOI: http://dx.doi.org/10.2749/101686698780488875.

Otieno, M., Beushausen, H., Alexander, M. (2011). “Prediction of corrosion rate in RC structures – A critical review.” *Modelling of Corroding Concrete Structures*, Vol. 5, pp. 15–37, DOI: 10.1007/978-94-007-0677-4_2.

Pantazopoulou, S. J. and Papoulia, K.D. (2001). “Modeling cover-cracking due to reinforcement corrosion in RC structures.” *Journal of Engineering Mechanics*, Vol. 127, No. 4, pp. 342–351, DOI: 10.1061/(ASCE)0733-9399(2001)127:4(342), 342-351.Rasheeduzzafar, Al-Saadoun, S. S. and Al-Gahtani, A. S. (1992). “Corrosion cracking in relation to bar diameter, cover, and concrete quality.” *Journal of Materials in Civil Engineering*, vol. 4, No. 4, pp. 327–342, DOI: 10.1061/(ASCE)0899-1561(1992)4:4(327).

Reddy, D. V., Edouard, J., and Sobhan, K. (2013). “Durability of fly ash–based geopolymer structural concrete in the marine environment.” *Journal of Materials in Civil Engineering*, Vol. 5, No. 6, pp, 781–787, DOI: 10.1061/(ASCE)MT.1943-5533.0000632.

Sarker, P. (2010). “Bond strengths of geopolymer and cement concretes,” *Materials and Structures*, vol. 44, pp. 1021–1030, DOI 10.1617/s11527-010-9683-8.

Selby, D. R. (2011). “An investigation into the bond of steel reinforcement in geopolymer and ordinary portland cement concrete.” Final thesis report submitted in partial fulfilment of the requirements of the subject: ZEIT 4500 Civil Engineering: Project, Thesis and Seminar of the Bachelor of Engineering Degree in Civil Engineering, School of Civil Engineering University College The University of New South Wales Australian Defence Force Academy, CANBERRA.

Sofi, M., van Deventer, J. S. J., Mendis, P. A. and Lukey, G. C. (2007). “Bond performance of reinforcing bars in inorganic polymer concretes (IPCs).” *Journal of Materials Science*, Vol. 42, No. 9, pp 3107–3116, DOI 10.1007/s10853-006-0534-5.

Song, G. and Shayan, A. (1998). “Corrosion of steel in concrete: causes, detection and prediction.” A state-of-the-art review, in: Review Report 4, ARRB Transport Research Ltd., Victoria, Vermont, 1998.

Vidal, T., Castel, A. and François, R. (2004). "Analyzing crack width to predict corrosion in reinforced concrete." *Cement and Concrete Research,* Vol. 34, pp. 165–174, DOI: 10.1016/S0008-8846(03)00246-1.

Vidal, T., Castel, A. and François, R. (2007). "Corrosion process and structural performance of a 17 year old reinforced concrete beam stored in chloride environment." *Cement and Concrete Research,* Nov 30; Vol. 30, No. 11, pp.1551-61, DOI: 10.1016/j.cemconres.2007.08.004.

Visintin, P., Oehlers, D.J., Haskett, M. (2013). "Partial-interaction time dependent behaviour of reinforced concrete beams." *Engineering Structures*, Vol. 49, pp. 408–420, DOI:10.1016/j.engstruct.2012.11.025.

Visintin, P., Oehlers, D., Wu, C., and Griffith, M. C. (2012). "The reinforcement contribution to the cyclic behaviour of reinforced concrete beam hinges." *Earthquake Engineering & Structural Dynamics*, Vol. 41, No. 12, pp. 1591–1608, DOI: 10.1002/eqe.1189.

Vu, K., Stewart, M.G. and Mullard, J. (2005). "Corrosion-induced cracking: experimental data and predictive models." *ACI structural journal*, Vol. 102, No. 5, pp. 719–726.

Winnefeld, F., Leemann, A., Lucuk, M., Svoboda, P. and Neuroth, M. (2010). "Assessment of phase formation in alkali activated low and high calcium fly ashes in building materials." *Construction and Building Materials*, Vol. 24, No. 6, pp. 1086–1093, DOI: 10.1016/j.conbuildmat.2009.11.007.

Zhang, T., Visintin, P., Oehlers, D. J., Griffith, M. (2014). "Presliding shear failure in prestressed RC beams. I: Partial-Interaction mechanism." *Journal of Structural Engineering*, Vol. 140, No. 10, DOI: 10.1061/(ASCE)ST.1943-541X.0000988.

Zhao, Y., Yu, J., Hu, B. and Jin, W. (2012). "Crack shape and rust distribution in corrosion-induced cracking concrete." *Corrosion science*, Vol. *55*, pp.385–393, DOI: 10.1016/j.corsci.2011.11.002.

CHAPTER 3: Tension–Stiffening Mechanisms

Background

Having established the mechanical properties and durability characteristics of geopolymer concretes, the tension–stiffening mechanism of geopolymer concrete is of a considerable importance. That is, in order to determine the deformation of reinforced concrete members, quantifying the tensile stresses carried by concrete between cracks that stiffens reinforced concrete members is essential. The bond properties of geopolymer concrete investigated in Chapter 2 can now be used to further study the tension–stiffening mechanisms of geopolymer concrete. This chapter presents the results of an investigation into the tension–stiffening and cracking mechanisms of conventional and geopolymer concretes. It also incorporates the mechanics–based solutions developed for OPC concrete with the bond properties that are set for geopolymer concrete to predict the performance of geopolymer concrete in terms of crack formation, crack width and crack spacing. It is shown that the tension–stiffening responses of geopolymer concretes are similar to that of OPC concrete, which suggests the required design guidelines can easily be modified to incorporate geopolymer concretes.

List of Manuscripts

Albitar, M., Mohamed Ali, M.S., and Visintin, P. (2016). "Evaluation of tension–stiffening, crack spacing and crack width of geopolymer concretes." *Engineering Structures*, submitted.

Statement of Authorship

Title of Paper	Evaluation of tension–stiffening, crack spacing and crack width of geopolymer concretes
Publication Details	Albitar, M., Mohamed Ali, M.S., and Visintin, P. (2016). "Evaluation of tension–stiffening, crack spacing and crack width of geopolymer concretes." *Engineering Structures*, submitted.
Publication Status	Submitted

Principal Author

Name of Principal Author (Candidate)	Albitar, M		
Contribution to the Paper	Performed the experiment, interpreted and analysed data and wrote manuscript.		
Overall percentage (%)	85%		
Certification:	This paper reports on original research I conducted during the period of my Higher Degree by Research candidature and is not subject to any obligations or contractual agreements with a third party that would constrain its inclusion in this thesis. I am the primary author of this paper.		
Signature		Date	

Name of Co-Author	Mohamed Ali, M.S.		
Contribution to the Paper	Supervised development of work, helped to evaluate and edit the manuscript.		
Signature		Date	20/10/16

Name of Co-Author	Visintin, P.		
Contribution to the Paper	Supervised development of work and assisted in manuscript evaluation.		
Signature		Date	20/10/2016

Evaluation of Tension–Stiffening, Crack Spacing and Crack Width of Geopolymer Concretes

ABSTRACT

An experimental study on the behaviour of reinforced geopolymer concretes in uniaxial tension is conducted to investigate the tension–stiffening effect on the deformation and crack width of geopolymer concretes. The knowledge related to tension–stiffening mechanisms can expedite implementing such a new material in concrete industry and be widely used in structural applications. The experimental program included 20 concentrically reinforced concrete prisms, 16 of which were manufactured using class–F fly ash and granulated lead smelter slag (GLSS)–based geopolymer concretes. The remaining four prisms were manufactured from ordinary Portland cement (OPC) as a reference for evaluating the tension–stiffening mechanism of geopolymer concretes. All prisms were reinforced with a single reinforcing bar placed longitudinally through the centroid of each specimen. Two different reinforcing bar diameters were investigated, namely 12mm and 16mm. The results show that both geopolymer and OPC concretes exhibit similar tension–stiffening mechanisms. The experimental results are subsequently compared with predictions from models developed for OPC concrete. The comparison suggests that the models provide reasonably accurate predictions for the spacing and crack width of geopolymer concrete, suggesting that provisions developed for OPC concrete can be applied to predict the behaviour of geopolymer concrete.

KEYWORDS: Geopolymer concrete; tension–stiffening; crack width; crack spacing; fly ash; granulated lead smelter slag.

List of symbols

A_c	Concrete area
$A_{c,eff}$	Effective concrete area (= $A_c - A_s$)
A_s	Steel bar area
B	Bond force
C_c	Concrete cover
d_b	Steel bar diameter
E_c	Elastic modulus of concrete
E_s	Elastic modulus of steel
F_r	Force in reinforcement
f'_c	Concrete stress
f'_{ct}	Tensile strength of concrete
f'_{cf}	Flexural strength of concrete
$f_{c,m}$	Axial tension stress of concrete in a reinforced prism
f_{sy}	Yield stress of steel
k	Member stiffness
k_b	Linear bond stiffness
k_t	Factor depending on the duration of load
L_{per}	Length of bonded perimeter
L_{pri}	Length of loaded prism
N	Axial load of tension member
N_c	average load carried by cracked concrete (= $\beta A_c f_{cr}$)
N_{cr}	Axial cracking stress

N_s	Average load carried by steel
N_{sb}	Bear steel stress (at crack locations)
$N_{sb,cr}$	Bear steel stress at first cracking (= N_{cr}/A_s)
P_{cr}	Load acting on concrete at first cracking
S_{linear}	Linear crack spacing
$S_{non\text{-}linear}$	Non-linear crack spacing
$S_{r,m}$	Maximum crack spacing
w_c	Width of crack
$w_{c,Max}$	Maximum crack width
$w_{c,Ave}$	Average crack width
$w_{c,Min}$	Minimum crack width
β	Tension stiffening bond factor (= N_c/P_{cr})
τ	Bond stress
τ_{max}	Maximum shear stress
Δ	Slip
Δ_1	Slip at τ_{max}
Δ_{max}	Maximum slip where the shear stress is zero
Δ'	Slip-strain (=$\varepsilon_s - \varepsilon_c$)
Δ_{cr}	Slip at crack face
Δ_r	Half of the crack width
$\Delta\varepsilon_{s,max}$	Tension stiffening strain at first cracking (= P_{cr} / A_sE_s)
$\Delta\varepsilon_s$	Tension stiffening strain (= $\beta\Delta\varepsilon_{s,max}$)
ε_m	Average member strain
ε_{cr}	Concrete cracking strain
ε_c	Concrete strain
ε_s	Steel strain
ε_{sb}	Bare steel strain
$\varepsilon_{sb,cr}$	Bare steel strain at concrete cracking
σ_s	Steel stress
ρ	Reinforcement ratio (= A_s/A_c)
ρ_{eff}	Effective reinforcement ratio (= $A_s/A_{c,eff}$)
α_e	Modulus ratio (= E_s/E_c)

INTRODUCTION

Tension–stiffening effect in a reinforced concrete member is the ability of concrete to carry tensile stresses between cracks, which has a significant influence on the member global serviceability limit states. The tensile stresses carried by the concrete between cracks under service load level plays a significant role in the deformation of reinforced concrete in which it effectively stiffens the member response (Bischoff 2001). The interaction theory shown in *Figure 1* illustrates the importance of bond properties between the reinforcement steel and the adjacent concrete. *Figure 1(a)* shows a loaded prism with an induced crack at the crack face (Δ_{cr}). In the case of full interaction where the bond between concrete and reinforcing steel is infinitely stiff, the load is shared by both the reinforcement and the concrete according to their respective axial rigidities, which results in extending the concrete by the exact amount of the applied force, as illustrated in the path O-A in *Figure 1(b)*. In contrast, the concrete will not move at all in the case of no interaction, as shown in path O-C in *Figure 1(b)*. Thus, the actual extension of the concrete in the case of full interaction is equal to the force in the bar (F_r) divided by the rigidity of the reinforcement plus the rigidity of the concrete ($F_r/E_sA_s+E_cA_c$), whilst only the reinforcement rigidity is considered when the interaction is absent. In reality, the interaction is assumed to be in between those two extreme cases depending on bond properties, which means that the extension of concrete depends on the stiffness of the member (k_b) (F_r/k_b), as shown in path O-B in *Figure 1(b)*.

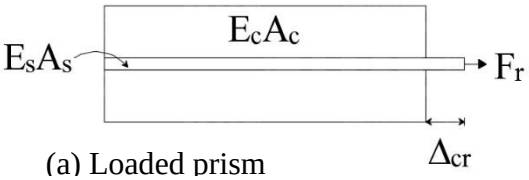

(a) Loaded prism

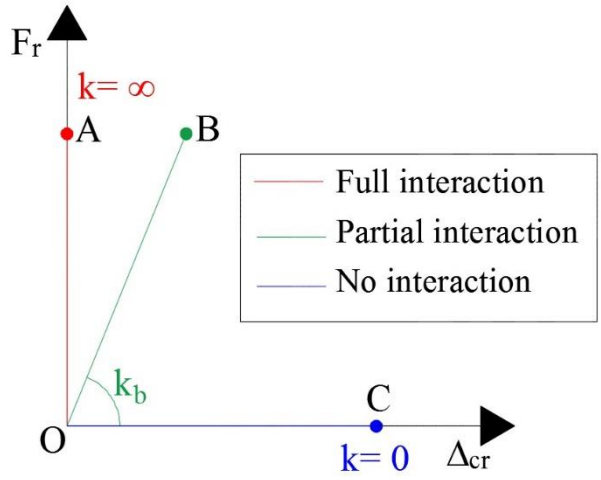

(b) Interaction conditions

Figure 1. Interaction theory

Considering the behaviour of tension–stiffening prism at the initial crack shown in *Figure 2* from which the mechanics of tension–stiffening have been described by (Muhamad et al. 2012; Knight et al. 2013). *Figure 1(a)* shows a concentrically loaded prism with a

concrete cross–section area (A_c), steel reinforcement cross–section area (A_s) and bonded perimeter length (L_{per}), while *Figure 2(b)* shows the loaded prism with length (L_{pri}).

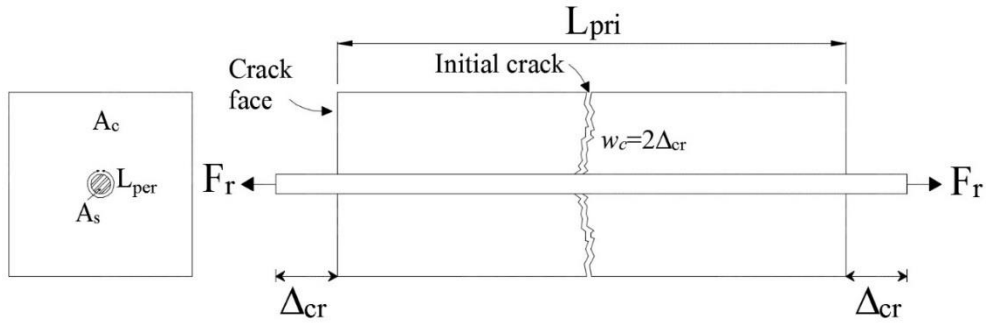

(a) Cross–section (b) Loaded prism

Figure 2. Tension–stiffening prism

A slip at the crack face (Δ_{cr}) is caused when a crack intercepts reinforcement due to the transferred applied load from the reinforcement steel to the adjacent concrete, which allows separation of crack face. Thus, the total crack width (w_c) at the level of reinforcement load is $2\Delta_{cr}$, which can be quantified through a partial–interaction theory that incorporates the bond stress–slip (τ–Δ) relationship. The idealised τ–Δ relationship is shown in *Figure 3* where τ_{max} is the maximum shear stress, Δ_1 is the slip at τ_{max} and Δ_{max} is the maximum slip where the shear stress is zero. It is with considerable importance to identify the bond between the reinforcement and the concrete, which controls the partial–interaction behaviour magnitude and hence influence the deflection (Bischoff 2005; Gilbert 2007), crack widths and tension–stiffening (Balazs 1993; Bischoff 2005; Albitar et al. 2016) of reinforced concrete members.

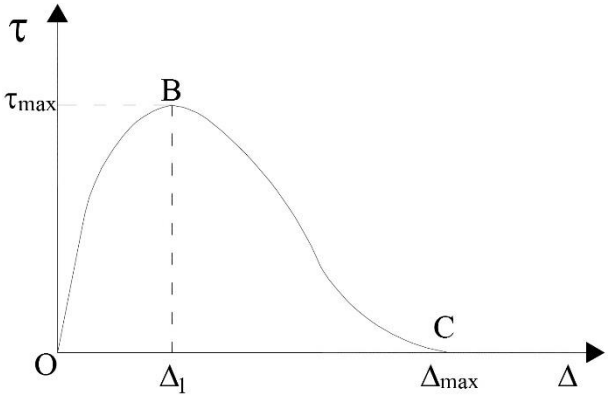

Figure 3. Bond stress–slip relationship

To date, only one study has been undertaken to quantify the tension–stiffening behaviour of geopolymer concrete (Ganesan et al. 2014). The study investigated ten reinforced geopolymer concrete (60m x 60 x 600 mm) prisms of which eight specimens were incorporated with steel-fibre-reinforced and only two specimens represent the tension–stiffening response of plain reinforced fly ash concrete under uniaxial tension force. The

study found that crack spacing can be accurately enough predicted using the expression provided by CEB–FIP (1992). However, due to the limited number of specimens and the incorporation of steel-fibre-reinforced, it is important to experimentally investigate the partial–interaction behaviour of geopolymer concrete including cracking pattern, crack widths, crack spacing and tension–stiffening. This study, therefore, has been undertaken with the aim of quantifying the tension behaviour of reinforced geopolymer concrete and hence verifying the accuracy of existing mechanics, semi–mechanics and empirical provisions developed for ordinary Portland cement (OPC) concrete.

Tension–stiffening mechanisms

Several numerical procedures for simulating partial–interaction mechanics have been developed (Mohamed Ali et al. 2008; Haskett et al. 2008; Oehlers et al. 2011; Muhamad et al. 2012; Visintin et al. 2012; Visintin et al. 2013a; Knight et al. 2013; Zhang et al. 2014). The loaded prism with length (L_{pri}) that is shown in *Figure 4* illustrates the tension–stiffening mechanism. According to the work of (Visintin et al. 2013b; Knight et al. 2013; Zhang et al. 2014), the prism in *Figure 2(b)* is sliced into *n* number of short elements of length (L_e) in which the slip within an element (Δ_n) can be assumed to be constant (Oehlers et al. 2011). *Figure 4* shows Element 1 with an imposed slip (Δ_1) and a force in reinforcement (F_r). An iterative shooting method can be used to find a solution by guessing the corresponding F_r that induces the required Δ_1:

- Based on the local bond stress–slip properties shown in *Figure 3*, the share stress τ_1 for a given slip can be calculated for Element 1 in *Figure 4*, which can then be integrated over the area to drive the bond force B_1, which is equal to $\tau_1 L_e L_{per}$.
- Based on the equilibrium, knowing the slip on the left hand side of the element and the bond force, the load in reinforcement on the other hand side can be calculated, which will be reduced to F_r-B_1.
- Knowing the force of the concrete on the left hand side, which is zero at the crack location, by equilibrium, the concrete force on the other had side can be calculated, which will be increased to B_1.
- Based on the modulus of the materials, the average strains of reinforcement and concrete can be calculated, and the difference between the two strains (ε_r-ε_c) is referred to as the slip–strain $d\Delta/dx$ (Δ').
- The change in the stiffness over the element is slip–strain multiplied by the element length $\Delta' L_e$.
- Based on the fact that $\Delta' L_e$ is equal to (ε_r-ε_c)L_e, the slip in Element 2 (Δ_2) equals Δ_1 minus (ε_r-ε_c)L_e.

By repeating the procedure outlined above all the way along the length of the prism in *Figure 4*, the variation of the slip Δ, the slip–strain Δ', the reinforcement strain ε_r and the concrete strain ε_c for a given slip at the bar end will be determined. It should be noted that to use this analysis, the prism must be concentrically loaded and symmetrically reinforced to ensure that the prism is without flexure and no bending stresses are developed.

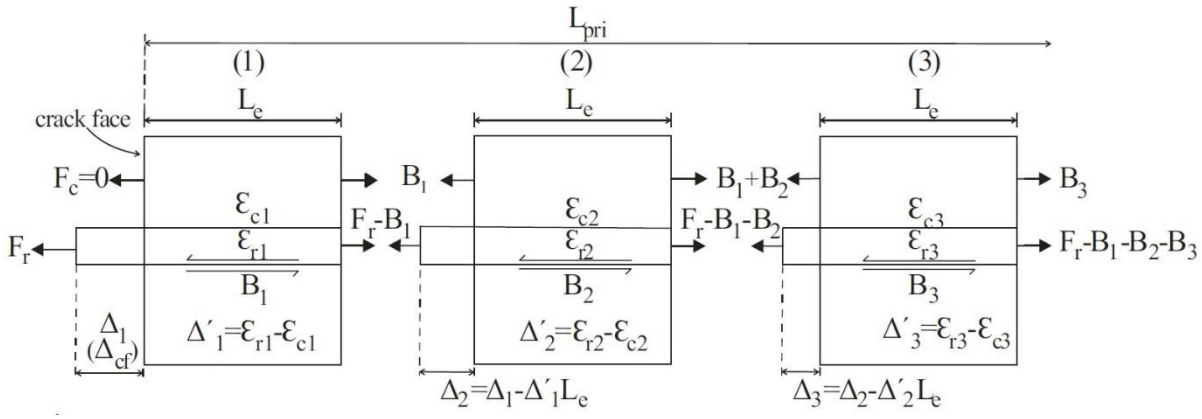

Figure 4. Tension–stiffening analysis

Load sharing approach

Tension–stiffening is characterised by a bond factor β which can be determined based on load sharing approach (Fields and Bischoff 2004). The typical tensile response of a reinforced prism is shown in *Figure 5*. The load sharing approach can be used to determine the post–cracking stress–strain response of concrete in tension using the average load carried by cracked concrete. That is, once the concrete had cracked, the axial load (N) of a tension member is shared between the reinforcing steel and the concrete. Thus, for a given average member strain (ε_m), the steel carries an average load (N_s) and the concrete carries the remaining average load (N_c) (*Eq. 1*).

$$N = N_s + N_c \leq A_s f_y \tag{1}$$

The first concrete crack occurs at an axial member load (N_{cr}) when the tensile strength of concrete (P_{cr}) is reached its maximum. Once the concrete is cracked, the P_{cr} will vary between zero at a crack location to a certain value between the cracks. Therefore, the average load carried by the concrete can be expressed by

$$N_c = \beta P_{cr} \tag{2}$$

The bond factor β accounts for the variation of concrete tensile stress between the cracks and it is equal to N_c/P_{cr}. The bond factor is a normalised value in which it is independent of the concrete tensile strength and the concrete area. The average load carried by the reinforcement steel can then be expressed by

$$N_s = A_s E_s \varepsilon_m = N - \beta P_{cr} \tag{3}$$

In order to use this load sharing approach, the average load carried by the concrete N_c needs to be determined first using an appropriate bond factor β for a given average

member strain ε_m. The axial load N can then be determined by adding the N_c to the corresponding average load carried by the reinforcement N_s.

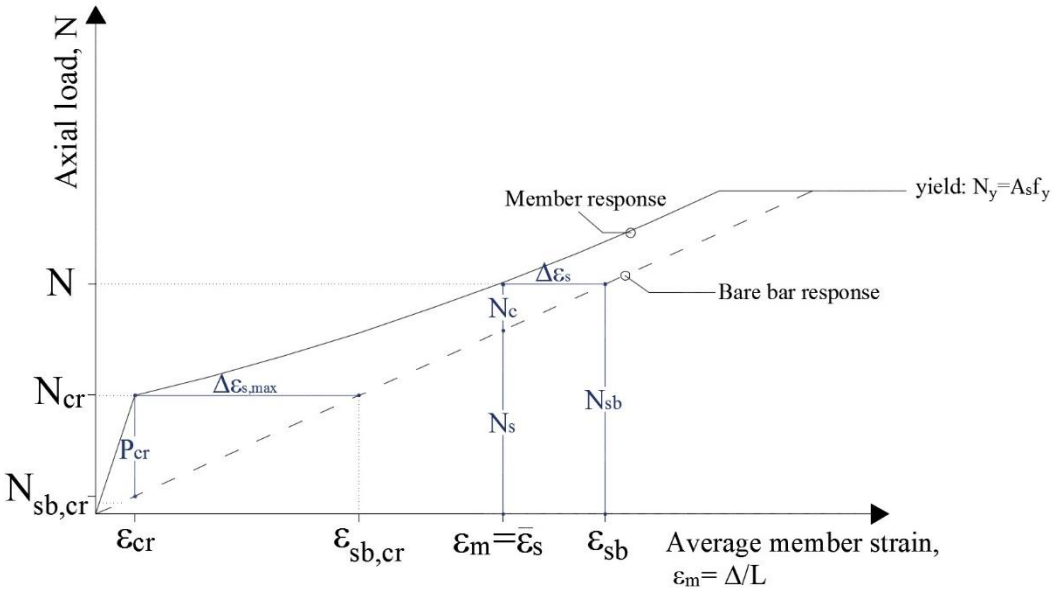

Figure 5. Typical response of tension–stiffening in a reinforced concrete

EXPERIMENTAL PROGRAM

Test specimens and materials

A total of 20 reinforced concrete prisms were designed, manufactured, and tested under direct tension at the laboratory of Adelaide University. All the specimens had a length of 650mm and the considered cross–sections were 75x75mm and 150x150mm. A single reinforcing conventional ribbed steel bar of either 12mm or 16mm was placed longitudinally through the centroid of each specimen. The tension axial load was applied at each extended end of the reinforcement bar as shown in *Figure 6*.

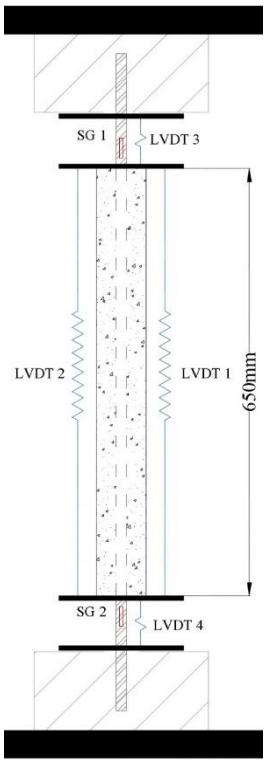

Figure 6. Test set–up

The specimens were manufactured using three different types of concrete: OPC, fly ash and GLSS. To manufacture fly ash–based geopolymer concrete, low–calcium class–F fly ash produced at Port Augusta Power Station in South Australia was used, whereas GLSS–based geopolymer concrete was manufactured using 50% fly ash and 50% granulated lead smelter slag sourced from Nystar port Pirie in South Australia. The alkaline solution phase in both concrete types, fly ash and GLSS, consisted of a combination of sodium silicate (Na_2SiO_3) and 14 M sodium hydroxide (NaOH) pre–mixed with a ratio of Na_2SiO_3/NaOH of 1.5. The chemical compositions of OPC, fly ash and GLSS were determined by x–ray fluorescence (XRF) and are summarised in *Table 1*. The mixtures proportions of fly ash and GLSS concretes were developed by Albitar et al. (2014; 2015) and are presented in *Table 2*, together with mixture proportion of OPC concrete.

Table 1. Chemical compositions of OPC, fly ash and GLSS, (%)

Oxides	Fe_2O_3	SiO_2	Al_2O_3	CaO	MgO	SO_3
OPC	2.7	21.5	5.8	61.5	2.2	2.4
Fly ash	2.8	49.0	31.0	5.4	2.5	0.3
Granulated lead smelter slag	33.8	27.5	7.4	19.4	2.1	-

Table 2. The mixtures proportions, (kg/m^3)

Ingredients	Fly ash	GLSS	OPC
OPC	0	0	391.3
Fly ash	424.8	212.4	0
Aggregate (10 mm)	1176	1176	1076
Sand	576	0	717.3
Granulated lead smelter slag	0	788.4	0
Sodium hydroxide (14M)	63.36	63.36	0
Sodium silicate	95.04	95.04	0
Superplasticiser (ViscoCrete 10)	48	48	0
Water	16.8	16.8	180

Instrumentation and testing procedure

Two linear variable displacement transformers (LVDTs) were placed on opposite sides of the prism as shown in *Figure 6* to measure the average axial elongation of the concrete prism form which the average concrete strain was determined. To measure the average axial strain in the reinforcing steel bar, two 5mm strain gauges were used, one on each end. In addition, two LVDTs were mounted on each edge of prisms to measure the slip of steel relative to concrete after deducting the strain of the steel, as shown in *Figure 7(b)*.

All test specimens were subjected to short–term uniaxial tensile load at a rate of 0.1 mm/min in a 900 kN capacity universal testing machine using tension grips to hold the extended bars at each end, as shown in *Figure 7(a)*. The test continued until yielding of the steel bar for specimens with a 75x75mm cross–section, whereas specimens with a 150x150mm cross–section the test continued until near rupturing of steel bar. Development of cracking, crack widths and spacing were measured at their occurrence, at the occurrence of other new cracks and at 10kN interval.

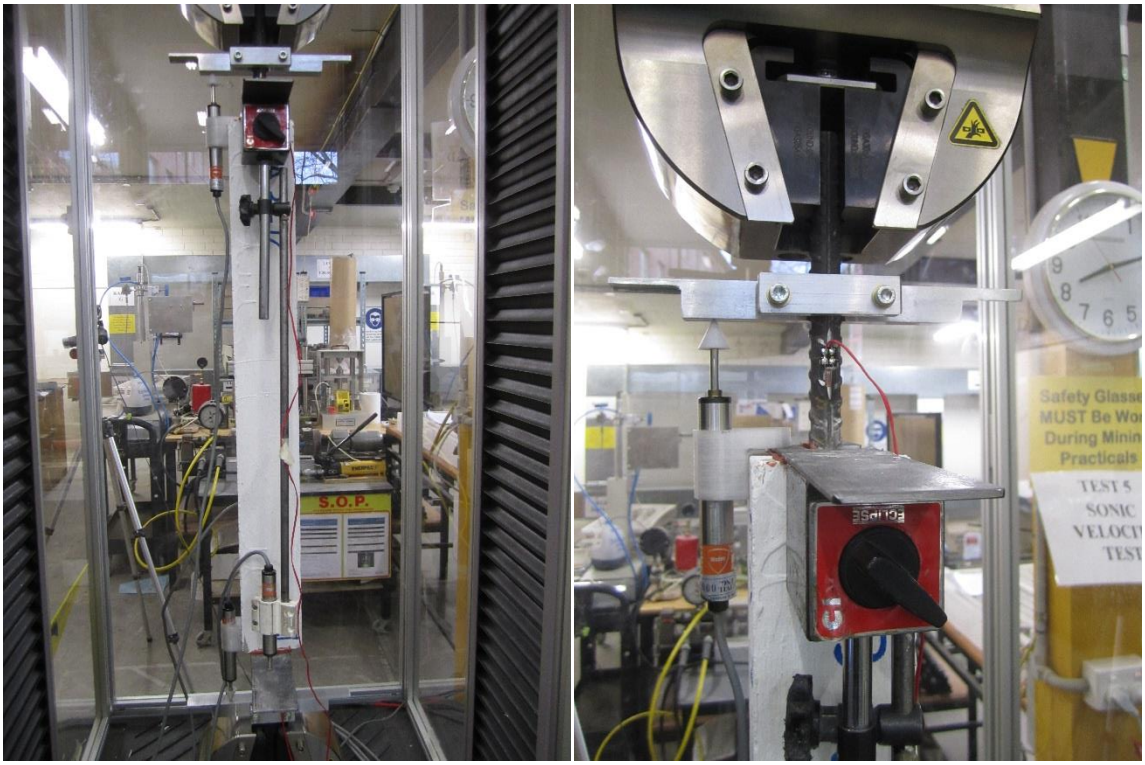

(a) Testing machine (b) Instrumentations

Figure 7. Testing machine and instrumentations.

EXPERIMENTAL RESULTS

Failure mode

The failure modes of all the test specimens are shown in *Figure 8*, together with the corresponding crack numbers and locations for each specimens. All the specimens developed transverse tensile cracks along the prism. The formation of the first transverse crack (primary crack) generally appeared near the middle portion of the specimens, and as the load increased, additional cracks appeared, while the first crack widened. In some specimens, two cracks appeared simultaneously in which each one took place near the edge on the opposite side as can be seen in *Figure 8(b-ii)* where cracks 1 and 2 appeared at the same time. Longitudinal splitting cracks appeared on some specimens tested until near rupturing of the steel bar, and two specimens, OPC 1 – 12 – 150 and OPC 2 – 12 – 150, did not develop any cracks.

(a-i) FA 1 – 12 – 75 (a-ii) Crack numbers and locations

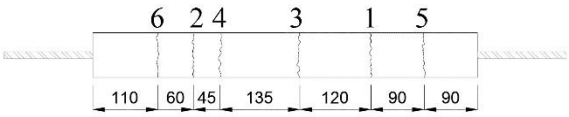

(b-i) FA 2 – 12 – 75

(b-ii) Crack numbers and locations

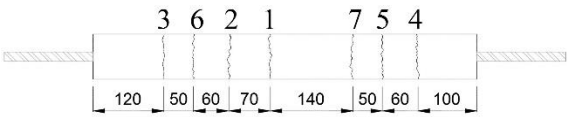

(c-i) FA 3 – 16 – 75

(c-ii) Crack numbers and locations

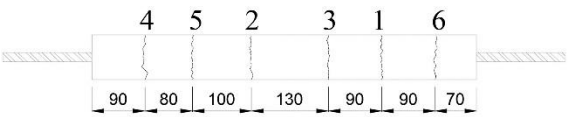

(d-i) FA 4 – 16 – 75

(d-ii) Crack numbers and locations

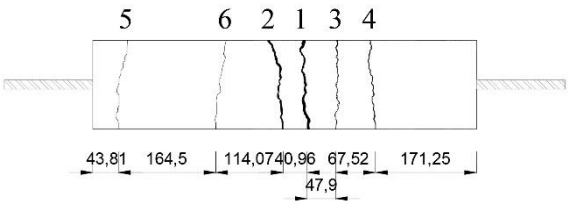

(e-i) FA 1 – 12 – 150

(e-ii) Crack numbers and locations

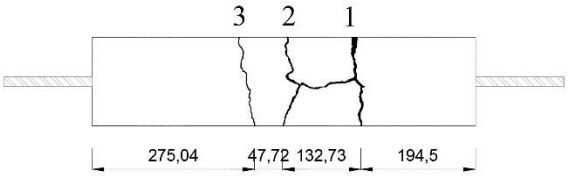

(f-i) FA 2 – 12 – 150

(f-ii) Crack numbers and locations

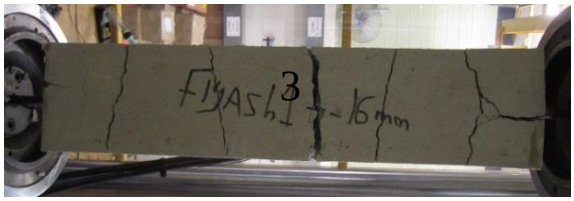

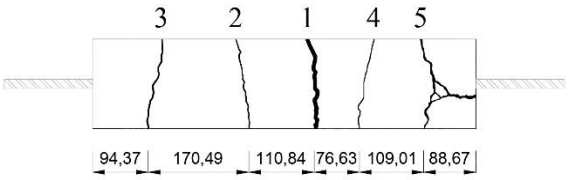

(g-i) FA 3 – 16 – 150

(g-ii) Crack numbers and locations

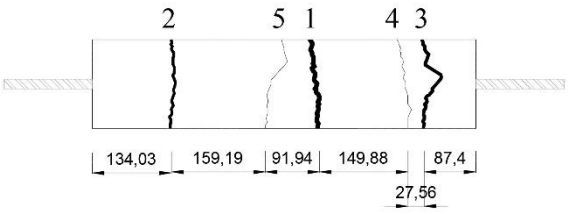

(h-i) FA 4 – 16 – 150

(h-ii) Crack numbers and locations

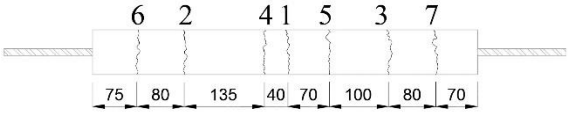

(i-i) GLSS 1 – 12 – 75

(i-ii) Crack numbers and locations

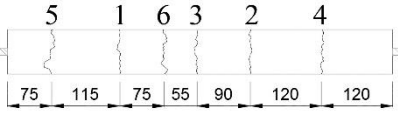

(j-i) GLSS 2 – 12 – 75

(j-ii) Crack numbers and locations

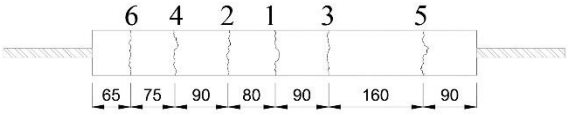

(k-i) GLSS 3 – 16 – 75

(k-ii) Crack numbers and locations

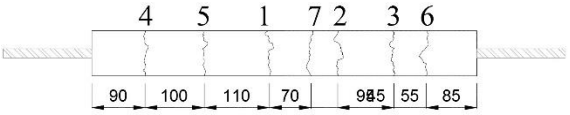

(l-i) GLSS 4 – 16 – 75

(l-ii) Crack numbers and locations

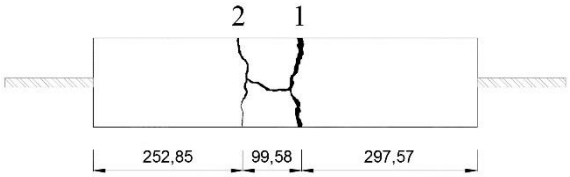

(m-i) GLSS 1 – 12 – 150

(m-ii) Crack numbers and locations

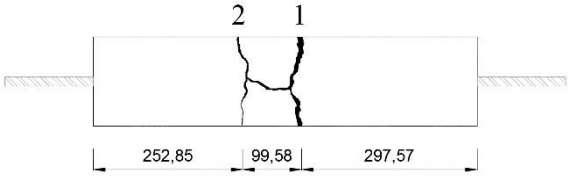

(n-i) GLSS 2 – 12 – 150

(n-ii) Crack numbers and locations

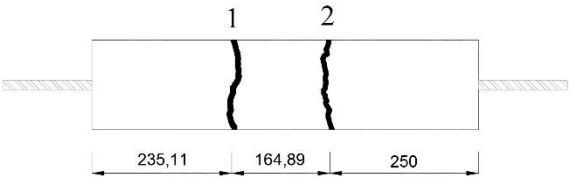

(o-i) GLSS 3 – 16 – 150

(o-ii) Crack numbers and locations

(p-i) GLSS 4 – 16 – 150

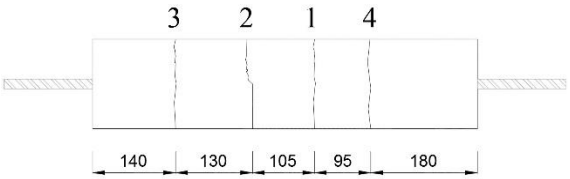

(p-ii) Crack numbers and locations

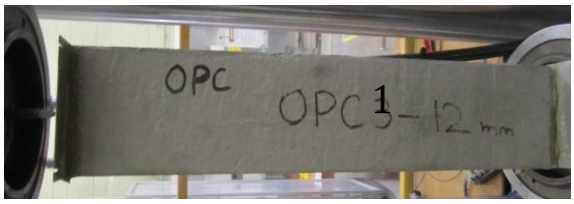

(q-i) OPC 1 – 12 – 150

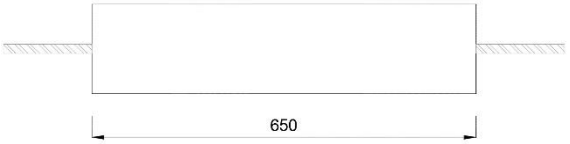

(q-ii) Crack numbers and locations

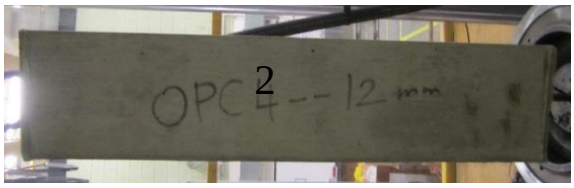

(r-i) OPC 2 – 12 – 150

(r-ii) Crack numbers and locations

(s-i) OPC 3 – 16 – 150

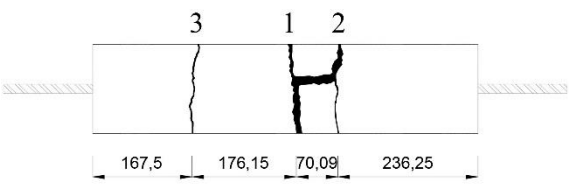

(s-ii) Crack numbers and locations

(t-ii) OPC 4 – 16 – 150

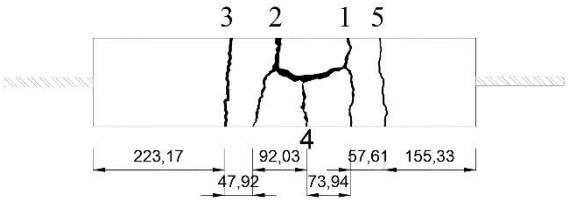

(t-ii) Crack numbers and locations

Figure 8. Failure modes of tension–stiffening specimens

Material properties

The measured material properties of each concrete including compressive strength (f'_c), splitting tensile strength (f'_{ct}), flexural strength (f'_{cf}) and elastic modulus of concrete (E_c) are tabulated in *Table 3*. It should be noted that the mix designs listed in *Table 2* were used to manufacture all the specimens, but prisms with a cross–section of 75mm were tested after 2 months of casting, whereas prisms with a 150mm cross–section were tested after 5 months of casting. This difference in testing time resulted in different strengths. Although the compressive strength of geopolymer concrete is different to that of OPC concrete, the results are used to validate and compare the mechanisms that govern the behaviour of tension stiffening. The properties of reinforcing steel bar were measured through tensile tests, which were performed on three bars of each diameter, and the mechanical properties of the reinforcement bars are documented in *Table 4*.

Table 3. Material properties of concretes

Concrete type	f'_c (MPa)	f'_{ct} (MPa)	f'_{cf} (MPa)	E_c (MPa)
Specimens with 75x75mm cross–section				
Fly ash	35	3.4	4.1	29123.5
GLSS	29	3.2	3.7	28879.3
Specimens with 150x150mm cross–section				
Fly ash	42	3.9	4.8	30957.6
GLSS	42	3.8	4.8	31563.2
OPC	62	4.2	5.5	32602.8

Table 4. Mechanical properties of the reinforcement bars

Nominal Diameter (mm)	Nominal area (mm^2)	Yield strength, f_{sy} (MPa)	Yield strain, ε_{sy}	Ultimate strength, f_{su} (MPa)	Ultimate strain, ε_{sh}
12	113	550	0.0030	628	0.0422
12	113	548	0.0028	620	0.0392
12	113	520	0.0026	610	0.0321
16	201	530	0.0035	583	0.0468
16	201	530	0.0033	590	0.0371
16	201	530	0.0034	600	0.0350

Tension–stiffening test results

Experimentally recorded axial cracking load (N_{cr}) of all the reinforced prisms are presented in *Table 5*, together with concrete cracking strain (ε_{cr}) and tensile strength of concrete at initial cracking (P_{cr}). The crack widths at different loading stages are presented in *Table S1*, which is available in the supplementary data. The axial load versus average axial strain relationships of each test specimens are depicted in *Figure 9*. It should be noted that the specimens are designated by letters FA, GLSS or OPC to describe the binder

material followed by the number that corresponds to their series and then the diameter of the steel bar and finally the cross–section.

Table 5. Test results of tension–stiffening specimens

Specimen ID	f_c (MPa)	Reinforcement ratio (%)	N_{cr} (kN)	ε_{cr} (x10^{-6})	$\varepsilon_{sb,cr}$ (x10^{-6})	$N_{sb,cr}$ (kN)	P_{cr} (kN)	f_{cr} (MPa)
FA 1 - 12 - 75	35	2.05	11.56	126.87	520.25	1.58	9.98	1.81
FA 2 - 12 - 75		2.05	12.66	191.93	553.20	3.89	8.77	1.59
FA 3 - 16 - 75		3.71	17.71	255.5	450.71	9.99	7.72	1.42
FA 4 - 16 - 75		3.71	18.28	243.88	463.86	9.47	8.81	1.62
FA 1 – 12 - 150	42	0.51	56.35	35.89	2530.56	0.66	55.69	2.49
FA 2 – 12 - 150		0.51	61.22	40.073	2887.68	0.8	60.42	2.70
FA 3 – 16 - 150		0.90	41.65	17.05	1061.49	0.62	41.03	1.84
FA 4 – 16 - 150		0.90	67.84	53.73	1733.08	2	65.84	2.95
GLSS 1 – 12 - 75	29	2.05	9.21	122.77	422.03	2.58	6.63	1.20
GLSS 2 – 12 - 75		2.05	9.64	237.84	444.53	4.88	4.76	0.86
GLSS 3 – 16 - 75		3.71	8.13	70.3	225.45	2.67	5.46	1.01
GLSS 4 – 16 - 75		3.71	9.24	64.54	252.24	2.3	6.94	1.28
GLSS 1 – 12 - 150	42	0.51	59.7	31.3	2688.15	0.57	59.13	2.64
GLSS 2 – 12 - 150		0.51	60.24	14.484	2737.38	0.25	59.99	2.68
GLSS 3 – 16 - 150		0.90	48.99	45.85	1250.64	1.75	47.24	2.12
GLSS 4 – 16 - 150		0.90	57.52	48.588	1465.55	1.75	55.77	2.50
OPC 1 – 12 - 150	62	0.51	-	-	-	-	-	-
OPC 2 – 12 - 150		0.51	-	-	-	-	-	-
OPC 3 – 16 - 150		0.90	66.81	16.298	1697.09	0.62	66.19	2.97
OPC 4 – 16 - 150		0.90	69.25	1.6476	1775.61	0.05	69.2	3.10

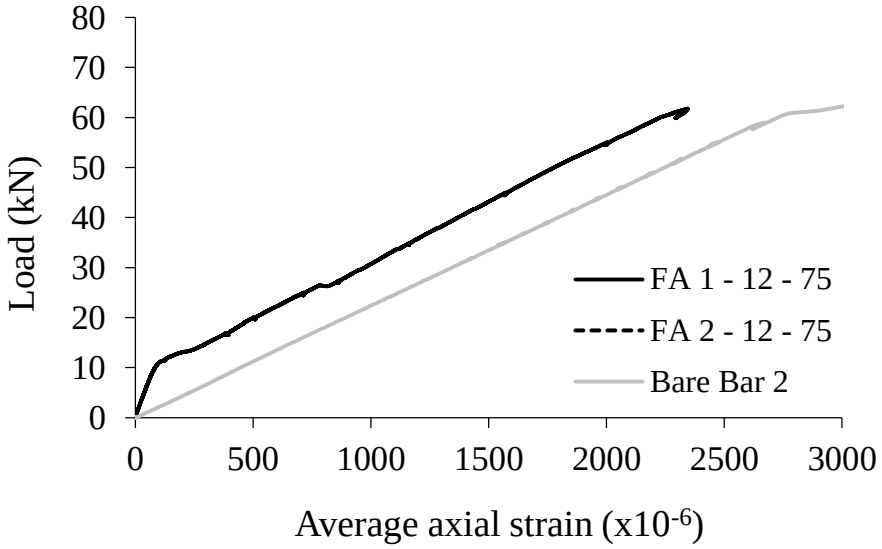

(a) Fly ash d_b= 12mm, *cross-section* = 75mm

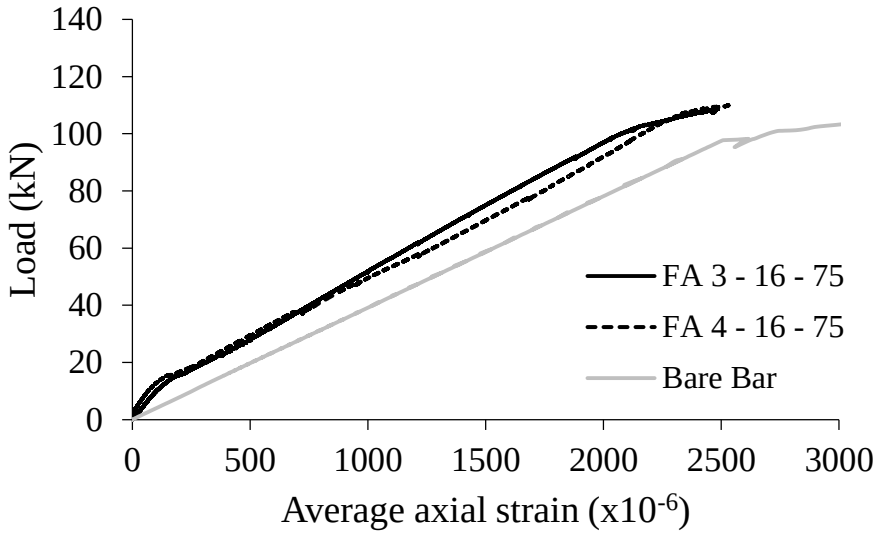

(b) Fly ash d_b= 16mm, *cross-section* = 75mm

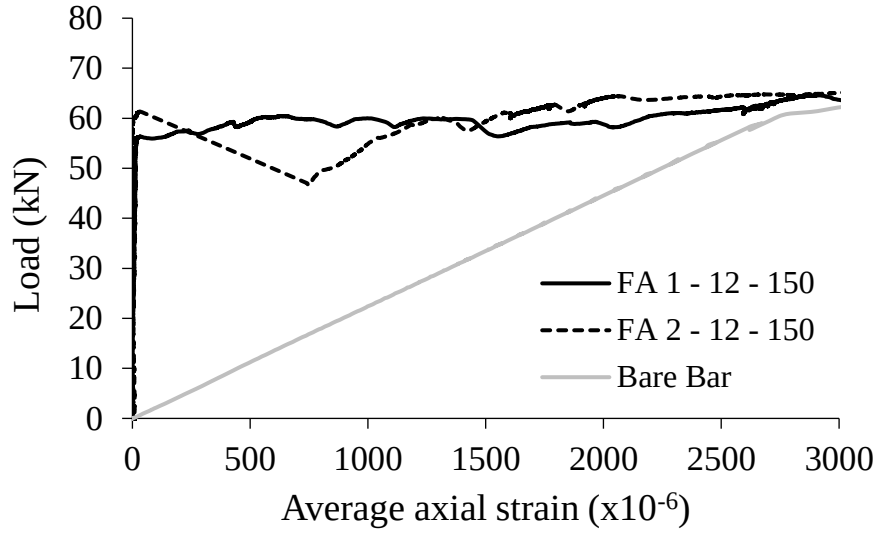

(c) Fly ash d_b= 12mm, *cross-section* = 150mm

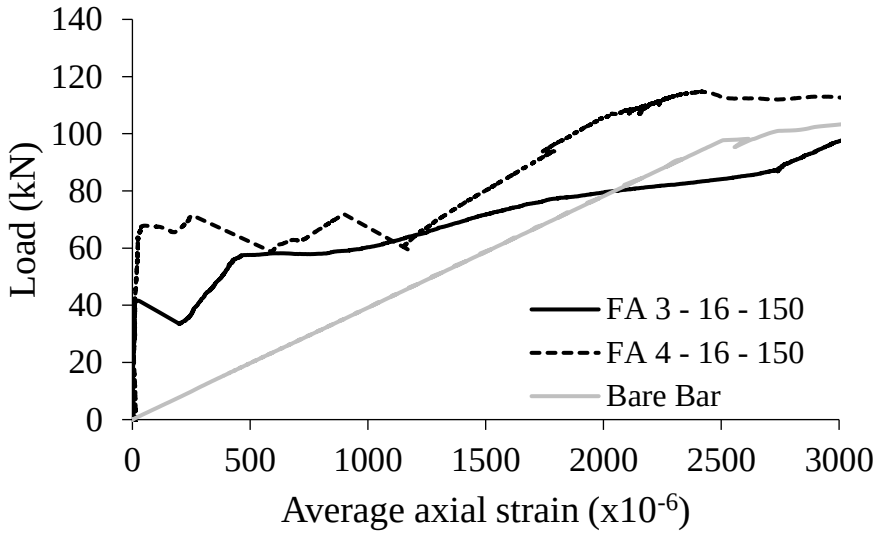

(d) Fly ash d_b= 16mm, *cross-section* = 150mm

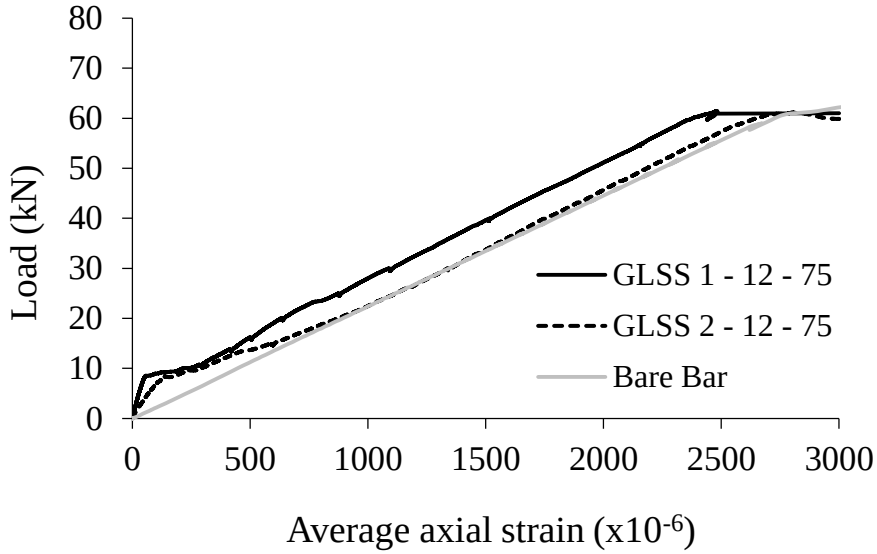

(e) GLSS d_b= 12mm, *cross-section* = 75mm

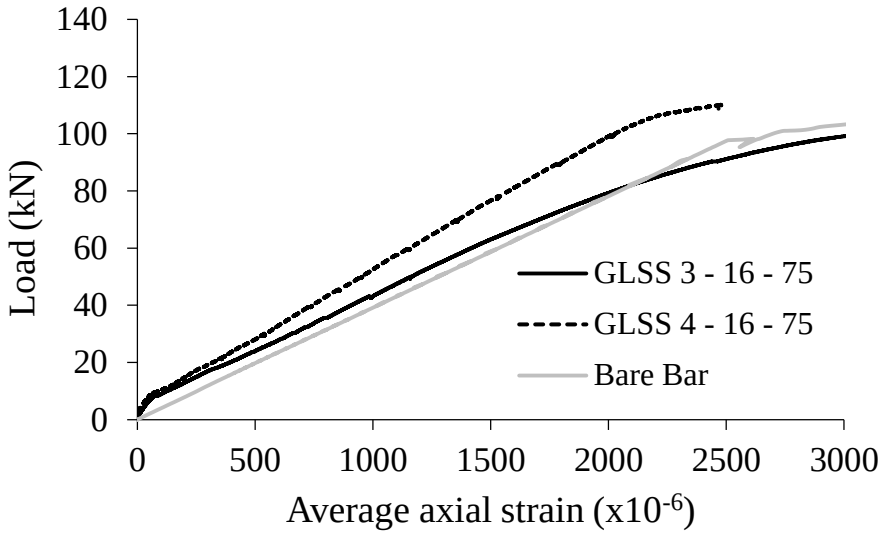

(f) GLSS d_b= 16mm, *cross-section* = 75mm

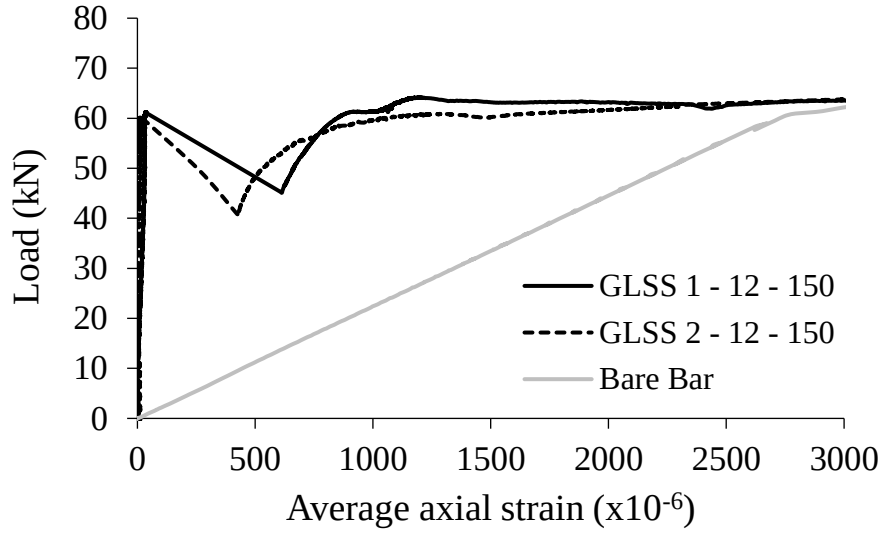

(g) GLSS d_b= 12mm, *cross-section* = 150mm

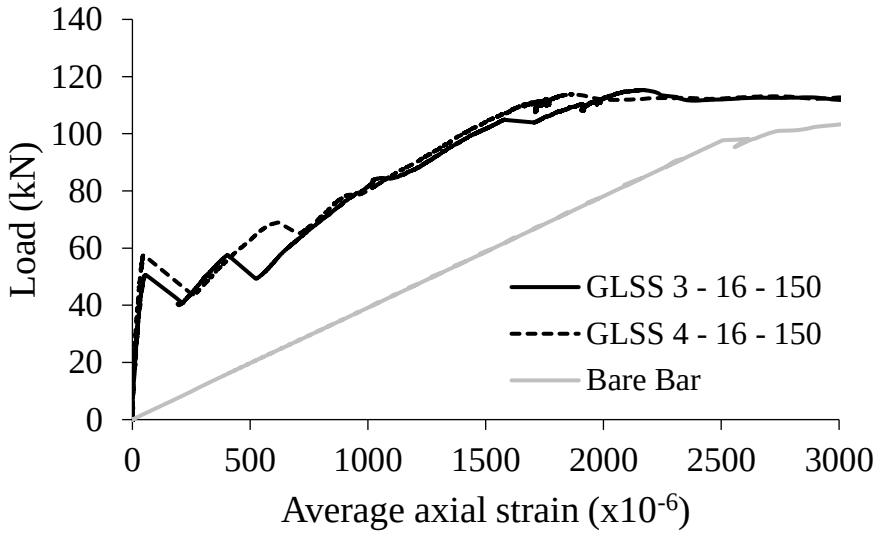

(h) GLSS d_b= 16mm, *cross-section* = 150mm

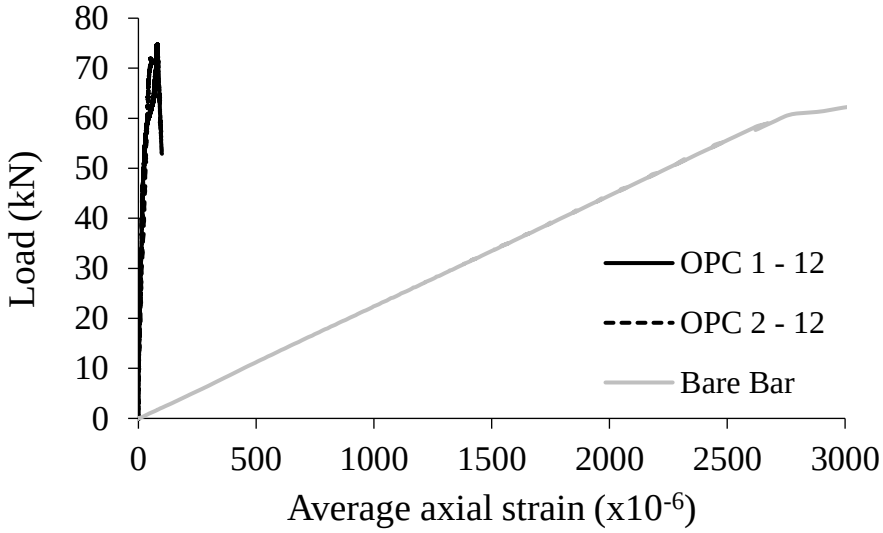

(i) OPC d_b= 12mm, *cross-section* = 150mm

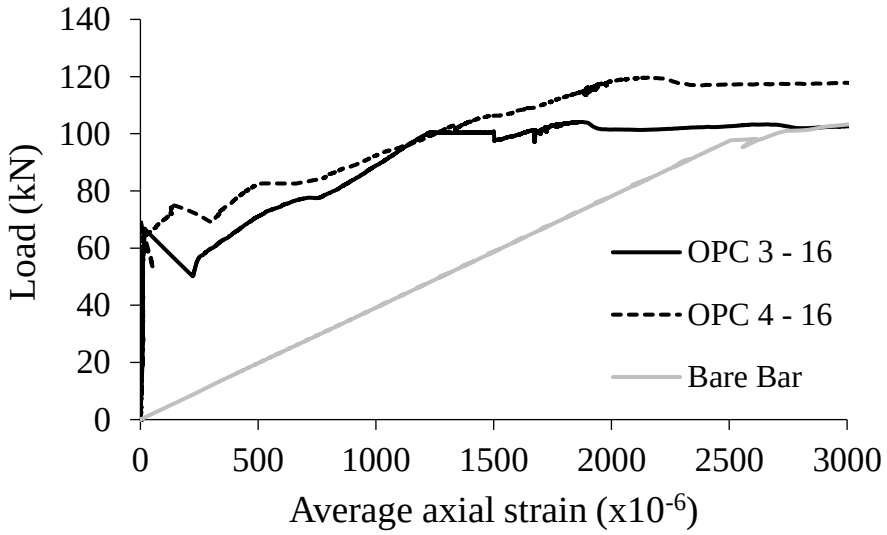

(j) OPC d_b= 16mm, *cross-section*= 150mm

Figure 9. Axial load–average strain response

DISCUSSION

Influence of concrete types

The axial tension stress ($f_{c,m}$) experienced by the concrete itself in a reinforced concrete prism can be defined as the load resisted by the cracked concrete (N_c) divided by its cross–section area. The applied tension load on the cracked concrete (N_c) was determined by subtraction the axial load resisted by the reinforcement steel bar (N_s) for a given axial strain from the total load resisted by the reinforced concrete prism (N) at the same axial strain. The resisted load by the bare bar was determined based on the results of steel bar tension tests, assuming that the load–strain behaviour of bare bar embedded in the reinforced concrete is similar to that of bare steel bar. The concrete response was then divided by the load acting on concrete at initial crack (P_{cr}) in order to obtain the tension–stiffening bond factor (β) of the cracked concrete (*Eq. 4*).

$$\beta = {}^{N_c}/_{P_{cr}} \tag{4}$$

The tension–stiffening bond factor is a highly variable material property that can be used for investigating cracked concrete because it is independent of concrete strength and the reinforcement ratio (Fields and Bischoff 2004). *Figure S1*, which is available in the supplementary data, shows the tension–stiffening bond factor of fly ash, GLSS and OPC cracked concretes. It can be observed from *Figure S1* that, in general, fly ash and GLSS concretes exhibited similar behaviour to that of OPC concrete. *Figure S1(a and e)* shows that the tension–stiffening bond factor of fly ash and GLSS prisms with a 75mm cross–

section and reinforced with a 12mm steel bar generally decreased after the initial cracking and then slightly increased to the same bond factor exhibited at the initial concrete cracking. *Figure S1(b and f)*, on the contrary, shows that specimens with the same cross–section but reinforced with a 16mm steel bar exhibited an increase in the bond factor after the initial concrete cracking.

Geopolymer concrete prisms with a 150mm cross–section and reinforced with a 12mm steel bar experienced a gradual reduction in the bond factor after initial cracking, indicating that the concrete did not carry a significant load between cracks, as can be seen in *Figure S1(c and g)*. This is because the concrete was able to carry a significant tensile load before concrete cracking, yet once the concrete cracked, the cracked concrete lost its ability to carry any more load, which resulted in reducing the tension–stiffening effect. Geopolymer concrete prisms with the same cross–section but reinforced with a 16mm steel bar, shown in *Figure S1(d and h)*, exhibited pronounced fluctuation in the tension–stiffening bond factor (β) after the initial concrete cracking. This is due to the intact concrete between the cracks being able to carry tensile stresses. In contrast, the β in OPC concrete prisms with a 150mm cross–section reinforced with a 16mm steel bar reduced as the deformation increased after the initial concrete cracking with less fluctuation than their geopolymer counterparts, as can be seen in *Figure S1(j)*. This indicates the intact concrete between the cracks was mainly able to maintain the tensile stress, but carried less tensile stress than that was carried by geopolymer cracked concrete. Therefore, it can be said that the tension–stiffening effect of geopolymer concrete, in general, is more significant than that of OPC concrete.

Influence of reinforcement ratio

The behaviour of concrete differs when it is combined with steel, and it also differs with different reinforcement ratios. The concrete stress versus concrete average strain responses of fly ash, GLSS and OPC concretes are depicted in *Figure 10(a–j)* in which the influence of the reinforcement ratio on the concrete response can be observed. It is evident from *Figure 10* that, in general, the stress of cracked concrete is slightly higher when prisms are reinforced with a 12mm diameter steel bar. This can be attributed to the reinforcement ratio ($\rho = A_s/A_c$) in the concrete prisms. It can be seen in *Figure 10(c and g)* that when the reinforcement ratio was 0.5%, the member reached its ultimate load at the initial crack, whereas *Figure 10 (d and h)* shows that a 0.9% reinforcement ratio allowed the concrete members to carry stresses beyond the initial crack. In the case of a high reinforcement ratio (i.e., 2% and 3.6%), *Figure 10(a, b, e and f)*, shows that the initial concrete cracking occurred at lower concrete stress, but the concrete was able to maintain the stresses after concrete cracking, and in some cases the stress was increased and exceeded the force at the initial concrete cracking (P_{cr}). This behaviour can be attributed to the residual stresses in the concrete due to shrinkage, which would be more significant for a smaller cross–section because the effective restraint provided by the steel bar is higher than that of a larger cross–section.

It is worth mentioning that the tensile stress of concrete (in effect the tension–stiffening) is greater when the reinforcement ratio is smaller. This is attributed to the volume of

concrete around the steel, which has an inverse relationship with the volume of steel, as the concrete volume increases with a decrease of the reinforcement ratio. Therefore, it can be said that the P_{cr} decreases with increasing the reinforcement ratio.

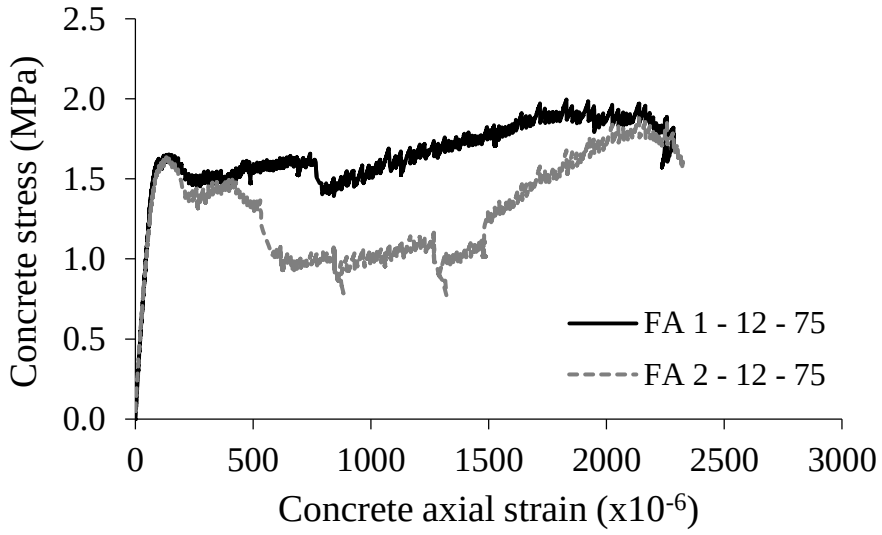

(a) Fly ash d_b= 12mm, *cross-section*= 75mm

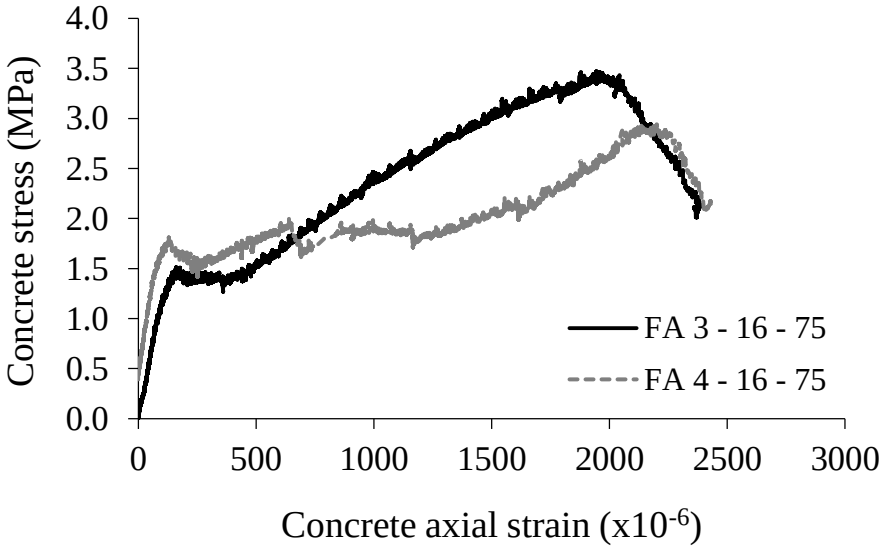

(b) Fly ash d_b= 16mm, *cross-section*= 75mm

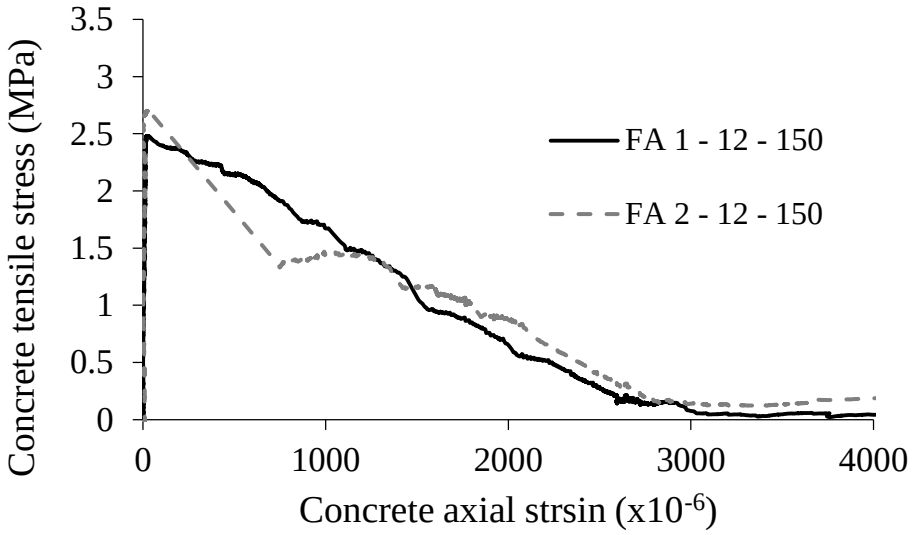

(c) Fly ash d_b= 12mm, *cross-section*= 150mm

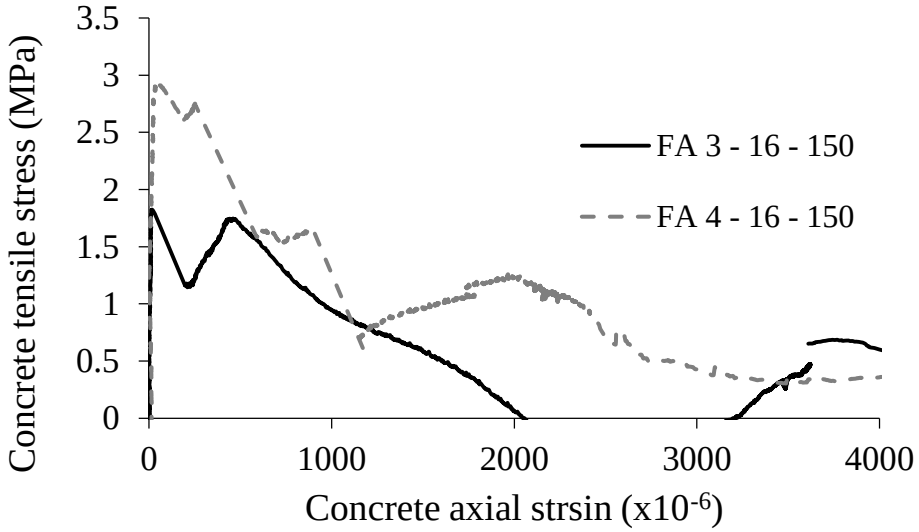

(d) Fly ash d_b= 16mm, *cross-section*= 150mm

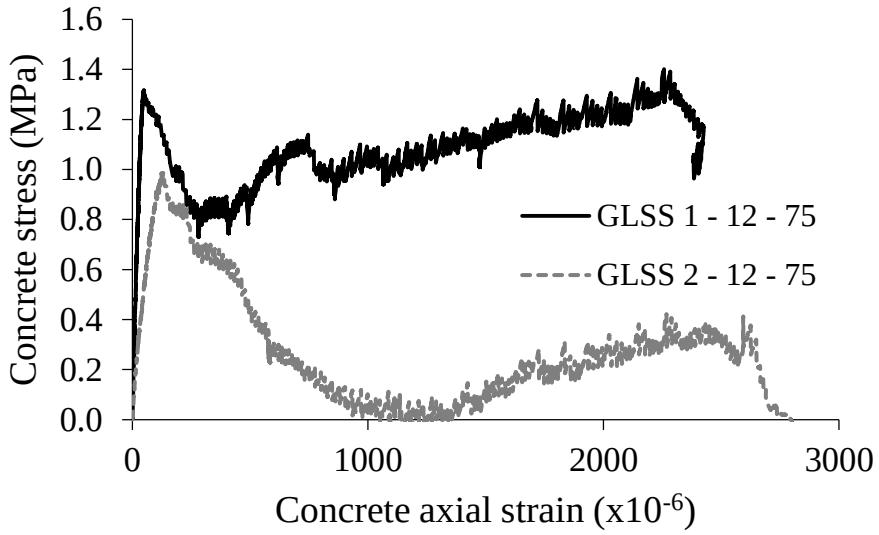

(e) GLSS d_b= 12mm, *cross-section*= 75mm

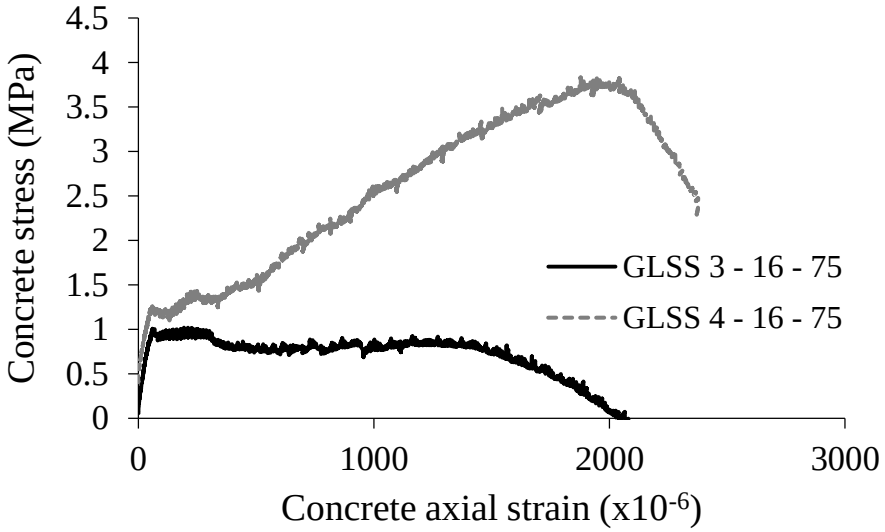

(f) GLSS d_b= 16mm, *cross-section*= 75mm

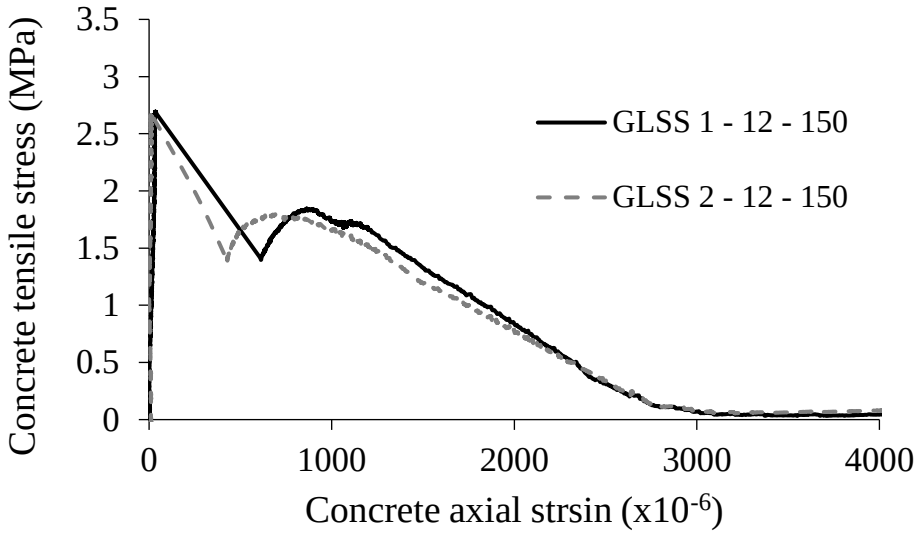

(g) GLSS d_b= 12mm, *cross-section*= 150mm

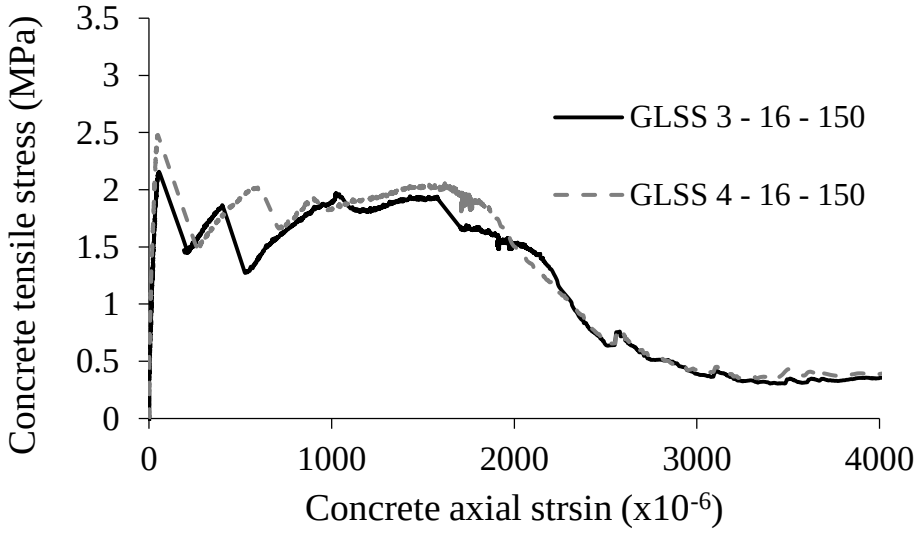

(h) GLSS d_b= 16mm, *cross-section*= 150mm

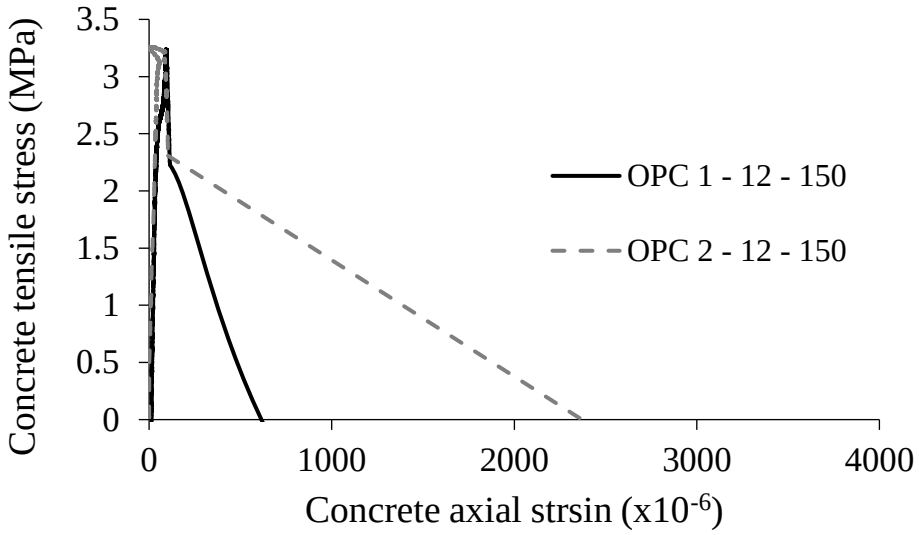

(i) OPC d_b= 12mm, *cross-section*= 150mm

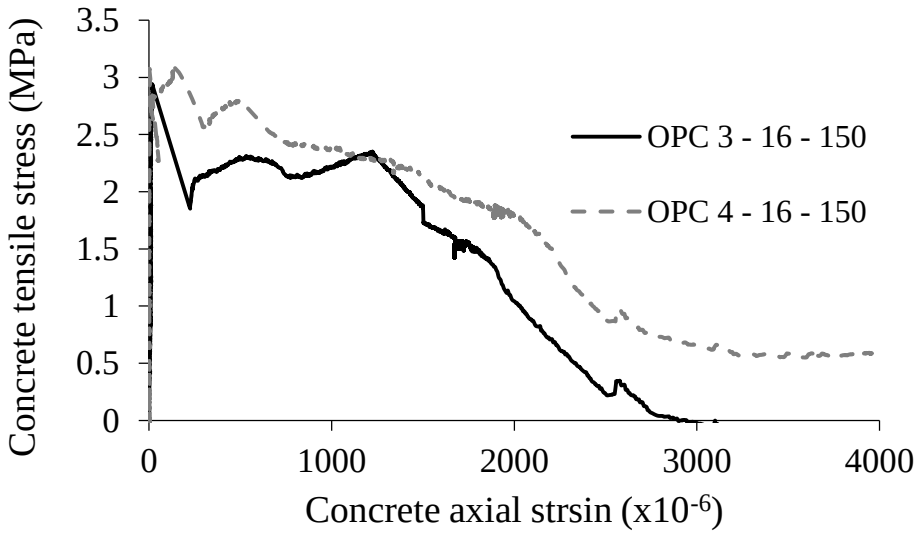

(j) OPC d_b= 16mm, *cross-section*= 150mm

Figure 10. Tensile stress of cracked concretes

Crack width

The maximum, average and minimum crack widths for each specimens are plotted against normalised steel stress to yield stress (σ_s/f_y) in *Figure S2*, which is available in the supplementary data. From *Figure S2(e, f, g, h, m, n, o, p, q and r)*, it can be seen that specimens with a 150mm cross–section developed cracks at high σ_s/f_y, especially those

reinforced with 12mm steel bar. This is attributed to the large stresses capacity carried by concrete before the occurrence of first crack. It is worth mentioning that two specimens (i.e., OPC 1 – 12 – 150 and OPC 2 – 12 – 150) did not crack and they failed due to steel bar rupturing. In contrast, specimens with a cross–section of 75mm developed cracks at early stages and the cracks widened as the steel stress increased, as can be seen in *Figure S2(a, b, c, d, i, j, k and l)*. The maximum, average and minimum increase of crack widths that are presented in *Table S1* and *Figure S2* can be expressed mathematically through a linear regression of the data. The expressions are provided in *Table S2*, which is available in the supplementary data. However, liner regression may not always represent all the data, and the best fit can be expressed in a logarithmic form as shown in *Eqs 5–10*. It should be noted that the influence of compressive strength and steel bar diameter was marginal due to the small variation considered, and hence the only significant impact was due to the concrete cross–section. *Figure 11(a and b)* presents the maximum, average and minimum crack widths of cross–sections 75mm and 150mm respectively, together with their predictive models presented in *Eqs. 5–10*.

For cross–section 75mm

$$w_{c,Max} = 0.195 \ln\left(\frac{\sigma_s}{f_y}\right) + 0.45 \qquad R^2 = 0.944 \qquad \text{(Eq. 5)}$$

$$w_{c,Ave} = 0.133 \ln\left(\frac{\sigma_s}{f_y}\right) + 0.30 \qquad R^2 = 0.894 \qquad \text{(Eq. 6)}$$

$$w_{c,Min} = 0.07 \ln\left(\frac{\sigma_s}{f_y}\right) + 0.15 \qquad R^2 = 0.893 \qquad \text{(Eq. 7)}$$

For cross–section 150mm

$$w_{c,Max} = 0.515 \ln\left(\frac{\sigma_s}{f_y}\right) + 0.49 \qquad R^2 = 0.633 \qquad \text{(Eq. 8)}$$

$$w_{c,Ave} = 0.305 \ln\left(\frac{\sigma_s}{f_y}\right) + 0.32 \qquad R^2 = 0.458 \qquad \text{(Eq. 9)}$$

$$w_{c,Min} = 0.142 \ln\left(\frac{\sigma_s}{f_y}\right) + 0.18 \qquad R^2 = 0.084 \qquad \text{(Eq. 10)}$$

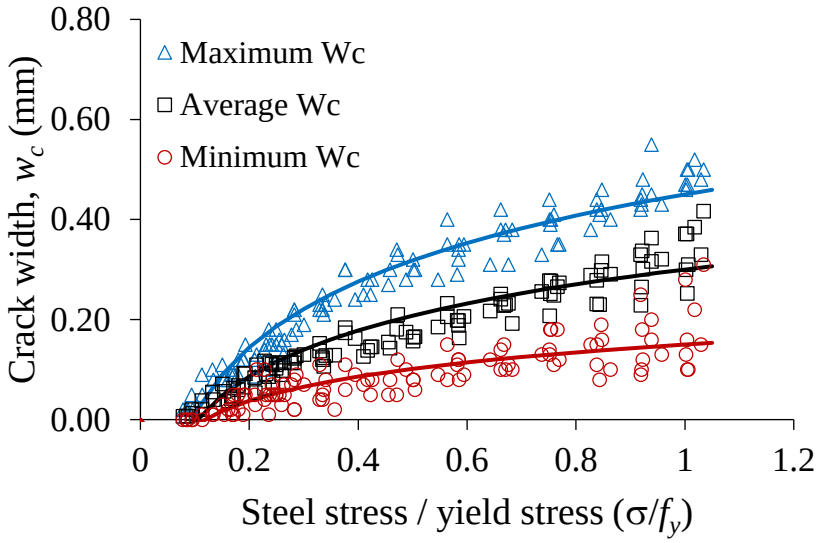

(a) Specimens with 75mm cross–section

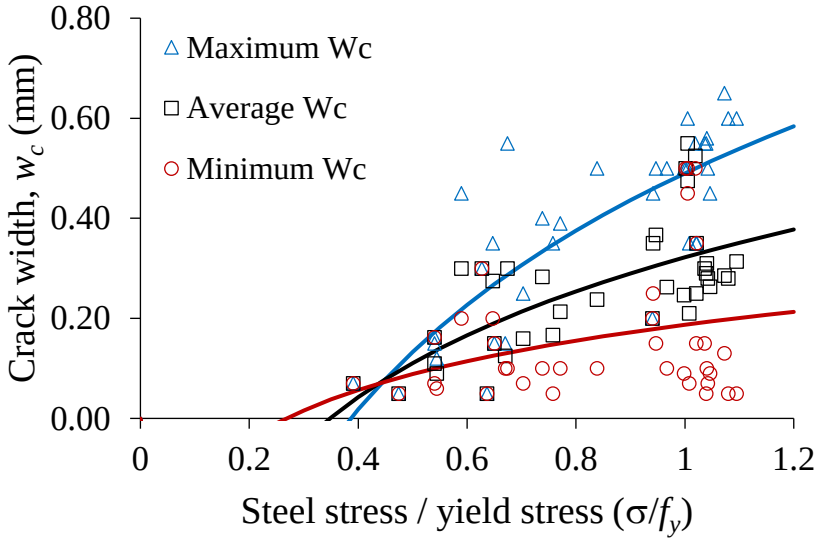

(b) Specimens with 150mm cross–section

Figure 11. Crack widths prediction

PREDICTION FORMULAE

Crack width and spacing

Crack width in concrete varies from concrete to another due to the heterogeneity of the material, which rises difficulties in the study of the cracking behaviour. Several simplified provisions to quantify tension cracking member have been proposed (CEB-FIP 1992; Eurocode2 2004). The majority of the models assume that the mean crack width is dependent on the mean steel strain (ε_{sm}) over the length of the member and the mean crack spacing (S_{rm}). This assumption is, in fact, based on the assumption that the concrete strain (ε_c) drops to zero. Although the concrete strain, which reduces the crack width, does not drop to zero in the uncracked region, it was assumed that the pre–existing shrinkage strain (ε_{sh}), which increases the crack width, substitutes the reduction of crack width due to ε_c. On the other hand, several numerically and analytically models based on partial–interaction theory have been proposed (Muhamad et al. 2012; Zhang et al. 2014) to incorporate the bond properties between reinforcement and concrete.

Eurocode2:

According to Eurocode2 (2004), the design crack width can be determined using the following expression

$$w_c = S_{r,max}(\varepsilon_{sm-}\varepsilon_{cm}) \tag{11}$$

where ε_{sm}-ε_{cm} is the difference between mean strains of steel and concrete, which is obtained from *Eq. 12*. $S_{r,max}$ is the maximum crack spacing, which is given in *Eq. 13*.

$$\varepsilon_{sm} - \varepsilon_{cm} = \frac{\sigma_s}{E_s} - \frac{k_t f_{ct,eff}\left(1 + \alpha_e \rho_{p,eff}\right)}{E_s \rho_{p,eff}} \geq 0.6\sigma_s/E_s \tag{12}$$

where σ_s is the stress in the reinforcement calculated assuming a crack section, E_s is the elastic modulus of reinforcement, $\rho_{p,eff}$ is the effective reinforcement ratio ($A_s/A_{c,eff}$), α_e is the modulus ratio (E_s/E_c), and k_t is a factor depending on the duration of the load, which can be taken as 0.6 for short–term loading.

$$S_{r,max} = 3.4C_c + 0.425k_1k_2\left(\frac{d_b}{\rho_{eff}}\right) \tag{13}$$

where C_c is the concrete cover, k_1 is the coefficient that takes account for bond properties of the steel bars, which for load induced–cracking can be taken as 0.8 for deformed bars

and 1.6 for plain bars, k_2 is the coefficient that accounts for the strain distribution in the concrete, which can be considered as 1.0 for pure tension, d_b is the steel bar diameter and ρ_{eff} is the effective reinforcement ratio.

Zhang et al. (2014) for linear ascending bond semi–mechanical solution

The crack spacing for a linear bond stress–slip relationship can be determined by *Eq. 13* using the recommended bond properties provided by CEB–FIP code 90 (CEB 1992) to determine the maximum shear stress (τ_{max}), which can be taken as $1.25\sqrt{f_c}$ where f_c is the compressive strength in MPa and the slip at τ_{max} (Δ_1) is 1.0mm. Thereafter, to find the stiffness (k_b), the crack spacing given in *Eq. 13* can be substituted into *Eq. 14*, which in effect is used to determine half of the crack width (Δ_r) in *Eq. 16*, as well as the axial stiffness of the tension–stiffening prism P_r/Δ_r as shown in *Eq. 17*. The strain in the reinforcement can then be determined by dividing the total extension of the bar over the length, which will be substituted into *Eq. 18* to calculate the strain in the prism.

$$S_{linear} = 1.21\left(\frac{A_r}{A_c}\right)^{-0.295}\left(\frac{L_{per}\sqrt{\frac{4\Delta_1}{\tau_{max}\beta}}}{2A_r}\right)^{-0.673\frac{A_r}{A_c}-0.399}\sqrt{\frac{4\Delta_1}{\tau_{max}\beta}} \tag{13}$$

$$S_{linear} = \sqrt{\frac{4}{k_b\beta}} \tag{14}$$

where

$$\beta = \frac{E_rA_r + E_cA_c}{E_rA_rE_cA_c}L_{per} \tag{15}$$

$$\Delta_r = \frac{P_r\tanh(1)}{E_rA_r\sqrt{k_b\beta}} \tag{16}$$

$$K_{a-linear} = \frac{E_rA_r\sqrt{k_b\beta}}{\tanh(1)} \tag{17}$$

$$\varepsilon_{prism-linear} = \frac{\sigma_r}{E_r}\tanh(1) = \varepsilon_r\tanh(1) \tag{18}$$

Zhang et al. (2014) for non–linear ascending bond

The crack spacing for non–linear bond stiffness can be determined by *Eq. 19*, which can then be substituted in *Eq. 20* and *Eq. 21* to obtain half the crack width (Δ_r) and the axial stiffness of the tension–stiffening prism, respectively. Thereafter, the strain of the prism

can be obtained by determining the reinforcement strain through dividing *Eq. 20* over the length and substitute the ε_r into *Eq. 22*.

$$S_{non-linear} = 29.1\left(\frac{A_r}{A_c}\right)^{0.207}\left[\frac{(1+\alpha)f_{ct}A_c\Delta_1^{\alpha}}{\tau_{max}L_{per}\left(\sqrt{2}\right)^{\alpha}}\right]^{\frac{1}{1+\alpha}} \quad (19)$$

$$\Delta_r = \left(\frac{P_r}{E_rA_r}\frac{S_{non-linear}}{2}\right)1.08\left(\frac{A_r}{A_c}\right)^{0.105} \quad (20)$$

$$K_{a,non-linear} = \frac{1.41E_rA_r}{\tanh(1)\,S_{non-linear}}\left(\frac{A_r}{A_c}\right)^{-0.105} \quad (21)$$

$$\varepsilon_{prism,non-linear} = \varepsilon_r(\tanh(1))\left(1.42\left(\frac{A_r}{A_c}\right)^{0.105}\right) \quad (22)$$

Comparison of the theoretical model with the experimental results

The mechanics–based solutions described by Zhang et al. (2014) to predict the crack spacing are compared with the experimental results in *Tables 6*. The crack width predictions using Eurocode2 (2004) and Zhang et al. (2014) are presented in *Table S3*, which is available in the supplementary data. The bond stress–slip properties in *Figure 12*, which rely on the CEB–FIP Model Code 90 (*Eq. 23*), were taken as recommended by CEB–FIP Model Code 90 (CEB 1992) in *Eqs. 24 and 25*, and as recommended by Albitar et al. (2016) in *Eqs. 26 and 27*, which were set for geopolymer concrete.

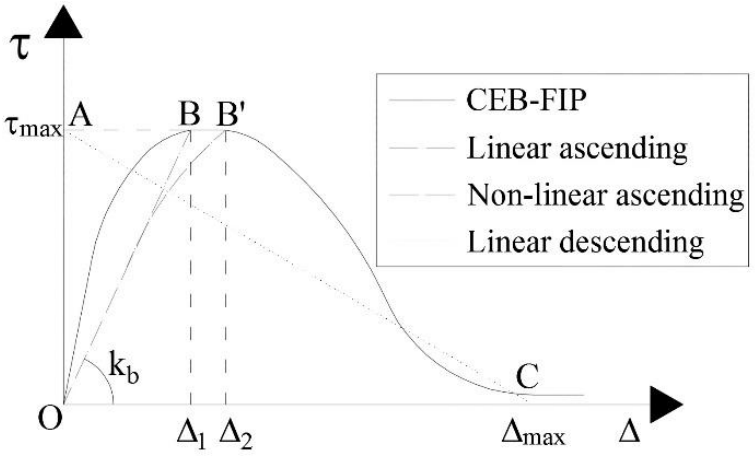

Figure 12. Idealised bond stress–slip relationship

$$\tau = \tau_{max}\left(\frac{\Delta}{\Delta_1}\right)^{\alpha} \quad (23)$$

CEB–FIP (CEB 1992)

$$\tau_{max} = 1.25\sqrt{f_{co}} \quad (24)$$

$$\Delta_1 = 1.0\ mm \quad (25)$$

Albitar et al. (2016)

$$\tau_{max} = 39.6f'_c - 76.5 \quad (26)$$

$$\Delta_1 = 0.088\tau_{max} - 0.32 \quad (27)$$

where τ_{max} is the maximum shear stress in MPa, Δ_1 is the slip at the maximum shear stress, α is the exponent value.

The comparison results shown in *Table 6* reveal that Zhang et al.'s (2014) linear approach using Albitar et al.'s (2016) bond stress–slip properties provided the closest prediction of crack spacing for geopolymer reinforced concrete. *Table 7* summarises the accuracy and precision of crack width predictive expressions. *Figure 13* plots the experimental crack width results against the calculated crack widths, in which the best fit denotes that $w_{c,Exp}=w_{c,Cal}$. It can be seen in *Figure 13* that the Eurocode2 (2004) expression slightly underestimated crack widths at lower steel stress. On the contrary, the mechanics–based solutions of both linear and nonlinear approaches accurately enough predicted the crack widths of geopolymer reinforced concrete. It is evident from *Table 7* and *Figure 13* that the mechanics–based solutions described by Zhang et al. (2014) using Albitar et al.'s (2016) recommendations for bond stress–slip properties provided the most accurate predictions for the crack width of geopolymer reinforced concrete.

Table 6. Crack spacing using *Eqs. 13 and 19*

ID No. (concrete type – steel diameter – cross-section)	Exp. spacing	Linear approach (mm)				Non-linear approach (mm)		
		Albitar et al. (2016)		CEB–FIP (1992)		CEB–FIP (1992)		
		S_{linear}	k_b	S_{linear}	k_b	$S_{non\text{-}linear}$ (α = 0.4)	$S_{non\text{-}linear}$ (α = 0.6)	$S_{non\text{-}linear}$ (α = 0.9)
FA 1 – 12 – 75	270	263.98	29.85	316.92	24.93	233.79	169.62	106.92
FA 2 – 12 – 75	470	263.98	29.85	316.92	24.93	233.79	169.62	106.92
FA 3 – 16 – 75	300	252.24	39.35	301.77	27.50	212.70	158.56	103.74
FA 4 – 16 – 75	490	252.24	39.35	301.77	27.50	212.70	158.56	103.74
FA 1 – 12 – 150	361	435.36	12.23	505.59	9.07	636.08	392.70	198.39
FA 2 – 12 – 150	454	435.36	12.23	505.59	9.07	636.08	392.70	198.39
FA 3 – 16 – 150	374	440.62	15.50	511.34	11.51	582.27	368.97	193.17
FA 4 – 16 – 150	385	440.62	15.50	511.34	11.51	582.27	368.97	193.17
GLSS 1 – 12 – 75	330	258.01	30.94	325.24	19.47	233.79	169.62	106.92
GLSS 2 – 12 – 75	190	258.01	30.94	325.24	19.47	233.79	169.62	106.92
GLSS 3 – 16 – 75	310	246.20	40.65	308.99	25.81	212.70	158.56	103.74
GLSS 4 – 16 – 75	300	246.20	40.65	308.99	25.81	212.70	158.56	103.74
GLSS 1 – 12 – 150	311	435.36	12.23	505.59	9.07	636.08	392.70	198.39
GLSS 2 – 12 – 150	351	435.36	12.23	505.59	9.07	636.08	392.70	198.39
GLSS 3 – 12 – 150	235	435.36	12.23	505.59	9.07	636.08	392.70	198.39
GLSS 4 – 12 – 150	375	435.36	12.23	505.59	9.07	636.08	392.70	198.39
OPC 1 – 12 – 150	0	370.30	16.98	477.70	10.21	635.47	392.38	198.25
OPC 2 – 12 – 150	0	370.30	16.98	477.70	10.21	635.47	392.38	198.25
OPC 3 – 16 – 150	167	375.44	21.53	483.77	12.97	581.72	368.66	193.05
OPC 4 – 16 – 150	435	375.44	21.53	483.77	12.97	581.72	368.66	193.05

Table 7. Comparison of experimental crack width to predictive models

Statistics	Experimental	Eurocode2 (2004)	Linear approach		Non-linear approach	
			Albitar et al. (2016)	CEB-FIP (1992)	Albitar et al. (2016)	CEB-FIP (1992)
Mean	0.28	0.25	0.26	0.31	0.12	0.22
COV	1.00	0.89	0.96	0.97	0.97	0.96
Confidence intervals	0.30 - 0.25	0.29 - 0.21	0.29 - 0.23	0.34 - 0.27	0.14 - 0.11	0.25 - 0.20

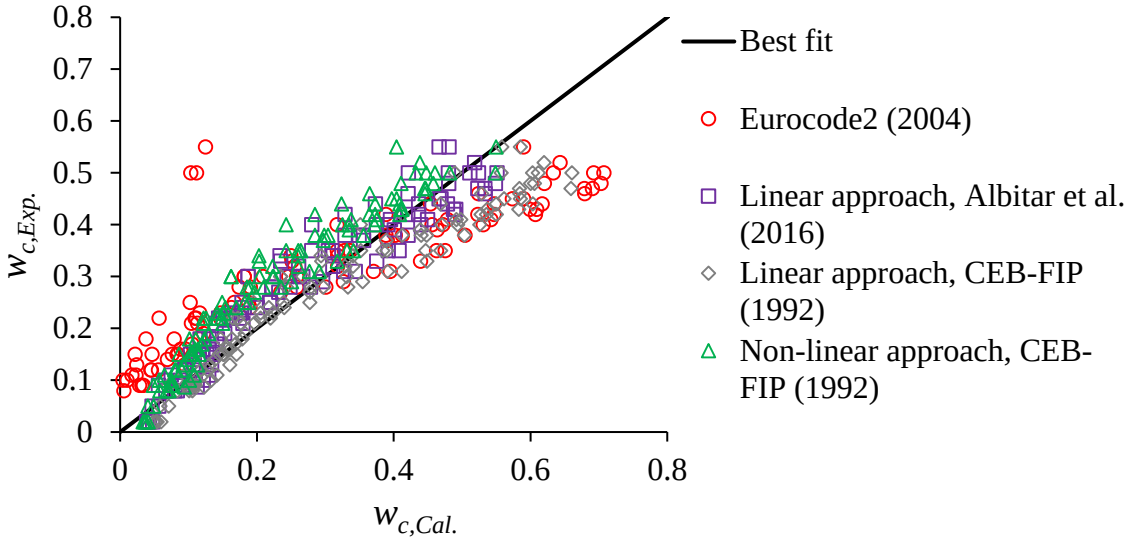

Figure 13. Comparison between experimental and calculated crack widths

CONCLUSION

This paper has presented the results of an experimental study that was undertaken to quantify the crack spacing, crack width and tension–stiffening behaviour of different concretes, including fly ash, granulated lead smelter slag (GLSS) and ordinary Portland cement (OPC). The mechanisms of tension–stiffening of concretes reinforced with two different steel bar diameters (i.e., 12mm and 16mm) and two different concrete cross–sections (i.e., 75mm and 150mm) have been explained. It was demonstrated that, in general, the tension–stiffening member response of geopolymer concrete is similar to that of OPC concrete. It was also shown that increasing the reinforcement ratio leads to a marginal decrease in the tensile stress of concrete, which in effect a decrease in the tension–stiffening. Moreover, the transverse tensile cracks were developed at higher steel stress in specimens with larger cross–sections, and the width of the cracks was wider. The tension–stiffening effect of geopolymer concrete was shown to be slightly more significant than that of OPC concrete. The results also showed that the mechanics–based solutions developed for OPC concrete can be used along with bond stress–slip properties set for geopolymer concrete to predict the crack spacing and crack width of geopolymer reinforced concrete. Finally, it has been shown that the tension–stiffening mechanisms of geopolymer and OPC concretes are in agreement, suggesting that the provisions developed for OPC concrete can be modified to predict the behaviour of geopolymer concrete.

Acknowledgement

The authors would like to thank Yipeng Chen, Wenhui Jiang, Shuming Sun, Jianhan Zhang, who have helped in undertaken the tests reported in this paper as part of their undergraduate project.

APPENDIX

SUPPLEMENTARY DATA – FIGURES

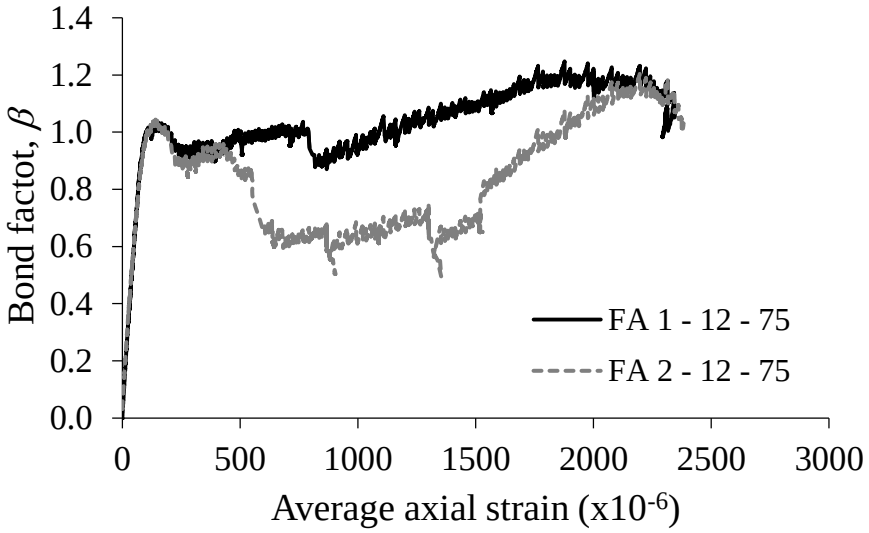

(a) Fly ash d_b= 12mm, *cross-section*= 75mm

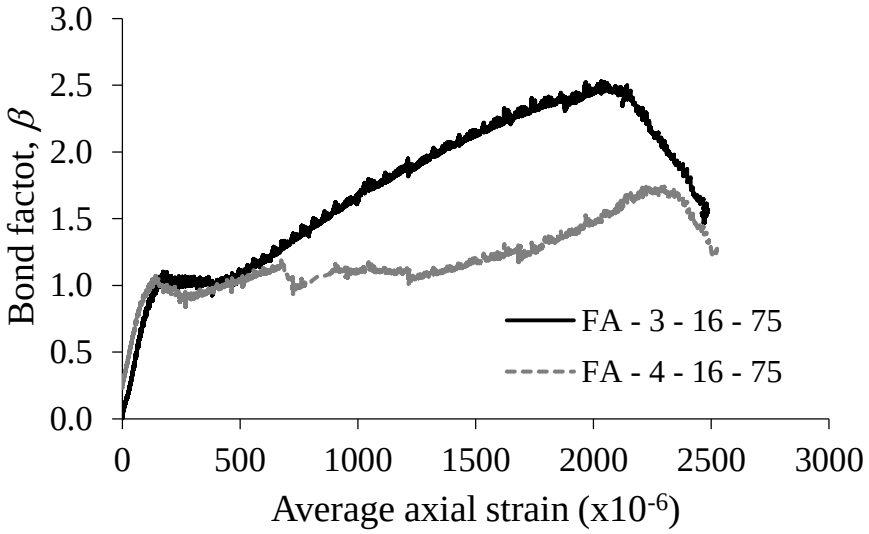

(b) Fly ash d_b= 16mm, *cross-section*= 75mm

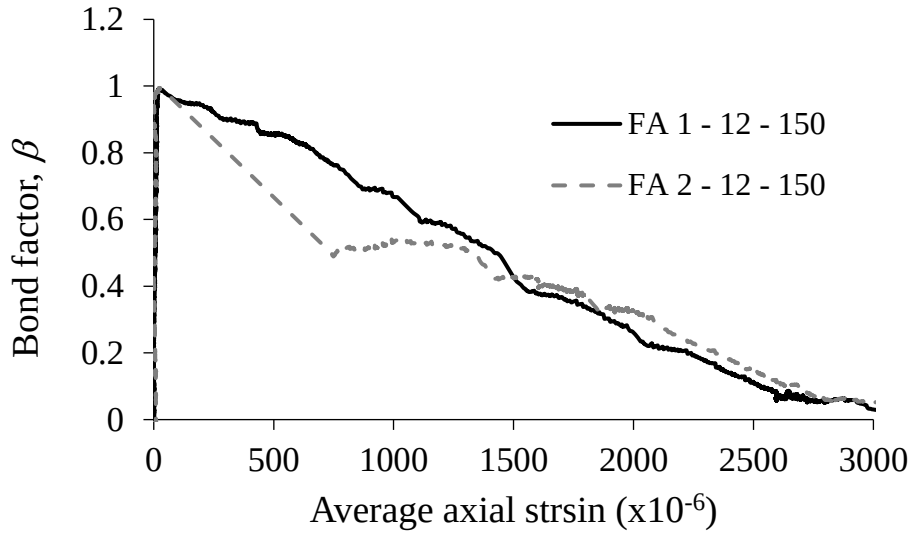

(c) Fly ash d_b= 12mm, *cross-section*= 150mm

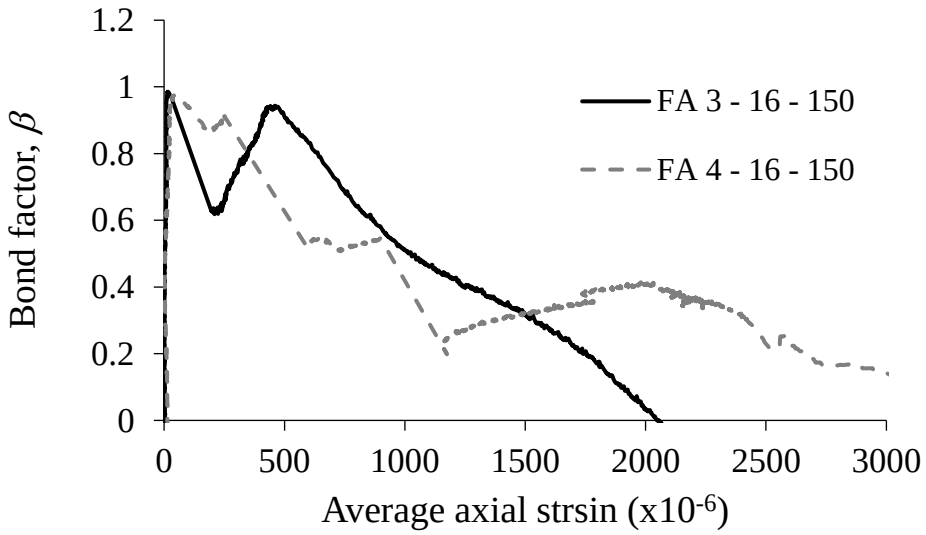

(d) Fly ash d_b= 16mm, *cross-section*= 150mm

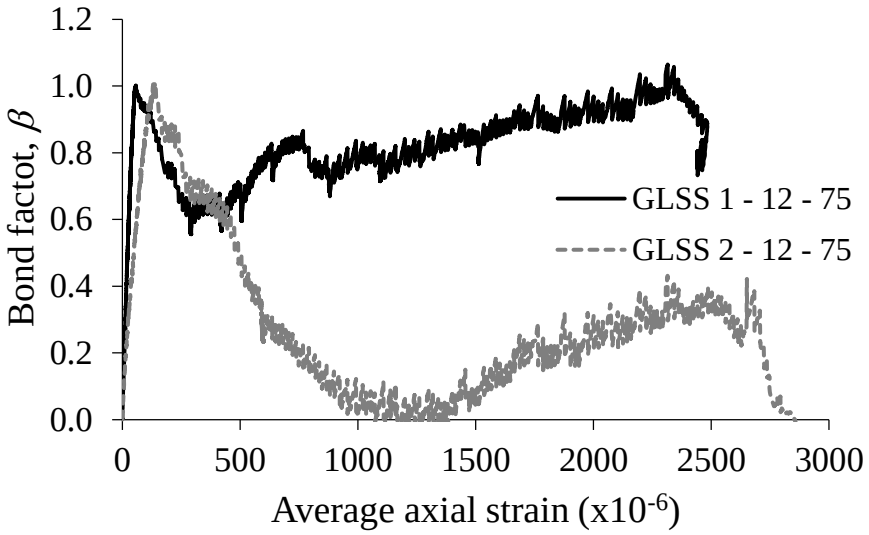

(e) GLSS d_b= 12mm, *cross-section*= 75mm

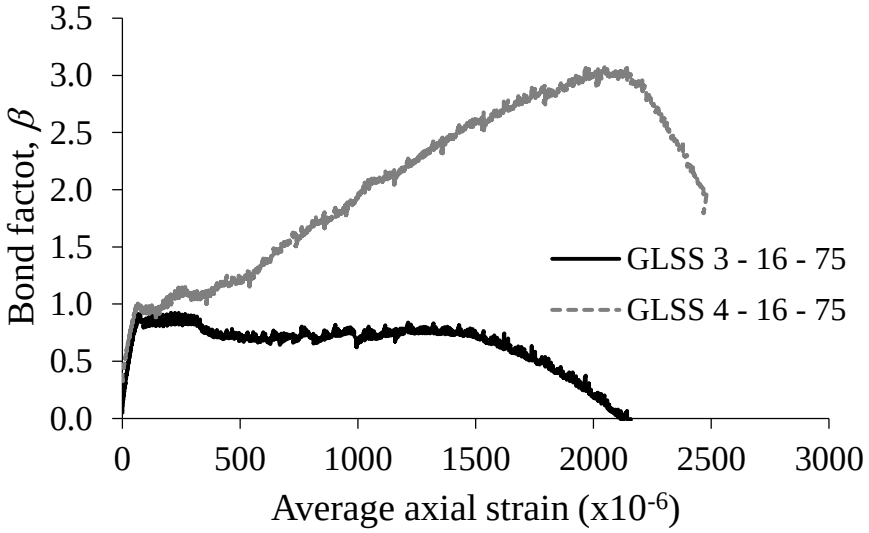

(f) GLSS d_b= 16mm, *cross-section*= 75mm

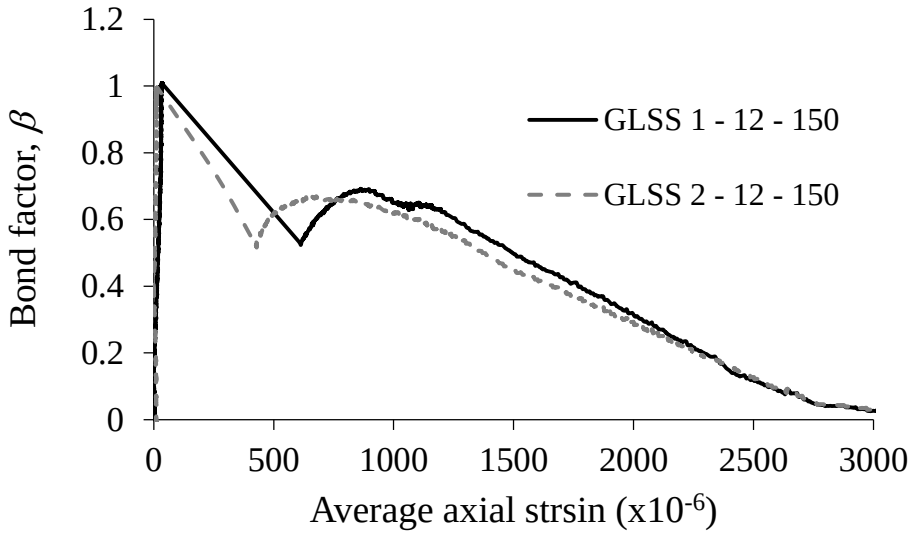

(g) GLSS d_b= 12mm, *cross-section*= 150mm

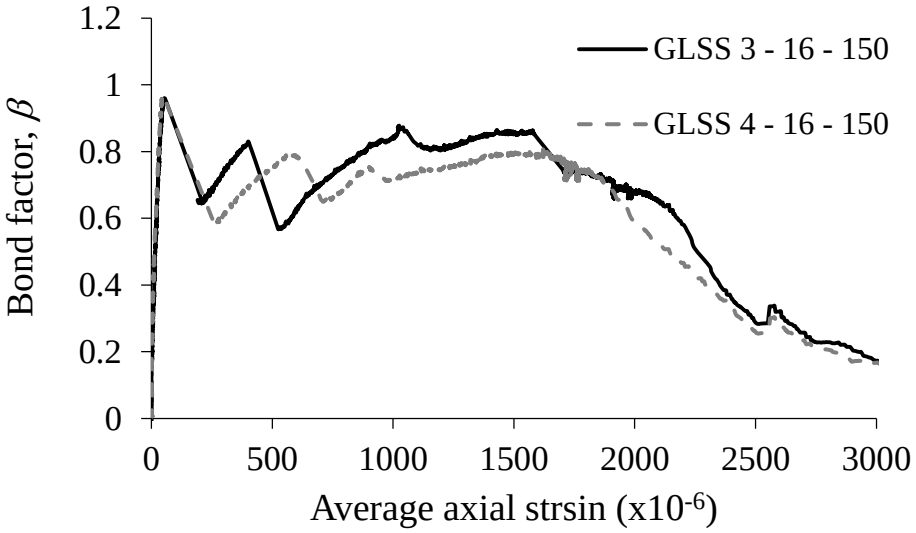

(h) GLSS d_b= 16mm, *cross-section*= 150mm

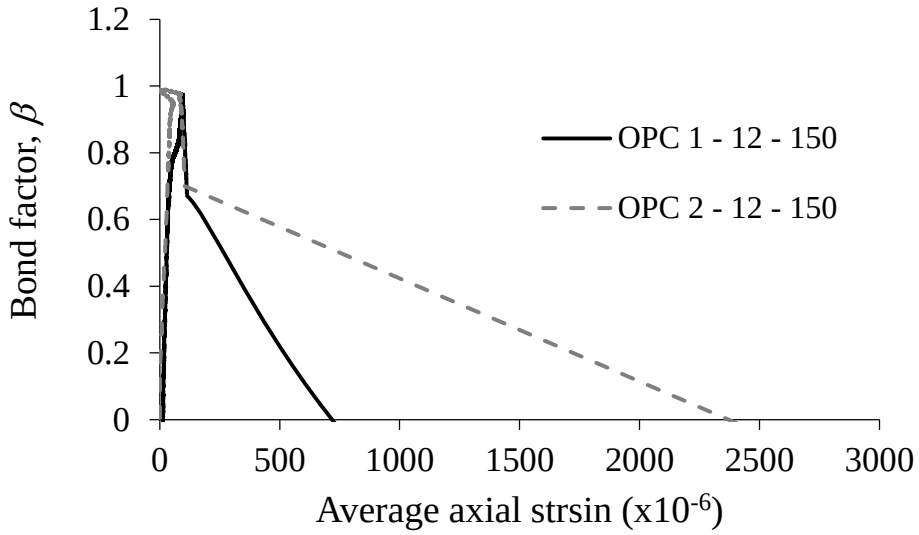

(i) OPC d_b= 12mm, *cross-section*= 150mm

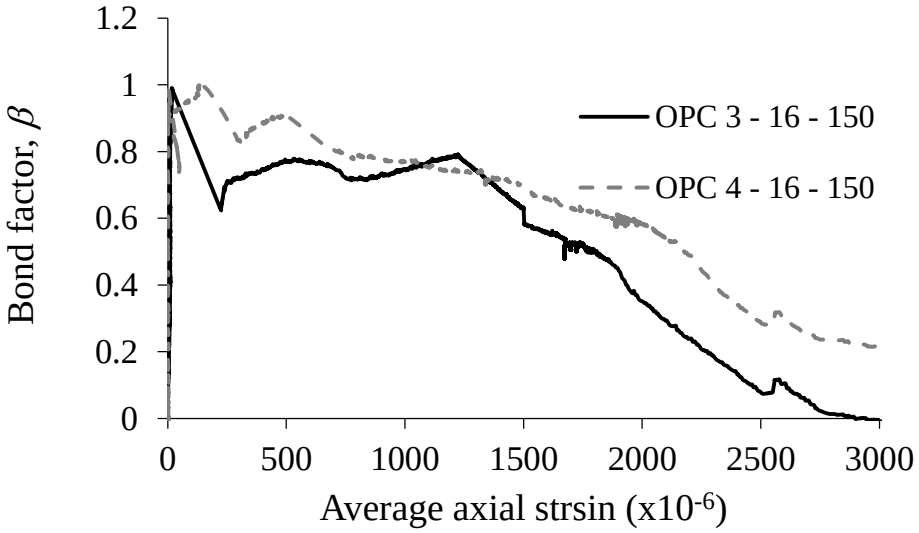

(j) OPC d_b= 16mm, *cross-section*= 150mm

Figure S1. Tension–stiffening bond factor, β, of cracked concrete

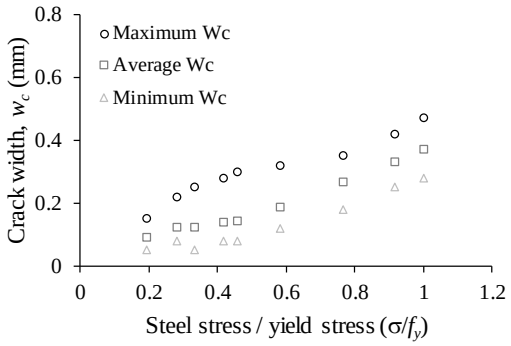

(a) FA 1 – 12 – 75

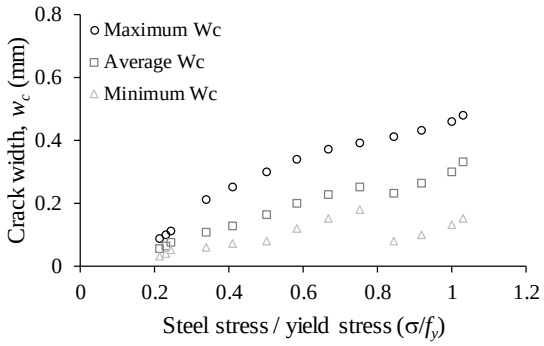

(b) FA 2 – 12 – 75

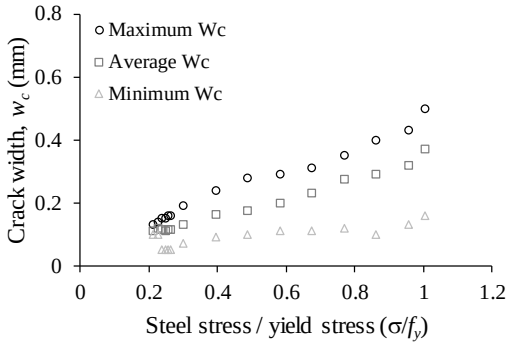

(c) FA 3 – 16 – 75

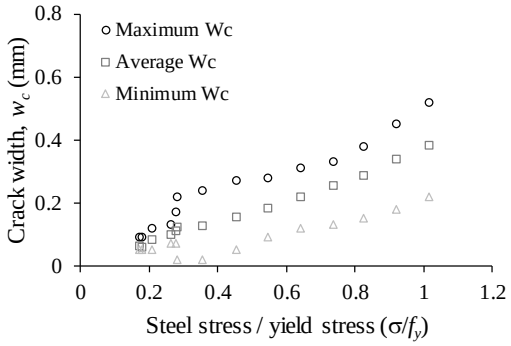

(d) FA 4 – 16 – 75

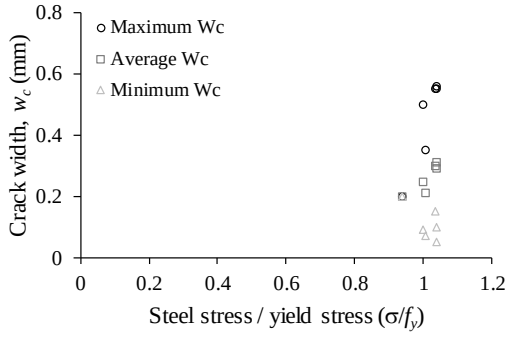

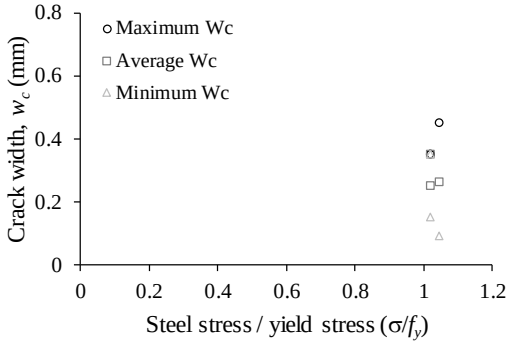

(e) FA 1 – 12 – 150

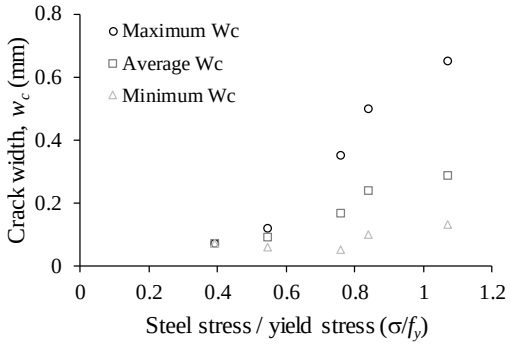

(f) FA 2 – 12 – 150

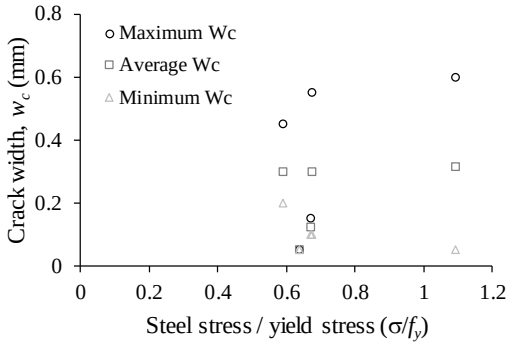

(g) FA 3 – 16 – 150

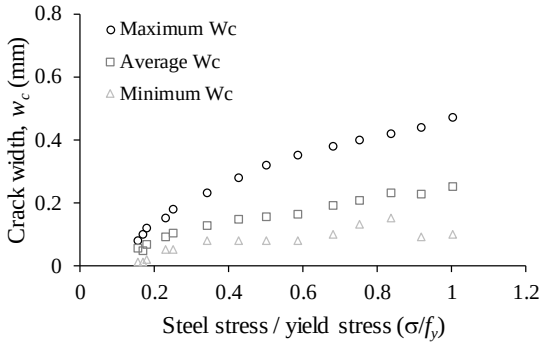

(h) FA 4 – 16 – 150

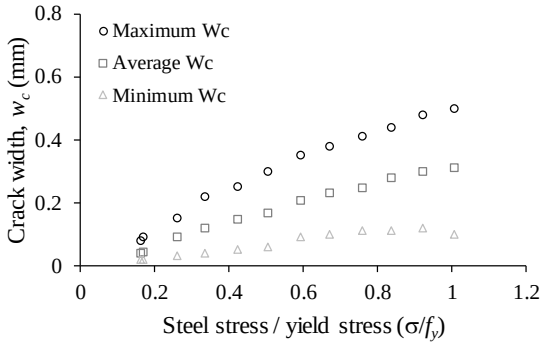

(i) GLSS 1 – 12 – 75

(j) GLSS 2 – 12 – 75

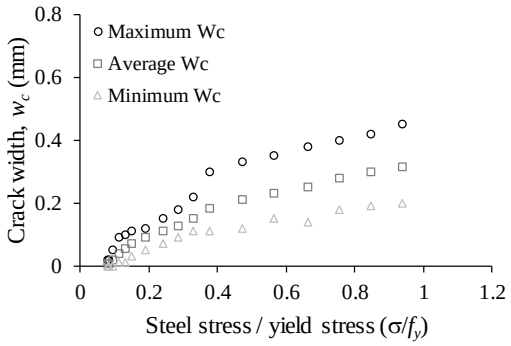

(k) GLSS 3 – 16 – 75

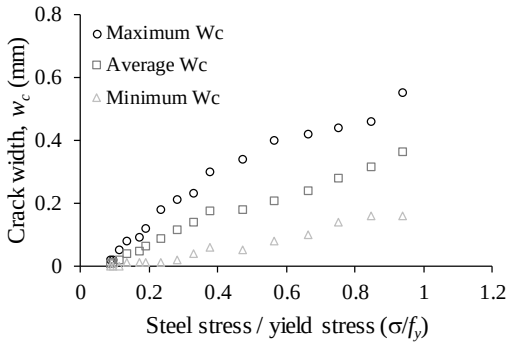

(l) GLSS 4 – 16 – 75

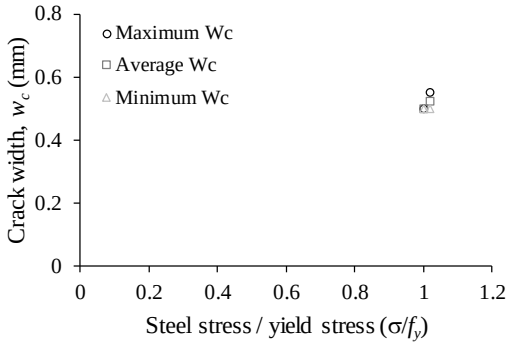

(m) GLSS 1 – 12 – 150

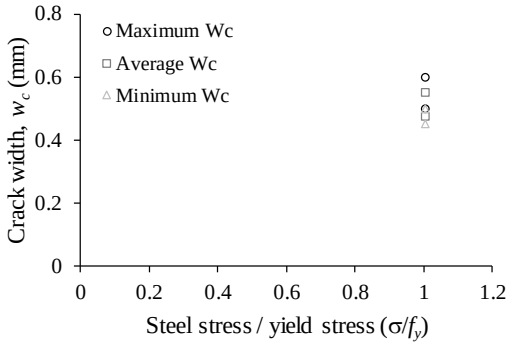

(n) GLSS 2 – 12 – 150

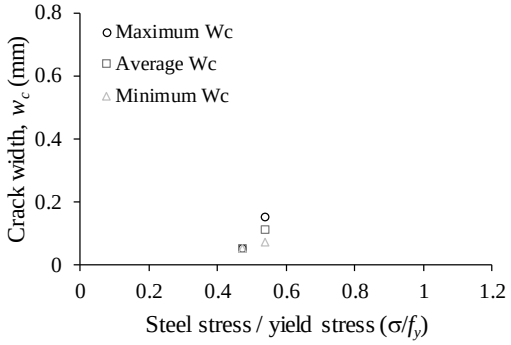

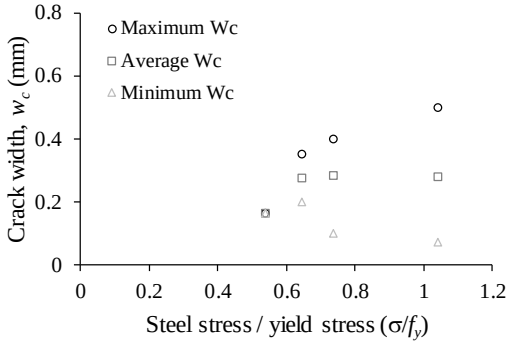

(o) GLSS 3 – 16 – 150

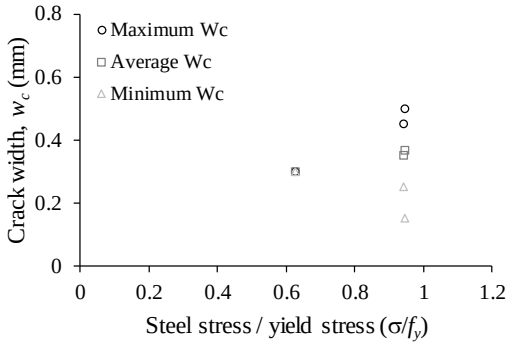

(p) GLSS 4 – 16 – 150

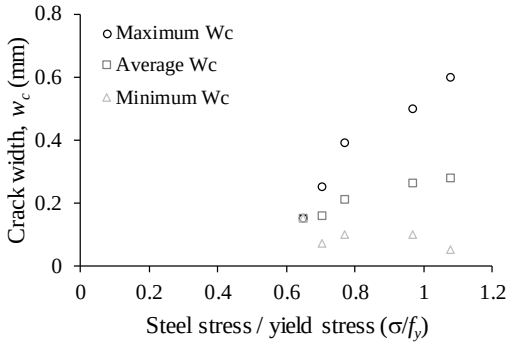

(q) OPC 3 – 16 – 150

(r) OPC 4 – 16 – 150

Figure S2. Crack widths versus steel stress/yield stress

SUPPLEMENTARY DATA – TABLES

Table S1. Crack widths at different loading stages

ID No.	Load stage	Load, P (kN)	σ_s (MPa)	Width of Top crack (mm)	Width of Bottom crack (mm)	Width of 1st crack (mm)	Width of 2nd crack (mm)	Width of 3rd crack (mm)	Width of 4th crack (mm)	Width of 5th crack (mm)	Width of 6th crack (mm)	Width of 7th crack (mm)	Max. crack width (mm)	Min. crack width (mm)	Ave. crack width (mm)
FA 1 – 12 – 75	1st	11.56	102.21	0.15	0.08	0.05	-	-	-	-	-	-	0.15	0.05	0.09
	2nd	16.93	149.69	0.22	0.10	0.1	0.08	-	-	-	-	-	0.22	0.08	0.13
	3rd	20.06	177.37	0.25	0.11	0.11	0.1	0.05	-	-	-	-	0.25	0.05	0.12
	4th	25.02	221.23	0.28	0.12	0.13	0.13	0.09	0.08	-	-	-	0.28	0.08	0.14
	5th	27.46	242.80	0.30	0.12	0.15	0.15	0.1	0.1	0.08	-	-	0.30	0.08	0.14
	6th	35.01	309.56	0.32	0.18	0.2	0.19	0.14	0.17	0.12	-	-	0.32	0.12	0.19
	7th	45.91	405.93	0.34	0.25	0.32	0.35	0.2	0.22	0.18	-	-	0.35	0.18	0.27
	8th	55.06	486.84	0.42	0.28	0.39	0.41	0.29	0.27	0.25	-	-	0.42	0.25	0.33
	9th	60.01	530.60	0.47	0.31	0.42	0.46	0.35	0.31	0.28	-	-	0.47	0.28	0.37
	10th	62	548.20	0.50	0.40	0.48	0.48	0.4	0.35	0.31	-	-	0.50	0.31	0.42
FA 2 – 12 – 75	1st	12.66	111.94	0.05	0.09	0.05	0.03	-	-	-	-	-	0.09	0.03	0.05
	2nd	13.68	120.96	0.06	0.10	0.05	0.04	-	-	-	-	-	0.10	0.04	0.06
	3rd	14.58	128.92	0.08	0.11	0.07	0.07	0.05	-	-	-	-	0.11	0.05	0.08
	4th	20.2	178.61	0.13	0.21	0.1	0.08	0.06	0.06	-	-	-	0.21	0.06	0.11
	5th	24.55	217.07	0.15	0.25	0.12	0.1	0.07	0.07	-	-	-	0.25	0.07	0.13
	6th	30.04	265.61	0.15	0.30	0.18	0.18	0.1	0.08	-	-	-	0.30	0.08	0.17
	7th	35.03	309.73	0.18	0.34	0.2	0.2	0.15	0.12	-	-	-	0.34	0.12	0.20
	8th	40.03	353.94	0.19	0.37	0.25	0.23	0.18	0.15	-	-	-	0.37	0.15	0.23
	9th	45.12	398.95	0.22	0.39	0.27	0.25	0.18	0.2	-	-	-	0.39	0.18	0.25
	10th	50.56	447.05	0.24	0.41	0.3	0.3	0.2	0.21	0.1	0.08	-	0.41	0.08	0.23
	11th	55.18	487.90	0.31	0.43	0.33	0.33	0.22	0.25	0.15	0.1	-	0.43	0.10	0.27

	12th	60.07	531.14	0.33	0.46	0.4	0.35	0.25	0.28	0.2	0.13	-	0.46	0.13	0.30
	13th	61.72	545.72	0.35	0.48	0.43	0.39	0.3	0.32	0.22	0.15	-	0.48	0.15	0.33
FA 3 – 16 – 75	1st	22.73	113.05	0.13	0.10	0.1	-	-	-	-	-	-	0.13	0.10	0.11
	2nd	24.3	120.86	0.14	0.11	0.12	0.1	-	-	-	-	-	0.14	0.10	0.12
	3rd	25.32	125.93	0.15	0.12	0.14	0.11	0.05	-	-	-	-	0.15	0.05	0.11
	4th	26.52	131.90	0.15	0.13	0.15	0.13	0.05	0.05	-	-	-	0.15	0.05	0.11
	5th	27.16	135.08	0.16	0.13	0.15	0.135	0.05	0.07	0.1	-	-	0.16	0.05	0.11
	6th	28.17	140.11	0.16	0.14	0.155	0.14	0.06	0.09	0.12	0.05	-	0.16	0.05	0.11
	7th	32	159.15	0.19	0.16	0.17	0.15	0.08	0.1	0.12	0.07	-	0.19	0.07	0.13
	8th	42	208.89	0.24	0.22	0.19	0.18	0.1	0.12	0.16	0.09	-	0.24	0.09	0.16
	9th	52	258.63	0.28	0.25	0.21	0.18	0.11	0.15	0.12	0.1	-	0.28	0.10	0.18
	10th	62	308.36	0.29	0.28	0.24	0.2	0.15	0.19	0.13	0.11	-	0.29	0.11	0.20
	11th	72	358.10	0.31	0.30	0.29	0.24	0.2	0.23	0.18	0.11	-	0.31	0.11	0.23
	12th	82	407.83	0.34	0.33	0.35	0.3	0.3	0.24	0.21	0.12	-	0.35	0.12	0.27
	13th	92	457.57	0.34	0.36	0.4	0.32	0.35	0.33	0.27	0.15	0.1	0.40	0.10	0.29
	14th	102	507.31	0.35	0.41	0.43	0.37	0.39	0.36	0.31	0.14	0.13	0.43	0.13	0.32
	15th	107	532.17	0.39	0.43	0.5	0.43	0.45	0.43	0.35	0.2	0.16	0.50	0.16	0.37
FA 4 – 16 – 75	1st	18.21	90.57	0.05	0.09	0.05	-	-	-	-	-	-	0.09	0.05	0.06
	2nd	19.1	95.00	0.05	0.09	0.05	0.05	-	-	-	-	-	0.09	0.05	0.06
	3rd	22.35	111.16	0.09	0.12	0.08	0.08	0.05	-	-	-	-	0.12	0.05	0.08
	4th	28.02	139.36	0.10	0.13	0.1	0.09	0.07	-	-	-	-	0.13	0.07	0.10
	5th	29.55	146.97	0.12	0.17	0.12	0.11	0.09	0.07	-	-	-	0.17	0.07	0.11
	6th	30.14	149.90	0.14	0.22	0.15	0.14	0.1	0.09	0.02	-	-	0.22	0.02	0.12
	7th	38.02	189.10	0.16	0.24	0.18	0.16	0.12	0.1	0.02	0.05	-	0.24	0.02	0.13
	8th	48.55	241.47	0.17	0.27	0.2	0.19	0.17	0.12	0.05	0.07	-	0.27	0.05	0.16
	9th	58.24	289.66	0.19	0.28	0.23	0.22	0.22	0.15	0.1	0.09	-	0.28	0.09	0.19
	10th	68.45	340.44	0.22	0.31	0.25	0.28	0.25	0.19	0.12	0.12	-	0.31	0.12	0.22

	11th	78.52	390.53	0.25	0.33	0.31	0.33	0.3	0.22	0.18	0.13	-	0.33	0.13	0.26
	12th	88.1	438.17	0.29	0.35	0.35	0.38	0.33	0.25	0.21	0.15	-	0.38	0.15	0.29
	13th	98.22	488.51	0.34	0.37	0.42	0.45	0.38	0.31	0.25	0.18	-	0.45	0.18	0.34
	14th	108.45	539.39	0.35	0.40	0.52	0.5	0.4	0.39	0.3	0.22	-	0.52	0.22	0.39
FA 1 – 12 – 150	1st	56.35	498.29	NA	NA	0.2	-	-	-	-	-	-	0.20	0.20	0.20
	2nd	60.41	534.15	NA	NA	0.35	0.07	-	-	-	-	-	0.35	0.07	0.21
	3rd	59.86	529.35	NA	NA	0.5	0.15	0.09	-	-	-	-	0.50	0.09	0.25
	4th	62.11	549.2	NA	NA	0.55	0.3	0.15	0.2	-	-	-	0.55	0.15	0.30
	5th	62.29	550.78	NA	NA	0.55	0.35	0.25	0.25	0.05	-	-	0.55	0.05	0.29
	6th	62.36	551.37	NA	NA	0.56	0.4	0.4	0.25	0.15	0.1	-	0.56	0.10	0.31
	Failure	69.38	613.46	NA	NA	3.58	1.6	0.46	0.7	0.2	0.1	-	3.58	0.10	1.11
FA 2 – 12 – 150	1st	61.22	541.34	NA	NA	0.35	-	-	-	-	-	-	0.35	0.35	0.35
	2nd	61.18	540.96	NA	NA	0.35	0.15	-	-	-	-	-	0.35	0.15	0.25
	3rd	62.71	554.51	NA	NA	0.45	0.25	0.09	-	-	-	-	0.45	0.09	0.26
	Failure	71.32	630.67	NA	NA	7	2	1.5	-	-	-	-	7.00	1.50	3.50
FA 3 – 16 – 150	1st	41.65	207.17	NA	NA	0.07	-	-	-	-	-	-	0.07	0.07	0.07
	2nd	58.01	288.53	NA	NA	0.12	0.06	-	-	-	-	-	0.12	0.06	0.09
	3rd	80.74	401.58	NA	NA	0.35	0.1	0.05	-	-	-	-	0.35	0.05	0.17
	4th	89.34	444.34	NA	NA	0.5	0.25	0.1	0.1	-	-	-	0.50	0.10	0.24
	5th	114.29	568.44	NA	NA	0.65	0.3	0.15	0.13	0.2	-	-	0.65	0.13	0.29
	Failure	132.21	657.57	NA	NA	7	0.45	2	1.5	3.2	-	-	7.00	0.45	2.83
FA 4 – 16 – 150	1st	67.84	337.42	NA	NA	0.05	-	-	-	-	-	-	0.05	0.05	0.05
	2nd	71.36	354.94	NA	NA	0.15	0.1	-	-	-	-	-	0.15	0.10	0.13
	3rd	62.8	312.36	NA	NA	0.45	0.25	0.2	-	-	-	-	0.45	0.20	0.30
	4th	71.83	357.28	NA	NA	0.55	0.3	0.25	0.1	-	-	-	0.55	0.10	0.30
	5th	116.64	580.25	NA	NA	0.6	0.45	0.3	0.17	0.05	-	-	0.60	0.05	0.31
	Failure	128.34	638.32	NA	NA	8	5	3	1.5	0.07	-	-	8.00	0.07	3.51

GLSS 1 – 12 – 75	1st	9.21	81.43	0.08	0.08	0.01	-	-	-	-	-	-	0.08	0.01	0.06
	2nd	10.1	89.30	0.10	0.09	0.02	0.01	0.01	-	-	-	-	0.10	0.01	0.05
	3rd	10.77	95.23	0.10	0.12	0.02	0.05	0.05	-	-	-	-	0.12	0.02	0.07
	4th	13.85	122.46	0.11	0.15	0.08	0.08	0.08	0.05	-	-	-	0.15	0.05	0.09
	5th	14.94	132.10	0.12	0.18	0.1	0.1	0.1	0.07	0.05	-	-	0.18	0.05	0.10
	6th	20.4	180.38	0.15	0.23	0.12	0.11	0.11	0.1	0.08	-	-	0.23	0.08	0.13
	7th	25.51	225.56	0.17	0.28	0.15	0.12	0.12	0.1	0.08	-	-	0.28	0.08	0.15
	8th	30.02	265.44	0.19	0.32	0.15	0.12	0.12	0.12	0.08	-	-	0.32	0.08	0.16
	9th	35.07	310.09	0.20	0.35	0.17	0.13	0.13	0.15	0.1	0.08	-	0.35	0.08	0.16
	10th	40.93	361.90	0.23	0.38	0.19	0.15	0.15	0.19	0.15	0.1	-	0.38	0.10	0.19
	11th	45.05	398.33	0.24	0.40	0.2	0.15	0.17	0.2	0.17	0.13	-	0.40	0.13	0.21
	12th	50.22	444.04	0.28	0.42	0.22	0.18	0.19	0.22	0.19	0.15	-	0.42	0.15	0.23
	13th	55.1	487.19	0.34	0.44	0.23	0.19	0.2	0.22	0.2	0.15	0.09	0.44	0.09	0.23
	14th	60.2	532.28	0.44	0.47	0.24	0.21	0.22	0.24	0.2	0.15	0.1	0.47	0.10	0.25
GLSS 2 – 12 – 75	1st	9.64	85.24	0.03	0.08	0.02	0.02	-	-	-	-	-	0.08	0.02	0.04
	2nd	10.02	88.60	0.05	0.09	0.03	0.02	0.02	-	-	-	-	0.09	0.02	0.04
	3rd	15.55	137.49	0.13	0.15	0.09	0.09	0.05	0.03	-	-	-	0.15	0.03	0.09
	4th	20.05	177.28	0.19	0.22	0.12	0.12	0.1	0.05	0.04	-	-	0.22	0.04	0.12
	5th	25.32	223.88	0.25	0.24	0.15	0.14	0.12	0.07	0.05	-	-	0.25	0.05	0.15
	6th	30.22	267.20	0.30	0.29	0.19	0.19	0.15	0.09	0.06	0.06	-	0.30	0.06	0.17
	7th	35.62	314.95	0.35	0.32	0.23	0.25	0.19	0.12	0.1	0.09	-	0.35	0.09	0.21
	8th	40.21	355.53	0.38	0.37	0.25	0.27	0.2	0.15	0.12	0.1	-	0.38	0.10	0.23
	9th	45.5	402.31	0.39	0.41	0.25	0.29	0.22	0.19	0.13	0.11	-	0.41	0.11	0.25
	10th	50.22	444.04	0.41	0.44	0.29	0.32	0.25	0.23	0.18	0.11	-	0.44	0.11	0.28
	11th	55.32	489.14	0.43	0.48	0.31	0.35	0.28	0.24	0.2	0.12	-	0.48	0.12	0.30
	12th	60.31	533.26	0.45	0.50	0.35	0.39	0.33	0.3	0.22	0.15	0.1	0.50	0.10	0.31
GLSS 3	1st	8.33	41.43	0.00	0.00	0.02	-	-	-	-	-	-	0.02	0.00	0.01

	2nd	8.93	44.41	0.00	0.00	0.02	0.01	-	-	-	-	-	0.02	0.00	0.01
	3rd	10	49.74	0.00	0.00	0.05	0.03	0.02	-	-	-	-	0.05	0.00	0.02
	4th	12.03	59.83	0.01	0.02	0.09	0.05	0.03	0.03	-	-	-	0.09	0.01	0.04
	5th	14.11	70.18	0.05	0.05	0.1	0.08	0.05	0.05	0.01	-	-	0.10	0.01	0.06
	6th	16.04	79.78	0.08	0.08	0.11	0.1	0.06	0.06	0.03	0.05	-	0.11	0.03	0.07
	7th	20.23	100.62	0.10	0.12	0.12	0.12	0.08	0.08	0.05	0.07	-	0.12	0.05	0.09
	8th	25.73	127.97	0.15	0.14	0.12	0.12	0.1	0.1	0.07	0.09	-	0.15	0.07	0.11
	9th	30.52	151.79	0.18	0.15	0.14	0.13	0.11	0.12	0.09	0.1	-	0.18	0.09	0.13
	10th	35.05	174.32	0.22	0.18	0.18	0.15	0.13	0.14	0.11	0.11	-	0.22	0.11	0.15
	11th	40.11	199.49	0.30	0.22	0.19	0.18	0.17	0.17	0.13	0.11	-	0.30	0.11	0.18
	12th	50.33	250.32	0.33	0.28	0.21	0.2	0.2	0.2	0.14	0.12	-	0.33	0.12	0.21
	13th	60.07	298.76	0.35	0.32	0.22	0.22	0.22	0.22	0.16	0.15	-	0.35	0.15	0.23
	14th	70.52	350.74	0.38	0.35	0.25	0.23	0.24	0.24	0.18	0.14	-	0.38	0.14	0.25
	15th	80.38	399.78	0.40	0.39	0.28	0.25	0.26	0.26	0.2	0.18	-	0.40	0.18	0.28
	16th	90.2	448.62	0.42	0.42	0.3	0.28	0.27	0.27	0.24	0.19	-	0.42	0.19	0.30
	17th	100.03	497.51	0.44	0.45	0.32	0.3	0.28	0.28	0.26	0.2	-	0.45	0.20	0.32
GLSS 4 – 16 – 75	1st	9.24	45.96	0	0.00	0.02	-	-	-	-	-	-	0.02	0.00	0.01
	2nd	10.2	50.73	0.02	0.00	0.02	0.01	-	-	-	-	-	0.02	0.00	0.01
	3rd	12.11	60.23	0.02	0.00	0.05	0.02	0.01	-	-	-	-	0.05	0.00	0.02
	4th	14.3	71.12	0.08	0.01	0.08	0.05	0.01	0.01	-	-	-	0.08	0.01	0.04
	5th	18.2	90.52	0.09	0.02	0.09	0.07	0.02	0.01	0.03	-	-	0.09	0.01	0.05
	6th	20.11	100.02	0.12	0.08	0.1	0.09	0.05	0.02	0.05	0.01	-	0.12	0.01	0.07
	7th	25.1	124.84	0.18	0.12	0.12	0.11	0.07	0.03	0.05	0.01	-	0.18	0.01	0.09
	8th	30.1	149.71	0.21	0.18	0.15	0.14	0.08	0.05	0.08	0.02	-	0.21	0.02	0.11
	9th	35.07	174.42	0.23	0.22	0.18	0.17	0.1	0.06	0.1	0.04	-	0.23	0.04	0.14
	10th	40.11	199.49	0.30	0.28	0.2	0.2	0.15	0.08	0.12	0.06	-	0.3	0.06	0.17
	11th	50.16	249.48	0.34	0.34	0.22	0.22	0.16	0.09	0.13	0.08	0.05	0.34	0.05	0.18

	12th	60.05	298.66	0.40	0.36	0.24	0.24	0.18	0.1	0.15	0.1	0.08	0.4	0.08	0.21
	13th	70.52	350.74	0.42	0.38	0.32	0.32	0.22	0.12	0.17	0.12	0.1	0.42	0.10	0.24
	14th	80.04	398.09	0.44	0.40	0.38	0.38	0.28	0.15	0.19	0.14	0.14	0.44	0.14	0.28
	15th	90.31	449.17	0.46	0.44	0.43	0.45	0.3	0.2	0.22	0.16	0.18	0.46	0.16	0.32
	16th	100.02	497.46	0.48	0.45	0.55	0.55	0.38	0.28	0.24	0.18	0.16	0.55	0.16	0.36
GLSS 1 – 12 – 150	1st	60.01	530.63	NA	NA	0.5	-	-	-	-	-	-	0.50	0.50	0.50
	2nd	61.1	540.27	NA	NA	0.55	0.5	-	-	-	-	-	0.55	0.50	0.53
	Failure	70.4	622.52	NA	NA	6	2	-	-	-	-	-	6.00	2.00	4.00
GLSS 2 – 12 – 150	1st	60.24	532.66	NA	NA	0.5	0.45	-	-	-	-	-	0.50	0.45	0.48
	2nd	60.24	532.66	NA	NA	0.6	0.5	-	-	-	-	-	0.60	0.50	0.55
	Failure	73.43	649.3	NA	NA	8	3	-	-	-	-	-	8.00	3.00	5.50
GLSS 3 – 16 – 150	1st	50.53	251.34	NA	NA	0.05	-	-	-	-	-	-	0.05	0.05	0.05
	2nd	57.61	286.13	NA	NA	0.15	0.07	-	-	-	-	-	0.15	0.07	0.11
	Failure	128.86	640.94	NA	NA	9.6	8.1	-	-	-	-	-	9.60	8.10	8.85
GLSS 4 – 16 – 150	1st	57.52	286.12	NA	NA	0.08	-	-	-	-	-	-	0.08	0.08	0.08
	2nd	68.94	342.88	NA	NA	0.35	0.2	-	-	-	-	-	0.35	0.20	0.28
	3rd	78.69	391.37	NA	NA	0.4	0.35	0.1	-	-	-	-	0.40	0.10	0.28
	4th	111.02	552.18	NA	NA	0.5	0.4	0.15	0.07	-	-	-	0.50	0.07	0.28
	Failure	128.38	638.51	NA	NA	10	7	3	0.1	-	-	-	10.00	0.10	5.03
OPC 1 – 12 – 150	Failure	74.73	660.81	NA	NA	-	-	-	-	-	-	-	0.00	0.00	0.00
OPC 2 – 12 – 150	Failure	74.15	655.67	NA	NA	-	-	-	-	-	-	-	0.00	0.00	0.00
OPC 3 – 16 – 150	1st	66.81	332.3	NA	NA	0.3	-	-	-	-	-	-	0.30	0.30	0.30
	2nd	100.34	499.08	NA	NA	0.45	0.25	-	-	-	-	-	0.45	0.25	0.35

	3rd	100.91	501.89	NA	NA	0.5	0.45	0.15	-	-	-	-	0.50	0.15	0.37
	Failure	119.01	591.49	NA	NA	10.7	8.4	2.3	-	-	-	-	10.70	2.30	7.13
OPC 4 – 16 – 150	1st	69.25	344.46	NA	NA	0.15	-	-	-	-	-	-	0.15	0.15	0.15
	2nd	74.9	372.54	NA	NA	0.25	0.07	-	-	-	-	-	0.25	0.07	0.16
	3rd	82.14	408.54	NA	NA	0.39	0.15	0.1	-	-	-	-	0.39	0.10	0.21
	4th	103.03	512.46	NA	NA	0.5	0.3	0.15	0.1	-	-	-	0.50	0.10	0.26
	5th	115.04	572.16	NA	NA	0.6	0.4	0.2	0.15	0.05	-	-	0.60	0.05	0.28

Table S2. Crack width regression analysis for each specimen.

Specimen	Crack widths (mm)		
	Maximum	Average	Minimum
FA 1 – 12 – 75	w_c= 0.335σ_s/f_y + 0.122 R^2 = 0.953	w_c = 0.345σ_s/f_y + 0.0073 R^2 = 0.972	w_c = 0.292σ_s/f_y - 0.031 R^2 = 0.943
FA 2 – 12 – 75	w_c = 0.455σ_s/f_y + 0.032 R^2 = 0.948	w_c = 0.306σ_s/f_y + 0.0021 R^2 = 0.970	w_c = 0.121σ_s/f_y + 0.023 R^2 = 0.585
FA 3 – 16 – 75	w_c = 0.409σ_s/f_y + 0.054 R^2 = 0.979	w_c = 0.304σ_s/f_y + 0.037 R^2 = 0.984	w_c = 0.093σ_s/f_y + 0.046 R^2 = 0.664
FA 4 – 16 – 75	w_c = 0.446σ_s/f_y + 0.037 R^2 = 0.952	w_c = 0.355σ_s/f_y + 0.0034 R^2 = 0.988	w_c = 0.193σ_s/f_y - 0.0042 R^2 = 0.852
FA 1 – 12 – 150	w_c = 3.480σ_s/f_y - 3.065 R^2 = 0.844	w_c = 1.056σ_s/f_y - 0.808 R^2 = 0.739	w_c = -0.935σ_s/f_y + 1.054 R^2 = 0.424
FA 2 – 12 – 150	w_c = 3.964σ_s/f_y - 3.698 R^2 = 0.999	w_c = -1.369σ_s/f_y + 1.697 R^2 = 0.134	w_c = -6.174σ_s/f_y + 6.552 R^2 = 0.436
FA 3 – 16 – 150	w_c = 0.918σ_s/f_y - 0.32 R^2 = 0.967	w_c = 0.343σ_s/f_y - 0.077 R^2 = 0.954	w_c = 0.09σ_s/f_y + 0.015 R^2 = 0.551
FA 4 – 16 – 150	w_c = 0.629σ_s/f_y - 0.101 R^2 = 0.275	w_c = 0.239σ_s/f_y + 0.042 R^2 = 0.161	w_c = -0.164σ_s/f_y + 0.220 R^2 = 0.302
GLSS 1 – 12 – 75	w_c = 0.447σ_s/f_y + 0.055 R^2 = 0.957	w_c = 0.226σ_s/f_y + 0.034 R^2 = 0.966	w_c = 0.119σ_s/f_y + 0.013 R^2 = 0.71
GLSS 2 – 12 – 75	w_c = 0.497σ_s/f_y + 0.028 R^2 = 0.981	w_c = 0.327σ_s/f_y + 0.0003 R^2 = 0.988	w_c = 0.124σ_s/f_y + 0.0021 R^2 = 0.909
GLSS 3 – 16 – 75	w_c = 0.505σ_s/f_y + 0.029 R^2 = 0.936	w_c = 0.361σ_s/f_y + 0.010 R^2 = 0.954	w_c = 0.240σ_s/f_y - 0.0033 R^2 = 0.934
GLSS 4 – 16 – 75	w_c = 0.602σ_s/f_y + 0.0094 R^2 = 0.953	w_c = 0.398σ_s/f_y - 0.012 R^2 = 0.985	w_c = 0.202σ_s/f_y - 0.025 R^2 = 0.970
GLSS 1 – 12 – 150	w_c = 2.749σ_s/f_y - 2.252 R^2 = 0.989	w_c = 1.374σ_s/f_y - 0.876 R^2 = 0.998	w_c = 1.345σ_s/f_y - 0.857 R^2 = 0.999
GLSS 2 – 12 – 150	w_c = 0.478σ_s/f_y - 0.012 R^2 = 0.987	w_c = 0.878σ_s/f_y - 0.012 R^2 = 0.999	w_c = 4.95σ_s/f_y - 0.012 R^2 = 0.915
GLSS 3 – 16 – 150	w_c = 1.523σ_s/f_y - 0.672 R^2 = 0.997	w_c = 0.914σ_s/f_y - 0.383 R^2 = 0.999	w_c = 0.304σ_s/f_y - 0.094 R^2 = 0.998
GLSS 4 – 16 – 150	w_c = 0.710σ_s/f_y - 0.194 R^2 = 0.730	w_c = 0.292σ_s/f_y + 0.0129 R^2 = 0.399	w_c = -0.103σ_s/f_y + 0.1891 R^2 = 0.139
OPC 3 – 16 – 150	w_c = 0.553σ_s/f_y - 0.047 R^2 = 0.948	w_c = 0.184σ_s/f_y + 0.184 R^2 = 0.948	w_c = -0.319σ_s/f_y + 0.500 R^2 = 0.585
OPC 4 – 16 – 150	w_c = 0.967σ_s/f_y - 0.429 R^2 = 0.938	w_c = 0.312σ_s/f_y - 0.047 R^2 = 0.946	w_c = -0.132σ_s/f_y + 0.204 R^2 = 0.404

Table S3. Crack width using *Eq. 11* for Eurocode, *Eq. 16* for leaner approach and *Eq. 20* for non-linear approach

ID No.	Load stage	Load, P (kN)	$w_{c,Exp.}$ (mm)	Eurocode 2 (2004)	Linear approach (mm)				Non-linear approach (mm)	
					Albitar et al. (2016)		CEB–FIP (1992)		CEB–FIP (1992)	
				w_c	Δ_r	w_c	Δ_r	w_c	Δ_r	w_c
FA 1 – 12 – 75	1st	11.56	0.15	-0.02	0.05	0.10	0.06	0.11	0.04	0.09
	2nd	16.93	0.22	0.06	0.08	0.15	0.08	0.16	0.06	0.13
	3rd	20.06	0.25	0.10	0.09	0.18	0.10	0.20	0.07	0.15
	4th	25.02	0.28	0.17	0.11	0.22	0.12	0.24	0.09	0.19
	5th	27.46	0.30	0.21	0.12	0.24	0.13	0.27	0.10	0.20
	6th	35.01	0.32	0.32	0.16	0.31	0.17	0.34	0.13	0.26
	7th	45.91	0.35	0.48	0.20	0.41	0.22	0.45	0.17	0.34
	8th	55.06	0.42	0.61	0.24	0.49	0.27	0.54	0.20	0.41
	9th	60.01	0.47	0.68	0.27	0.53	0.29	0.58	0.22	0.45
	10th	62.00	0.50	0.71	0.28	0.55	0.30	0.60	0.23	0.46
FA 2 – 12 – 75	1st	12.66	0.09	0.00	0.06	0.11	0.06	0.12	0.05	0.09
	2nd	13.68	0.10	0.01	0.06	0.12	0.07	0.13	0.05	0.10
	3rd	14.58	0.11	0.02	0.06	0.13	0.07	0.14	0.05	0.11
	4th	20.20	0.21	0.10	0.09	0.18	0.10	0.20	0.07	0.15
	5th	24.55	0.25	0.17	0.11	0.22	0.12	0.24	0.09	0.18
	6th	30.04	0.30	0.25	0.13	0.27	0.15	0.29	0.11	0.22
	7th	35.03	0.34	0.32	0.16	0.31	0.17	0.34	0.13	0.26
	8th	40.03	0.37	0.39	0.18	0.36	0.19	0.39	0.15	0.30
	9th	45.12	0.39	0.46	0.20	0.40	0.22	0.44	0.17	0.33
	10th	50.56	0.41	0.54	0.22	0.45	0.25	0.49	0.19	0.38
	11th	55.18	0.43	0.61	0.25	0.49	0.27	0.54	0.20	0.41
	12th	60.07	0.46	0.68	0.27	0.53	0.29	0.58	0.22	0.45
	13th	61.72	0.48	0.70	0.27	0.55	0.30	0.60	0.23	0.46
FA 3 – 16 – 75	1st	17.71	0.13	0.02	0.05	0.11	0.06	0.13	0.05	0.09
	2nd	24.30	0.14	0.07	0.06	0.12	0.07	0.14	0.05	0.10
	3rd	25.32	0.15	0.08	0.06	0.12	0.07	0.14	0.05	0.10
	4th	26.52	0.15	0.08	0.06	0.13	0.08	0.15	0.05	0.11
	5th	27.16	0.16	0.09	0.06	0.13	0.08	0.16	0.05	0.11
	6th	28.17	0.16	0.10	0.07	0.13	0.08	0.16	0.06	0.11
	7th	32.00	0.19	0.12	0.08	0.15	0.09	0.18	0.06	0.13
	8th	42.00	0.24	0.19	0.10	0.20	0.12	0.24	0.08	0.17
	9th	52.00	0.28	0.26	0.12	0.25	0.15	0.30	0.11	0.21
	10th	62.00	0.29	0.33	0.15	0.30	0.18	0.35	0.13	0.25

	11th	72.00	0.31	0.39	0.17	0.34	0.21	0.41	0.15	0.29
	12th	82.00	0.35	0.46	0.20	0.39	0.23	0.47	0.17	0.33
	13th	92.00	0.40	0.53	0.22	0.44	0.26	0.53	0.19	0.37
	14th	102.00	0.43	0.60	0.24	0.49	0.29	0.58	0.21	0.41
	15th	107.00	0.50	0.63	0.26	0.51	0.31	0.61	0.22	0.43
FA 4 – 16 – 75	1st	18.28	0.09	0.03	0.04	0.09	0.05	0.10	0.04	0.07
	2nd	19.10	0.09	0.03	0.05	0.09	0.05	0.11	0.04	0.08
	3rd	22.35	0.12	0.06	0.05	0.11	0.06	0.13	0.05	0.09
	4th	28.02	0.13	0.09	0.07	0.13	0.08	0.16	0.06	0.11
	5th	29.55	0.17	0.11	0.07	0.14	0.08	0.17	0.06	0.12
	6th	30.14	0.22	0.11	0.07	0.14	0.09	0.17	0.06	0.12
	7th	38.02	0.24	0.16	0.09	0.18	0.11	0.22	0.08	0.15
	8th	48.55	0.27	0.23	0.12	0.23	0.14	0.28	0.10	0.20
	9th	58.24	0.28	0.30	0.14	0.28	0.17	0.33	0.12	0.24
	10th	68.45	0.31	0.37	0.16	0.33	0.20	0.39	0.14	0.28
	11th	78.52	0.33	0.44	0.19	0.38	0.22	0.45	0.16	0.32
	12th	88.10	0.38	0.50	0.21	0.42	0.25	0.50	0.18	0.36
	13th	98.22	0.45	0.57	0.23	0.47	0.28	0.56	0.20	0.40
	14th	108.45	0.52	0.64	0.26	0.52	0.31	0.62	0.22	0.44
FA 1 – 12 – 150	1st	56.35	0.20	0.03	0.41	0.83	0.48	0.96	0.49	0.98
	2nd	60.41	0.35	0.10	0.44	0.89	0.51	1.03	0.53	1.05
	3rd	59.86	0.50	0.09	0.44	0.88	0.51	1.02	0.52	1.04
	4th	62.11	0.55	0.12	0.46	0.91	0.53	1.06	0.54	1.08
	5th	62.29	0.55	0.13	0.46	0.91	0.53	1.06	0.54	1.09
	6th	62.36	0.56	0.13	0.46	0.91	0.53	1.06	0.54	1.09
	Failure	69.38	3.58	0.24	0.51	1.02	0.59	1.18	0.60	1.21
FA 2 – 12 – 150	1st	61.22	0.35	0.11	0.45	0.90	0.52	1.04	0.53	1.07
	2nd	61.18	0.35	0.11	0.45	0.90	0.52	1.04	0.53	1.07
	3rd	62.71	0.45	0.13	0.46	0.92	0.53	1.07	0.55	1.09
	Failure	71.32	7.00	0.27	0.52	1.05	0.61	1.21	0.62	1.24
FA 3 – 16 – 150	1st	41.65	0.07	-0.10	0.17	0.35	0.20	0.40	0.20	0.40
	2nd	58.01	0.12	0.02	0.24	0.48	0.28	0.56	0.28	0.55
	3rd	80.74	0.35	0.18	0.34	0.67	0.39	0.78	0.39	0.77
	4th	89.34	0.50	0.24	0.37	0.75	0.43	0.87	0.43	0.85
	5th	114.29	0.65	0.42	0.48	0.95	0.55	1.11	0.55	1.09
	Failure	132.21	7.00	0.55	0.55	1.10	0.64	1.28	0.63	1.26
FA 4 – 16 – 150	1st	67.84	0.05	0.09	0.28	0.57	0.33	0.66	0.32	0.65
	2nd	71.36	0.15	0.11	0.30	0.60	0.35	0.69	0.34	0.68
	3rd	62.80	0.45	0.05	0.26	0.52	0.30	0.61	0.30	0.60
	4th	71.83	0.55	0.12	0.30	0.60	0.35	0.70	0.34	0.69

	5th	116.64	0.60	0.44	0.49	0.97	0.56	1.13	0.56	1.11
	Failure	128.34	8.00	0.52	0.54	1.07	0.62	1.24	0.61	1.22
GLSS 1 – 12 – 75	1st	9.21	0.08	-0.05	0.04	0.08	0.05	0.10	0.03	0.07
	2nd	10.10	0.10	-0.03	0.04	0.09	0.06	0.11	0.04	0.07
	3rd	10.77	0.12	-0.02	0.05	0.09	0.06	0.12	0.04	0.08
	4th	13.85	0.15	0.02	0.06	0.12	0.08	0.15	0.05	0.10
	5th	14.94	0.18	0.04	0.06	0.13	0.08	0.16	0.06	0.11
	6th	20.40	0.23	0.12	0.09	0.18	0.11	0.22	0.08	0.15
	7th	25.51	0.28	0.19	0.11	0.22	0.14	0.28	0.09	0.19
	8th	30.02	0.32	0.26	0.13	0.26	0.16	0.33	0.11	0.22
	9th	35.07	0.35	0.33	0.15	0.30	0.19	0.38	0.13	0.26
	10th	40.93	0.38	0.41	0.18	0.36	0.22	0.45	0.15	0.30
	11th	45.05	0.40	0.47	0.20	0.39	0.25	0.49	0.17	0.33
	12th	50.22	0.42	0.55	0.22	0.44	0.27	0.55	0.19	0.37
	13th	55.10	0.44	0.62	0.24	0.48	0.30	0.60	0.20	0.41
	14th	60.20	0.47	0.69	0.26	0.52	0.33	0.66	0.22	0.45
GLSS 2 – 12 – 75	1st	9.64	0.08	-0.04	0.04	0.08	0.05	0.11	0.04	0.07
	2nd	10.02	0.09	-0.03	0.04	0.09	0.05	0.11	0.04	0.07
	3rd	15.55	0.15	0.05	0.07	0.14	0.09	0.17	0.06	0.12
	4th	20.05	0.22	0.11	0.09	0.17	0.11	0.22	0.07	0.15
	5th	25.32	0.25	0.19	0.11	0.22	0.14	0.28	0.09	0.19
	6th	30.22	0.30	0.26	0.13	0.26	0.17	0.33	0.11	0.22
	7th	35.62	0.35	0.34	0.15	0.31	0.20	0.39	0.13	0.26
	8th	40.21	0.38	0.40	0.17	0.35	0.22	0.44	0.15	0.30
	9th	45.50	0.41	0.48	0.20	0.40	0.25	0.50	0.17	0.34
	10th	50.22	0.44	0.55	0.22	0.44	0.27	0.55	0.19	0.37
	11th	55.32	0.48	0.62	0.24	0.48	0.30	0.61	0.21	0.41
	12th	60.31	0.50	0.69	0.26	0.52	0.33	0.66	0.22	0.45
GLSS 3 – 16 – 75	1st	8.13	0.02	-0.04	0.02	0.04	0.02	0.05	0.02	0.03
	2nd	8.93	0.02	-0.03	0.02	0.04	0.03	0.05	0.02	0.04
	3rd	10.00	0.05	-0.02	0.02	0.05	0.03	0.06	0.02	0.04
	4th	12.03	0.09	-0.01	0.03	0.06	0.04	0.07	0.02	0.05
	5th	14.11	0.10	0.00	0.03	0.07	0.04	0.08	0.03	0.06
	6th	16.04	0.11	0.02	0.04	0.07	0.05	0.09	0.03	0.06
	7th	20.23	0.12	0.05	0.05	0.09	0.06	0.12	0.04	0.08
	8th	25.73	0.15	0.08	0.06	0.12	0.08	0.15	0.05	0.10
	9th	30.52	0.18	0.12	0.07	0.14	0.09	0.18	0.06	0.12
	10th	35.05	0.22	0.15	0.08	0.16	0.10	0.21	0.07	0.14
	11th	40.11	0.30	0.18	0.09	0.19	0.12	0.23	0.08	0.16
	12th	50.33	0.33	0.25	0.12	0.23	0.15	0.29	0.10	0.20
	13th	60.07	0.35	0.32	0.14	0.28	0.18	0.35	0.12	0.24

	14th	70.52	0.38	0.39	0.16	0.33	0.21	0.41	0.14	0.29
	15th	80.38	0.40	0.46	0.19	0.37	0.24	0.47	0.16	0.32
	16th	90.20	0.42	0.52	0.21	0.42	0.26	0.53	0.18	0.36
	17th	100.03	0.45	0.59	0.23	0.47	0.29	0.59	0.20	0.40
GLSS 4 – 16 – 75	1st	9.24	0.02	-0.03	0.02	0.04	0.03	0.05	0.02	0.04
	2nd	10.20	0.02	-0.02	0.02	0.05	0.03	0.06	0.02	0.04
	3rd	12.11	0.05	-0.01	0.03	0.06	0.04	0.07	0.02	0.05
	4th	14.30	0.08	0.01	0.03	0.07	0.04	0.08	0.03	0.06
	5th	18.20	0.09	0.03	0.04	0.08	0.05	0.11	0.04	0.07
	6th	20.11	0.12	0.04	0.05	0.09	0.06	0.12	0.04	0.08
	7th	25.10	0.18	0.08	0.06	0.12	0.07	0.15	0.05	0.10
	8th	30.10	0.21	0.11	0.07	0.14	0.09	0.18	0.06	0.12
	9th	35.07	0.23	0.15	0.08	0.16	0.10	0.21	0.07	0.14
	10th	40.11	0.30	0.18	0.09	0.19	0.12	0.23	0.08	0.16
	11th	50.16	0.34	0.25	0.12	0.23	0.15	0.29	0.10	0.20
	12th	60.05	0.40	0.32	0.14	0.28	0.18	0.35	0.12	0.24
	13th	70.52	0.42	0.39	0.16	0.33	0.21	0.41	0.14	0.29
	14th	80.04	0.44	0.45	0.19	0.37	0.23	0.47	0.16	0.32
	15th	90.31	0.46	0.52	0.21	0.42	0.26	0.53	0.18	0.37
	16th	100.02	0.55	0.59	0.23	0.47	0.29	0.59	0.20	0.40
GLSS 1 – 12 – 150	1st	59.70	0.50	0.10	0.21	0.42	0.24	0.49	0.24	0.48
	2nd	61.10	0.55	0.12	0.24	0.48	0.28	0.56	0.27	0.55
	Failure	70.40	6.00	0.27	0.54	1.08	0.62	1.25	0.61	1.23
GLSS 2 – 12 – 150	1st	60.24	0.50	0.11	0.24	0.48	0.28	0.56	0.27	0.55
	2nd	60.24	0.60	0.11	0.29	0.58	0.33	0.67	0.33	0.66
	Failure	73.43	8.00	0.32	0.33	0.66	0.38	0.76	0.38	0.75
GLSS 3 – 16 – 150	1st	48.99	0.05	-0.04	0.46	0.93	0.54	1.08	0.53	1.06
	2nd	57.61	0.15	0.02	0.54	1.07	0.62	1.24	0.61	1.22
	Failure	128.86	9.60	0.53	0.44	0.88	0.51	1.02	0.52	1.05
GLSS 4 – 16 – 150	1st	57.52	0.08	0.02	0.45	0.90	0.52	1.04	0.53	1.07
	2nd	68.94	0.35	0.10	0.52	1.03	0.60	1.20	0.61	1.23
	3rd	78.69	0.40	0.17	0.44	0.88	0.51	1.03	0.53	1.05
	4th	111.02	0.50	0.40	0.44	0.88	0.51	1.03	0.53	1.05
	Failure	128.38	10.00	0.53	0.54	1.08	0.63	1.25	0.64	1.28
OPC 1 – 12 – 150	Failure	74.73	0.00	0.26	0.24	0.48	0.31	0.61	0.32	0.64

OPC 2 – 12 – 150	Failure	74.15	0.00	0.25	0.36	0.71	0.46	0.92	0.48	0.96
OPC 3 – 16 – 150	1st	66.81	0.30	0.05	0.36	0.72	0.46	0.92	0.48	0.96
	2nd	100.34	0.45	0.29	0.42	0.85	0.55	1.09	0.57	1.13
	3rd	100.91	0.50	0.30	0.25	0.49	0.32	0.63	0.33	0.66
	Failure	119.01	10.70	0.43	0.27	0.53	0.34	0.69	0.36	0.71
OPC 4 – 16 – 150	1st	69.25	0.15	0.07	0.29	0.58	0.38	0.75	0.39	0.78
	2nd	74.90	0.25	0.11	0.37	0.73	0.47	0.94	0.49	0.98
	3rd	82.14	0.39	0.16	0.41	0.82	0.53	1.05	0.55	1.10
	4th	103.03	0.50	0.31	0.48	0.96	0.62	1.23	0.64	1.28
	5th	115.04	0.60	0.40	0.47	0.93	0.39	0.77	0.65	1.30
	Failure	134.34	8.50	0.53	0.46	0.92	0.38	0.77	0.65	1.29

REFERENCE

Albitar, M., Mohamed Ali, M. S., Visintin, P., Drechsler, M. (2015). "Effect of granulated lead smelter slag on strength of fly ash–based geopolymer concrete." *Construction and Building Materials*, vol. 83, pp. 128–135, DOI: 10.1016/j.conbuildmat.2015.03.009.

Albitar, M., Visintin, P., Mohamed Ali, M. S. and Drechsler, M. (2014). "Assessing behaviour of fresh and hardened geopolymer concrete mixed with class–F fly ash." *KSCE Journal of Civil Engineering*, Vol. 19, No. 5, pp. 1445–1455, DOI 10.1007/s12205-014-1254-z.

Albitar, M., Visintin, P., Mohamed Ali, M. S., Lavigne, O. and Gamboa, E. (2016). "Effect of corrosion on the bond between reinforcement and class–f fly ash–based geopolymer concrete." *Journal of Materials in Civil Engineering*, DOI: 10.1061/(ASCE)MT.1943-5533.0001713.

Balazs, G.L. (1993). "Cracking analysis based on slip and bond stresses." *ACI Materials Journal*, Vol. 90, No. 4, pp. 340–348.

Bischoff, P. H. (2001). "Effects of shrinkage on tension stiffening and cracking in reinforced concrete." *Canadian Journal of Civil Engineering*, Vol. 28, pp. 363–374, DOI: 10.1139/cjce-28-3-363.

Bischoff, P.H. (2005). "Revaluation of deflection prediction for concrete beams reinforced with steel and fiber reinforced polymer bars." *Journal of Structural Engineering*, (ASCE), Vol. 131, No. 5, pp. 752–767, DOI: org/10.1061/(ASCE)0733-9445(2005)131:5(752).

CEB (1992). *CEB-FIP Model Code 90*, Thomas Telford, London, UK.

Eurocode-2 (2004). *Eurocode 2: Design of Concrete Structures-Part 1: General Rules and Rules for Buildings*, European Committee for Standardization, Brussels, Belgium.

Fields, K. and Bischoff, P.H. (2004). "Tension stiffening and cracking of high-strength reinforced concrete tension members." ACI Structural Journal, Vol. 101, No. 4, pp. 447–456.

Ganesan, N., Indira, P.V. and Santhakumar, A. (2014). "Influence of steel fibres on tension stiffening and cracking of reinforced geopolymer concrete." *Magazine of Concrete Research*, Vol. 66, No. 6, pp. 268–276, DOI: org/10.1680/macr.13.00273.

Gilbert, R.I. (2008). “Revisiting the tension stiffening effect in reinforced concrete slabs.” *Australian Journal of Structural Engineering*, Vol. 8, No. 3, pp. 189–196, DOI: org/10.1080/13287982.2008.11464997.

Haskett, M., Oehlers, D.J. and Mohamed Ali, M.S. (2008). “Local and global bond characteristics of steel reinforcing bars.” *Engineering Structures*, Vol. 30, No. 2, pp. 376–383, DOI: org/10.1016/j.engstruct.2007.04.007.

Knight, D., Visintin, P., Oehlers, D. J. and Jumaat, M. Z. (2013). “Incorporating residual strains in the flexural rigidity of RC members with varying degrees of prestress and cracking.” *Advances in Structural Engineering*, Vol. 16, No. 10, pp. 1701–1718, DOI: 10.1260/1369-4332.16.10.1701.

Mohamed Ali, M.S., Oehlers, D.J. and Griffith, M. (2008). “Shear transfer across cracks in FRP strengthened RC structures.” *Journal of Composites for Construction*, Vol. 12, No. 4, pp. 416–424, DOI: 10.1061/(ASCE)1090-0268(2008)12:4(416).

Muhamad, R., Mohamed Ali, M.S., Oehlers, D.J. and Griffith, G. (2012). “The tension stiffening mechanism in reinforced concrete prisms.” *Advances in Structural Engineering*, Vol. 15 No. 12, pp. 2053–2069, DOI: 10.1260/1369-4332.15.12.2053.

Oehlers, D., Mohamed Ali, M.S., Haskett, M., Lucas, W., Muhamad, R. and Visintin, P. (2011). “FRP-reinforced concrete beams: unified approach based on IC theory.” *Journal of Composites for Construction*, Vol. 15, NO. 3, pp. 293–303, DOI: 10.1061/(ASCE)CC.1943-5614.0000173.

Visintin, P., Oehlers, D.J., Haskett, M. and Wu, C. (2013a). “Mechanics-based hinge analysis for reinforced concrete columns.” *Journal of Structural Engineering: ASCE*, Vol. 139, No. 11, pp. 1973–1980, DOI: 10.1061/(ASCE)ST.1943-541X.0000761.

Visintin, P., Oehlers, D.J., Muhamad, R. and Wu, C. (2013b). “Partial-interaction short term serviceability deflection of RC beams.” *Engineering Structures*, Vol. 56, pp. 993–1006, DOI: org/10.1016/j.engstruct.2013.06.021.

Visintin, P., Oehlers, D.J., Wu, C. and Haskett, M. (2012). “A mechanics solution for hinges in RC beams with multiple cracks.” *Engineering Structures*, Vol. 36, pp. 61–69, DOI: org/10.1016/j.engstruct.2011.11.028.

Zhang, T., Visintin, P. and Oehlers, D.J. (2016). “Partial-interaction tension-stiffening properties for numerical simulations.” *Advances in Structural Engineering*, DOI: 10.1177/1369433216660654.

CHAPTER 4: Structural Performance of Geopolymer Concrete Columns

Background

All the previous geopolymer properties investigated in Chapters 1, 2 and 3 have shown that geopolymer concrete has the potential to be used in structural applications. Therefore, in this chapter, the structural performance of geopolymer concrete columns manufactured using blended fly ash with granulated lead smelter slag (GLS) is investigated in "Experimental study on fly ash and lead smelter slag–based geopolymer concrete columns". This paper investigates the structural behaviour of fly ash with GLSS–based geopolymer concrete short and slender columns subjected to axial compression with different eccentricities. It is shown that the performance of blended fly ash with GLSS–based geopolymer concrete columns and beam is similar to that of OPC concrete, and hence the design provision contained in the current codes of practice can be adopted to design reinforced fly ash/GLSS–based geopolymer concrete structural members.

List of Manuscripts

Albitar, M., Mohamed Ali, M. S. and Visintin, P. (2016). "Experimental study on fly ash and lead smelter slag–based geopolymer concrete columns." *Magazine of Concrete Research*, submitted.

Statement of Authorship

Title of Paper	Experimental study on fly ash and lead smelter slag–based geopolymer concrete columns
Publication Details	Albitar, M., Mohamed Ali, M.S. and Visintin, P. (2016). "Experimental study on fly ash and lead smelter slag–based geopolymer concrete columns." *Magazine of Concrete Research*, submitted.
Publication Status	Published

Principal Author

Name of Principal Author (Candidate)	Albitar, M		
Contribution to the Paper	Performed the experiment, interpreted and analysed data and wrote manuscript and acted as corresponding author.		
Overall percentage (%)			
Certification:	This paper reports on original research I conducted during the period of my Higher Degree by Research candidature and is not subject to any obligations or contractual agreements with a third party that would constrain its inclusion in this thesis. I am the primary author of this paper.		
Signature		Date	

Co-Author Contributions

By signing the Statement of Authorship, each author certifies that:

i. the candidate's stated contribution to the publication is accurate (as detailed above);
ii. permission is granted for the candidate in include the publication in the thesis; and
iii. the sum of all co-author contributions is equal to 100% less the candidate's stated contribution.

Name of Co-Author	Mohamed Ali, M.S.		
Contribution to the Paper	Supervised development of work, helped to evaluate and edit the manuscript		
Signature		Date	20/10/2016

Name of Co-Author	Visintin, P.		
Contribution to the Paper	Supervised development of work and assisted in manuscript evaluation.		
Signature		Date	20/10/2016

Experimental Study on Fly Ash and Lead Smelter Slag–Based Geopolymer Concrete Columns

M. Albitar, M.S. Mohamed Ali and P. Visintin

ABSTRACT

Geopolymer concrete is an emerging technology with the potential to significantly reduce the environmental footprint of concrete manufacture and utilise high volumes of industrial waste materials. Although significant experimental research has focused on the development of geopolymer mix design, there is far less information available regarding the performance of geopolymer concretes at a member level. This has implications in transferring geopolymer concretes from a laboratory material to a material in which can be specified in practice. This paper addresses the application of geopolymer concrete at a member level through an experimental investigation on the behaviour of fly ash/granulated lead smelter slag (GLSS)–based geopolymer concrete columns and beams tested under concentric and eccentric loading. Slenderness effect of the geopolymer concrete columns is investigated and axial load–moment interaction envelopes are generated experimentally. The analytical interaction diagrams are compared to those calculated using classical methods for normal reinforced concrete beams and columns. The results of the comparison show that the analytical interaction diagrams overestimated the test results due to variation in material properties. The results also highlight potential issues with the scaling of ambient–cured geopolymer concrete to the structural level.

Keywords: Geopolymer; columns; beams; lead smelter slag; eccentricity; slenderness.

1. INTRODUCTION

The manufacture of ordinary Portland cement (OPC) is a major contributor to anthropogenic carbon dioxide (CO_2) emissions and hence global warming [1, 2]. During the past two decades, significant research has sought alternatives to OPC concrete, one of which is geopolymer concrete, which can be manufactured from industrial waste materials, such as fly ash and slags [3-5]. As such geopolymer concretes have the potential to be the next generation of highly sustainable construction material.

Geopolymer concrete has been demonstrated to be suitable for the use in civil engineering applications, such as in the construction of roads, footpaths and pipes. A broader demonstration of its behaviour is however required prior to widespread adoption in structural applications and for the development of national codes of practice. To date, the major focus of research into geopolymer concretes has focused on material development and the quantification of mechanical behaviour [6-15], with comparably few studies available that consider the behaviour of geopolymer concrete structural elements [16-19].

To this end, only two studies in the open literature devoted to the behaviour of slender columns [20, 21].

Sumajouw et al. [20] studied the behaviour of twelve fly ash concrete slender columns (175 x 175 x 1500mm) subjected to axial compression and uniaxial bending. The key parameters of the study involved compressive strength (i.e., 40MPa and 60MPa), longitudinal reinforcement ratio (i.e., 1.47 and 2.95), and load eccentricity (i.e., 15, 35 and 50mm) and it was shown that fly ash geopolymer concrete columns exhibit similar behaviour to that of OPC concrete and hence the design provisions contained in the current standards and codes can be used to design reinforced fly ash–based geopolymer concrete columns. Rahman and Sarker [21] similarly studied the behaviour of twelve fly ash concrete slender columns (175 x 175 x 1500mm) subjected to axial compression and different combination of biaxial load eccentricities. The key parameters of the study involved compressive strength (i.e., 37MPa to 63MPa), longitudinal reinforcement ratio (i.e., 1.47 and 2.95), load eccentricity in *x* direction (i.e., 15, 30, 35, 50 and 70mm), and load eccentricity in *y* direction (i.e., 15, 30, 35, 50 and 70mm). Their findings indicate the potential for fly ash geopolymer concrete to be used in structural applications.

This paper presents the results of a study on the behaviour of short and slender blended fly ash/lead smelter slag–based geopolymer concrete columns under concentric and eccentric loadings. This research follows on from previous research by the authors who have shown the potential for using non–ferrous slags, such as lead smelter slag (LSS) in the manufacture of geopolymer concrete [6]. The previous research demonstrated that LSS can be utilised in high volumes in the manufacture of geopolymer concrete either by blending granulated slags with fly ash or by grinding granulated slags to a similar fineness to that of fly ash. The use of LSS in concrete industry is considered significant because the demand for lead is increasing dramatically as it is necessary for the development of other 'green' technologies, such as the manufacture of battery storage for solar power. Although it is necessary for the manufacture of other green technologies, LSS has negative impacts on the environment and community health from fugitive dust, increased sediment loads of surface waters and heavy metal contamination of groundwater. Therefore, reducing the volumes of slags going to landfills by developing commercial applications, such as encapsulating GLSS in geopolymer and OPC concretes, can provide the community and smelting companies with significant environmental and economic benefits.

2. EXPERIMENTAL PROGRAM

2.1. Test specimens and geometric properties

The results presented in this study are of nine fly ash/granulated lead smelter slag (GLSS) –based geopolymer concrete columns and one beam all with the 150mm square cross–section shown in *Fig. 1(a)*. Five of the columns were designed as short columns with a length of 900mm, and the other four columns were designed as slender columns with a length of 1600mm as can be seen in *Fig. 1(b)*. The beam in *Fig. 1(c)* was designed to fail in bending and hence was tested under 3-point loading with a clear span of 2700mm. The

columns are subjected to axial load with eccentricities of 0, 10, 35, 50 or 85mm for the short columns, and 0, 30, 125, 145mm for the slender columns. All the columns and beam were reinforced longitudinally with four 12mm diameter bars with 32 mm cover to the centre of the bar. Transverse reinforcement consisting of 6mm diameter stirrups placed at 85mm centres was provided in all specimens.

The short and slender columns are designated by letters “SHC” and “SLC”, respectively, followed by the number that corresponds to their series and then the applied load eccentricity, such as the third short column tested under load eccentricity of 35mm can be represented as SHC3-35. The beam specimen is designated by Beam1.

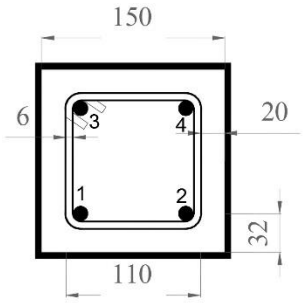

(a) Cross-section of the columns and the beam

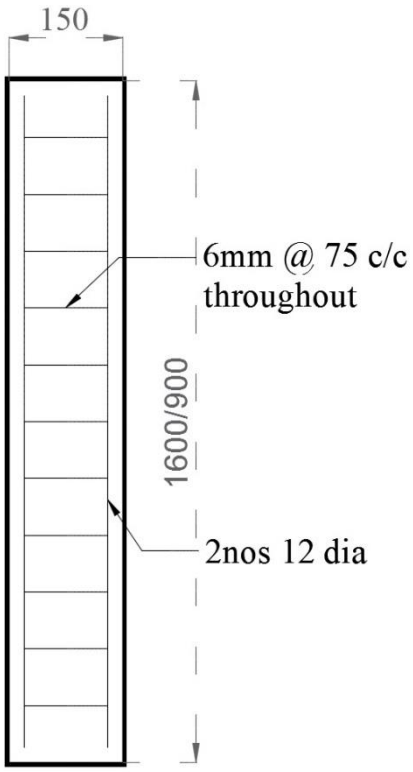

(b) Dimensions and reinforcement arrangement of short and slender columns

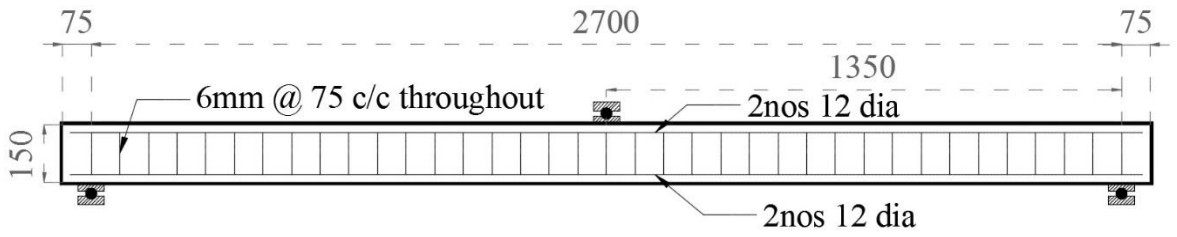

(c) Dimensions and reinforcement arrangement of the beam

Figure 1. Reinforcement arrangement of columns and beam (all dimensions are in mm).

2.2. Materials and properties

Granulated lead smelter slag (GLSS) and low calcium class–F fly ash were used as the cementitious material to manufacture the geopolymer concrete. The chemical compositions of GLSS and fly ash are listed in *Table 1*. The mix design was developed by the authors in previous works [6], which incorporates granulated lead smelter slag (GLSS) with fly ash as a blended binder. To maximise the usage of GLSS, GLSS was also utilised as fine aggregate, resulting in a mix comprising a total of 32.85% of GLSS by weight and only 8.85% fly ash. Crushed bluestone with 10mm maximum size was used as coarse aggregate.

Table 1. Chemical compositions by mass (%)

Oxides	Fe_2O_3	SiO_2	Al_2O_3	CaO	MgO	SO_3
Granulated lead smelter slag	33.8	27.5	7.4	19.4	2.1	-
Class– F Fly ash	2.8	49.0	31.0	5.4	2.5	0.3

To manufacture the geopolymer concrete, all the dry constituents were electronically weighed and mixed in dry state in a pan mixer for at least 3 minutes. The activator, which consisted of sodium silicate (Na_2SiO_3) and 14-molar sodium hydroxide (NaOH) pre–mixed with Na_2SiO_3–to–NaOH ratio of 1.5, high range water reducer retarder and water were added and mixed for further seven minutes. The proportions of the mix design are documented in *Table 2*. Control specimens with dimensions of 100mm diameter and 200mm height were used for the determination of compressive strengths of the mixes. All the specimens were ambient cured for 56 days prior to testing. This period of ambient curing was chosen as it has previously been shown by the authors [8] that ambient curing of cylinders for this period leads to the same strength development as that obtained when heat curing.

Table 2. Mixture proportions

Components	Note	(%)	(kg/m^3)
Coarse aggregate	10 mm	49	1176
GLSS		32.85	788.4
Fly ash		8.85	212.4
NaOH + sodium silicate	14M	6.6	158.4
*Superplasticiser		2	48
Water		0.7	16.8
Total		100	2400
* ViscoCrete 10 was used for short columns and Sika ViscoCrete-5-500 was used for slender columns			

The control specimens were tested before and after the test of the columns and beam. The measured compressive strength of the short columns and beam was 35MPa with an axial strain of 0.0020, whereas the compressive strength of the slender columns was 30MPa with an axial strain of 0.0016. It should be noted that the difference in the compressive strength is attributed to the different high range water reducer retarder used in the mixes in which ViscoCrete 10 was used for short columns and beam, and Sika ViscoCrete-5-500 was used for slender columns. The deformed bars used as longitudinal reinforcement were tested to determine the steel properties from which the mean yield strength (f_{sy}) was 510MPa, the yield strain (ε_{sy}) was 0.0025 and the ultimate tensile strength (f_{su}) was 620MPa.

2.3. Instrumentation and testing procedure

All specimens were fabricated horizontally from two batches of concrete. One column in each series was subjected to a monotonically increasing concentrically applied axial compression load to determine the squash load; the remaining columns were tested under an eccentrically applied compression load that produced a coupled axial load and bending moment. All the columns were tested with 5000kN capacity AMSLER testing machine, whereas the pure bending beam was tested using a 1000kN capacity Avery testing machine. High strength steel pins and bearing plates were placed eccentrically at the end of each column to produce combined bending and axial loads.

The columns and beam were extensively instrumented for measuring displacement and strain profiles. A total of nine linear variable displacement transformers (LVDTs) and eight electrical unidirectional strain gauges were used to measure axial and lateral deformation of the columns. *Figs. 2(a)* and *(b)* show the test setup schematically for the short and slender columns, respectively.

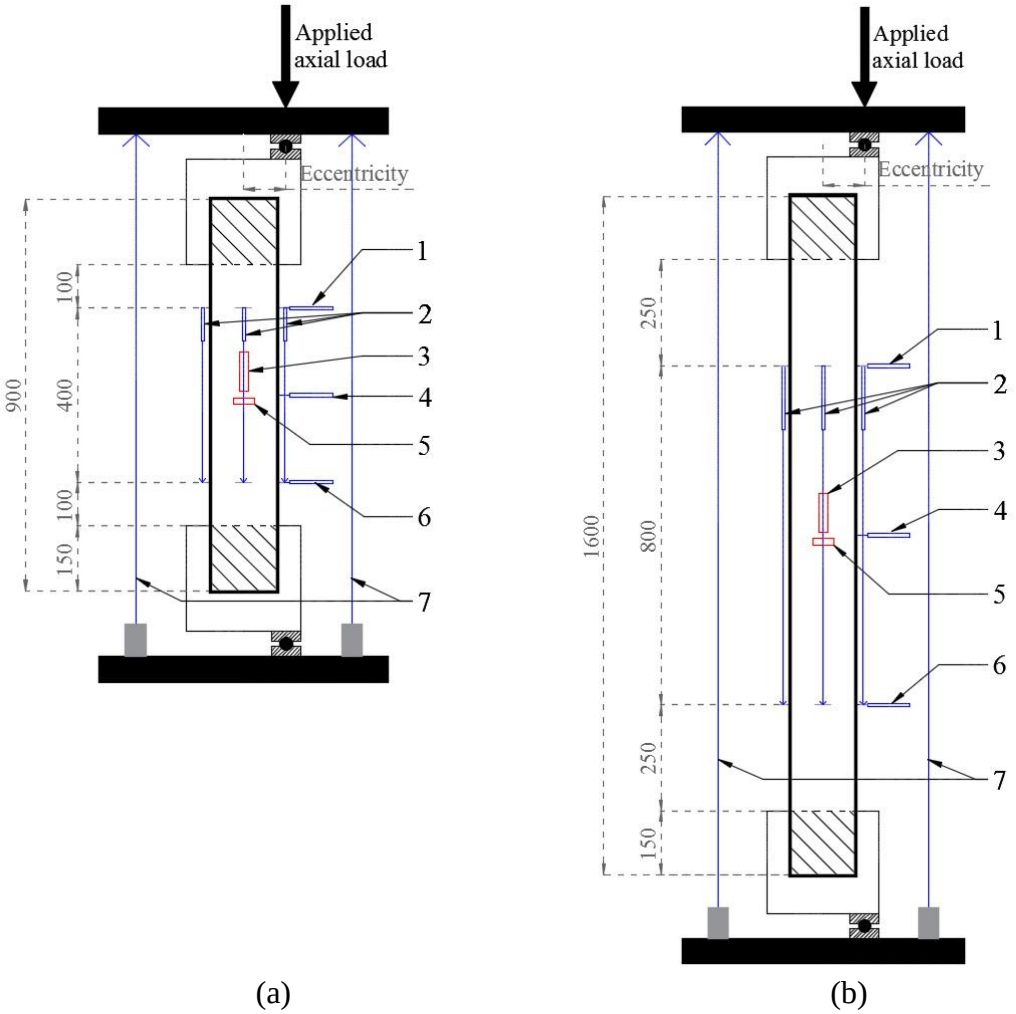

(a) (b)

(1, 4, 6) Lateral LVDTs, (2) Axial mid-height LVDTs, (3) Axial 900mm electrical strain gauge, (5) Lateral 30mm electrical strain gauge, (7) Axial global LVDTs.

Figure 2. Test setup: (a) short columns under testing rig, (b) slender columns under testing rig

To measure the average axial deformation along the entire height of the columns, a platen to platen displacement was measured by two LVDTs placed adjacent to the centre line of the columns. To measure the average axial deformation along the mid–height region within a length of 400mm for the short columns and 800mm for the slender columns, four LVDTs were placed at the mid–height regions of the columns. Moreover, the axial and lateral strain values were measured by eight unidirectional electrical strain gauges with a gauge length of 90mm for the axial strain, and 30mm for the lateral strain. All the strain gauges were placed around the centre at the mid–height of the columns. To measure the lateral deformation, three LVDTs were mounted on the mid–height and 200mm above and below the mid–height of the short columns and 400mm above and below the mid–height of the slender columns.

The instrumentation of the beam consisted of seven LVTDs and four unidirectional electrical strain gauges, as shown in *Fig. 3*. To measure the beam deflection, three LVDTs were placed underneath the beam at the middle and 250mm either side of the centre line. To measure the extension of the tension face and the contraction of the compression face, four LVDTs and four strain gauges were attached to the beam at the mid region and on the front and back of the beam at 5 mm from the surface.

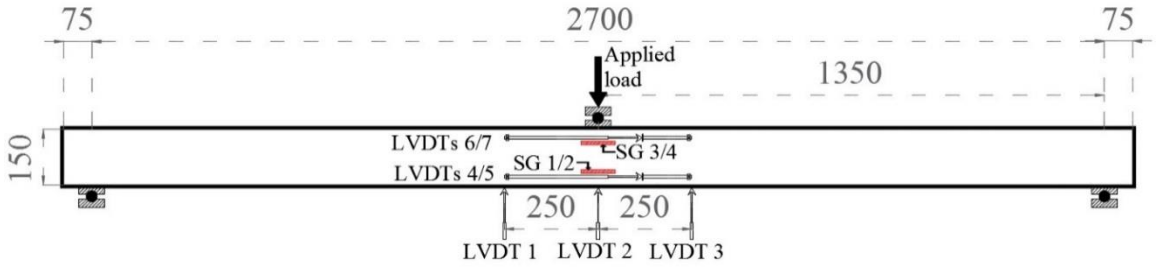

Figure 3. Test set up of the beam

3. EXPERIMENTAL TEST RESULTS AND OBSERVATION

All the short columns (SHCs) and slender columns (SLCs) were tested until failure. The location of failure, ultimate load (P_u), moment at ultimate load (M_u), corresponding lateral displacement at the mid–height of specimen ($\Delta_{u,mid}$), eccentricity (e), axial strain at ultimate load, and the rotation at ultimate load (θ) are presented in *Table 3*. The moment (M_u) is calculated as $M_u = P_u\,(e + \Delta_{u,mid})$. The corresponding test results for the beam are also given in *Table 3.*

Table 3. Test results all columns and beam

Specimen	*Failure location (mm)	f_c *(MPa)*	P_u (kN)	Δ_{mid} at P_u (mm)	e (mm)	M_u (kN.m)	Axial strain at P_u	Rotation at P_u (rad)
SHC1-0	+350 to -200	35	775.55	0.73	0	0.57	0.00307	0.000179
SHC2-10	+200 to -200	35	545.34	3.58	10	7.40	0.00090	0.000068
SHC3-35	+25 to -150	35	354.83	6.16	35	14.61	0.00033	0.000084
SHC4-50	+50 to -150	35	272.41	8.52	50	15.94	0.00026	0.000084
SHC5-85	+200 to -200	35	170.34	10.83	85	16.32	0.00059	0.006022
SLC6-0	+400 to +50	30	597.47	0.50	0	0.30	0.00180	0.000116
SLC7-30	+150 to -150	30	302.66	9.69	30	12.01	0.00155	0.000158
SLC8-125	+250 to -30	30	91.89	20.48	125	13.37	0.00104	0.000592
SLC9-145	+100 to -100	30	76.29	19.66	145	12.56	0.00100	0.000678
Beam1	+250 to -250	35	17.92	96.23	-	12.10	-	-

* "+" is above and "-" is below column mid-height

3.1. Test results of short columns

The failure mode of the concentrically loaded short columns was observed to be abrupt and was associated with little residual load capacity. The failure occurred between 350mm above and 200mm below the mid–height. The concentrically loaded columns failed by concrete crushing while the eccentrically loaded short columns failed in a typical flexural failure mode, that is formation of flexural cracks followed by concrete crushing. The crack pattern varied depending on the eccentricities and, in general, the number of crack increased with increasing eccentricity. The failure modes of all short columns are depicted in *Fig. 4*.

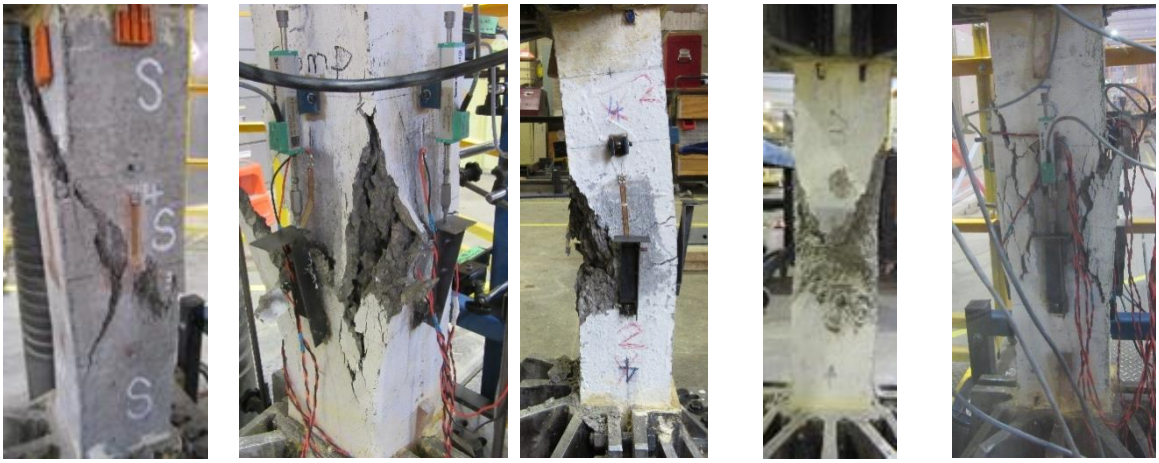

(a) SHC1-0 (b) SHC2-10 (c) SHC3-35 (d) SHC4-50 (e) SHC5-85

Figure 4. Failure modes of all short columns

The variation of axial compression strains with increasing applied loads for short columns are shown in *Fig. 5*. It can be seen that the ultimate load (P_u) has an inverse relationship with the load eccentricity, as it decreases with increasing the eccentricity of the axial load. The load capacities of the eccentrically loaded short columns were reduced by 29.68%, 54.24%, 64.87% and 78.03% for specimens SHC2-10, SHC3-35, SHC4-50 and SHC5-85, respectively, in comparison to the squash load of the concentrically loaded short column (SHC1-0). This reduction in the ultimate load is associated with a reduction in the axial compression strain of the concrete. The mid-height lateral deflection increased proportionally to the increasing eccentricity of the load (*Fig. 6*).

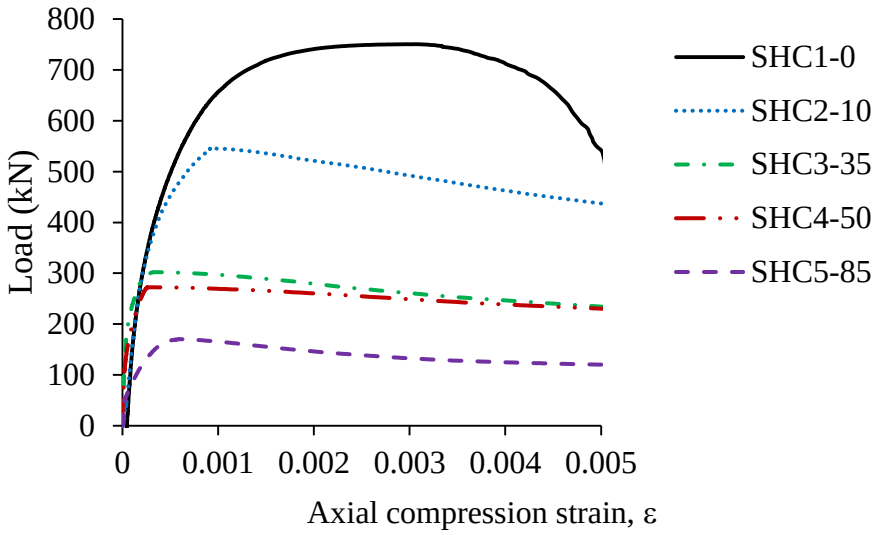

Figure 5. Load versus axial compression strain of short columns

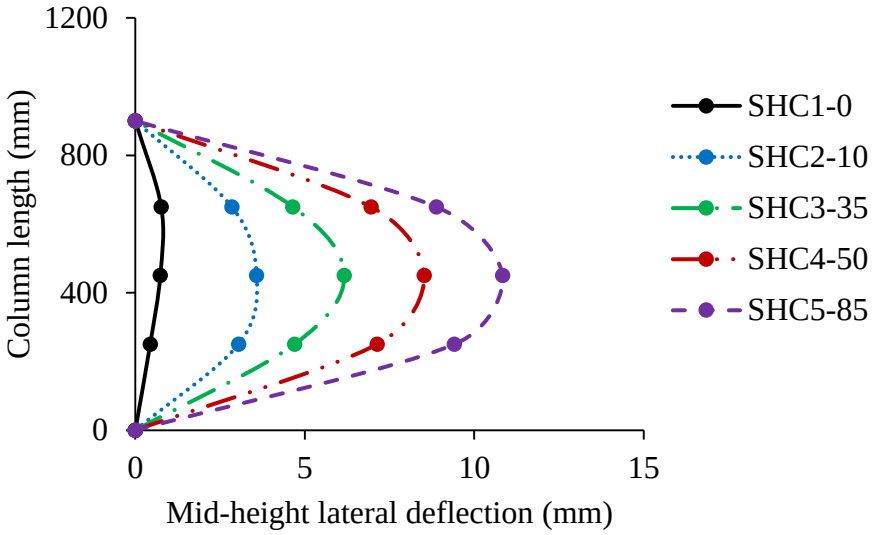

Figure 6. Column length versus mid–height lateral deflection at failure load of short columns

It is evident from *Fig. 7*, which depicts the relationship between the applied load and mid–height lateral displacement that concentrically loaded columns behaved differently to eccentrically loaded columns. The concentrically loaded columns (i.e., SHC1-0) failed in a brittle fashion as the load dropped abruptly after the squash load was achieved, whereas eccentrically loaded columns (i.e., SHC4-50, SHC5-85) exhibited gradual failure as the load drop was gradual with a long plateau.

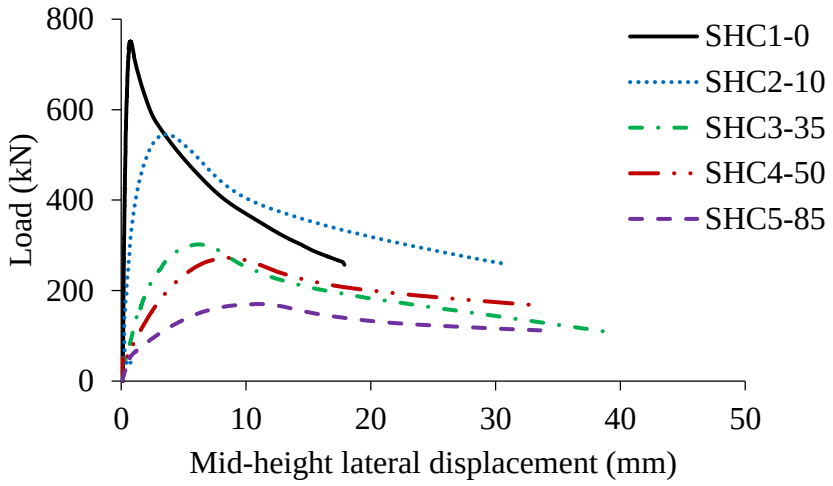

Figure 7. Load versus mid–height displacement of short columns

3.2. Test results of slender columns

Slender columns were observed to fail in a similar fashion to that of short columns in which the concentrically loaded columns exhibited a brittle failure with localised concrete crushing, whereas the eccentrically loaded columns failed with the development of flexural cracks followed by concrete crushing on the compression face. The failure modes of all slender columns are depicted in *Fig. 8*.

(a) SLC6-0 (b) SLC7-30 (c) SLC8-125 (d) SLC9-145

Figure 8. Failure modes of all slender columns

The general performance of the slender columns test results is similar to that of short columns test results in which the P_u and the axial strain at P_u decrease with an increase in the eccentricity of load (*Fig. 9*), whereas the lateral deflection increases with an increase in the eccentricity due to buckling of columns (*Fig. 10*). The load capacities of the eccentrically loaded slender columns were reduced by 49%, 85%, and 87% for specimens SLC7-30, SLC8-125, SLC9-145, respectively, in comparison to the squash load of the concentrically loaded slender column (SLC6-0).

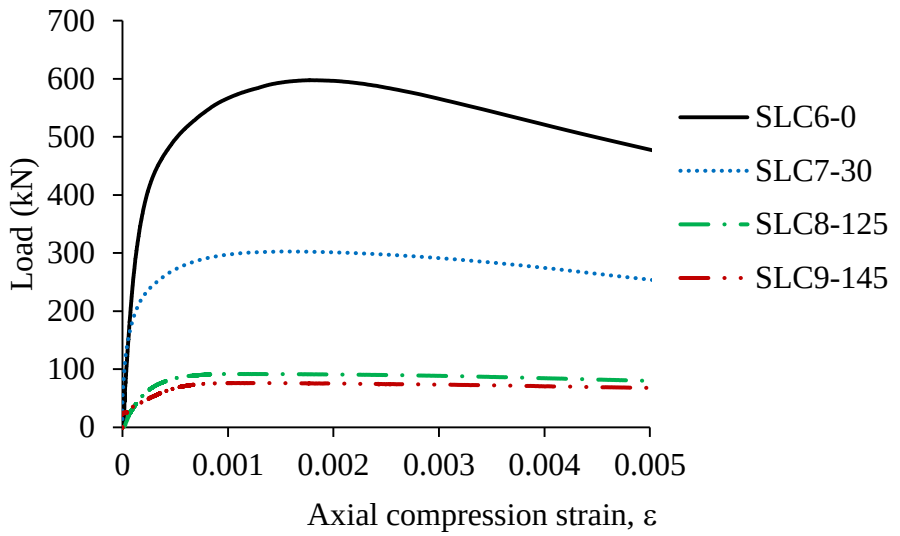

Figure 9. Load versus axial compression strain of slender columns

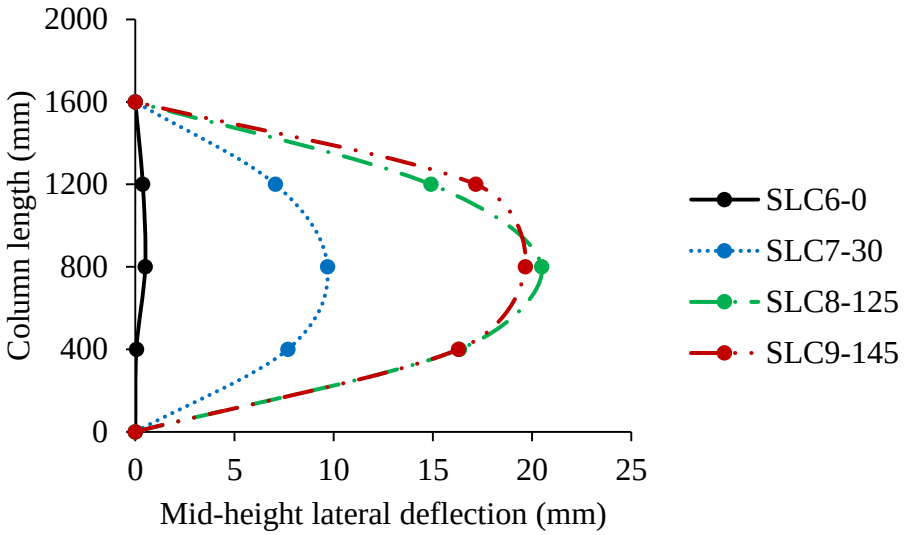

Figure 10. Column length versus mid-height lateral deflection at failure load of slender columns

It can be observed that the squash load, P_u, of short column subjected to concentric load is larger than that of the corresponding slender column; however, there is no major difference between the load versus mid–height deformation responses of short and slender columns. Nevertheless, it can be seen from *Fig. 11* that slender columns developed greater deformation than the corresponding short columns due to excessive buckling. It is worth mentioning that short and slender columns behaved in a similar way with final failure occurring well beyond the peak load, P_u.

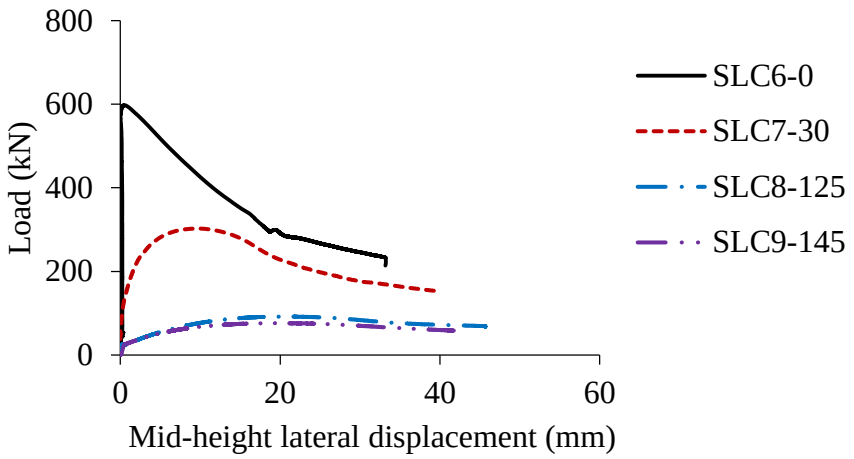

Figure 11. Load versus mid–height displacement of slender columns

3.3. Test results of the beam

The simply supported beam was centrally loaded until failure. Flexural cracks occurred in the maximum bending region at early stages of loading (i.e., 4kN). The number of cracks increased with the increase in the applied load. The cracks kept on widening with increasing applied load, and eventually lead to failure (*Fig. 12*). After attaining the peak load of 17.9kN (M= 12.1kN.m), the applied load dropped steadily with a long plateau due to the onset of concrete crushing.

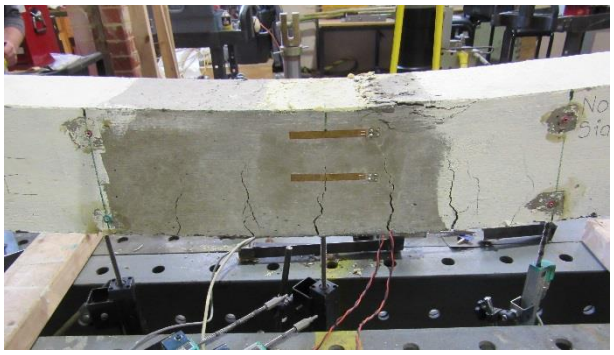

Figure 12. Failure mode of the beam

Fig. 13 shows the plot of applied load–deflection at mid–span the beam. The concrete crushing occurred at an applied load of 14.52kN (M= 9.8kN.m) with a mid–span displacement of 31.32mm, whereas the beam failed completely when the applied load was 17.9kN (12.1kN.m) and the corresponding mid–span deflection was 96.2mm, as can be seen in *Table 4*. It is worth mentioning that the load–deflection behaviour of the geopolymer concrete beam is similar in nature to that of OPC concrete beam and the long plateau of the post peak load–deflection relationship indicates that the beam failed generally in a ductile fashion.

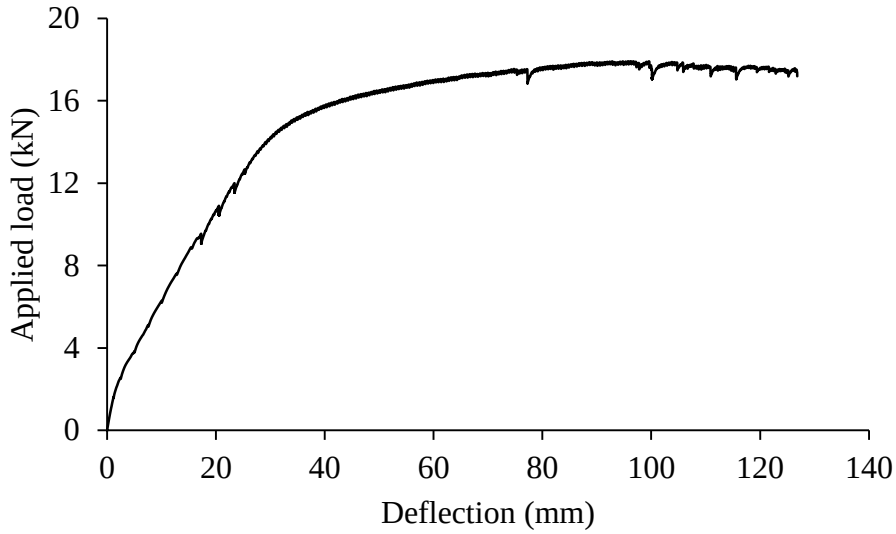

Figure 13. Load versus deflection of the beam

Table 4. Details of the beam

Load stage	Load (kN)	Bending moment (kN.m)	Disp Mid (mm)	Disp East (mm)	Disp West (mm)
Initial failure	14.5	9.8	31.6	28.9	29.2
Failure load	17.9	12.1	96.2	83.7	84.7

3.4. Slenderness effect

The ratio of secondary moment to primary moment in the critical cross–section of a pin–ended column controls the reduction in strength caused by slenderness effect. The primary moment depends on the applied axial, *P*, and the initial eccentricity, *e*, whereas the secondary moment depends on *P*, as well as on the length of the column and the bending stiffness of the column section [22]. Thus, the lateral deflection and secondary moment in short pin–ended column are negligible, which leads to a proportional increase in both *P* and *M* with gradual increase in the applied load in the critical section at the mid–height. However, in the case of slender column with the same cross–section, increasing the applied

axial load results in a progressive increase in deflection, which leads to a reduction in the load–carrying capacity. This is due to the lateral deflection at mid–height is perceptible, and hence the secondary moment is significant. Therefore, slender columns resist lower axial loads than their short columns counterparts due to the slenderness effect, which must be taken into consideration over and above the sectional capacity considerations incorporated in the interaction diagrams.

In this study, 5 short columns and 4 slender columns were tested under different eccentricities. As the compressive strengths were different, the P_u was divided by the compressive strength, f'_c, for a meaningful comparison. *Table 5* presents the major required data for a comparison between short and slender columns. The significance of slenderness effect is expressed through nominal slenderness ratio (λ_n), which is calculated in *Eq. 1*.

$$\lambda_n = \frac{k l_u}{r_g} \tag{1}$$

where, l_u is unsupported column length; k is effective length factor reflecting the end restraint and lateral bracing conditions of a column (= 1 for pin–ended column); and r_g is the radius of gyration, reflecting the size and shape of a column cross–section, which can be taken as $r_g = 0.3h$ for square shape, or can be defined as *Eq. 2*.

$$r_g = \sqrt{\frac{I}{A}} \tag{2}$$

in which I is the moment of inertia of the section; and A is the area of the section.

Table 5. Comparison between short and slender columns

Column	e (mm)	f_c (MPa)	P_u (kN)	P_u/f_c	Δ_{mid} (mm)	M_u (kN.m)	M_u/f_c	λ_n
SHC1-0	0	35	775.55	22.15	0.73	0.57	0.01	13.86
SHC2-10	10	35	545.34	15.58	3.58	7.40	0.21	13.86
SHC3-35	35	35	354.83	10.14	6.16	14.61	0.42	13.86
SHC4-50	50	35	272.41	7.78	8.52	15.94	0.46	13.86
SHC5-85	85	35	170.34	4.87	10.83	16.32	0.47	13.86
SLC6-0	0	30	597.47	19.91	0.50	0.30	0.01	30.02
SLC7-30	30	30	302.66	10.08	9.69	12.01	0.40	30.02
SLC8-125	125	30	91.89	3.06	20.48	13.37	0.44	30.02
SLC9-185	145	30	76.29	2.54	19.66	12.56	0.42	30.02

It is evident from *Table 5* that concentrically loaded slender column (i.e., SLC6-0) had lower load carrying capacity (P_u/f_c) than its companion short column (i.e., SHC1-0). This can be attributed to the slenderness effect.

3.5. Axial Load–moment interaction envelopes

The axial load versus bending moment interaction curves obtained from the tests are plotted in *Figs. 14(a)* and *(b)* for short and slender columns, respectively, together with the axial load versus bending moment interaction curves obtained from a standard sectional analysis. The sectional analysis procedure as explained in Warner et al. [22] and AS 3600 [23] is adopted in this study. From *Fig. 14(a)*, it can be seen that the sectional analysis overestimated the axial load results of short columns by an average of 25%, whereas *Fig. 14(b)* shows an overestimation of 30% for the axial load of slender columns. *Table 6* compares the load capacities of the experimentally obtained values with the calculated values with the average overestimation of bending moment for both short and slender columns was 15%. This discrepancy could be attributed to the fact that the concrete compressive strength used in the analyses is based on the 100mm (diameter) x 200mm (height) cylinders, whereas the actual material strength in a large size structural members using a geopolymer concrete that was cured under ambient conditions could be less. Hence there is a need to investigate the variation in rate of gain of compressive strength in large scale elements as otherwise standard compression cylinder test results may lead to misleading analytical results.

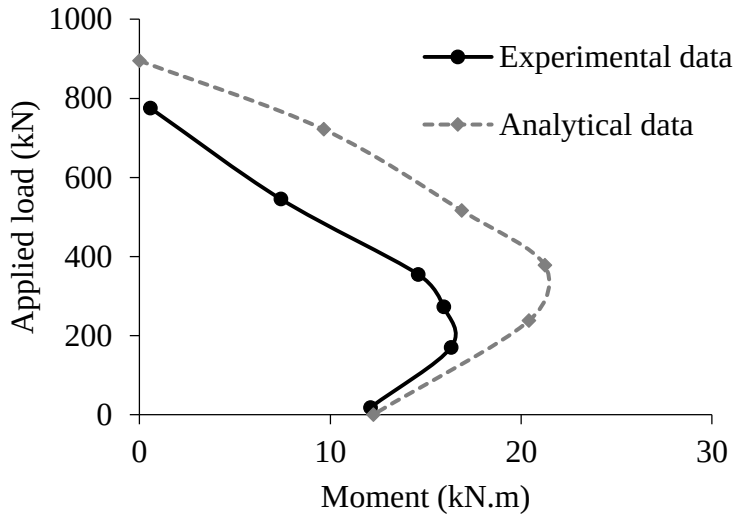

(a)

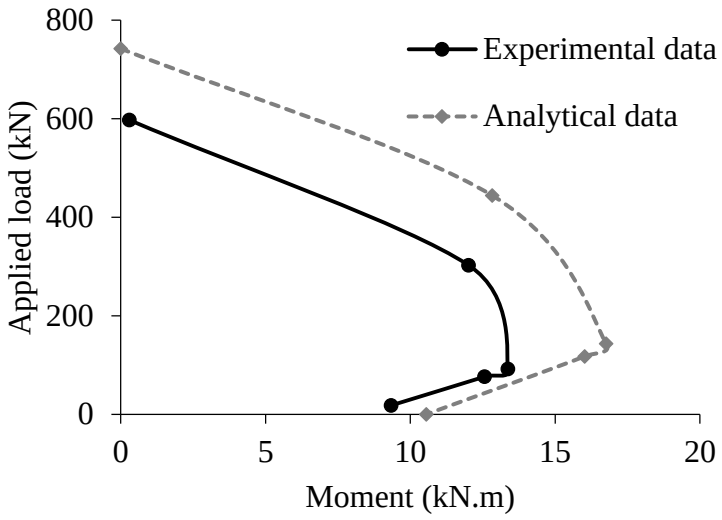

(b)

Figure 14. Load–moment interaction plots: (a) short columns, and (b) slender columns

Table 6. Experimental and theoretical predicted ultimate load for columns

Column	(Experiment)	(Predicted)	$P_{u(Exp.)}/P_{u(Theo.)}$
	$P_{u(Exp.)}$ kN	$P_{u(Theo.)}$ kN	
SHC1-0	775.55	895.37	0.86
SHC2-10	545.34	721.64	0.75
SHC3-35	354.83	516.35	0.69
SHC4-50	272.41	377.96	0.72
SHC5-85	170.34	237.71	0.72
SLC6-0	597.47	742.38	0.80
SLC7-30	302.66	444.11	0.68
SLC8-125	91.89	143.52	0.64
SLC9-145	76.29	117.50	0.64

4. CONCLUSIONS

This paper has presented the results of an experimental study undertaken to investigate the structural behaviour of reinforced short and slender fly ash/GLSS–based geopolymer concrete columns subjected to axial compressive loads coupled with bending moment. The following conclusions can be drawn based on the results and discussions reported in this paper:

1. The failure mode of the geopolymer concrete columns and beams were similar in nature to that of OPC concrete columns and beams.
2. The axial load at failure of the eccentrically loaded short columns were reduced by 30%, 54%, 65% and 78% for specimens SHC2-10, SHC3-35, SHC4-50 and SHC5-85, respectively, when compared to the squash load obtained for concentrically loaded short column (SHC1-0).
3. The corresponding load capacities of the eccentrically loaded slender columns were reduced by 49. %, 85%, and 87% for specimens SLC7-30, SLC8-125, SLC9-145, respectively, of the squash load of the concentrically loaded slender column (SLC6-0).
4. The current design provisions of the available analytical methods for determining the interaction curve overestimated the axial load of short columns by 25%, and the axial load of slender columns by 30%.
5. The strength obtained from standard cylinder tests may be inadequate for predicting the strength of ambient–cured geopolymer concrete in large scale elements.

It is evident that geopolymer concrete has the potential to be used in a wide range of applications in order to reduce the amount of OPC used worldwide and hence reduce the environmentally damaging effects from the production of OPC concrete. It is shown that fly ash/slag–based geopolymer concrete structural members exhibit similar structural response to that of OPC concrete. Thus, the current design provisions contained in the standards for OPC reinforced concrete columns can easily be modified and adopted for the applications of blended fly ash and GLSS–based geopolymer concrete columns; however, further research effort is required to identify methods for predicting the strength of geopolymer concrete when placed in large volumes.

ACKNOWLEDGEMENTS

The authors would like to thank Dylan Anderson, Michael Moshos, Christopher Silbor, John Zunis, Ka Ho Leung, Mengyu Tang, Kin Yeung Wong and Qianping Ye, who have helped in undertaken the tests reported in this paper as part of their undergraduate project. Thanks are due to Dr. M Ridha, Dr. MS Mohamed Ali and Mr. J Ayoub for the usage of steel cap arrangement for the column tests. This research is part of an ongoing program at the University of Adelaide on geopolymer concrete.

This research was funded by the Department of Planning, Transport and Infrastructure of South Australia and The South Australian Department of Further Education, Employment, Science and Technology through Catalyst Research Grant “Development of Geopolymer Concrete”. The authors declare that they have no conflict of interest.

REFERENCES

[1] Bosoaga, O. Masek, J.E. Oakey, CO_2 capture technologies for cement Industry, Energy. Procedia. 1 (2009) 133–140.

[2] L. Barcelo, J. Kline, G. Walenta, E. Gartner, Cement and carbon emissions, Mater. Struct. 47 (2014) 1055–1065.
[3] P. Duxson, J.L. Provis, G.C. Lukey, J.S.J. van Deventer, The role of inorganic polymer technology in the development of 'green concrete', Cem. Concr. Res. 37 (2007) 1590–1597.
[4] H. Yildirim, M. Sümer, V. Akyüncü, E. Gürbüz, Comparison on efficiency factors of F and C types of fly ashes, Constr. Build. Mater. 25 (2011) 2939–2947.
[5] E. Ivan Diaz-Loya, E.N. Allouche, S. Vaiday, Mechanical properties of fly-ash-based geopolymer concrete, ACI. Mater. J. 108 (2011) 300–306.
[6] M. Albitar, M.S. Mohamed Ali, P. Visintin, M. Drechsler, Effect of granulated lead smelter slag on strength of fly ash-based geopolymer concrete, Constr. Build. Mater. 83 (2015) 128–135.
[7] A.I. Laskar, R. Bhattacharjee, Effect of plasticizer and superplasticizer on rheology of fly-ash-based geopolymer concrete, ACI. Mater. J. 110 (2013) 513–518.
[8] M. Albitar, P. Visintin, M.S. Mohamed Ali, M. Drechsler, Assessing behaviour of fresh and hardened geopolymer concrete mixed with class-F fly ash, J. Korean. Soc. Civil. Eng. 19 (2014) 1445–1455.
[9] T. Sugama, T. Pyatina, Effect of sodium carboxymethyl celluloses on water-catalyzed self-degradation of 200 ^{o}C-heated alkali-activated cement, Cem. Concr. Comp. 55 (2015) 281–289.
[10] S. Ioannou, K. Paine, L. Reig, K. Quillin, Performance characteristics of concrete based on a ternary calciumsulfoaluminate–anhydrite–fly ash cement, Cem. Concr. Comp. 55 (2015) 196–204.
[11] R. Yu, P. Spiesz, H.J.H. Brouwers, Development of an eco-friendly Ultra-High Performance Concrete (UHPC) with efficient cement and mineral admixtures uses, Cem. Concr. Comp. 55 (2015) 383–394.
[12] M. Albitar, P. Visintin, M.S. Mohamed Ali, O. Lavigne, E. Gamboa, Bond slip models for uncorroded and corroded steel reinforcement in class-F fly ash geopolymer concrete, J. Mater. Civ. Eng. (2016) 04016186-1–04016186-10.
[13] R. Kovács, Effect of the hydration products on the properties of fly-ash cements, Cem. Concr. Res. 5 (1975) 73–82.
[14] E.E. Berry, R.T. Hemmings, B.J. Cornelius, Mechanisms of hydration reactions in high volume FA pastes and mortars, Cem. Concr. Comp. 12 (1990) 253–61.
[15] R.F. Feldman, G.G. Carette, V.M. Malhotra, Studies on mechanics of development of physical and mechanical properties of high-volume FA-cement pastes, Cem. Concr. Comp. 12 (1990) 245–51.
[16] J.R. Yost, A. Radli ska, S. Ernst, M. Salera, Structural behaviour of alkali activated fly ash concrete. Part 1: Mixture design, material properties and sample fabrication, Mater. Struct. 46 (2013) 435–447.
[17] P. Kathirvel, S.R.M. Kaliyaperumal, Influence of recycled concrete aggregates on the flexural properties of reinforced alkali activated slag concrete, Constr. Build. Mater. 102 (2016) 51–58.

[18] G.B. Maranan, A.C. Manalo, B. Benmokrane, W. Karunasena, P. Mendis, Behavior of concentrically loaded geopolymer-concrete circular columns reinforced longitudinally and transversely with GFRP bars, Eng. Struct. 117 (2016) 422–436.
[19] X. Fan, M. Zhang, Experimental study on flexural behaviour of inorganic polymer concrete beams reinforced with basalt rebar, Compos. Part. B-Eng. 93 (2016) 174–183.
[20] D.M.J. Sumajouw, D. Hardjito, S.E. Wallah, B.V. Rangan, Fly ash-based geopolymer concrete: study of slender reinforced columns, J. Mater. Sci. 42 (2007) 3124–3130.
[21] M.M. Rahman, P.K. Sarker, Geopolymer concrete columns under combined axial load and biaxial bending, Research Project. Curtin University of Technology, Perth, Australia, 2011.
[22] R.F. Warner, B.V. Rangan, A.S. Hall, K.A. Faulkes, Concrete structures, Addison Wesley Longman Australia Ltd., Melbourne, 1998.
[23] AS 3600, Australian Standard for concrete structures, 2009.

CHAPTER 5: Conclusion and Recommendation for Future Work

Conclusion

Geopolymers have emerged as innovative engineering materials with a broad range of potential fields of applications. However, the knowledge associated with geopolymers is based on the assumption that geopolymer concretes have the exact same mechanisms as the conventional ordinary Portland cement (OPC) concrete. Therefore, an extensive experimental work is required to understand and evaluate the behaviour of geopolymer concretes. This thesis has contributed to the present knowledge on the development of geopolymer concretes at the material and structural level.

The mechanical properties of class–F fly ash–based geopolymer concrete were first determined and analysed in Chapter 1 to address the inadequacy of the current knowledge. Having optimised a mix design of fly ash–based geopolymer, the approach extended to incorporate granulated lead smelter slag (GLSS) with the fly ash to introduce the first comprehensive experimental–based investigation on the utilisation of GLSS in the concrete industry. The broad investigation into mix design mechanical properties of fly ash and GLSS geopolymer concretes enabled generic models based on a mathematical regression for fresh and hardened concrete to be established. Specific findings from these studies are outlined below:

- Class–F fly ash–based geopolymer concrete has comparable mechanical properties to OPC concrete, and hence it has a great potential for the utilisation in construction industries.
- Lead smelter slag can be used as a solo binder if its particles are crushed to produce fractions with grain size similar to that of fly ash.
- Partial replacement of fly ash with GLSS has a positive impact in terms of utilising raw GLSS, which results in reducing the vast stockpiles of GLSS and increasing the green credentials of the concrete.

Once the mechanical properties were thoroughly established in Chapter 1, an extensive durability study was performed on fly ash, GLSS and OPC concretes in Chapter 2. The durability evaluation aimed at investigating the performance of each concrete when exposed to various chemical attacks. The durability characteristic of fly ash–based geopolymer concrete was also investigated in Chapter 2 through the influence of reinforcement corrosion on the bond stress. In this work, a total of 102 pull–out test specimens were considered covering corrosion levels from 0% to 85%. Through these extensive investigations, the major findings include:

- The water absorption and sorptivity of OPC concrete were observed to be lower than that of both fly ash and GLSS geopolymer concretes, which is indicates that OPC concrete is more durable and sustainable in regards to limiting water access.

Nevertheless, the water absorptions of both fly ash and GLSS geopolymer concretes were less than 5%.

- In an acidic environment, OPC concrete lost 26.6% of its compressive strength, whereas the performance of both fly ash and GLSS geopolymer concretes was substantially superior in which their reduction magnitudes were 10.9% and 7.3% respectively. However, in a sulphate environment, durability performance of fly ash and GLSS was marginally better with reduction magnitudes of 13.4% and 12.3%, respectively, compared to 15.4% corresponding reduction magnitude of OPC concrete.
- The bond performance of uncorroded reinforcement in fly ash–based geopolymer concrete was slightly stronger than that in OPC concrete.
- The bond performance of corroded reinforcement in fly ash concrete was significantly stronger than that in OPC concrete when the reinforcement mass loss due to corrosion ranged between 7-30%.
- The bond behaviour between conventional ribbed steel bars and fly ash concrete was subsequently compared with predictive models developed for OPC concrete. The comparison suggests that predictive models developed for OPC concrete can be used as a reliable lower bound to predict the bond stress of fly ash–based geopolymer concrete.
- For more accurate analysis, new bond models for geopolymer concrete with uncorroded and corroded reinforcements were proposed from statistical analyses of the test results.

In Chapter 3, the geopolymer mix development conducted in Chapter 1 and geopolymer bond properties conducted in Chapter 2 were used to further investigate the tension–stiffening mechanism in geopolymer concrete. In this study, an experimental investigation was conducted to quantify the tension behaviour of reinforced geopolymer concrete and verify the accuracy of existing mechanics, semi–mechanics and empirical provisions developed for OPC concrete. The following findings can be drawn based on the results of the experimental program and the comparison with mechanics–based solutions:

- The mechanisms of tension–stiffening in geopolymer concrete, in general, is similar to that of OPC concrete.
- The tension–stiffening effect decreases with increasing the reinforcement ratio.
- Specimens with larger cross–section develop transverse tensile cracks at higher steel stress.
- The tension–stiffening effect of geopolymer concrete was shown to be slightly more significant than that of OPC concrete.
- Crack spacing and crack width of geopolymer reinforced concrete can be accurately predicted using mechanics–based solutions developed for OPC concrete along with bond stress–slip properties set for geopolymer concrete.

Finally, the structural behaviour of short and slender geopolymer concrete columns was studied in Chapter 4. It was shown that the strength of geopolymer concrete columns could be determined using classical methods for normal reinforced concrete beams and columns.

Therefore, it can be said that the current design provisions contained in the standards for OPC reinforced concrete can easily be modified and adopted for the applications of geopolymer concrete.

Through a study of the material, mechanical durability and structural performance of geopolymer concretes, this research has shown the potential for normalising the use of geopolymer concrete in construction industry. Therefore, based on the results and the aforementioned observations, the cement industry should expect the emergence of major environmentally friendly binder–manufacturing technologies in the foreseeable future.

Recommendation for Future Work

Having investigated a broad base of the utilisation of fly ash and lead smelter slag in concrete, several research aspects are to follow. During the investigation, certain inscrutable aspects that have either a major role in manufacturing geopolymer concrete or a significant influence on geopolymer concrete strength arose.

- Size effect on strength development:
  Geopolymer concrete is sensitive to curing, which makes strength development a critical aspect. Therefore, further research effort is required to study the size effect and identify methods for predicting the strength of geopolymer concrete when used in large volumes.
- Activator solution:
  Geopolymer concrete is usually activated by sodium hydroxide with sodium silicate. These two activators are expensive, hazardous and have a negative impact on the environment. Furthermore, this research found that sodium hydroxide has a detrimental impact on the strength of geopolymer concrete when an interaction with sodium sulphate takes place. Therefore, it is a particularly important consideration to find an alternative activator solution.
- Confinement effect:
  Fibre-reinforce-polymer (FRP) confinement generally enhances the ductility behaviour of concrete. The behaviour of confined geopolymer concrete columns under axial compressive strength with different eccentricities is an important research to conduct.
- Void filling mechanisms:
  Geopolymer concrete displays a wide range of pore variation, such as entrapped air voids, entrained air voids, capillary pores and nanoscale gel pores. The void filling mechanisms can be enhanced by incorporating graphene oxide, which enhances the durability of geopolymer concrete, as well as the mechanical properties.
- Attenuation of Nuclear Radiation:
  Nuclear radiation emits three different waves or particles, including: alpha particles, beta particles and gamma rays. Gamma rays are usually much higher frequency and more energetic. This radiation requires concrete containing high

amount of lead slag to shield and reduce the danger. The amount of lead slag that reduces the gamma rays needs to be investigated.